

UNIVERSITY OF NATAL

A STUDY OF PROCESSES  
OCCURRING IN FLOTATION FROTHS



BY

MICHAEL HUGH MOYS  
B. SC. (ENG.) (RAND)  
M. SC. (ENG.) (NATAL)

A THESIS SUBMITTED IN PARTIAL FULFILMENT OF  
THE REQUIREMENTS FOR A DEGREE OF DOCTOR OF  
PHILOSOPHY, IN THE DEPARTMENT OF CHEMICAL  
ENGINEERING, UNIVERSITY OF NATAL.

DURBAN,  
SOUTH AFRICA,  
DECEMBER 1979.

A C K N O W L E D G E M E N T S

I wish to express my sincere appreciation to:

Professor E.T. Woodburn for the opportunity to perform this work in his department and for many helpful and inspiring discussions.

Mr. M.F. Dawson for his encouraging supervision of the project.

The National Institute for Metallurgy for providing financial support.

My wife Denise for her tolerance, understanding and support, and for typing most of this manuscript, and Mrs. Lilian Fourie who assisted her.

Mr. Alan Perumal for drawing many of the diagrams.

The staff and graduate students of the Department of Chemical Engineering for their varied and valuable contributions.

Declaration:

I hereby declare that this is my own work and that it has not been submitted for a degree at any other university.

M.H. Moys.

December 1979.

S Y N O P S I S

While the significant effect that the froth phase has on the performance of a flotation operation has recently been widely recognised, little work has been published which promotes an understanding of the physical processes occurring in the froth phase. A more intimate understanding of these processes and their relative importance and interactions would lead to a more rational design of froth chambers and froth removal methods, with resultant improvements in flotation plant performance. In pursuit of this understanding the following investigations were performed:

- (1) In a specially designed cell the variation of mineral grade with height above the froth-slurry interface - as affected by gas rate, frother concentration, the presence of froth baffles (to minimise mixing) and final product removal rate - was measured. A mathematical model was formulated to assist in the interpretation of this data.
- (2) The residence time distribution of a 2-phase froth (air and water without solid particles) was measured as a function of froth height, gas rate and frother concentration. Small polystyrene balls were used as a tracer. The results were interpreted using two theoretical models:
  - (a) a streamline model which involved the solution of the 2-dimensional Laplace equation for frictionless flow of froth in the froth chamber;
  - (b) a semi-phenomenological model which relates the froth residence time distribution to cell dimensions, gas rate and froth stability.

On the basis of insights gained in these investigations, a number of objectives which should be met by froth removal methods were formulated:

- (1) froth removal efficiency should be maximised, i.e. there should be no stagnant zones in the froth;
- (2) froth stability should be optimised;
- (3) the minimum residence time of froth elements in the froth phase should be maximised.

One novel method of froth removal was designed, and this and a number of other methods of froth removal were compared experimentally. It was found that substantial improvement in flotation performance could be obtained by

- (1) sprinkling the froth with water, which removed entrained particles and improved froth stability;
- (2) inserting a baffle in the froth phase near the concentrate weir which increased the minimum residence time of a froth element in the froth phase, thereby improving the drainage of entrained particles from the froth; and
- (3) placing a froth scraper near the back of the cell, thus ensuring that no stagnant froth zones developed.

C O N T E N T S

TITLE PAGE

ACKNOWLEDGEMENTS

SYNOPSIS

CONTENTS

LIST OF TABLES

LIST OF FIGURES

CHAPTER 1 THE FROTH PHASE : THE CINDERELLA OF FLOTATION RESEARCH?

1.1 Introduction

1.2 Literature Survey

CHAPTER 2 PREPARATION FOR EXPERIMENTATION : EQUIPMENT, SLURRY PRODUCTION  
AND SAMPLE ANALYSIS

2.1 Introduction

2.2 Design and Construction of Flotation Cell

2.3 Production and Conditioning of Feed Slurry

2.3.1 Description of Ore Used

2.3.2 Grinding of the Ore

2.3.2.1 Batch Grinding

2.3.2.2 Continuous Operation

2.3.3 Feed to Flotation Circuit

2.3.4 Conditioning of the Feed Slurry

2.4 Sampling Procedures

2.4.1 Sampling of Concentrate and Tailings Streams

2.4.2 Sampling of Froth Chamber Contents

2.5 Analysis of Samples

CHAPTER 3 VARIATION OF FROTH PROPERTIES WITH HEIGHT IN THE FROTH COLUMN

3.1 Introduction

3.2 Processes occurring during vertical, plugflow removal  
of froth

3.3 Mathematical Model for plugflow froth behaviour

3.4 Scope of Experimentation

3.5 Discussion of Results

3.6 Summary and Conclusions

CHAPTER 4 RESIDENCE TIME DISTRIBUTIONS IN FLOTATION FROTHS : INTRODUCTION  
AND THEORETICAL DEVELOPMENTS.

4.1 Introduction

4.2 Theoretical Determination of Residence Time Distributions

4.2.1 Two-dimensional Streamline Behaviour of Flotation Froths

4.2.1.1 Solution of the Laplace Equation

4.2.1.2 Determination of Streamlines

4.2.1.3 Air and Particle Residence Times

4.2.1.4 Discussion of Simulations

4.2.2 One-dimensional flow approximation: a tractable model

4.2.2.1 Variation of froth velocity with distance from the back  
of the cell

4.2.2.2 Froth Residence Time Distribution

4.2.2.3 Model for Mass Flowrate of Concentrate Components

4.2.2.4 Comparison with other Simple Models of Froth Phase RTD

4.2.2.5 Comparison of Model 2 with the 2-dimensional streamline  
model

CHAPTER 5 RESIDENCE TIME DISTRIBUTION IN FLOTATION FROTHS: EXPERIMENTAL  
DETERMINATIONS

5.1 Development of Apparatus and Technique

5.1.1 Production of a Uniform Tracer Distribution at the Base of  
the Froth

5.1.2 Measurement of RTD of Tracer Particles in the Liquid Phase

5.1.3 Measurement of the Residence Time of Particles on the Overflow  
Weir

5.1.4 Measurement of the Cell Residence Time Distribution

5.1.5 Measurement of the Velocity of the Surface of the Froth

5.2 Experimental Design and Analysis of Data

5.2.1 Estimation of Parameters in Model 2

5.2.1.2 Estimation of Parameters for  $E_c(\tau)$

5.2.2 Testing of Hypotheses Concerning the Model

5.2.3 Confidence Limits on the Parameters

5.2.4 Dependence of RTD Parameters on Control Variables

5.2.5 Estimation of Froth Stability from Froth Velocity Measurements

5.2.6 Conclusion

CHAPTER 6 DESIGN OF FROTH REMOVAL METHODS

- 6.1 Introduction
- 6.2 Use of the froth RTD model for rationalising real flotation data
- 6.3 Effect of changes in the RTD Model parameters on flotation performance
  - 6.3.1 Simulation of grade-recovery curves
  - 6.3.2 Implications for design and control
- 6.4 Effect of changes in froth removal method on concentrate RTD
- 6.5 Experimental tests of various froth removal methods
  - 6.5.1 Tests on Prieska Ore
  - 6.5.2 Tests on Gasifier Cinder from African Explosives and Chemical Industries' Ammonia Plant

CHAPTER 7 CONCLUSIONS

REFERENCES

APPENDIX A DISCUSSION OF PAPER BY GREAVES AND ALLAN ON TRANSIENT RESPONSE OF CONCENTRATE FLOWRATE TO CHANGES IN SLURRY FEED RATE.

APPENDIX B USE OF THE MODEL OF HARRIS AND RIMMER FOR ESTIMATING FROTH VOLUME.

APPENDIX C CONCENTRATION OF COMPONENTS IN THE FROTH PHASE: PLUG FLOW MODEL

APPENDIX D CONFIDENCE LIMITS FOR THE PARAMETERS  $\alpha$  AND  $\delta$  IN THE FROTH RESIDENCE TIME DISTRIBUTION

NOMENCLATURE

LIST OF TABLES

TABLE 2.1	Results of Conditioning Tests.
TABLE 4.1	Results of simulations using the solution of the Laplace Equation.
TABLE 4.2	Comparison of Models for Froth Phase RTD.
TABLE 4.3	Comparison of Model 2 and Streamline Model.
TABLE 5.1	Attempts to obtain a uniform distribution of tracer particles at the base of the froth.
TABLE 5.2	Data for Residence Time Distribution Measurements.
TABLE 5.3	Parameters and Sum of Squares for Hypotheses $H_1$ , $H_2$ and $H_3$ (data: Series A, experiments 1-17).
TABLE 5.4	Comparison of methods for estimating froth RTD parameters.
TABLE 6.1	Results of hypothesis testing of the froth model on Dunne's data.
TABLE 6.2	Residence Time Distribution parameters as affected by presence or absence of flow modifier.
TABLE A.1	Analysis of data from Greaves and Allan's paper.
TABLE B.1	Values of parameters and control variables used in simulations.



LIST OF FIGURES

- Figure 1.1 Schematic representation of the flotation process for the development of a two-phase model.
- Figure 2.1 Deep Flotation Cell used for both batch and continuous tests. Plan view shows froth baffles inserted.
- Figure 2.2 View of cell showing concentrate launder and "wig-wag" sampler.
- Figure 2.3 Flow diagram of mill circuit for grinding, conditioning and floating the ore.
- Figure 3.1 Variation of froth grades and density with height, illustrating general trends and reproducibility (continuous bulk sulphide floats with baffles in the froth phase; no froth removal).
- Figure 3.2 Simulation of froth behaviour using a simple mathematical model.
- Figure 3.3 Variation of froth properties with height showing inflection in pyrite grade curve. (Batch float with pyrite depressed under "steady state" conditions. No baffles in the froth phase).
- Figure 3.4 Simulation of froth behaviour involving detachment of pyrite particles in the froth phase.
- Figure 3.5 Effect of froth removal on froth grades (continuous bulk sulphide float with no baffles in the froth phase).
- Figure 3.6 Effect of froth removal on froth grades (Batch bulk sulphide float with no baffles in the froth phase).
- Figure 3.7 Variation of froth grade profiles with gas rate (Continuous bulk float with baffles in the froth phase, with and without froth removal).
- Figure 3.8 Effect of baffles designed to reduce mixing in the froth phase on pyrite and gangue grades (Continuous bulk float, concentrate removal rate approximately 10% of feed rate).
- Figure 3.9 Effect of position in froth on variation of mineral grades with particle size (Batch sulphide float).

- Figure 4.1                    Boundary conditions for the solution of the Laplace equation for streamline flow of froth.
- Figures 4.2.1 to 4.2.15        Results of simulations of froth behaviour using the solution of the Laplace equation. In each diagram the effect of varying the parameters given in Table 4.1 on bubble streamlines, various velocity profiles and residence times is shown.
- Figure 4.3                    Variation of residence time ratio  $\delta$  with froth stability  $\alpha$  (obtained from the solution of the Laplace equation).
- Figure 4.4                    Volume balance across a differential element in the froth phase.
- Figure 5.1                    Arrangement used for injecting tracer into impeller region, and for achieving a uniform distribution of tracer at the pulp/froth interface.
- Figure 5.2                    Division of pulp surface into 9 segments for measurement of distribution of tracer in the pulp/froth interface.
- Figure 5.3                    Device used for scraping tracer particles from the surface of the cell while measuring the RTD of these particles in the pulp.
- Figure 5.4                    Plan View showing how the device illustrated in Figure 5.3 was mounted on the cell.
- Figure 5.5                    Circuit used for timing pulp phase RTD measurements.
- Figure 5.6                    Recorder output and data obtained from pulp phase RTD measurements.
- Figure 5.7                    Variation of  $\alpha$  with gas rate for pulp phase RTD.
- Figure 5.8                    Variation of concentrate weir residence time and its inverse with water flowrate.
- Figure 5.9                    Measurement of froth velocity by recording photographically the co-ordinates of blackened polystyrene particles at a sequence of time intervals.
- Figure 5.10.1                Points at which froth RTD measurements were performed. (Series A, Table 5.2).
- Figure 5.10.2                Points at which froth RTD measurements were performed (Series B, Table 5.2)

- Figure 5.11      Variation of froth removal efficiency  $\epsilon$  with gas flux, froth height and frother concentration.
- Figure 5.12      Froth breakage parameter  $g_2$  vs gas flux, as a function of froth height. Lack of correlation between  $g_2$ ,  $h$  and  $g$  is evident. (Data: Series A, Experiments 1-17).
- Figure 5.13      Ratio of  $\alpha(H_1)$  to  $\alpha(H_2)$  vs  $g_2$ , demonstrating high correlation between the two estimates of  $\alpha$ .
- Figures 5.14.1 and 5.14.2      Effect of gas rate and froth height on concentrate residence time distribution.
- Figure 5.14.3      Effect of frother concentration on concentrate residence time distribution.
- Figure 5.15      Standard Deviation of RTD cumulative distribution at  $\tau_{\min} = \delta h/g_0$ .
- Figure 5.16      Standard Deviation of Cumulative RTD at  $\tau_{\text{av}} = h/\alpha g_0$
- Figure 5.17      Variation of parameter  $\beta_\alpha$  in equation 5.8 with froth height.
- Figure 5.18      Gas flux at zero concentrate flowrate ( $g_0^0$ ) as a function of froth height.
- Figure 5.19      Intercept  $\hat{g}$  of gas flux at zero concentrate flowrate and slope of  $\beta_\alpha$  vs  $h$  as a function of (frother concentration)<sup>-1</sup>
- Figure 5.20      Froth stability  $\alpha$  as a function of gas flux, froth height and frother concentration.
- Figures 5.21.1 to 5.21.7      Froth Velocity data and Laplace Equation solution for Experiments 41-47.
- Figure 5.22      Comparison of froth stability values estimated from froth velocity measurements with values estimated from froth RTD measurements.
- Figure 5.23      Comparison of effective cell length values estimated from froth velocity measurements with values estimated from froth RTD measurements.
- Figure 6.1      Average froth stability calculated from froth rise time measurements, and estimated by regression on froth flow rates.

- Figure 6.2 Comparison of recoveries produced by the model (using equation (6.1) to evaluate the froth stability) with recoveries obtained experimentally.
- Figure 6.3 Effect of changes in parameters on grade-recovery curves (base case parameters are:  $\alpha=0,5$   $\delta=0,5$   $k_{f1}=0,08$   $k_{f2}=0,5$   $k_{f3}=0,6$ ).
- Figure 6.4 Grade-recovery curves using expressions for  $\alpha$  and  $\epsilon$  determined in Chapter 5: effect of variations in froth height  $h$  and frother concentration  $FC$  (base case:  $h=2$  cm and  $FC=10 \times 10^{-6}$  g/cc).
- Figure 6.5 Grade-recovery curves using expressions for  $\alpha$  and  $\epsilon$  determined in Section 6.2 (Dunne's data): effect of variations in froth height  $h$  and frother concentration  $FC$ . (base case:  $h=2$  cm,  $FC=15$ g/ton).
- Figure 6.6 The froth crowder and two versions of flow modifier discussed in (i) section 6.3.2 and (ii) section 6.4
- Figure 6.7.1 Effect of flow modifier on froth phase residence time to 6.7.3 distribution.
- Figure 6.8 Effect of froth crowder on froth phase residence time distribution.
- Figure 6.9 Effect of flow modifier on grade-recovery curves for components of the Prieska ore.
- Figure 6.10.1 Effect of flow modifier on grades within particle size classes for chalcopyrite and sphalerite (Prieska ore).
- Figure 6.10.2 Effect of flow modifier on grades within particle size classes for pyrite and gangue. (Prieska ore).
- Figure 6.11 Grade-recovery curves for flotation of gasifier cinder.
- Figure 6.12 Variation of various experimental parameters with particle size for experiments 3,16A and 18 (experiments with gasifier cinder).
- Figure B-1 Variation of air-free froth volume  $V_f$  with operating parameters feed rate, feed concentration and froth removal rate.
- Figure D-1 Variation of residence time distribution  $F(\tau)$  and its derivatives with  $\tau$  for  $g_o=0,5$   $h=5$ cm  $\delta=0,5$  and  $\alpha=0,5$

## CHAPTER ONE

### The Froth Phase : The Cinderella of Flotation Research?

#### 1.1 Introduction

The *thesis* of this work may be summarised in the following points:

- (i) In all cases the performance of the flotation process (as measured by grade and recovery) is affected by processes that occur in the froth phase;
- (ii) In some cases (where pulp phase processes operate at a relatively high efficiency) froth phase processes assume a predominating or rate-controlling role.
- (iii) In most cases, but particularly for the latter, substantial improvements can be obtained in cell performance through design and control actions (based on a thorough understanding of froth phase processes) which seek to improve the efficiency of the froth removal process.

There is of course nothing new in the above - the need for a deeper understanding of what occurs in the froth phase has been expressed by many workers especially in the last decade; however there is a dearth in the literature of reports on how froth removal efficiency has actually been improved, and demonstrably inefficient methods of froth removal (eg the conventional paddle) are still in wide, unquestioned use.

In the following pages an attempt is made to identify some of the processes occurring in the froth phase, to assess their function, and to evaluate various methods (some conventional, some as yet only sporadically mentioned in the literature and one original) of taking advantage of these processes with a view to improving the efficiency of the froth removal process.

One method in particular has been found to be particularly effective in improving both the grade and recovery of a mixed sulphide float, and its simplicity and ease of installation make its investigation on plant level an easy and attractive option.

## 1.2 Literature Survey

While the importance of the part played by the froth phase was recognised early in the history of flotation research, comparatively little work has been devoted to investigating it. This is due probably to

- (i) the large volume of research effort that undeniably important aspects such as chemical conditioning, impeller design, particle-bubble interactions etc. have attracted and held to themselves and
- (ii) the extreme complexity of the processes occurring in the froth phase which reveals itself to any who have the temerity to attempt an analysis at any level below the macrokinetic level defined by Flint (1973) i.e. kinetics which relate an observable rate of concentrate production to macroscopic parameters such as tailings concentration or residence time. Even Mika and Fuerstenau (1969) in their ambitious attempt to formulate a microscopic model of the flotation process were forced to make an unrealistic and essentially macroscopic assumption concerning the behaviour of the froth phase (i.e. that it is perfectly mixed) and came to the conclusion that "the absence of a detailed representation of the froth subprocesses frustrates the attempt to arrive at a complete microscopic model of the overall flotation process."

Before reviewing work that has been done on the froth phase a few comments should be made about the work that has been done on the process as a whole and on the pulp phase. Woodburn (1976) has reviewed the wide range of models which are available for describing at least the macrokinetic behaviour of the particle-bubble aggregate which exist in the pulp phase.

Most of these are based on the first order chemical kinetic analogy applied to a perfectly mixed cell. Models involving other than first order are not advocated widely now, and Ball and Fuerstenau (1974) are of the opinion that the controversy concerning the order of the rate equation has been settled in favour of the first order option. The models range from the purely macrokinetic level where rate of flotation is proportional to tailings concentration, to the more detailed representations (e.g. King, et al., 1970) where gas rate, particle size and composition, bubble loading and froth effects are taken into account. Further development by Harris et al (1975) of a recycle model for the pulp phase has given a good description of observed departures from ideal mixing in the pulp phase. It seems that an investigator will always be able to find a model of the pulp phase process which is appropriate to his needs.

On the microkinetic level much still remains to be understood and, for example, the controversy concerning the mechanism of particle-bubble attachment still continues. The lack of detailed understanding on this level is part of the reason why for example so many different designs of impeller are on the market, all claiming superior performance - supported by operating data but based on different and sometimes opposing understandings of what is occurring in the cell. No wonder "strength of personality of manufacturer's representatives" and "operator prejudice" are listed among the reasons why a machine may be selected for a particular duty. (Flint - op cit.)!

The first attempt to incorporate the effect of froth processes into a kinetic framework is that of Bushell (1962). He assumed that the rate of return of particles from the froth to the pulp was proportional (with prop. factor  $k_f$ ) to the rate of entry of particles into the froth phase, the latter rate being obtained from the conventional chemical reaction rate analogy model with rate constant  $k_p$ . This model reduces to the same form as the latter model with a modified rate constant  $k' = k_p(1-k_f)$  and hence constitutes no significant advance on previous models. However in the same year Harris and Arbiter proposed a model which has been the basis for most subsequent attempts to incorporate descriptions of the froth phase in flotation modelling. They assume that each of the froth and pulp phases is perfectly mixed, and that particle transfer into and return from the froth are first order processes. (see Figure 1.1)

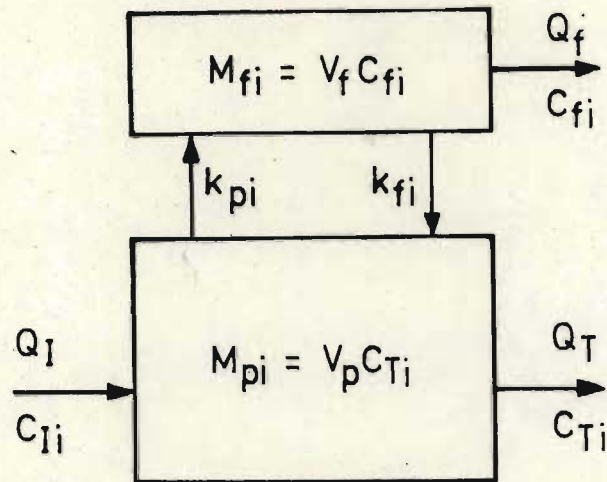


Figure 1.1 Schematic representation of the flotation process for the development of the two-phase model.

Thus

rate of flotation

$$Q_f C_{fi} = k_{pi} V_p C_{Ti} - k_{fi} V_f C_{fi}$$

The main difficulty raised by this model (aside from the invalid assumption of a perfectly mixed froth phase) is the definition of  $V_f$  and  $Q_f$ . No methods have thus far been developed for measuring  $Q_f$  as volume of froth (air + slurry) per unit time, and hence  $V_f$  and  $Q_f$  have been defined on an air-free basis. The problem then reduces to the determination of  $V_f$ ; and most workers thus far reported have assumed that  $V_f$  is invariant over the range of independent variables considered, and hence have lumped it with the froth return rate constant  $k_f' = k_f V_f$ . Greaves and Allen (1974) are the one exception thus far encountered in the literature; they estimate  $V_f$  by assuming that the residence times of air and other components in the froth are identical, and obtain

$$V_f = \frac{\text{Vol of froth zone}}{1 + G/Q_f}$$

Their basic assumption is challenged by the results given later in this work, and by their own results as shown in Appendix A.



Had they taken cognisance of the fact that the air-free fraction of the froth has a significantly larger residence time than that of the air because

- (i) the air-free fraction rises at a velocity lower than that of the air bubbles in the froth and
- (ii) some of the air escapes through the top of the froth due to bubble breakage

they would have obtained substantially improved correlations between experiment and theory

Thus in general

$$V_f = \frac{\text{Vol of froth phase}}{1 + \bar{\alpha}G/Q_c}$$

where  $\bar{\alpha} < 1,0$  is a function of froth stability and relative rates of drainage (and hence of bubble size, liquid viscosity, bubble loading etc.) It is clear that  $V_f$  is unlikely to remain constant under varying operating conditions, in spite of the fact that the ratio  $G/Q_c$  may not vary over a wide range since in many cases  $Q_c$  is proportional to  $G$ . As shown in Appendix B, if the behaviour of the water can be modelled on the same basis as that of the solid, then  $V_f$  can be obtained as a function of operating variables eg. feed rate,  $Q_I$  feed concentration  $C_{Ii}$  and froth removal rate  $Q_I$  (see Figure B.1).

The model has however been used to interpret continuous flotation data - most dramatically in a paper by Harris, Jowett and Ghosh (1963) where coal-flotation results for a wide range of feed rates and feed concentrations were analyzed. They assumed that the froth return rate constant  $k_f$  was proportional to  $C_I$  which allowed them to obtain an excellent straight line correlation with the equation

$$\frac{C_T}{C_I C_f} = \frac{k''_f}{k'_p} + \frac{Q_f}{k'_p C_I}$$

where  $k'_f$  and  $k'_p$  are defined by

$$k_f = k'_f V_f C_I$$

$$k_p = k'_p V_p$$

$V_f$  is assumed constant. It is surprising that the authors do not attempt to improve on their assumption concerning  $k_f$  i.e.  $k_f$  proportional to  $C_I$  e.g., had they postulated that  $V_f$  is proportional to  $C_I$ , they would have obtained the same correlation while avoiding the need to justify their assumption concerning the dependence of  $k_f$  on  $C_I$ . It should be pointed out that the authors do not claim that their results can be interpreted as a justification of their model assumptions; the equation that results from them, however, has shown its value in correlating their data. This attitude to the model has not changed; Harris (1978) states "it is the generality of the equation which succeeds, not the model from which it is derived ... Although the advantage of a general equation is clear, there may be an important disadvantage which should be noted: it is that the information gained from steady-state studies may not be directly applicable to the transient state."\* This latter point is borne out by the studies of dynamic froth behaviour conducted by Greaves and Allen (op cit.) and Sadler (1973).

A number of authors (Harris and Rimmer 1966; Harris and Chakravarti 1970; Ball and Fuerstenau 1970 and 1974) have used the model to simulate both batch and continuous operations, and have extended it to include distribution of the various species over the pulp rate constant,  $k_p$ . The main difficulty is the estimation of the froth return rate constant and, as Ball and Fuerstenau point out, until sufficiently accurate estimates can be found, the utility of the model for gaining insight into macroscopic flotation kinetics is limited.

On a more practical level, the effect of the froth phase on the recovery of the various components in the pulp has been measured and described by various authors. This applies particularly to hydrophilic gangue particles.

---

\* For further discussion see Section 4.2.2.4

Jowett (1966) was the first to highlight the importance of an entrainment mechanism for the recovery of such particles and propose a kinetic description of it. In most other work the recovery of gangue was modelled on the same basis as the recovery of valuable minerals, the only difference being the magnitude of the rate constants involved. In his model the rate of recovery of gangue is proportional to the rate of recovery of water and the concentration of gangue in the pulp, the proportionality constant being a function of gangue size distribution, since the hydraulic classification that occurs in the froth will be affected by particle diameter. An explicit form for the effect of particle size was first proposed by Johnson and Lynch (1972), and developed further by them and their co-workers (Lynch et al, 1974; Johnson et al, 1972). They defined the classification function

$$CF_i = \frac{\text{solid/water ratio for free gangue in concentrate for size } i}{\text{solid/water ratio for free gangue in pulp for size } i}$$

and showed (Lynch et al, op cit.) that it was constant for a particular gangue component over the normal range of water recoveries encountered in plant operation. Once the  $CF_i$  have been determined for the full range of particle sizes, the recovery of gangue is given by

$$R_g = Q_w \sum CF_i C_{Ti}$$

and  $R_g$  can be controlled by varying control variables which affect  $Q_w$  i.e. frother concentration, froth height and gas rate.

The fact that  $Q_w$  also affects the recovery of valuables and sulphide gangue (though to a far smaller extent) is recognised in their analysis.

Bisshop and White (1974) measured  $CF_i$  for a wide range of particle densities, pulp densities and water recovery rates, and attempted to elucidate the dependence of  $CF_i$  on these variables. Assuming that air-free froth volume  $V_f$  is proportional to froth height  $h$  with proportionality constant  $r_0$  they define froth residence time as

$$\tau = V_f/Q_w = r_0 h/Q_w$$

They then make the assumption that concentrate flowrate is given by

$$\dot{M}_i = k_{ci} \left(\frac{1}{\tau}\right) M_i$$

where  $k_{ci}$  is a proportionality constant and  $M_i$  is the mass of gangue in the froth. Using Harris and Rimmer's model they show that

$$CF_i = \frac{1 + (k_{fw}/k_{cw}) \tau}{1 + (k_{fi}/k_{ci}) \tau}$$

The introduction of the parameters  $k_{ci}$  and  $k_{cw}$  is unnecessary, however, since for the dilute froths they obtained these parameters have values very close to unity. Thus

$$CF_i = \frac{1 + k_{fw} \tau}{1 + k_{fi} \tau}$$

If their definition for  $\tau$  is substituted into this expression we find

$$CF_i = \frac{1 + k'_{fw} h / Q_w}{1 + k'_{fi} h / Q_w}$$

which is a much clearer statement of the relationship between  $CF_i$  and the control variables  $h$  and (through manipulation of the gas rate)  $Q_w$ . The introduction of the residence time is attractive but is not essential for model development. Together with other definitions (e.g. that of Greaves and Allen) it does not yield good estimates of the true froth residence times, being subject to large errors depending upon the stability of the froth. (See Section 5.2.6)

They find that  $k_{fw}$  is a function of solids density (their justification of this is obscure; why should the drainage rate of water depend upon solids density?) while  $k_{fi}$  is an exponential function of the hydraulic settling diameter.

In spite of these reservations good agreement between predicted and experimental recovery of gangue is obtained; individual  $CF_i$  values are poorly predicted, however.

Woodburn (1976) in his comprehensive review of flotation kinetics has developed a model for batch flotation involving a froth residence time distribution. Unfortunately the solution is complex even for the simplest distribution function. No analysis of experimental data is reported. Because of the large number of variables in batch flotation it seems that little reliable information can be gained about froth behaviour from batch tests.

Watson and Grainger-Allen (1974) have pioneered a technique which circumvents this objection while avoiding the difficulties associated with continuous operation. In their specially designed "equilibrium cell" froth is not removed, but allowed to build up above the pulp phase. Once steady state is achieved (at an experimentally determined time where both froth height and mass of components in the froth is constant) a slide is interposed between froth and pulp and both are removed for assay. They investigated the effect of varying reagent levels, pH, airflow rate and proportions of feed minerals, and their results show that froth stability (defined as bulk froth volume per unit gas rate) varied over wide ranges which are linked to the levels of the experimental variables. In particular it was found that fine gangue particles play a significant role in stabilising the froth, a result which has been supported by other work (Gaudin 1932, Livshits and Dudenkov 1960). Flint (1974) in a concurrent research programme used the same technique to estimate some of the parameters in his model of the flotation process. He showed that it was possible to determine which of the processes occurring in the flotation process (e.g. attachment of particles to bubbles, removal into froth phase, or removal of froth from the cell) is rate controlling. In the case where froth removal is the rate-controlling step (as is the case for highly floatable minerals) the modelling of pulp phase processes becomes relatively unimportant and the kinetics of the system depend on the rate at which froth is removed from the cell, and any model of the process which fails to recognise this will be inadequate.

Cutting and Devenish (1975) have continued the work of Watson and Grainger-Allen with a modified "equilibrium cell" in which the froth is partitioned into four sections with the addition of three more horizontal slides. This allowed them to investigate the variation of froth properties with height and by using a semi-empirical approach to develop a model of froth behaviour which might be used in the simulation of complex plant behaviour. This "steady-state batch technique" - to use Flint's term - is discussed further in Chapter 3.

Klassen and Makrousov (1959) report measurements of concentration gradients in the froth phase that were done on industrial plants. The upper layers of froth contained less gangue material but also less large mineral particles, because of the inability of well-drained froths to support such particles. Effects of various types of frother, bubble size and particle size and shape on froth properties are discussed in detail and the importance of enhancing (e.g. by froth height control and by froth spraying) the "secondary enrichment" which occurs in the froth is highlighted.

Recognition of the importance of froth phase processes has led to the modification of conventional flotation cells, and to a number of innovative designs. In the pneumomechanical cells discussed by Zakhvatkin (1970) impellers are designed so that agitation is limited to a particular zone in the cell and the pulp below the froth is relatively quiescent. This "separation zone" minimises the amount of entrainment of gangue particles into the froth. In addition to this, the cell banks have removable weirs between cells and adjustable overflow weirs to allow channelling of froth flow counter-current to the direction of pulp flow, and the forward-sloping back wall of the cell ensures that stagnant regions do not occur near the back of the cell.

Klassen, et. al. (1956) and later Millar (1969) are among a number of authors who discuss the effect of froth sprinkling on coal flotation efficiency. Klassen showed that froth sprinkling washes loosely held gangue particles from the froth and compensates for the water lost in the upper froth layers, increasing froth stability. Thus both grade and recovery can be improved; Miller showed that single-stage flotation coupled with froth sprinkling produced a product comparable to that obtained in a conventional rougher/cleaner combination. Substantial savings in flotation volume (35%) were found to be possible.

Lukina and Bogatikov (1971) tested an idea proposed by Malinovski (undated), whereby adhesion drums are mounted near the overflow weir. The paddles are used to feed the froth onto the slowly rotating adhesion drums. The well-drained froth product is removed from the drum by a knife assembly. This resulted in dramatic improvements in grade on a molybdenum float (from 9 to 14%) at comparable or improved recoveries.

The column flotation method of Boutin and Wheeler (1969) is a radical departure from conventional practice. Bubbles rise through a 9-metre column countercurrent to the flotation pulp, which enters the column about 3 m. below the top. Wash water is added at the top of the column where the concentrate is removed. These authors and later Matthieu (1972) report comparable grade and recovery characteristics for the flotation of fine material when compared with conventional methods, at greatly reduced pulp retention time, power and frother consumption. Coarse particles, due to their large settling velocity, experience very low retention times and are perhaps best floated by conventional means.

Malinovskii (1970) describes the development of Rebinder's (1960) "froth separation" method, where pulp is distributed onto the surface of the froth phase from above. Due to the virtual absence of disruptive forces large particles (of 1-2 mm) are recovered. The high concentration of hydrophobic bubble surfaces results in greatly reduced pulp retention times; power consumption is also reduced several-fold.

In the cylindrical Maxwell cell the unique design of the froth removal system (a circular annulus mounted in the froth phase so that no froth element has a great distance to travel before being removed in the concentrate stream) results in a large weir length to cell surface area ratio and hence reduced removal rate per meter of weir length. Thus the high grades associated with low froth removal rates in conventional cells are obtained in the Maxwell cell at substantially higher overall froth removal rates.

In spite of the wide range of flotation methods available, the conventional cell is still the most commonly used unit in flotation plants. They enjoy the testimony of experience and the inertia of conservatism, and will only be replaced or improved upon by innovations of unquestioned superiority.

As Flint (1973) points out, a comprehensive understanding of the microkinetic subprocesses will provide a sound basis for the development of such innovations; it is hoped that this work makes some contribution towards such an understanding.



## CHAPTER TWO

### Preparation for Experimentation : Equipment, Slurry Production and Sample Analysis.

#### 2.1 Introduction

In preliminary investigations attempts were made on a large  $1,0 \text{ m}^3$  Denver cell to measure the rate at which solids were transferred into the froth from the pulp. This was done by trapping all bubbles that would have entered the froth over a small crosssectional area in a device similar to that used by Maksimov and Khainman(1965). The air was continually removed from the device at a measured rate, and all solids that entered the device were prevented, as far as possible, from leaving it. Thus a measure of the load of solid particles per volume of air was obtained. The results were however difficult to interpret because of suspected entrainment into the device and the wide variation of gas flux across the froth-pulp interface, and are not considered worthy of presentation. However these experiments did reveal the distributed nature of the behaviour of the froth in a conventional flotation cell, and motivated the construction of a smaller cell which would produce a more uniform froth, allow closer examination of its behaviour, eliminate the presence of the impeller column in the froth phase and allow easier and less expensive experimentation because of the reduced scale of operation. In particular the new cell would have transparent sides and would be designed to allow the production of froths with depth varying over a wide range, so that detailed examinations of froth properties as a function of height above the pulp might be made.

The feed to the cell was produced by the grinding circuit described below. The mismatch between the minimum production rate that the grinding circuit could produce and the range of flowrates required in the flotation cell, together with difficulties associated with the inevitably variable nature of the slurry produced by the grinding circuit and with continuous

conditioning of this slurry made it almost impossible to run the grinding circuit and the flotation experiments at the same time. For this reason a large volume of slurry was produced before flotation experiments began and this was batch conditioned before being fed to the cell. This allowed adequate control of feed rate, density and composition, but suffered from the disadvantage of imperfect mixing in the feed tank, with the result that feed particle size distribution and density changed slowly as the run progressed. The effect of time on the floatability of the ore was found to be of secondary importance. Because of the slowly changing nature of the feed, it was only possible to compare experiments that had been performed within intervals which were small compared with the duration of the run. These disadvantages were considered far preferable to those associated with simultaneous production, conditioning and flotation of slurry.

## 2.2 Design and Construction of Flotation Cell.

The cell shown in Figure 2.1 and 2.2 is similar to the "batch steady state cell" of various worker's mentioned in Chapter 1. Various requirements were met by design parameters in the following way:

- (i) To permit visual observation of the froth structure and behaviour, the cell was constructed from 6 mm thick perspex.
- (ii) To avoid the presence of the impeller shaft in the froth phase the impeller was driven by a shaft entering through the base of the cell. The seal was a tightly-fitting neoprene ring which was held to the base of the cell with a brass collar and was replaced when necessary. A stuffing box was mounted outside the cell and packing designed for abrasive slurries was used to fill it. The bearings were mounted well below the cell and additional protection was provided by a spray deflector attached to the shaft above them. The use of two pulley blocks consisting of 3 and 4 pulleys respectively allowed the choice of a number of impeller speeds to be made. The impeller consists of a 10 cm stainless steel disc with eight 1,3 x 3,5 cm. ribs welded in symmetrically spaced radial positions.
- (iii) Air was introduced to the cell via a fine canvas ring-shaped sparger mounted on the base of the cell concentric with the

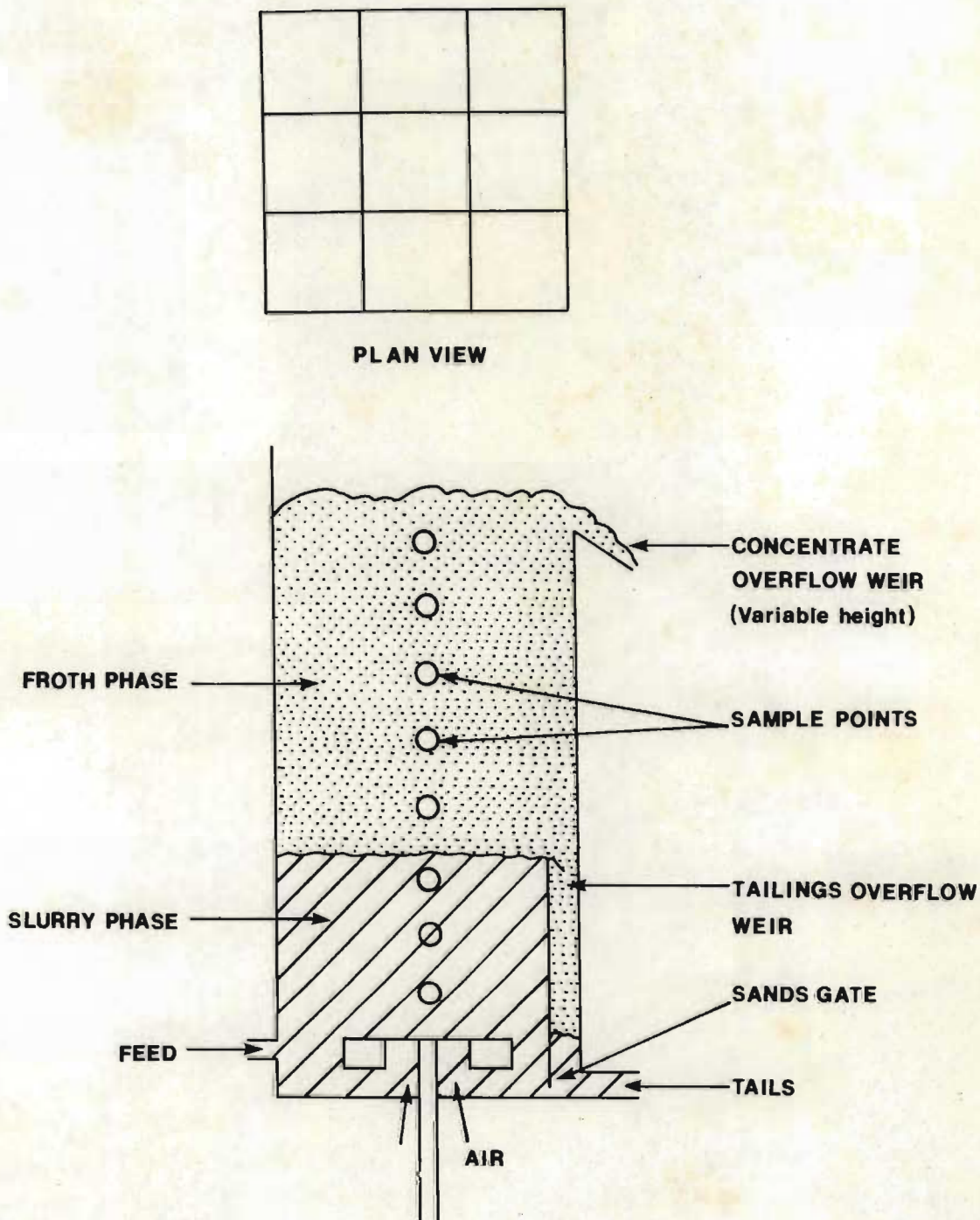


Figure 2.1 Deep Flotation Cell used for both batch and continuous tests. Plan view shows froth baffles inserted.



Figure 2.2 View of cell showing concentrate launder and "wig-wag" sampler.

shaft axis. Control of the air rate was achieved with an air pressure regulator supplying air at a constant pressure to a gate-valve/ rotameter combination.

- (iv) The cell was 20 cm. square and a small tailings box mounted inside the cell allowed a pulp depth of 18 cm (and resulted in a volume of 7,2 l.). The sides of the cell were 60 cm high and removable slats at the front of the cell allowed the choice of froth heights between 2 and 35 cm in 2 cm steps. Feed pulp was introduced through a hole in the back of the cell.
- (v) To minimise rotation of the slurry 12 baffles were mounted in radial positions around the impeller. Further modifications aimed at improving the distribution of gas flux across the froth/slurry interface are described in Chapter 5.

### 2.3 Production and Conditioning of Feed Slurry

The ore and methods used for crushing, grinding and conditioning it are described.

#### 2.3.1 Description of Ore Used.

A detailed mineralogical description of the ore is given by de Kok (1972) and is briefly summarised here. The three main minerals are pyrite, chalcopyrite and sphalerite. Small amounts of silver, gold, galena and various metal sulphides occur as well. The gangue consists of a wide range of minerals, including quartz, muscovite, biotite, calcite, chlorite and talc (many others are mentioned by de Kok). The pyrite occurs in a number of forms which present no problems in obtaining complete liberation, except that in one form sphalerite and pyrite are finely intergrown. Chalcopyrite and sphalerite are contaminated with pyrite to a limited degree. A small percentage of sphalerite has been shown to contain up to 10% Fe. It should be noted that many of the gangue minerals contain varying amounts of Fe as well.

Great difficulty was experienced in developing suitable reagent recipes. The methods used in this work are described in a later section. Grinding to 65% - 75 $\mu$  was considered the optimum from an economic point of view.

The average concentration of major minerals in the ore used in this work (part of a 40 ton batch) were: pyrite (45%), chalcopyrite (3,5%) sphalerite(2,7%) and the balance (48,8%) is gangue.

### 2.3.2 Grinding of the Ore

Batch grinding was used to produce slurry for the development of conditioning recipes and for some of the experiments described in Chapter 3. The balance was produced continuously.

#### 2.3.2.1 Batch Grinding

All the ore used in batch tests was first crushed to -3mm in a 3" jaw crusher. To produce feed for conditioning batch tests, six kg of this ore was wet ground in a 30 x 30 cm laboratory ball mill with a load of 30 mm balls for 30 minutes. The balls were cleaned by grinding silica for 10 minutes before grinding the ore. The ground sample was allowed to stand overnight to allow short-term changes in the surface properties of the particles to dissipate themselves and the sample was then split into 8 equal samples using a riffler and floated sequentially in a 1 liter Denver lab cell.

Feed for batch tests in the experimental cell was produced in a 20 x 20 cm ball mill with a 12 kg load of balls under wet grinding conditions. Since the whole batch of slurry was used in the subsequent test, it was not necessary to allow it to stand for any length of time, and it was conditioned and floated immediately.

Grinding under the above conditions had been shown by Dunne and Dawson (1975) to produce a product with 60% less than 75 $\mu$  which is close to the specification applied at the Prieska Flotation Plant.

### 2.3.2.2 Continuous Operation

The flow diagram for feed slurry production is shown in Figure 2.3. The 40 ton crushed (- 13,5mm) and blended ore sample was stored in a large storage bin and fed batchwise to a 500 kg capacity hopper as shown. A conveyor belt transferred the feed at a controlled rate to a conventional ball mill (0,90 m x 1,2 m) circuit. The mill load consisted of 900 kg of balls ranging from 70 down to 30 mm in proportions required to simulate a steady-state ball load with additions of 70 mm balls. The computer control of the circuit is described in detail by Hulbert (1977) whose assistance in producing the slurry is acknowledged. A brief description of the circuit suffices. Water was added together with the feed solids to the mill inlet at a steady rate. The mill discharge flowed into a sump where the slurry density (monitored by a  $\gamma$  gauge) was controlled to a set point by water addition. A variable speed pump producing feed for a 15 cm diameter cyclone (12 mm spigot) controlled the level in the sump. The cyclone overflow flowed into a surge box and gravitated to the flotation feed conditioning tank.

### 2.3.3 Feed to Flotation Circuit

The product from the mill circuit was allowed to flow through a 2 mm screen before entering the conditioning tank to ensure that no oversize due to possible spigot blockages entered the flotation feed. The tank was baffled and agitated by a 3,7 kW stirrer with inclined blades which produced satisfactory agitation when the tank was full, but proved too powerful when the level of slurry in the cell dropped below the 40% mark. At this point the impeller began to draw air and produced a thick layer of heavily laden froth on the surface of the pulp, resulting in removal and possible oxidation of floatable particles. The situation was considerably improved by lowering a heavy metal disc onto the impeller when this began to occur. This ensured that all slurry leaving the impeller zone did so in a radial direction, resulting in substantially less agitation and minimal aeration of the pulp.

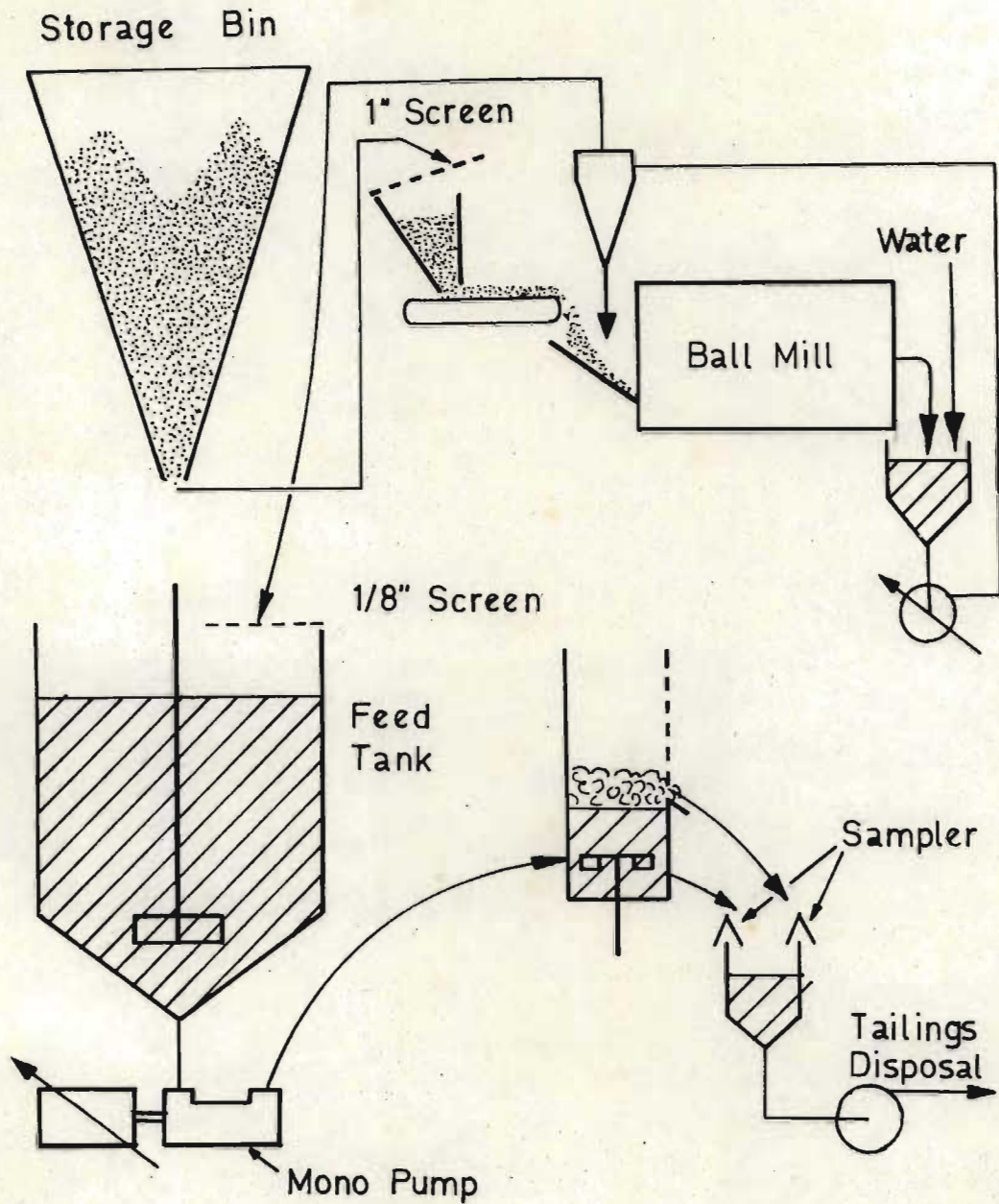


Figure 2.3 Flow diagram of mill circuit for grinding, conditioning and floating the ore.



Flotation feed was withdrawn from a pipe set in the base of the tank with its inlet below the impeller. A monopump driven by a motor with Kopp variable speed coupling was used to control the feed rate to the cell. Since the monopump is a positive displacement pump, excellent control of feed rate was obtained, and no decrease in performance due to impeller wear was measured. Maximum feedrate obtainable was 15 l/min. An occasional pipe blockage was experienced so a simple transistorised warning system connected to electrodes mounted in the feed stream near the cell was designed. Whenever the flow of slurry to the cell ceased, this was immediately detected and an alarm bell called attention to the problem.

The concentrate and tailings streams drained into a sump below the sampling mechanism as shown in Figure 2.2, and was pumped away to a large tailings disposal bin.

#### 2.3.4. Conditioning of the Feed Slurry

Most of the tests reported were a simple bulk float of the chalcopyrite, sphalerite and pyrite in the feed. A few experiments were done with pyrite depressed and the recipe used (developed by Dunne 1975) is given where those experiments are described.

Finlayson (1976) recommended the following recipe for obtaining a bulk sulphide float:

- (i) Add 200 g/ton hydrated  $\text{CuSO}_4$ , condition for 3 minutes.
- (ii) Add 135 g/ton Sodium Ethyl Xanthate (SEX) and condition for four minutes.
- (iii) Add 90 g/ton Dowfroth 250, condition for one minute, then float.

Preliminary tests had indicated that improved flotation rates could be obtained by decreasing the  $\text{CuSO}_4$  addition.\* Five tests were thus

\* Finlayson has recently shown that adding no  $\text{CuSO}_4$  produced a slight overall improvement in the recovery of the sulphides. (Finlayson 1976)



done around the centrepoint :  $\text{Cu SO}_4$  175 g/ton and SEX 135 g/ton and the results are summarised in Table 2.1. The above recipe was followed in each case except that the different  $\text{CuSO}_4$  and SEX dosages were used. Gas rate was maintained constant for all experiments, using a rotameter to monitor it. Froth was allowed to flow for 2 minutes without scraping and collected in one pan, then scraping was commenced and the product collected separately. The first sample gave an idea of the rate at which particles were removed, the total sample gave an estimate of the total amount of each element that was floatable. As the data shows, both measures were fairly insensitive to reagent levels, but Test III showed the most rapid rate and highest total recovery. For this reason the dosages used in that test (200 g/t  $\text{CuSO}_4$  and 110 g/ton SEX) were used in all bulk sulphide floats described herein.

Two more floats were done using this recipe to determine the effect of conditioning time on amount of floatable material in the pulp. Test VI was conditioned for an extra 10 minutes and Test VII for an extra 30 minutes before floating. Results showed no definite trend, and the largest change in final recovery was a decrease in Zn recovery by 5,8% after an extra 30 minutes conditioning (Cu recovery increased by 3,0%). This corroborated the work of Dunne (op. cit.) that conditioning time had little effect on mineral floatability. To eliminate short term effects, however, in subsequent tests on the large volume of slurry used in continuous testing, the conditioning time was extended to 40 minutes before commencing tests.

## 2.4 Sampling Procedures

Sampling was designed to enable the determination of flowrates of all components in the concentrate and tailings streams, and to obtain measurements of mineral grades and concentrations in the froth column as a function of height above the froth-slurry interface. The feed stream was not sampled.

### 2.4.1 Sampling of Concentrate and Tailings Streams

The pneumatically operated "wig-wag" sampler shown in Figure 2.2 was used for cutting samples from these streams. The timing of the sampling was controlled by the Real-Time CDC 1700 Computer available in the department.

Before the commencement of a run the sampling policy was specified in terms of the number of seconds to be spent by the wig-wag in each position (10 seconds sampling, 10 seconds not sampling was used for all experiments). The operation of a 3-way switch mounted near the cell informed the computer when to start sampling and when to stop, at which point the clock time and duration of the sampling operation was recorded on a nearby teletypewriter.

The above sampling policy was tested by collecting 20 successive 10 second tailings samples, and measuring their volumes. The values obtained had a standard deviation of less than 3% and the flowrates thus measured differed from the flowrate measured by collecting the whole stream over a 1 minute period by less than 2%. Since between 6 and 15 10-second sub-samples were taken for any particular sample, this policy was considered adequate.

Under conditions where a low concentrate flowrate was obtained, the duct transferring the concentrate stream from the overflow weir to the sampler was removed and the whole sample was taken manually, using a stopwatch. The tailings sample was taken as described above.

#### 2.4.2 Sampling of Froth Chamber Contents

The most accurate method of obtaining the variation of froth properties with height would be that of Watson and Grainger-Allen (1974) i.e. using horizontal slides to partition the froth phase into a number of segments, and removing the samples by suction dredging. The difficulties involved in both constructing and operating such a cell are considerable, and in view of the limited effort that was to be devoted to this aspect of the experimentation, samples were removed from the side of the cell through the holes that are shown in Figure 2.1 and Figure 2.2 while the cell was allowed to continue operating. Various methods of obtaining known volumes of sample (slurry plus air) were tested but no adequate method was developed, and the method eventually used was simply to remove the stopper from the hole and to allow the sample to flow into a beaker. Since a sample of large volume removed from a hole would not necessarily be characteristic of the froth at that level (in the limit, all the froth above any hole could be removed through it) small samples were taken from each hole in turn, starting from the topmost hole, and this process was repeated (at intervals long enough

to allow the froth to reestablish itself) until a sufficient amount of sample was obtained at each level.

## 2.5 Analysis of Samples

Wet and dry weights were obtained for all samples. Where particle size distributions were desired samples were wet screened to remove the  $-38\ \mu\text{m}$  fraction, dried and then screened on Tyler sieves in  $\sqrt{2}$  sequences, from  $425\ \mu\text{m}$  down to  $38\ \mu\text{m}$ . A Warman cyclosizer was used to obtain sub-sieve samples. The slimes fractions from the cyclosizer were (unwisely) discarded since reliance was placed on the ability to deduce their concentrations from a knowledge of the concentrations in the total  $-38\ \mu\text{m}$  fraction and the other cyclosizer samples.

To obtain Cu, Zn and Fe concentrations the samples were ground to powder in a Siebtechnik pulveriser and analyzed using a Lab-X radio-isotope excited X-ray fluorescence analyser. Considerable work was done to improve the accuracy of this instrument by linking it up to the CDC 1700 Real-time computer, which monitored the counting rate for each element, applied statistical tests to determine when the rate was known with a user-specified accuracy and, when all 3 rates were known, applied a calibration to obtain element concentrations. These element concentrations were used to obtain mineral and gangue concentrations and all concentrations were reported on a teletype next to the Lab-X analyser. Provision was made for standardising the instrument before measurements were made so that the effect of drift could be eliminated.

The calculation of the amount of each mineral from the element assays presented serious problems. Mineralogical analysis (de Kok) had revealed the qualitative complexity of the ore, where sphalerite has Zn atoms replaced by Fe in varying degrees and a lot of the gangue minerals contain Fe. Four samples of widely differing composition were accurately analysed for Fe, Cu, Zn and S content, and Dawson (1976) showed that Fe could be distributed between pyrite, sphalerite and gangue (as pyrrhotite) in a way which satisfied very closely all the stoichiometric relations involved. This, however was no good for calculating mineral concentrations within particle size classes, presumably because the Fe in sphalerite and

gangue was not uniformly distributed over the full range of particle sizes. Thus (particularly in some of the cyclosizer samples) it was often found that, once the mineral concentrations had been deduced, the gangue was found by difference to have a negative concentration.

Attempts were made to obtain an extra measurement by obtaining accurate (within 0,1%) measurements of the sample density using an air pycnometer. It was hoped that this would allow one to adjust mineral concentrations to obtain a better estimation of the true gangue concentration of a sample, since the density of the sample would be a strong function of gangue concentration, gangue density (approx 2,9) being much lower than that of the valuable minerals (4,1 to 5,0). This method did not work either, due probably to variations in mineral and gangue component densities.

The only option left open was to assume simple stoichiometric relationships for chalcopyrite, sphalerite and pyrite, and to assume that any weight remaining once these had been satisfied constituted the gangue content of the sample. The percentage of Cu, Zn and Fe in all samples in any suite of experiments was then artificially reduced by a constant fraction (0,92) to ensure that no negative gangue concentrations were obtained. Thus while mineral concentrations quoted are lower than those actually measured, they still bear the same relationship to one another. This approach was considered adequate since relative, not absolute effects were being investigated in all the experiments performed.

## CHAPTER THREE

### Variation of Froth Properties with Height in the Froth Column

#### 3.1 Introduction

As pointed out in Chapter One, most attempts to model the behaviour of the froth phase have been based on Harris and Rimmer's (1962) assumption of perfect mixing. At the other end of the scale we have the work of Cutting and Devenish (1975), who assumed plug flow of the froth in the vertical direction, and supported their work with experimental measurements of froth concentration gradients in their "equilibrium cell".

All the work thus far published on the "equilibrium cell" technique has been limited to batch operations. While the experimental advantages are obvious, serious practical objections and limitations may be raised. In continuous operations the residence time of particles in the froth phase is generally very different from that of the pulp phase, particularly for low-grade ores where low froth removal rates dictate that several cell volumes of pulp are required to produce the mass of solids that is held up in the froth at any particular instant. In addition, no investigation of the effect of froth removal rates is possible in the "equilibrium cell" technique.

In this chapter the results of a few experiments in which concentration gradients in the froth phase were measured during both batch and continuous operation, with and without froth removal, are discussed. A plugflow model is developed, based on a brief description

---

\* Note: the work described in this chapter was recently published in the International Journal of Mineral Processing (Moys 1978).

of the processes occurring in the froth phase. No attempt at quantitative prediction is made; the model is regarded simply as a device used to investigate the consequences of assumptions about the process, so that their validity might be checked.

Since the data were obtained in experiments where transverse motion is effectively eliminated and to that extent does not correspond with what occurs in practice, this work should be regarded as a study of the "other extreme" of flotation behaviour to the perfectly mixed concept of Harris and Rimmer. A realistic model would be a compromise between these two extremes.

### 3.2 Processes occurring during vertical, plugflow removal of froth

By various mechanisms the bubbles rising through the pulp phase pick up and carry with them mineral particles of varying composition. These bubbles with their load of attached particles enter a zone in the pulp at the base of the froth where they begin to crowd together and interact. It may reasonably be postulated that, associated with each bubble and its load of attached particles is an envelope of slurry liquid containing solid particles. These particles fall through the liquid because of their greater density. The relative velocity at which the particle falls, for any particle-liquid system, is determined by the spatial distribution of the bubbles in the froth and the size, shape and density of the particle. This relative velocity together with the net upward velocity of the slurry liquid in the froth determines whether particles in the froth liquid have a net upward or downward velocity. The velocity differential between bubbles and slurry liquid causes a steady decrease in slurry volume fraction with height, and the bubbles crowd more closely together to form firstly a foam and then a true froth consisting of polyhedral bubbles separated by thin films with Plateau Borders at the intersection of these films. Liquid and particles continue to drain from these films into the Plateau Borders and hence downwards along these Borders. The bubbles coalesce at a rate dependent on many factors and thus bubble surface area per froth volume decreases with height.



Thus the properties of the froth change continuously as the fluid drains from it. The concentrate is removed from the top of the froth by various methods which may themselves cause an increased rate of bubble coalescence, and hence reduce froth recovery.

The processes occurring in the froth either enhance or retard the "secondary cleaning" which generally occurs there. Froth drainage removes particles not strongly attached to the bubble surface (generally gangue particles); froth coalescence introduces shocks and reduces bubble surface area, both of which encourage particles to detach from the bubble films. If no attachment of strongly hydrophobic particles (i.e. valuables) occurs lower down in the froth phase, coalescence will not improve the grade of the froth and recovery of valuable minerals is reduced. However, if preferential attachment of valuables does occur, then the concentrate grade will improve, and regulating the degree of coalescence becomes a potential control action (through changing reagent concentration, froth residence time or froth removal method). In practice froth does not rise in true plugflow fashion, and the axial mixing that occurs {e.g. the "column drainage" observed by Cutting and Devenish (op cit) and mixing caused by the need for transverse motion towards the froth lip} has a deleterious effect on froth grade.

In the work to be described, transverse motion and mixing of the froth was largely eliminated and, as anticipated above, a rapid increase in the grade of valuable minerals and a rapid decrease in the gangue grade was in general obtained.

### 3.3 Mathematical Model for plugflow froth behaviour

The model discussed below is formulated to facilitate the rationalisation of the data obtained in the experimental work and may be used for predicting trends in situations resulting from altered control actions or design modifications. Most of the large number of parameters involved can be estimated independently because of the nature of the data obtained experimentally. Since the model will be used only to predict trends, a high precision is not required for the numerical values of the parameters.

In the development of the model no attempt is made to describe the attachment of mineral particles to the bubble films in the froth phase because this results in equations requiring iterative numerical solution. All streams are assumed to follow plug flow behaviour. The following assumptions are made:

- (i) Mineral particles attach to the bubbles in the pulp phase at a rate proportional to the available bubble surface area  $A \text{ m}^2$  in the cell and the concentration  $C_{Ti} \text{ kg/m}^3$  of particles in the cell, and rise at a rate  $m_{fi}(0) \text{ kg/s}$  into the froth:

$$m_{fi}(0) = k_{pi} A C_{Ti}$$

where  $k_{pi}$  is the first order rate constant (floatability) and  $A$  is determined from the bubble population parameters and the gas rate  $G \text{ m}^3/\text{s}$ . If all bubbles have diameter  $D_b$  and residence time  $\hat{t}$ , then it can easily be shown that

$$A = \frac{6\hat{t}G}{D_b}$$

Crowding of particles on the bubble surface will reduce  $A$ .

- (ii) Particles may detach from the bubble films and enter the liquid in the froth, depending on their strength of attachment and on the presence of mechanisms which encourage detachment, e.g. bubble coalescence. The rate of detachment is proportional to the concentration of the component in question. Taking a mass balance over a differential element we obtain

$$\frac{dm_{fi}(z)}{dz} = -k_{fi} m_{fi}(z)/v(z), \quad z > z_{di}$$

where  $z_{di}$  is the level at which detachment commences,  $k_{fi}$  is the detachment rate constant and  $v(z)$  the velocity of the bubble

films.  $v(z)$  is given by

$$v(z) = G/A_c \{1 - \bar{\epsilon}(z)\}$$

where  $A_c$  is the cell cross-sectional area and  $\bar{\epsilon}(z)$  is the slurry volume fraction, which is a complex function of  $z$ . In order to avoid the need for iterative numerical solutions of the differential equations it is necessary to assume  $\bar{\epsilon}(z) \ll 1.0$ , which is not true at the base of the froth. This however allows us to write

$$\frac{dm_{fi}(z)}{dz} = -k_{fi} A_c m_{fi}(z)/G$$

which yields an analytical solution.

- (iii) Slurry is entrained between the bubbles and contains particles in the same concentration as that in the cell. The initial flowrate of water,  $q_1(0)$ , is obtained by assuming that each bubble carries with it a layer of slurry of thickness  $\eta$  into the base of the froth: initial flowrate of slurry is

$$q_s(0) = 6G\eta/D_b$$

from which both solid and water flowrates can be obtained; both water and entrained particles rise at a rate  $q_1(z)$  and  $m_{ei}(z)$  respectively at a velocity  $v(z)$  towards the top of the froth column.

- (iv) Slurry liquid returns to the pulp phase in a downward-flowing stream at a rate  $q_2(z)$  at a velocity  $u(z)$ . This accords with what has been observed in practice; in certain areas of the froth small portions of the froth do have a net downward velocity, while froth channelling results in high upward velocities of the froth in other areas. At any level, however, the net upward flowrate of water is constant and equal to the concentrate water flowrate  $q_c$  :

$$q_c = q_1(z) - q_2(z)$$

- (v) The water and entrained particles in the upward flowing stream enter the downward flowing stream at a rate proportional to their concentration at the point of interest. Hence we obtain

$$\frac{dq_1(z)}{dz} = -k_q A_c q_1(z)/G$$

and

$$\frac{dm_{ei}(z)}{dz} = -k_{ei} A_c m_{ei}(z)/G$$

where  $k_q$  and  $k_{ei}$  are the first order rate constants for water and entrained particles respectively.

- (vi) At the top of the froth ( $z = z_w$ ) the froth removal process removes a fraction  $\alpha$  of the froth that arrives there, while a fraction  $(1-\alpha)$  collapses and enters the downward flowing streams. Thus the concentrate flowrates of water and particles are given by

$$q_c = \alpha q_1(z_w)$$

and

$$m_{ci} = \alpha \{m_{fi}(z_w) + m_{ei}(z_w)\}$$

The solutions of the above three differential equations are as follows:

- (i)  $m_{fi}(z) = m_{fi}(0) \quad z < z_{di}$   
 $= m_{fi}(0) \exp \left[ -\frac{k_{fi} A_c}{G} (z - z_{di}) \right] \quad z > z_{di}$
- (ii)  $q_1(z) = q_1(0) \exp \left[ -\frac{k_q A_c}{G} z \right]$

$$(iii) \quad m_{ei}(z) = m_{ei}(0) \exp \left| - \frac{k_{ei} A c z}{G} \right|$$

All solid particles which diffuse from the upward flowing stream enter a stream flowing downward at velocity  $u$  and rate  $m_{ri}(z)$  given by

$$m_{ri}(z) = m_{fi}(z) + m_{ei}(z) - m_{ci}$$

The velocity  $u(z)$  of downward-flowing streams is unknown. A simple model which takes into account the fact that  $u(z)$  will decrease as  $v(z)$  increases is based on the assumption that there is a constant velocity difference  $\Delta v$  between the upward and downward flowing streams. Thus, remembering that  $u(z)$  is positive for downward-flowing streams, we get

$$u(z) = \Delta v - v(z)$$

Given the flowrates and flow velocities at any point, mineral mass fractions in the froth can be calculated by noting that the mass of a particular mineral in the froth between heights  $z$  and  $z+dz$  is given by

$$dm_i(z) = \left[ \frac{m_{fi}(z) + m_{ei}(z)}{v(z)} + \frac{m_{ri}(z)}{u(z)} \right] dz$$

and mass fraction of mineral is obtained from

$$g_i(z) = \frac{dm_i(z)}{\sum_j dm_j(z)}$$

Note that, while the flowrates involved in these equations exhibit an exponential dependence on  $z$ , mineral mass fraction does not, as shown in Figure 3.2 (The discontinuities at  $z = 0$  are a result of the assumption that  $\epsilon(z) \ll 1,0$  for all  $z$ ; in practice as  $z$  tends to 0,  $\epsilon(z)$  tends to 1,0). Other properties such as froth density and bulk concentrations can easily be calculated.

The large number of parameters involved makes it essential to obtain independent estimates of as many of them as possible.

- (i) Bubble population parameters: methods have been developed (Dunne et al 1976) for the measurement of average bubble diameter  $D_b$ , while the bubble residence time  $\hat{\tau}$  can be incorporated in the flotation rate constants  $k_{pi}$ , which must be inferred from experimental data:

$$m_{fi}(0) = k_{pi} AC_{Ti} = 6(k_{pi} \hat{\tau}) GC_{Ti} / D_b$$

- (ii) The thickness  $\eta$  of the layer of slurry associated with each bubble is given a value which ensures that the slurry volume fraction at the base of the froth is comparable with that found in practice.
- (iii) The efficiency of froth removal  $\alpha$  is obtained by estimating  $Q_c$ , the volume flowrate (air plus slurry) of the froth flowing over the concentrate weir. Then

$$\alpha \approx Q_c / G$$

$Q_c$  will be related to the width, depth and velocity of the concentrate stream as it flows over the concentrate weir. As shown in Chapter 5, measurements of froth residence time distribution or horizontal froth velocity enable one to estimate  $\alpha$ . For some methods of froth removal, however,  $\alpha$  is known e.g. if no bubble breakage occurs on the top of the froth, or if the design of the froth chamber forces all froth into the concentrate launder  $\alpha = 1.0$ . If no froth is removed,  $\alpha = 0$ .

- (iv) The  $z_{di}$  will be fixed by noting the point on the grade vs height curve at which a change of direction occurs; e.g. refer to the discussion of figures 4 and 5. The  $k_{fi}$  must be adjusted to simulate the experimental results.

- (v)  $\Delta v$ , the velocity difference between upward and downward flowing streams cannot be measured, and will best be estimated by adjusting it and  $k_q$  to simulate as closely as possible the water hold-up profile in the froth column.
- (vi) The  $k_{ei}$  may be related directly to  $k_q$ . The density difference between the particles and water ensures that the rate of transport of particles into the downward stream is greater than the rate of such transport of water. Particles of specific gravity 1,0 will behave as the water does.\* Thus a reasonable model for the  $k_{ei}$  is

$$k_{ei} = k_q + \beta_e (\rho_i - 1,0) \quad (3.1)$$

where  $\rho_i$  is the particle specific gravity and  $\beta_e$  is an arbitrary parameter. This proposal is supported by the results obtained by Bishop and White (1974).

The ability of this model to simulate what is found experimentally is shown in Figures 3.2 and 3.4 and discussed in a subsequent section.

### 3.4 Scope of Experimentation

All details relating to cell construction, slurry conditioning, sampling, etc. are given in the previous chapter. Measurements of the variation of mineral grades with height in the froth were made for each of the experiments. These varied with respect to the following choices as indicated in the captions for each figure:

- (i) Bulk sulphide float or float with pyrite depressed.
- (ii) Batch or continuous operation.
- (iii) Removal of froth or so-called "equilibrium" operation where the gas rate is adjusted so that a negligible amount of froth flows over the weir.

\* This ignores interference between particles and bubble films, and will thus be valid only at the base of the froth (where most of the drainage occurs).

- (iv) Inclusion or exclusion of baffles (designed to minimise froth circulation) in the froth phase.

Particle size analyses were performed on all samples from the last experiment described so that the behaviour of particles within size fractions could be observed.

### 3.5 Discussion of Results

Figure 3.1 contains data from replicate experiments and shows the reproducibility obtainable. The trends are consistent with what is expected on the basis of the discussion in section 3.2. The grades of the activated minerals and % solids in the froth increase with height above the froth level, while % gangue decreases. This occurs most rapidly at the base of the froth due to preferential drainage of large gangue particles from entrained slurry liquid, as shown by the rapid decrease in gangue concentration (% gangue in the slurry by weight) at that level. Above the 5 cm level the gangue concentration remains essentially constant, due probably to the fact that the relatively well-drained froth hinders the preferential settling of interstitial particles.

The mathematical model was used to simulate this "normal behaviour" and the results are shown in Figure 3.2. The preferential settling of particles with respect to water was suppressed by assuming that  $\beta_e$  in equation 3.1 was equal to zero, with the result that gangue concentration remained constant. No detachment of particles from the bubble films is assumed ( $k_{fi} = 0$ ). The slurry contains 35% solids at the grades shown in Figure 3.2, and the other parameters are:  $\tau = 2,0s$ ,  $G = 0,25 \times 10^{-3} \text{ m}^3/s$ ,  $D_b = 0,001m$ ,  $\eta = 0,0006m$ ,  $\alpha = 0,3$  and  $\Delta v = 0,02 \text{ m/s}$ . The  $k_{fi}$  for sphalerite, chalcopyrite and gangue are respectively  $0,3 \times 10^{-3}$ ,  $0,3 \times 10^{-3}$ ,  $0,16 \times 10^{-3}$  and  $0,04 \times 10^{-6} \text{ s}^{-1}$ .

In Figure 3.3, the rapid increase and subsequent decrease in Fe grade is not consistent with the behaviour of the model illustrated in Figure 3.2 and requires the selective return of pyrite particles to the pulp. The following explanation is advanced (this effect occurs to



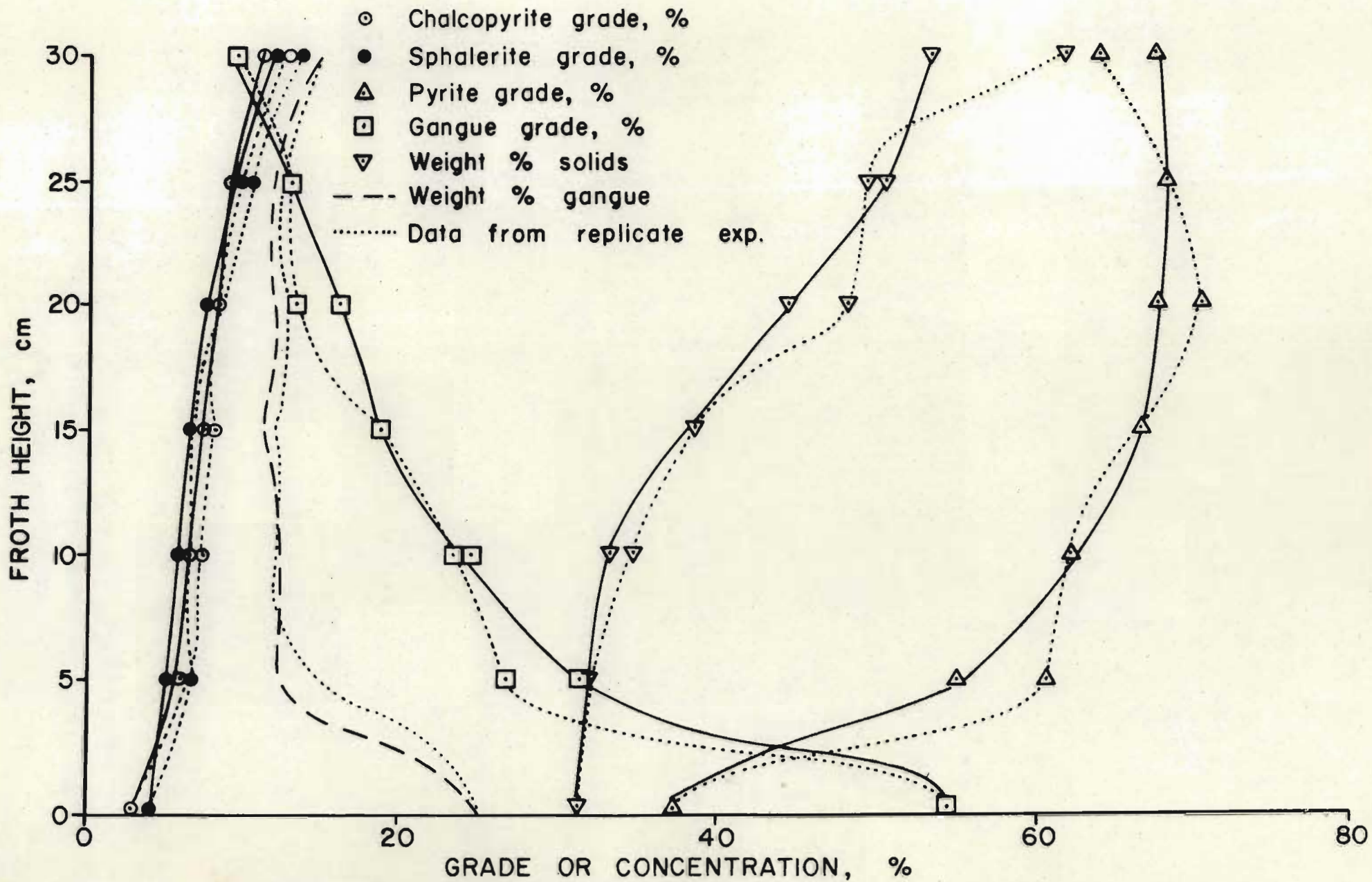


Figure 3.1 Variation of froth grades and density with height, illustrating general trends and reproducibility (continuous bulk sulphide floats with baffles in the froth phase; no froth removal).

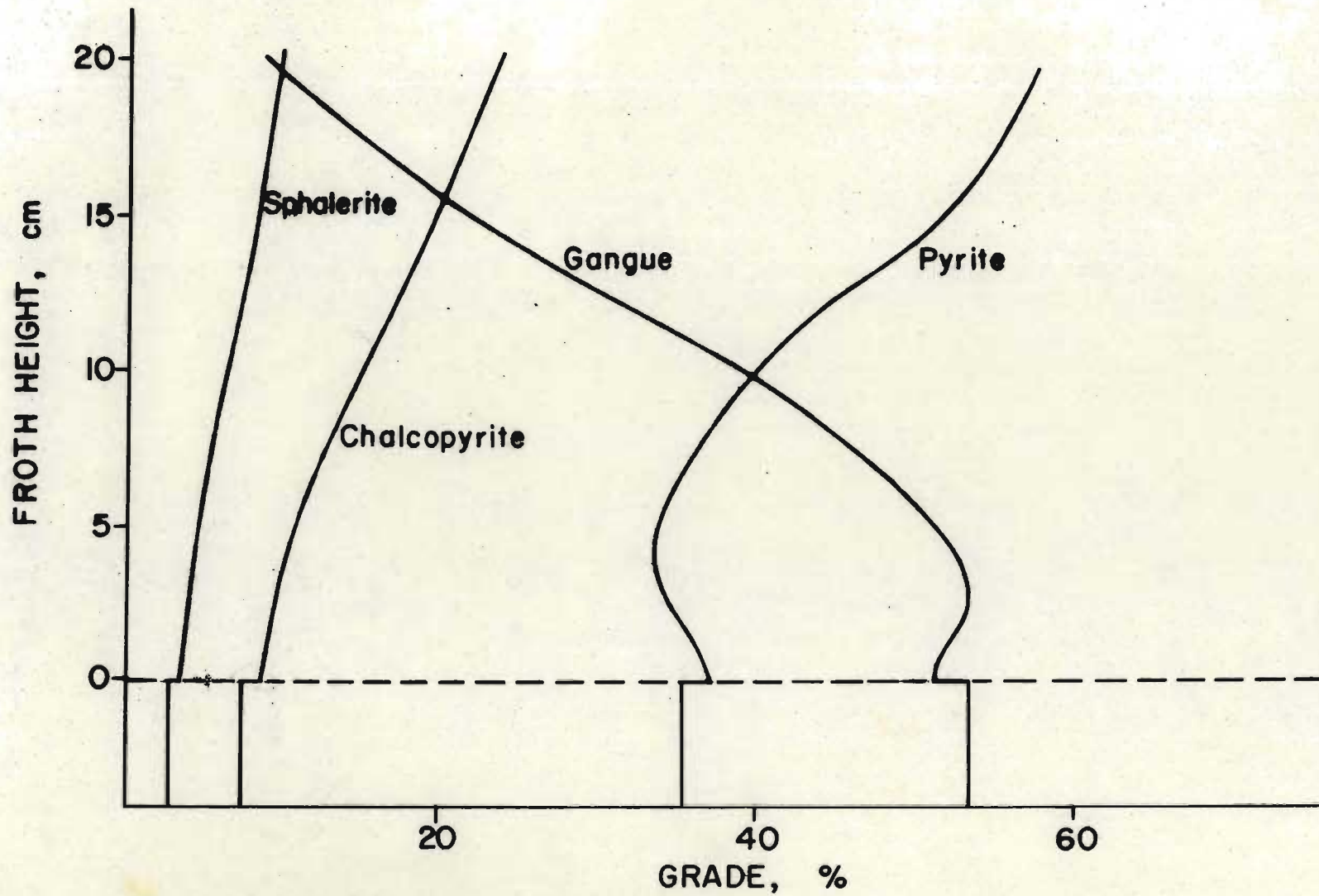


Figure 3.2 Simulation of froth behaviour using a simple mathematical model.

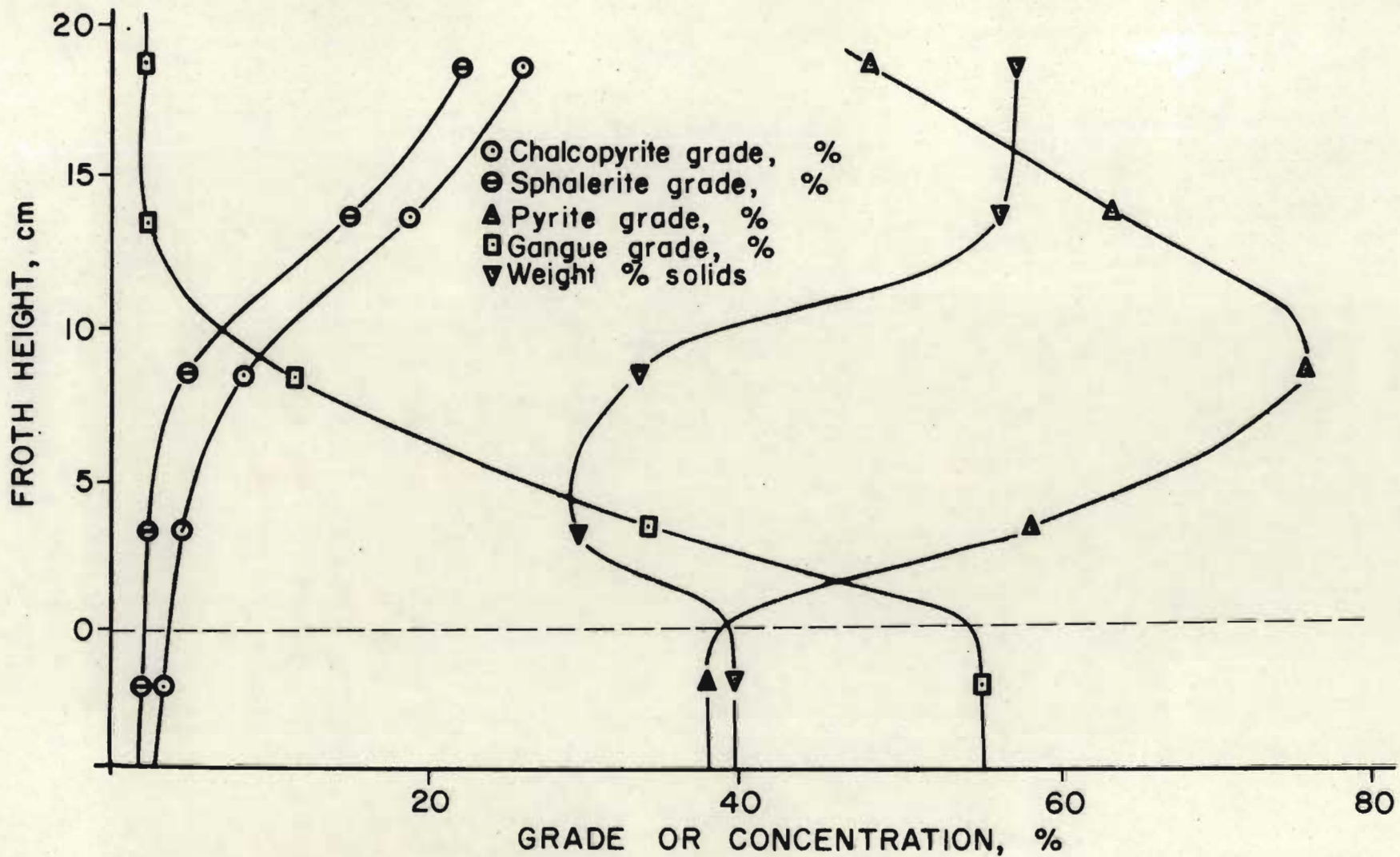


Figure 3.3 Variation of froth properties with height showing inflection in pyrite grade curve. (Batch float with pyrite depressed under "steady state" conditions. No baffles in the froth phase).

a lesser extent in Figures 3.5 and 3.7 as well). Fe, Cu and Zn become attached to the bubble films, Fe more weakly than the other two since the conditioning was such that Fe was depressed. As the froth rises in the cell, drainage occurs, the bubble walls thin to the point where coalescence commences. This results in progressively decreasing film surface area for attachment of mineral particles to the point where the particles start competing for attachment sites. At this point the Fe particles are displaced by the more hydrophobic Cu and Zn particles, and the Fe grade decreases as shown; at the same time the Cu and Zn grades increase rapidly. This effect was simulated successfully, as shown in Figure 3.4, using the mathematical model described above, by allowing Fe to diffuse off the film into the downward flowing stream above a froth height of 10 cm. (i.e.  $z_{di}$  for Fe = 10 cm,  $k_{f,Fe} = 0,085s^{-1}$ ). In this case where bubble coalescence occurs, a more rapid drainage of the froth is assumed ( $k_q = 0,1 s^{-1}$ ,  $\beta_e = 0,04$ ). The pulp rate constants for sphalerite, chalcopyrite, pyrite and gangue are respectively  $0,2 \times 10^{-3}$   $0,14 \times 10^{-3}$   $0,10 \times 10^{-3}$  and  $0,4 \times 10^{-6}$  m/s. All other parameters are identical to those used for the simulation illustrated in Figure 3.2.

Figure 3.5 indicates the effect of froth removal. When no froth is being removed, the gangue concentration at the top of the froth is very low, and the concentration of valuables is high. When the froth is being removed, such that the concentrate mass flowrate is approximately 10% of that of the feed, the grade of Cu and Zn decreases markedly, while the gangue concentration is increased. This effect has been observed by many authors {e.g. Casson (1973)}, who studied the effect of pulling rate on grade-recovery curves for an industrial plant; nevertheless there is a dearth in the literature of reports on attempts to design froth removal methods which seek to minimize this loss of grade with increase in froth removal rate. The performance of large cells in particular could be improved with the use of improved froth removal methods. The Maxwell cell is a case in point, where the annular launder situated in the froth phase ensures that no element of froth has to travel a large distance before being removed.

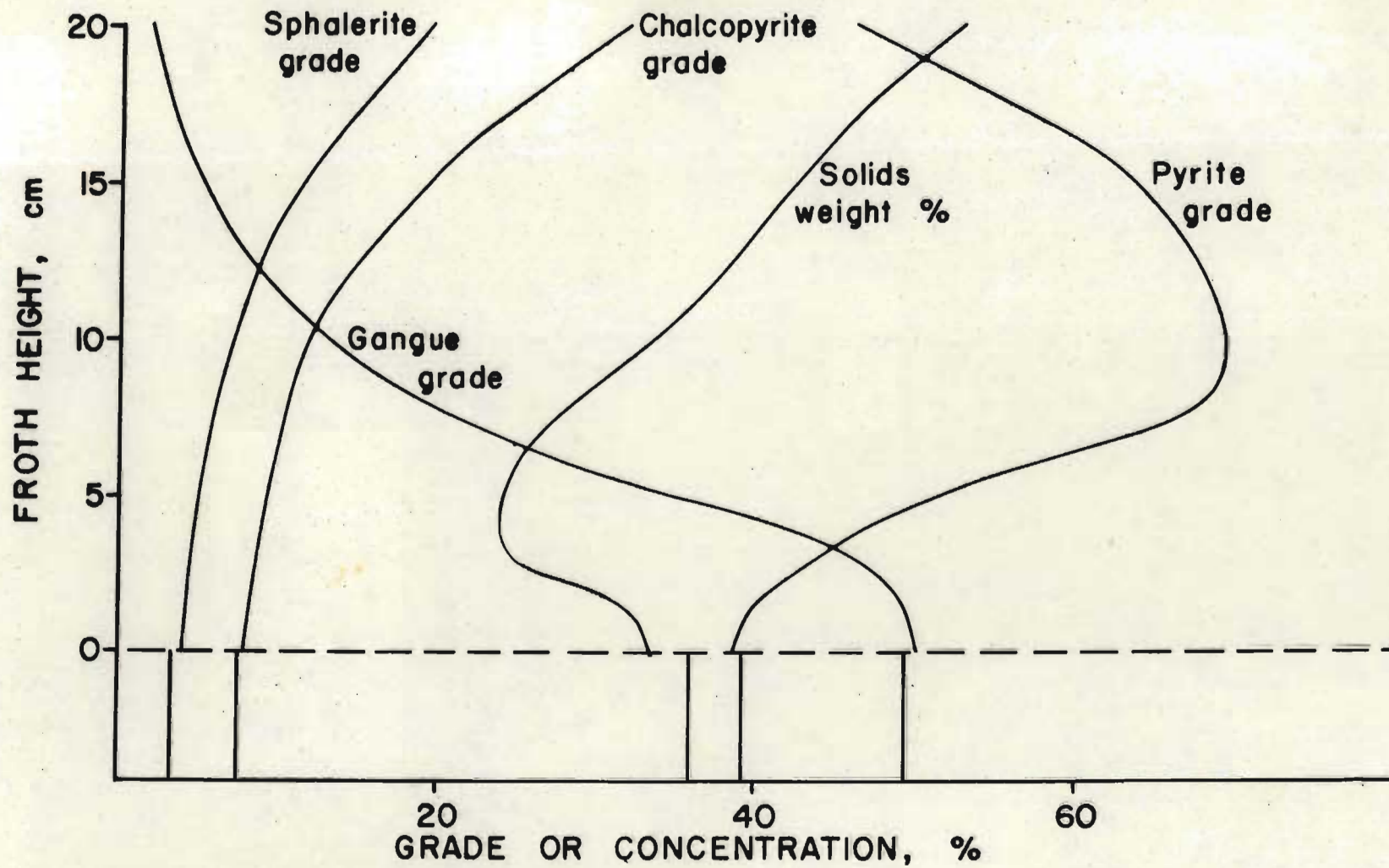


Figure 3.4 Simulation of froth behaviour involving detachment of pyrite particles in the froth phase.

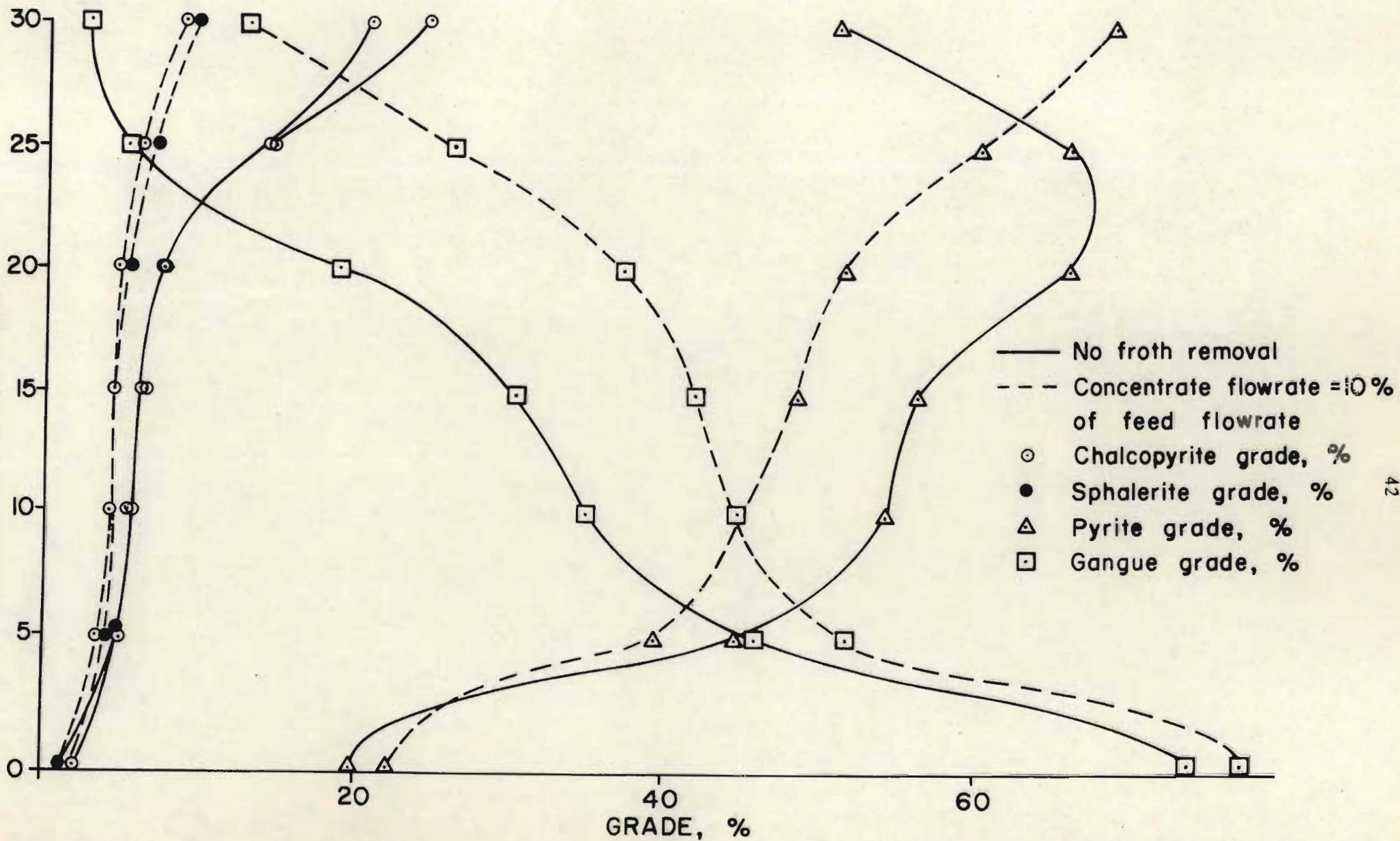


Figure 3.5 Effect of froth removal on froth grades (continuous bulk sulphide float with no baffles in the froth phase).

Figure 3.6 is used to illustrate the same effects on a batch float. Cu and Zn grades are not given since they were low and largely unaffected in the experiment. Under initial steady-state conditions, the high separation between Fe and gangue is evident; during the removal of concentrate this is largely reduced, the gangue contamination having increased four-fold; however, the initial separation is again achieved once froth removal is discontinued, in spite of the fact that a large percentage of the pyrite has been removed in the concentrate.

The effects observed in both Figures 3.5 and 3.6 would be explained by recognising that, in the case where no concentrate is removed, the froth at the top of the column is well drained and hence the volume of interstitial slurry containing low-grade ore is small. This is because the gas rate to the cell must be reduced to achieve the "steady-state" condition where no concentrate is flowing over the weir, resulting in decreased transport of interstitial slurry into the upper portions of the froth. In addition the continual froth coalescence which occurs at the top of the froth under these conditions gives rise to the preferential growth in concentration of hydrophobic particles at the top of the froth, even in cases where a large percentage of these particles have been removed previously by flotation with concentrate removal.

In Figure 3.7 the effect of froth removal rate is given. With no froth removal (low gas rate) a rapid separation of pyrite and gangue occurs at the base of the froth. This increases steadily to the top of the froth, where a rapid increase in Cu and Zn and decrease in Fe grades occurs (discussed above). By increasing the gas rate, a point is reached where froth starts flowing over the weir. As the froth removal rate is increased, the separation between gangue and pyrite in the lower regions of the froth is progressively decreased, indicating that in these regions where the froth is still relatively mobile, mixing of the froth phase occurs and becomes more marked as gas rate increases, in spite of the presence of baffles designed to reduce this. (Since gas rate changes were small (total change = 20%), the expected upward movement of the profiles with increase in gas rate would not be large enough to account for the effect observed here, and a mixing mechanism must be invoked.)

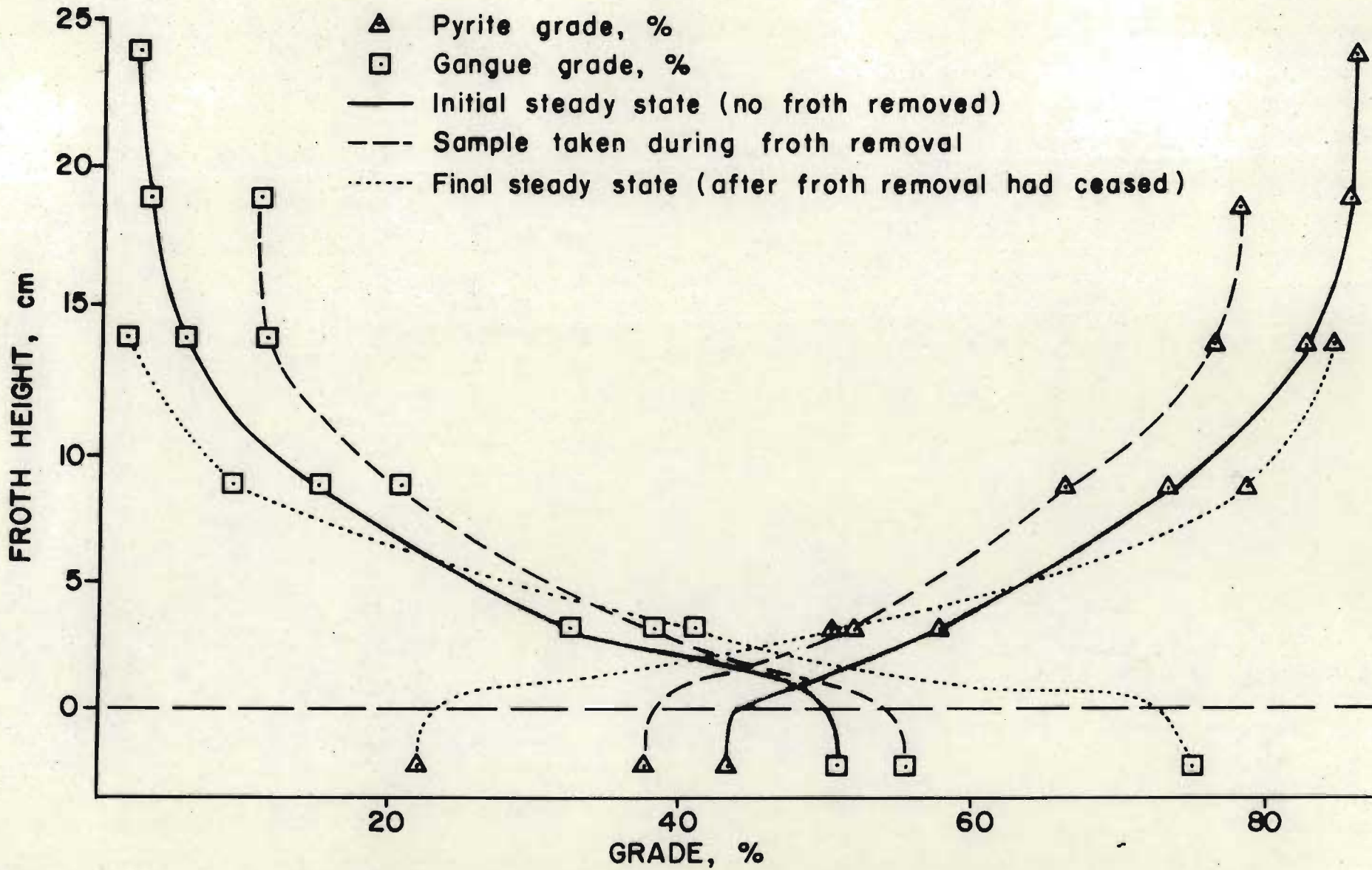


Figure 3.6 Effect of froth removal on froth grades (Batch bulk sulphide float with no baffles in the froth phase).



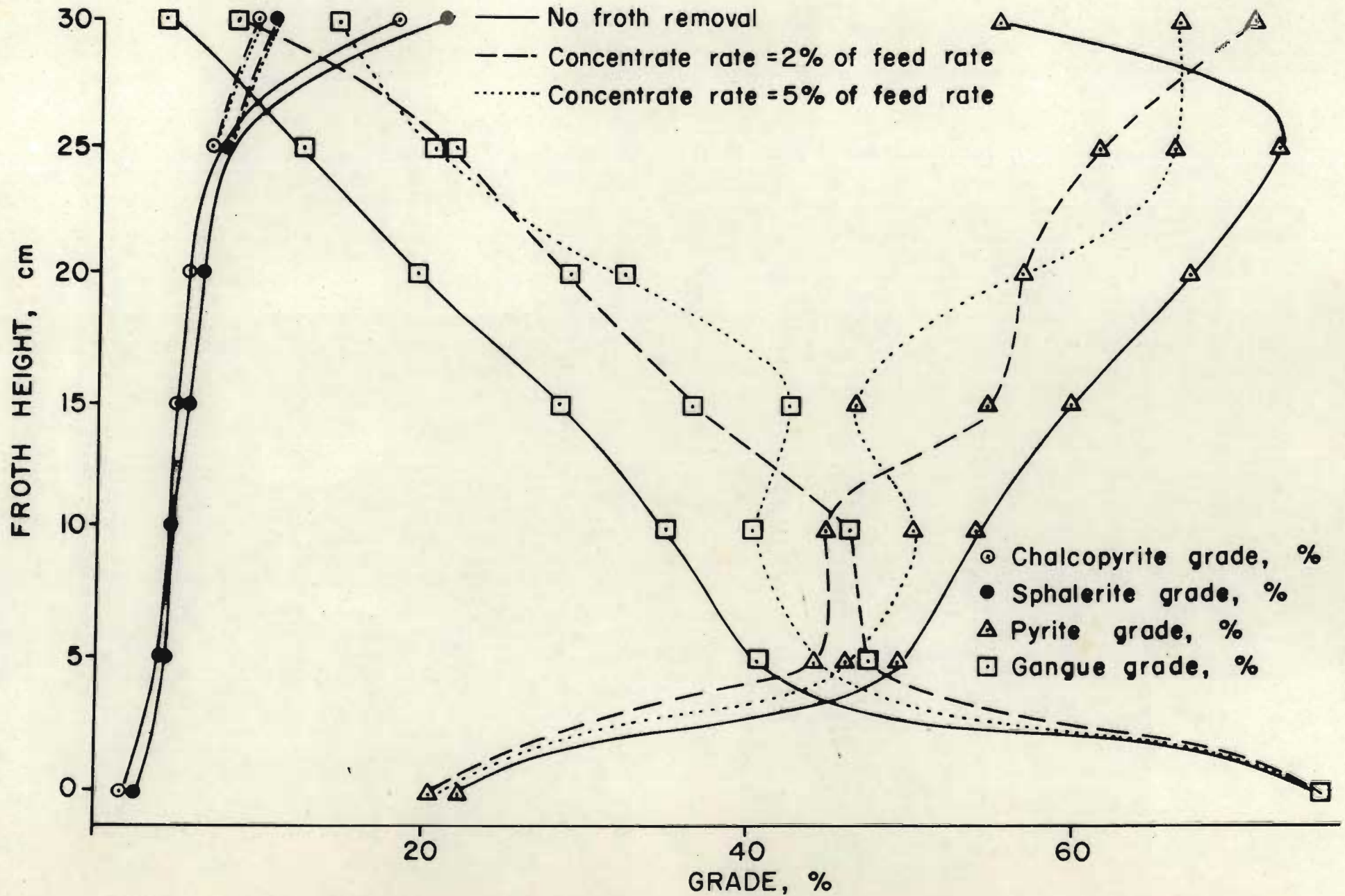


Figure 3.7 Variation of froth grade profiles with gas rate (Continuous bulk float with baffles in the froth phase, with and without froth removal).

The effect of baffles is indicated in Figure 3.8 where their presence hastens the establishment of pyrite-gangue separation. No significant effect on grades at the top of the froth is noted, however.

In Figure 3.9, the effect of froth cleaning action within particle size classes is demonstrated. The variation of Cu grade with particle size is strongly affected by froth height, large particles showing a greater tendency to detach from the froth than smaller particles. With Zn this effect is not as marked except at the top of the froth, while with Fe no significant effect is noted at all, the increase in grade with height (largely a result of gangue drainage) being essentially uniform over the whole particle size range.

### 3.6 Summary and Conclusions

The following points summarise what has been learnt from the data. Practical applications are discussed:

- (i) The results obtained conform in most cases with what is expected on the basis of the simple mathematical model outlined above. The effects of selective detachment of particles from the film can be simulated; deviations from the model are ascribed to mixing in the froth phase, i.e. departure from plug flow behaviour.
- (ii) The solid mass fraction of valuable mineral in the froth increases as the interstitial slurry drains from it; the practical advantages one can obtain from this are limited, however, because well-drained froths are generally unstable and do not flow easily. Any attempt to remove them by conventional methods will cause them to collapse and recovery is lost. Thus froth removal methods should be designed which allow maximum froth drainage while minimising the breakage of the resulting unstable froth.
- (iii) Substantial reduction in the concentration of gangue in entrained slurry occurs at the base of the froth due to the settling of these particles. A baffle grid inserted below the base of the froth would increase this effect by reducing turbulence at the base of the froth. Baffles in the froth have not been shown to produce a marked improvement in separation, however.

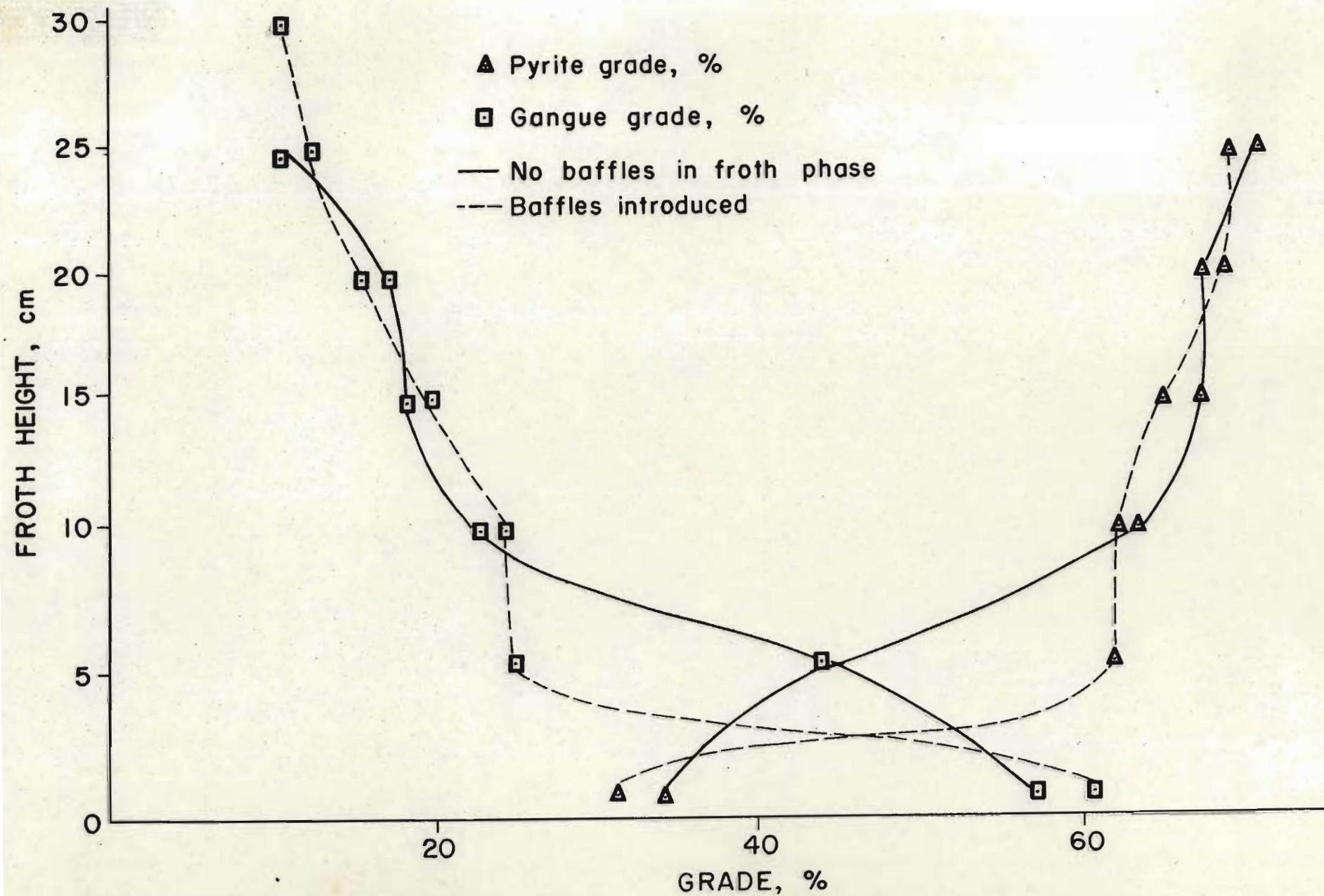


Figure 3.8 Effect of baffles designed to reduce mixing in the froth phase on pyrite and gangue grades (Continuous bulk float, concentrate removal rate approximately 10% of feed rate).

Symbol Froth height, cm

○ 20

⊖ 15

□ 10

⊠ 5

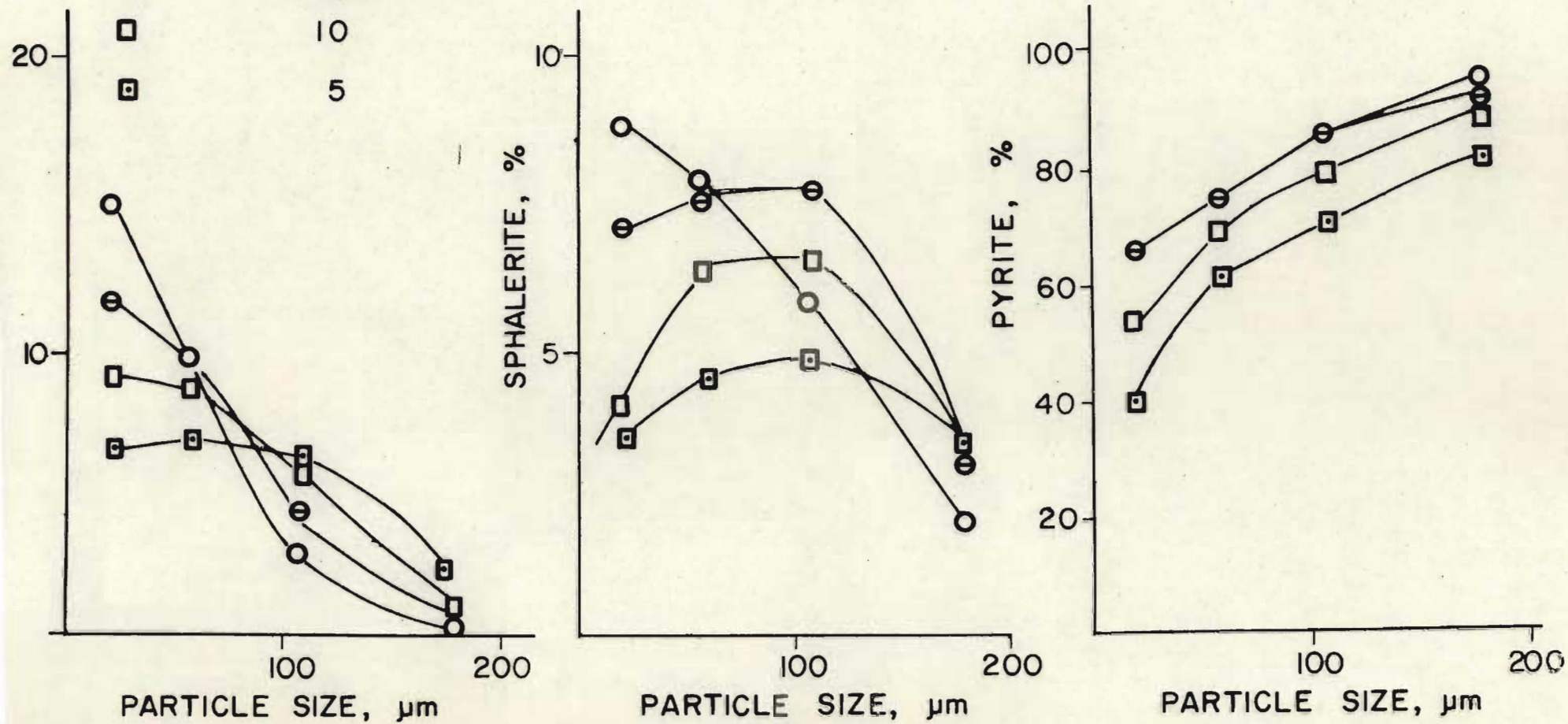


Figure 3.9 Effect of position in froth on variation of mineral grades with particle size (Batch sulphide float).

- (iv) The variation of grade within particle size fractions with froth height varies with each mineral. Information of this sort will assist in deciding degree of grind, for example.

A study of processes occurring in the flotation froth column have led to a clearer insight into what is happening there and provides some of the foundation for more rational design of froth removal methods.

## CHAPTER FOUR

### Residence Time Distributions in Flotation Froths: Introduction and Theoretical Developments.

#### 4.1 Introduction

The fact that the residence time of froth elements passing through the froth phase in conventional flotation cells is distributed over a wide range is evident to anyone familiar with the flotation process. Elements entering near the overflow are removed rapidly (especially if scrapers are used) while elements entering near the back of the cell may in fact never be removed. Thus in cases where a substantial fraction of the mass of a component entering the froth falls back into the pulp phase, the residence time distribution (RTD) will be an important factor determining the recovery of that component. This is particularly true for water and gangue and weakly floatable particles. Strongly floatable particles may be affected if too long a residence time in the froth causes their deactivation, or if certain fractions of the froth are never removed. A quantitative measure of froth RTD will thus be an important diagnostic tool in both design and control of flotation cells.

Very little work has been done in this area. Woodburn (1976) has reviewed work done on the modelling of the froth phase in general and has pointed out the need for quantitative measures of froth RTDs. The two phase model of Harris and Arbiter (1962) has been widely accepted as a major advance, but is based on the very questionable assumption of a perfectly mixed froth phase. Lynch and his co-workers have included either implicitly or explicitly the same assumption in their models of froth phase behaviour. No measurements of froth phase RTDs have been reported.

The froth residence time distribution  $E_f(\tau)d\tau$  is defined as the fraction of perfectly floatable material entering the froth phase which spends a time between  $\tau$  and  $\tau+d\tau$  in the froth phase before being withdrawn in the concentrate. It must be recognised that a certain fraction of these particles may never be removed in the concentrate stream, due to inefficiencies in the froth removal process, eg. when part of the froth moves towards the back of the cell where it collapses and returns its load of particles to the pulp phase. Accordingly it is convenient to define the concentrate residence time distribution  $E_c(\tau)d\tau$  as that fraction of the perfectly floatable particles in the concentrate which have spent a time between  $\tau$  and  $\tau + d\tau$  in the froth phase. In this case

$$\int_0^{\infty} E_c(\tau)d\tau = 1,0$$

The efficiency of the froth removal process is then defined as

$$\epsilon_f = \int_0^{\infty} E_f(\tau)d\tau$$

and is the fraction of perfectly floatable particles entering the froth phase which are removed in the concentrate. It is easily shown that

$$E_f(\tau) = \epsilon_f E_c(\tau) \quad (4.1)$$

Once  $E_f(\tau)$  has been determined the behaviour of real components is characterised by postulating a mechanism for the detachment and/or drainage of these particles, leading to expressions for their recovery in the concentrate stream.  $\epsilon_f$  and  $E_c(\tau)$  are functions of the design of the cell, the froth removal method, the froth height and the gas rate, at least, and should be useful concepts in rationalising the design, control and scale-up of flotation equipment. In this and the following chapter various models for froth phase behaviour are considered and compared with experimental data. Forms for both  $\epsilon_f$  and  $E_c(\tau)$  are

found which are physically realistic and quantify the phenomenon being studied with sufficient accuracy. The parameters involved can be determined either by pulse testing or, less accurately by other methods.

#### 4.2 Theoretical Determination of Residence Time Distributions

Two approaches have been adopted:

- (i) certain assumptions allow the Laplace equation for streamline flow in the froth chamber to be solved. Here the two-dimensional behaviour of the froth i.e. its simultaneous movement upwards towards the surface of the froth and horizontally towards the concentrate lip is described. The solution allows residence times of froth elements to be obtained as a function of froth height, froth stability, gas rate and the profile of the flux of the gas through the froth/slurry interface. This represents the closest one can get to the quantitative description of the behaviour of the froth without performing extremely complex numerical calculations which, for example, would allow one to take frictional and inertial forces into account. As it is, the solution is complex and is not appropriate for plant simulation, flotation parameter estimation or control;
- (ii) by quantifying the effect of vertical movement on the residence time of a froth element with a single parameter, a simple, very tractable model is produced which lends itself to parameter estimation and hence to interpretation of experimental measurements of the residence time distribution. Comparison of this model with the streamline model leads to the implementation of certain modifications to it which make it suitable for the interpretation of experimental RTD data.



Other models involving various combinations of plug-flow and perfectly mixed models are shown either to produce the same form for the RTD expression (with poorly defined parameters) or to fail to describe the phenomenon under study.

#### 4.2.1 Two-dimensional Streamline Behaviour of Flotation Froths

Two assumptions allow us to determine the streamlines for the flow of particles and air in the flotation froth phase:

- (i) the volume of liquid and solid in the froth phase is much less than the volume of air, i.e. the froth is well drained;
- (ii) no frictional forces act in the froth.

These two assumptions conflict since a well-drained froth consists of a relatively rigid bubble structure, and hence substantial frictional forces will be present. This must therefore be borne in mind when interpreting the results obtained below.

##### 4.2.1.1 Solution of the Laplace Equation

Under the above assumptions the flow of froth is governed by the two-dimensional Laplace equation

$$\frac{\partial^2 \phi}{\partial x^2} + \frac{\partial^2 \phi}{\partial z^2} = 0$$

where  $\phi$  is the stream function,  $x$  is the distance from the back of the cell and  $z$  the height above the slurry-froth interface. Figure 4.1 shows the geometry of the problem;  $w$  is the height of the concentrate weir,  $h$  is the height of the froth,  $g_f(x)$  is the flux of froth across the froth/slurry interface ( $\text{cm}^3/\text{cm}^2\text{s}$ ), (which,

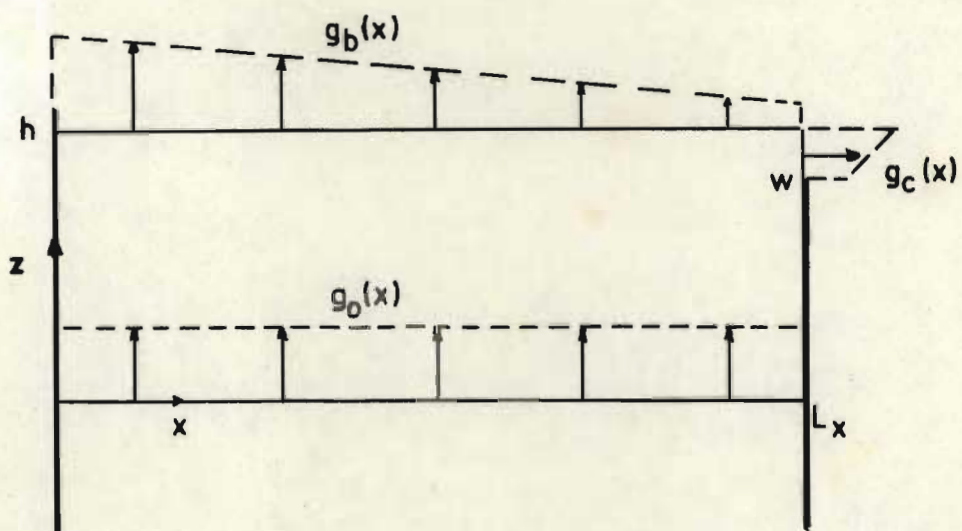


Figure 4.1 Boundary conditions for the solution of the Laplace equation for streamline flow of froth

according to assumption (i), is the flux of gas across the interface),  $g_b(x)$  is the flux of air through the froth surface, and  $g_c(z)$  is the flux of concentrate froth flowing from the cell. Various forms for these fluxes were considered:

(i)  $g_f(x)$  invariant with  $x$ :

$$g_f(x) = g_o \quad (4.2)$$

Measurements have shown (section 2.1) that  $g_f(x)$  varies substantially with  $x$ , being highest near the centre of the cell. Accordingly another form for  $g_f(x)$  was also considered:

$$g_f(x) = \hat{g}_o \sin \frac{\pi x}{L} \quad (4.3)$$

(ii) Rate of froth breakage varying linearly with  $x$ :

$$g_b(x) = g_{b1} + 2g_{b2}x \quad (4.4)$$

(iii) Concentrate flux invariant with  $z$

$$g_c(z) = g_{c1}$$

A froth stability parameter  $\alpha$  is defined as the ratio between the volume flowrate leaving the froth phase in the concentrate and the volume flowrate crossing the froth/slurry interface. If no froth breakage occurs,  $\alpha$  has a value of unity. Once  $\alpha$  and  $G$  are specified, all flowrates to and from the froth phase are defined.

According to streamline theory, the solution of the Laplace equation is subject to the boundary conditions

$$(1) \quad 0 \leq x \leq L, z = 0 : f_1(x) = \phi(x,0) = \int_0^x g_f(s) ds$$

$$(2) \quad 0 \leq x \leq L, z = h : f_2(x) = \phi(x,h) = \int_0^x g_b(s) ds$$

$$(3) \quad \begin{aligned} x = L, 0 \leq z \leq w : f_3(z) = \phi(L,z) &= \phi(L,0) \\ w \leq z \leq h : f_3(z) = \phi(L,z) &= \phi(L,0) - \int_w^z g_c(s) ds \end{aligned}$$

$$(4) \quad x = 0, 0 \leq z \leq h : f_4(z) = \phi(0,z) = 0$$

Carslaw and Jaeger (1959) give a solution for the Laplace equation where a boundary condition  $f_i(x)$  exists on the  $z = 0$  line with all other boundary values zero:

$$\phi_i(x_i, z_i) = \sum_{n=1}^{\infty} a_{in} \frac{\sin \frac{n\pi x_i}{a_i}}{a_i} \frac{\sinh \frac{(b_i - z_i)n\pi}{b_i}}{b_i} \operatorname{Cosech} \frac{n\pi b_i}{a_i} \quad (4.6)$$

Where  $i = 1, 2$  and  $3$  correspond to the nonzero b.c.s. (1), (2) and (3) respectively,  $a_i$  and  $b_i$  are the lengths in the  $x_i$  and  $z_i$  directions respectively, and the  $a_{in}$  are the coefficients of the sine fourier series for  $f_i(x)$ . This solution is applied to each nonzero boundary condition in our problem in turn, and the final solution is the sum of the three solutions obtained (bearing in mind that axes have to be translated and/or rotated through  $90^\circ$  to obtain the correct solutions). Thus

$$\phi(x,z) = \phi_1(x,z) + \phi_2(x,h-z) + \phi_3(z,L-x)$$

#### 4.2.1.2 Determination of Streamlines

A streamline is the locus of points defined by

$$\phi(x,z) = \Phi \quad (4.7)$$

where  $\phi$  is a constant. If the streamline corresponds to a bubble entering the froth phase at  $x$ , then

$$\phi = \phi(x, 0) = \int_0^x g_0(s) ds$$

Equation (4.7) is solved numerically for  $z$  at values of  $x$  covering the streamline's range using Newton's iteration formula. Rapid convergence was obtained in most cases; only in isolated cases were more than 3 iterations required to obtain  $z$  to within less than .01 cm.

Velocities in the  $x$  and  $z$  directions at the point  $(x, z)$  are given respectively by

$$v_x = -\frac{\partial \phi}{\partial z} \quad v_z = \frac{\partial \phi}{\partial x}$$

Expressions for the sine fourier series coefficients  $a_{ni}$  and the equations used for determining  $v_x$  and  $v_z$  are obtained by conventional rules of calculus.

#### 4.2.1.3 Air and Particle Residence Times

Once the locus of 9 streamlines covering the solution space, together with the values of  $v_x$  and  $v_z$  along each streamline were found, the residence time for air and particles were obtained by evaluating the following line integral numerically:

$$\tau = \int_{\phi} \frac{1}{v} ds$$

where  $v$  is the velocity tangential to the streamline and  $s$  is the distance along the streamline.

The streamline for a particle is the streamline for the bubble to which it is attached; if the bubble reaches the surface and bursts, then the particle is assumed to travel along the surface of the froth at the velocity  $v_x(h)$  and eventually leave the cell in the concentrate stream. Thus

$$\tau_p(x) \geq \tau_b(x)$$

where  $\tau_p(x)$  and  $\tau_b(x)$  are the residence times of particles and bubbles respectively which enter the froth at point  $x$ .

#### 4.2.1.4 Discussion of Simulations

Solutions were obtained for the conditions listed in the Table 4.1 and the results are shown graphically in Figures 4.2.1 to 4.2.15. In addition to streamlines and air and particle residence times, velocity profiles across 3 planes in the  $x$ -direction (at  $x = 1, 10, \text{ and } 19$  cm) and one in the  $z$  direction (at 0,5 cm below the overflow weir lip), and the variation of surface velocity with  $x$  are plotted. (Also shown are residence times produced by Model 1 described in Section 4.2.2.4. These are discussed in that section). Table 4.1 also lists various numerical results of the solutions:

(i) The residence time ratio is defined by

$$\delta = \frac{\tau_{\min}}{\tau_{\text{plug}}} = \tau_{\min} \cdot G / (hL_x L_y)$$

(ii)  $\tau_{\max}$  is a practical measure of the maximum residence time, obtained by straight-line extrapolation of the  $\tau$  vs  $x$  curve from the point  $x = 1.0$  to the point  $x = 0,0$ . In theory  $\tau_{\max} = \infty$  in all cases, since a particle rising at  $x = 0$  would never move off the back wall of the cell.

Table 4.1 Results of simulations using the solution of the Laplace Equation

Fig. No.	$g_0(x)$ : Equ <sup>n</sup> No	Froth Height cm	Nature of Froth Breakage			Froth Stability $\alpha$	Average Residence Time $\tau_{AV} = \frac{VF}{QF}$	Residence Time Ratio $\delta = \frac{\tau_{min}}{\tau_{plug}}$	$F(3\tau_{AV})$	$F(\infty)$	$\tau_{max}$ (Secs)
			Comment (Variation of flux with x)	$g_{b1}$	$g_{b2}$						
4-2-1	4.2	6.0	Constant	0,75	0,0.	0,25	20,0	0,53	0,91	1,0	87
4-2-2	4.2	6.0	Decreasing	1,00	-0,0125	0,25	20,0	0,56	0,67	0,78	8
4-2-3	4.2	6.0	Constant	0,50	0,0	0,50	10,0	0,41	0,93	1,0	45
4-2-4	4.2	6.0	Decreasing	1,00	-0,025	0,50	10,0	0,43	0,69	0,78	8
4-2-5	4.2	6.0	Constant	0,25	0,0	0,75	7,5	0,34	0,94	1,0	30
4-2-6	4.2	6,0	Decreasing	0,5	-0,0125	0,75	7,5	0,35	0,88	1,0	43
4-2-7	4.2	6,0	Constant	0,0	0,0	1,00	5,0	0,29	0,96	1,0	27
4-2-8	4.3	6,0	Constant	0,75	0,0	0,25	20,0	0,77	0,62	0,78	8
4-2-9	4.3	6,0	Constant	0,5	0,0	0,5	10,0	0,57	0,78	1,0	100
4-2-10	4.3	6,0	Constant	0,25	0,0	0,75	7,5	0,46	0,83	1,0	82
4-2-11	4.3	6,0	Constant	0,0	0,0	1,0	5,0	0,38	0,79	1,0	100
4-2-12	4.2	2,0	Constant	0,75	0,0	0,25	8,0	0,25	0,96	1,0	30
4-2-13	4.3	2,0	Constant	0,75	0,0	0,25	8,0	0,31	0,66	0,68	8
4-2-14	4.3	3,0	Constant	0,75	0,0	0,25	12,0	0,35	0,75	0,72	8
4-2-15	4.2	11,0	Constant	0,50	0,0	0,50	22,0	0,55	0,96	1,0	75

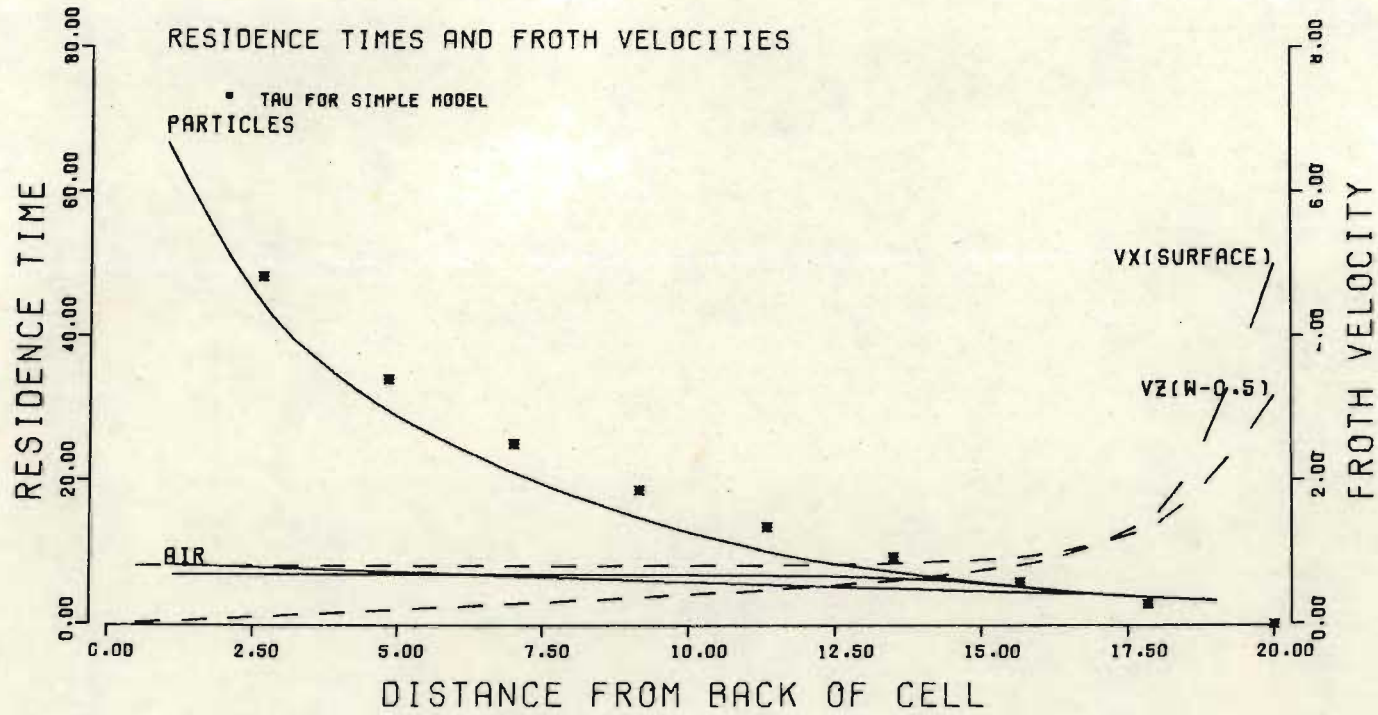
Figures 4.2.1 to 4.2.15 (on following pages).

Results of simulations of froth behaviour using the solution of the Laplace equation. In each diagram the effect of varying the parameters given in Table 4.1 on bubble streamlines, various velocity profiles and residence times is shown.

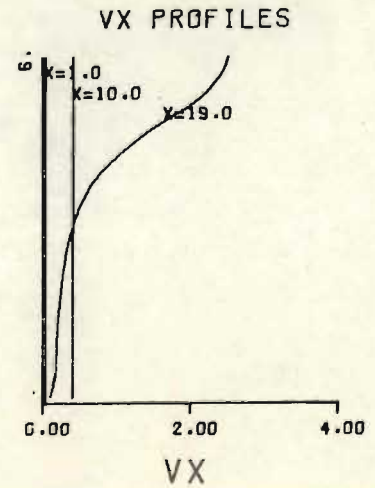
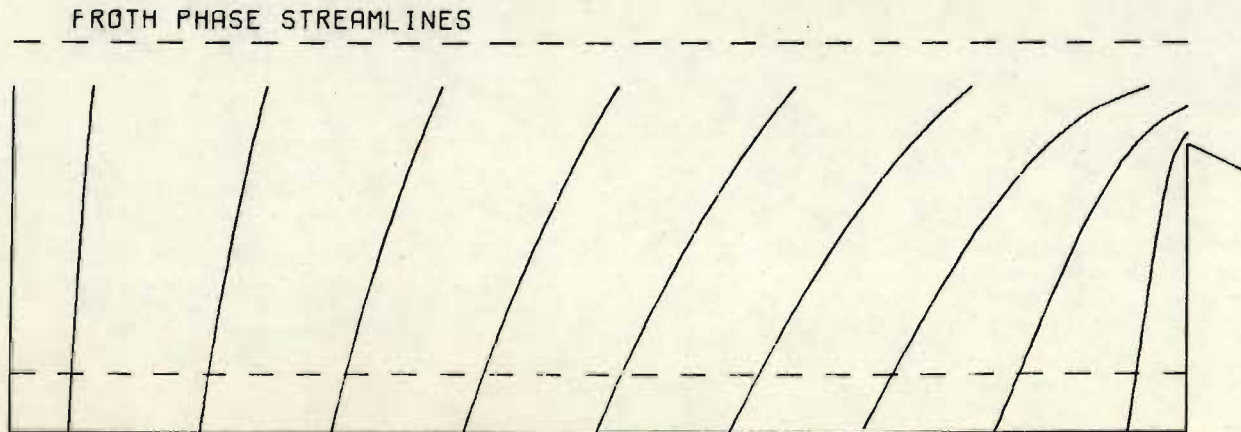
Explanation of graphs: At the bottom of the page, the streamlines followed by bubbles entering the froth phase are shown. The dashed lines indicate the profiles of the gas flux entering the froth phase and leaving through the surface of the froth (due to froth breakage). To the right of this diagram, the profiles of froth velocity crossing vertical planes at  $x=10$  and  $19$  cm. are shown. Just above the froth phase streamlines diagram the values of the parameters  $\alpha$ ,  $g_{b1}$ ,  $g_{b2}$ ,  $g_{c1}$  and  $G$  are given. A number of graphs are shown on the "RESIDENCE TIMES AND FROTH VELOCITIES" figure.

- (i) "TAU FOR SIMPLE MODEL" is  $\tau$  obtained from equation (4-11)
- (ii) The "PARTICLES" locus indicates the variation of particle residence time with distance from the back of the cell.
- (iii) The "AIR" locus shows the corresponding residence time for air bubbles.
- (iv) "VX(SURFACE)" is the velocity of the surface of the froth towards the froth lip.
- (v) "VX(W-0,5)" is the vertical velocity of froth elements across a plane  $0,5$  cm below the weir level.

Figure 4.2.1 Simulation of froth behaviour using the solution of the Laplace equation (Refer Table 4.1).



ALFR	GB1	GB2	GC1	G
0.250	0.750	0.000	5.0	400.0





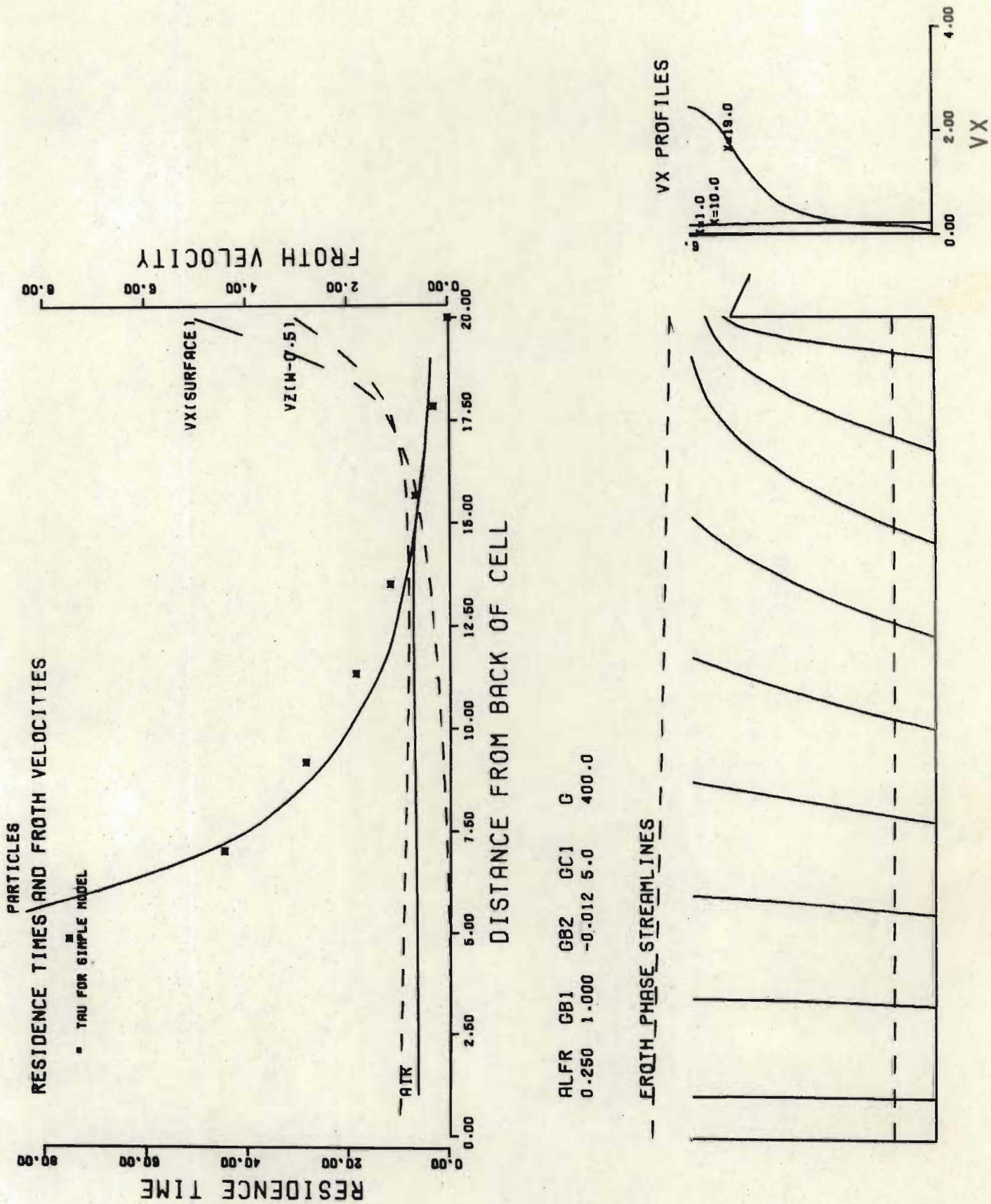


Figure 4.2.2 Simulation of froth behaviour using the solution of the Laplace equation (Refer Table 4.1).

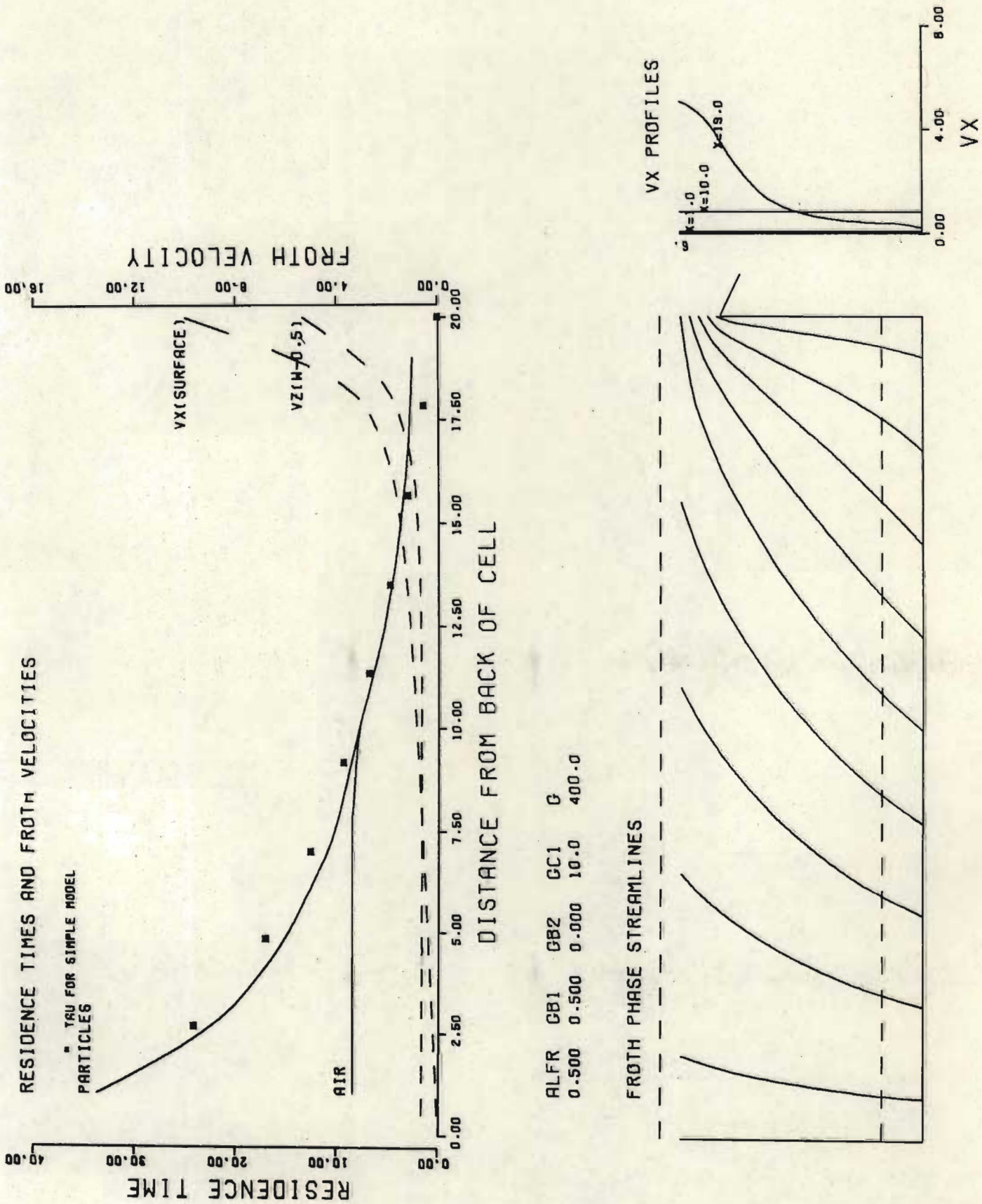


Figure 4.2.3 Simulation of froth behaviour using the solution of the Laplace equation (Refer Table 4.1).

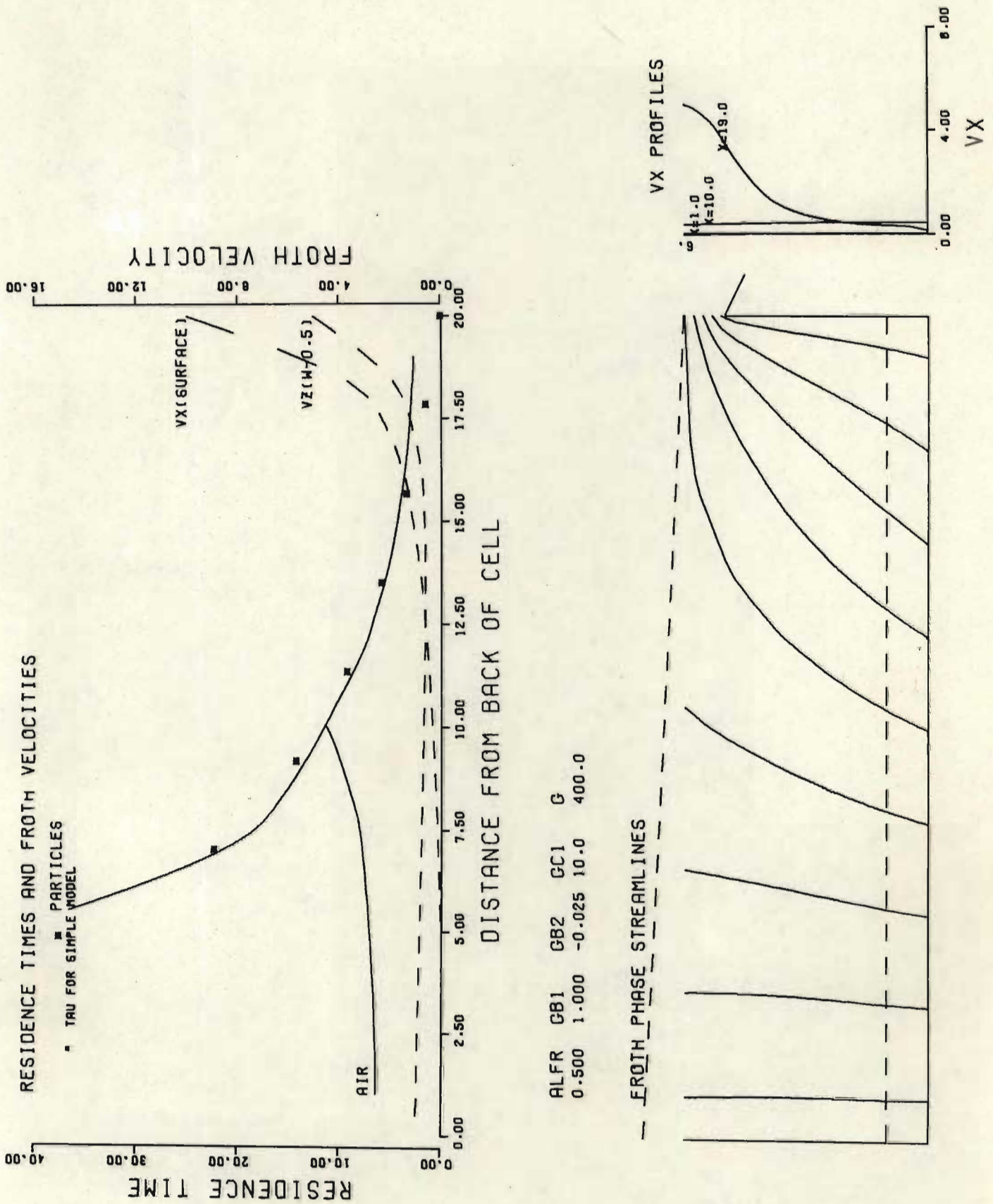


Figure 4.2.4 Simulation of froth behaviour using the solution of the Laplace equation (Refer Table 4.1).

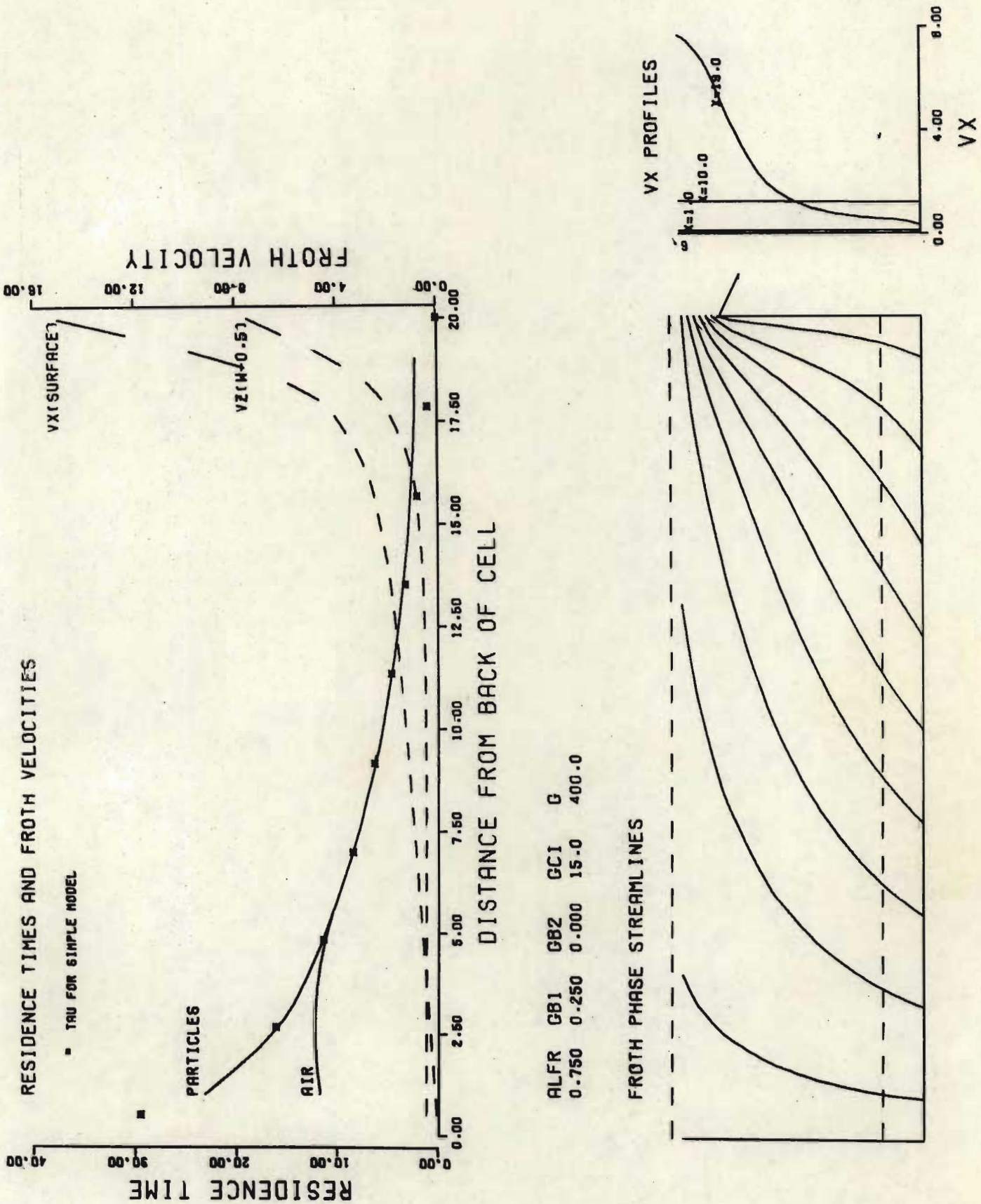
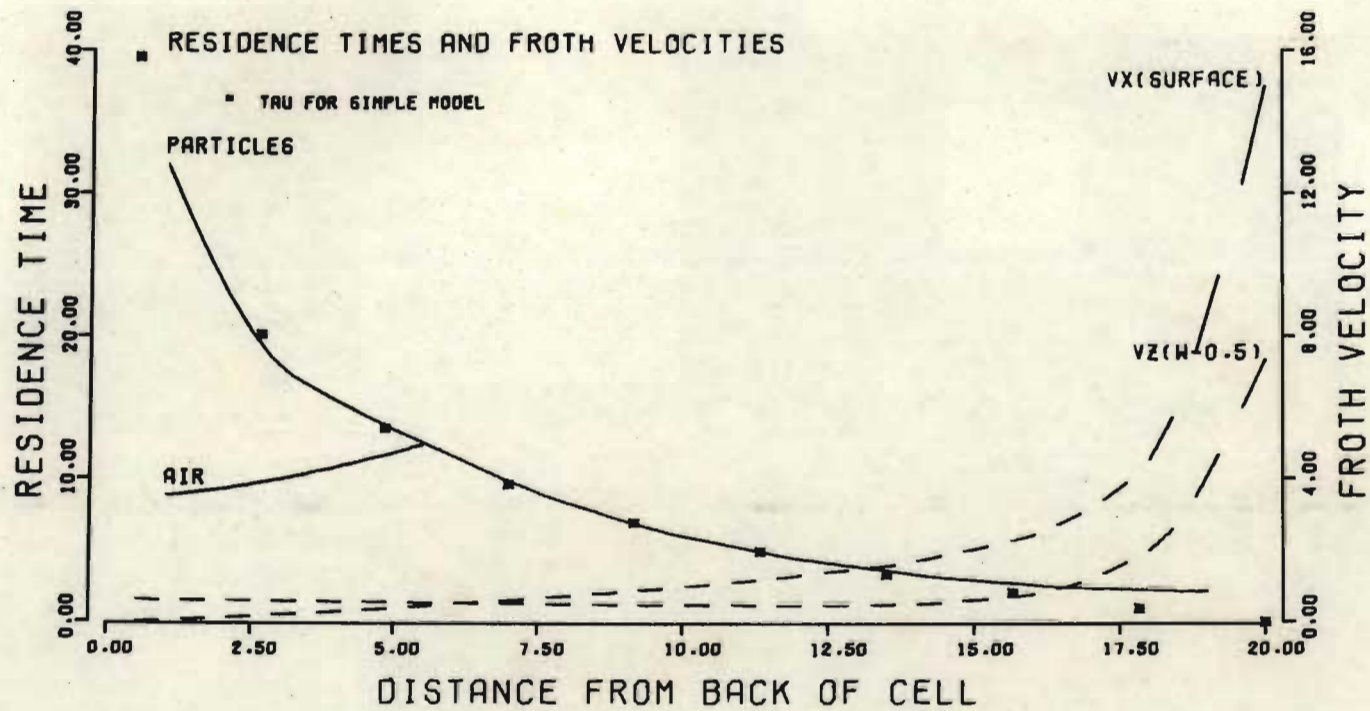
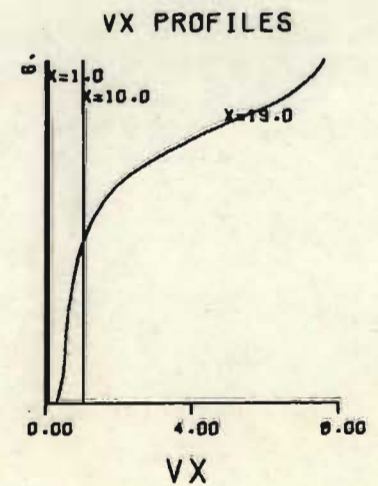
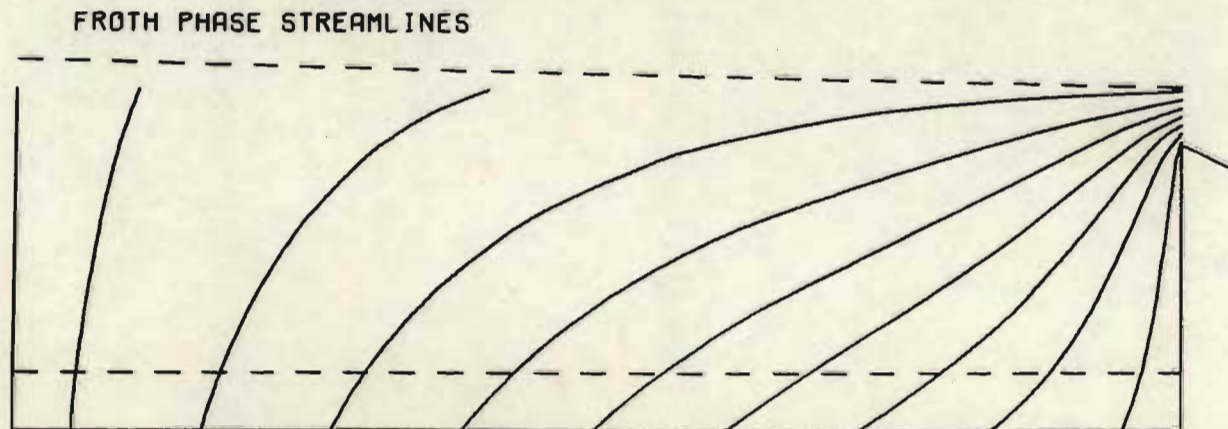


Figure 4.2.5 Simulation of froth behaviour using the solution of the Laplace equation (Refer Table 4.1).

Figure 4.2.6 Simulation of froth behaviour using the solution of the Laplace equation (Refer Table 4.1).



ALFR	GB1	GB2	GC1	G
0.750	0.500	-0.012	15.0	400.0



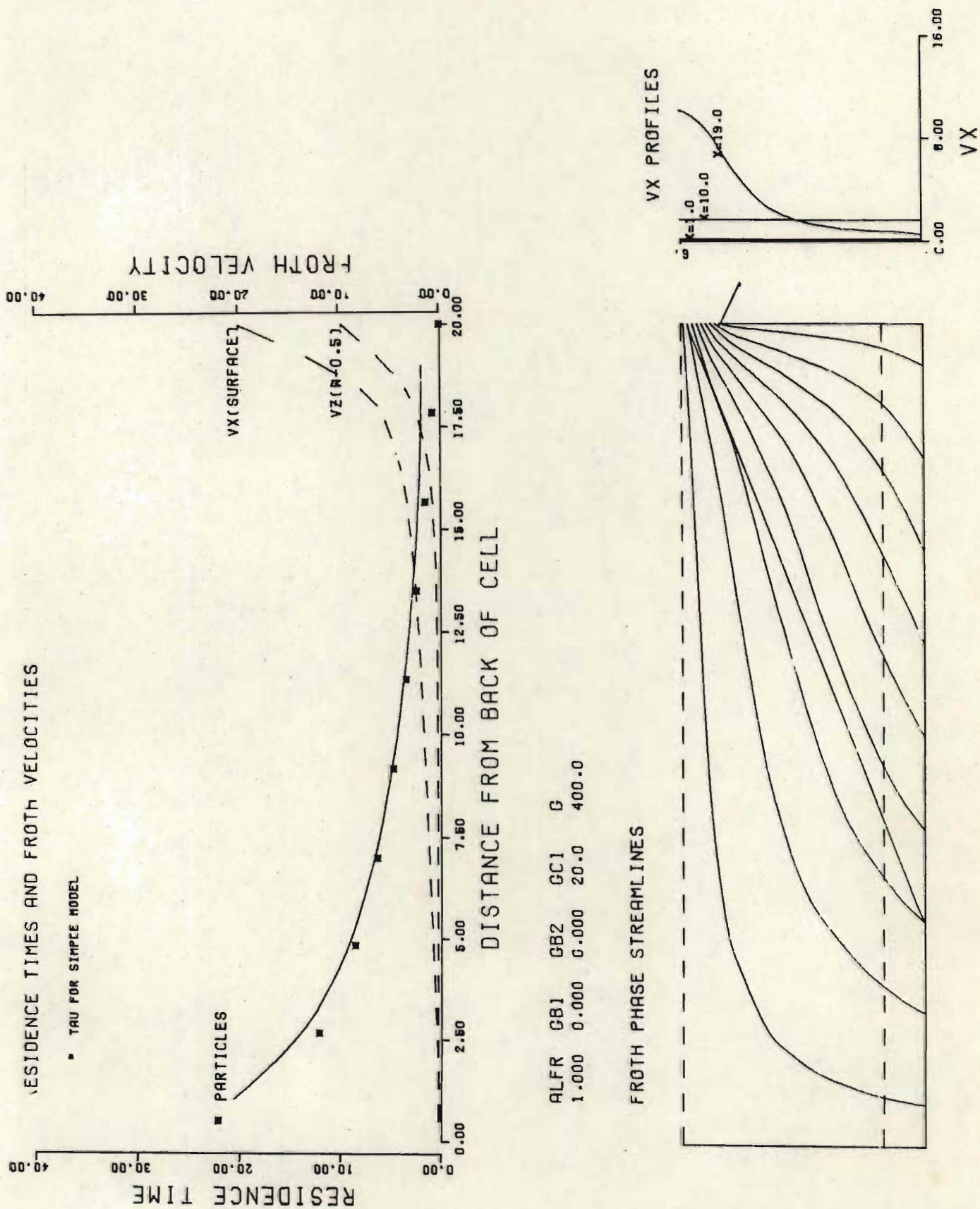
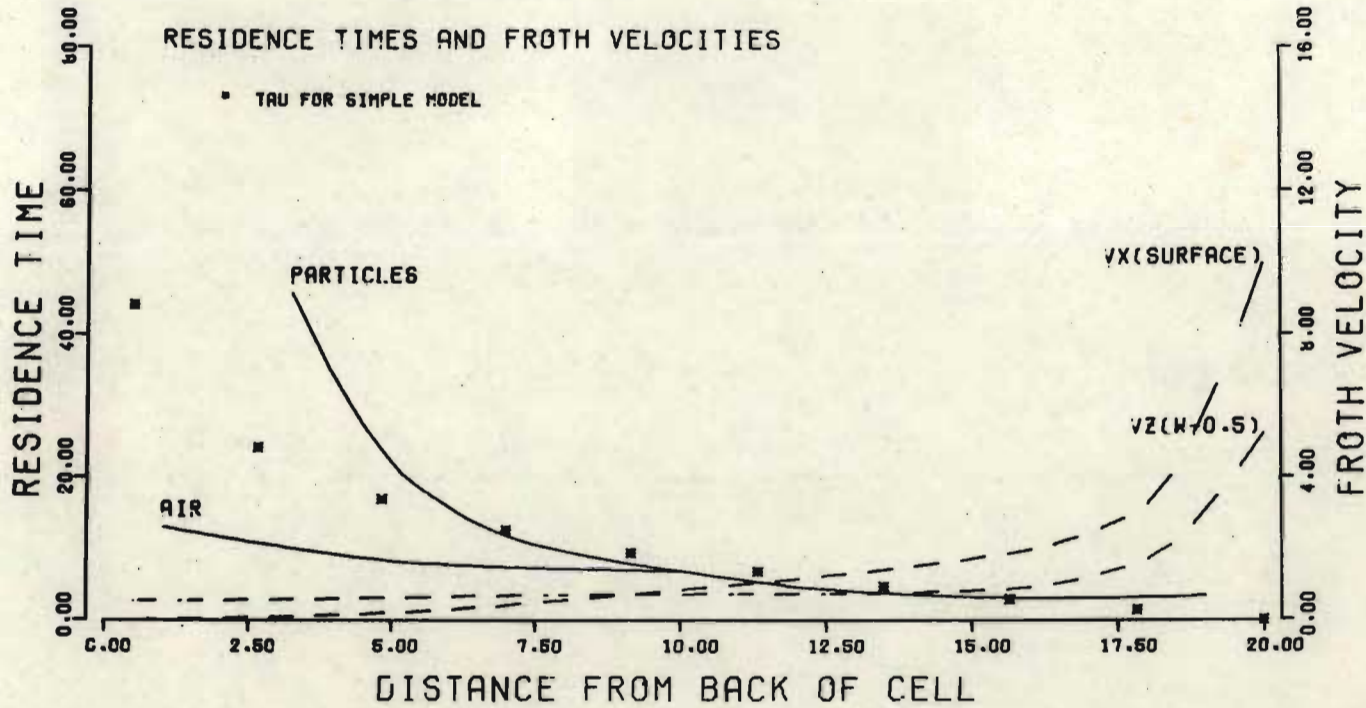


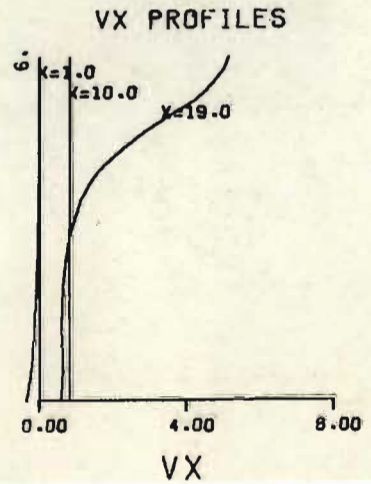
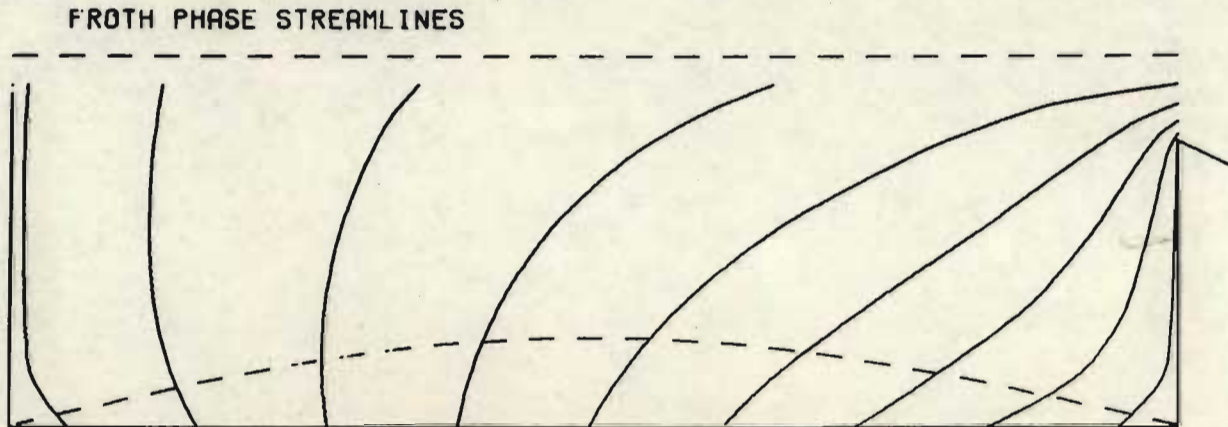
Figure 4.2.7 Simulation of froth behaviour using the solution of the Laplace equation (Refer Table 4.1).



Figure 4.2.9 Simulation of froth behaviour using the solution of the Laplace equation (Refer Table 4.1).



ALFR	GB1	GB2	GC1	G
0.500	0.500	0.000	10.0	400.0





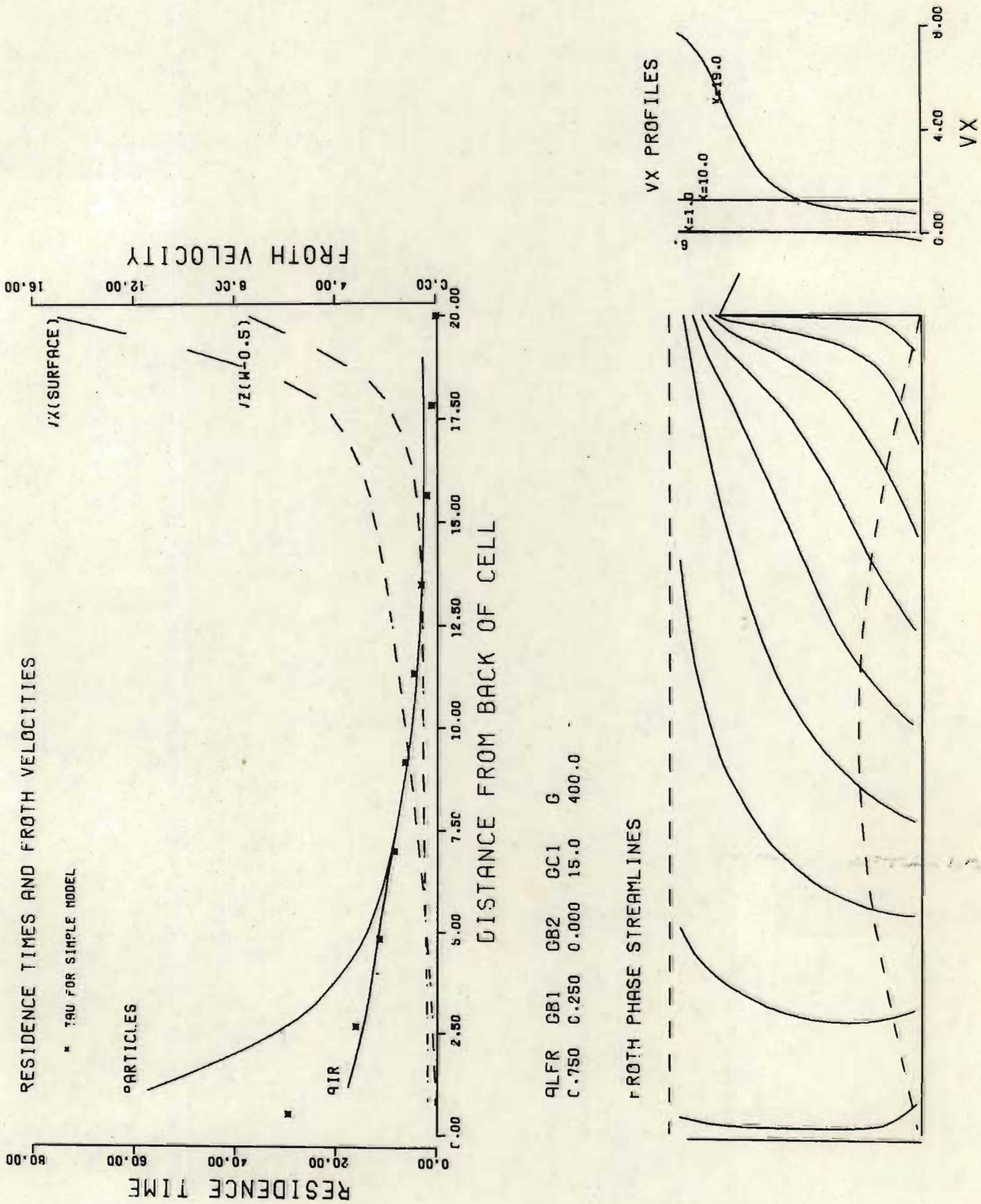


Figure 4.2.10 Simulation of froth behaviour using the solution of the Laplace equation (Refer Table 4.1).

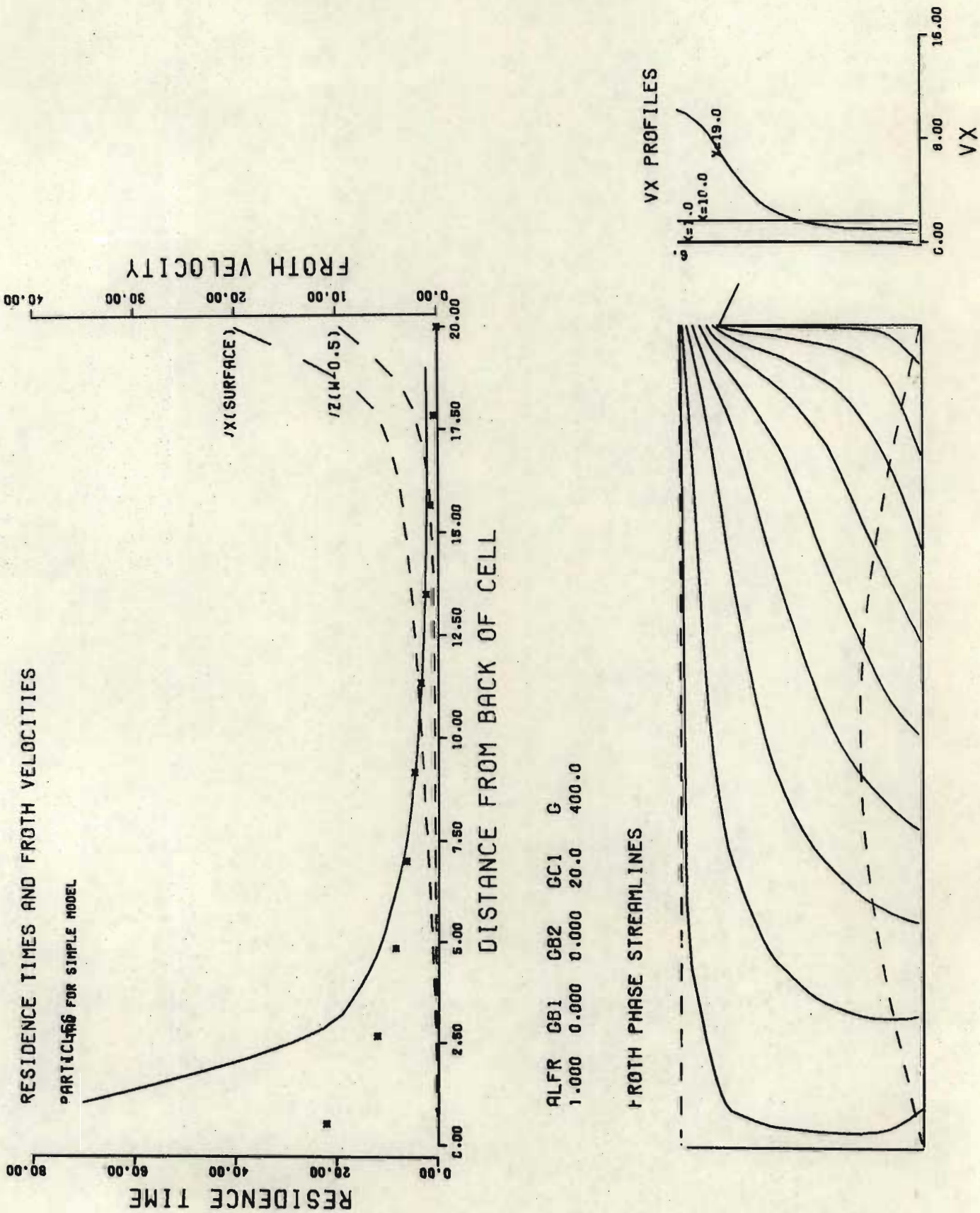


Figure 4.2.11 Simulation of froth behaviour using the solution of the Laplace equation (Refer Table 4.1).

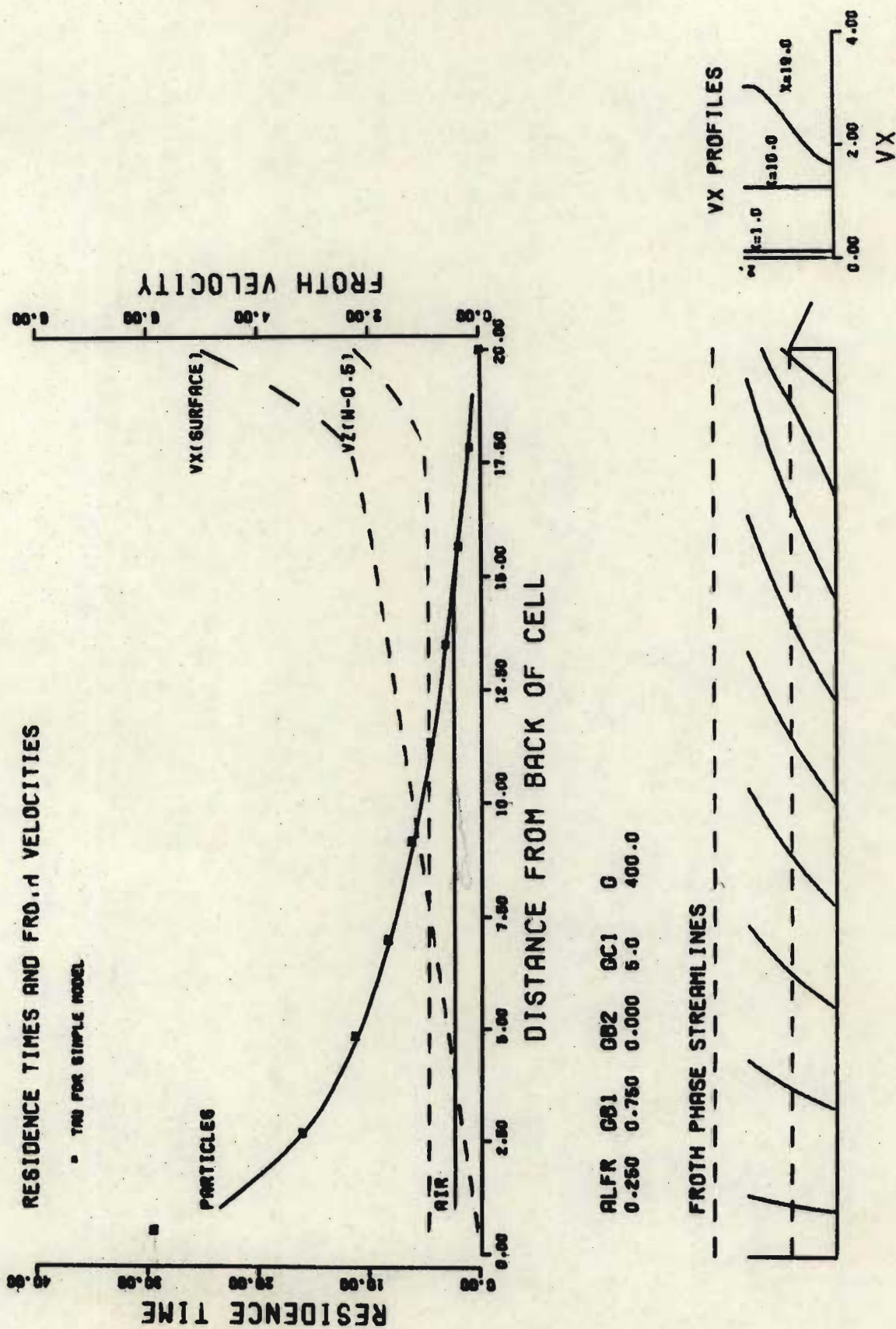


Figure 4.2.12 Simulation of froth behaviour using the solution of the Laplace equation (Refer Table 4.1).

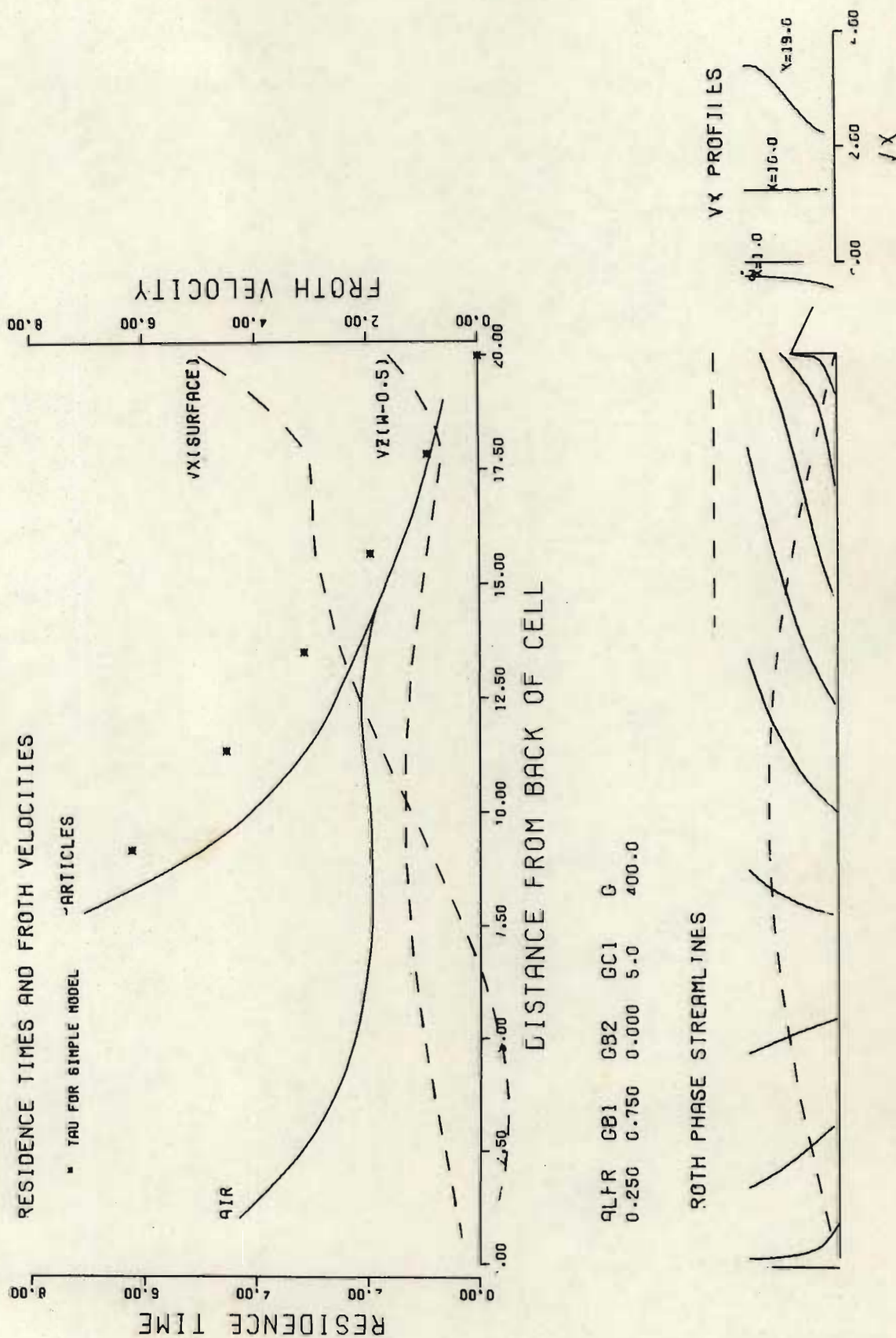


Figure 4.2.13 Simulation of froth behaviour using the solution of the Laplace equation (Refer Table 4.1).

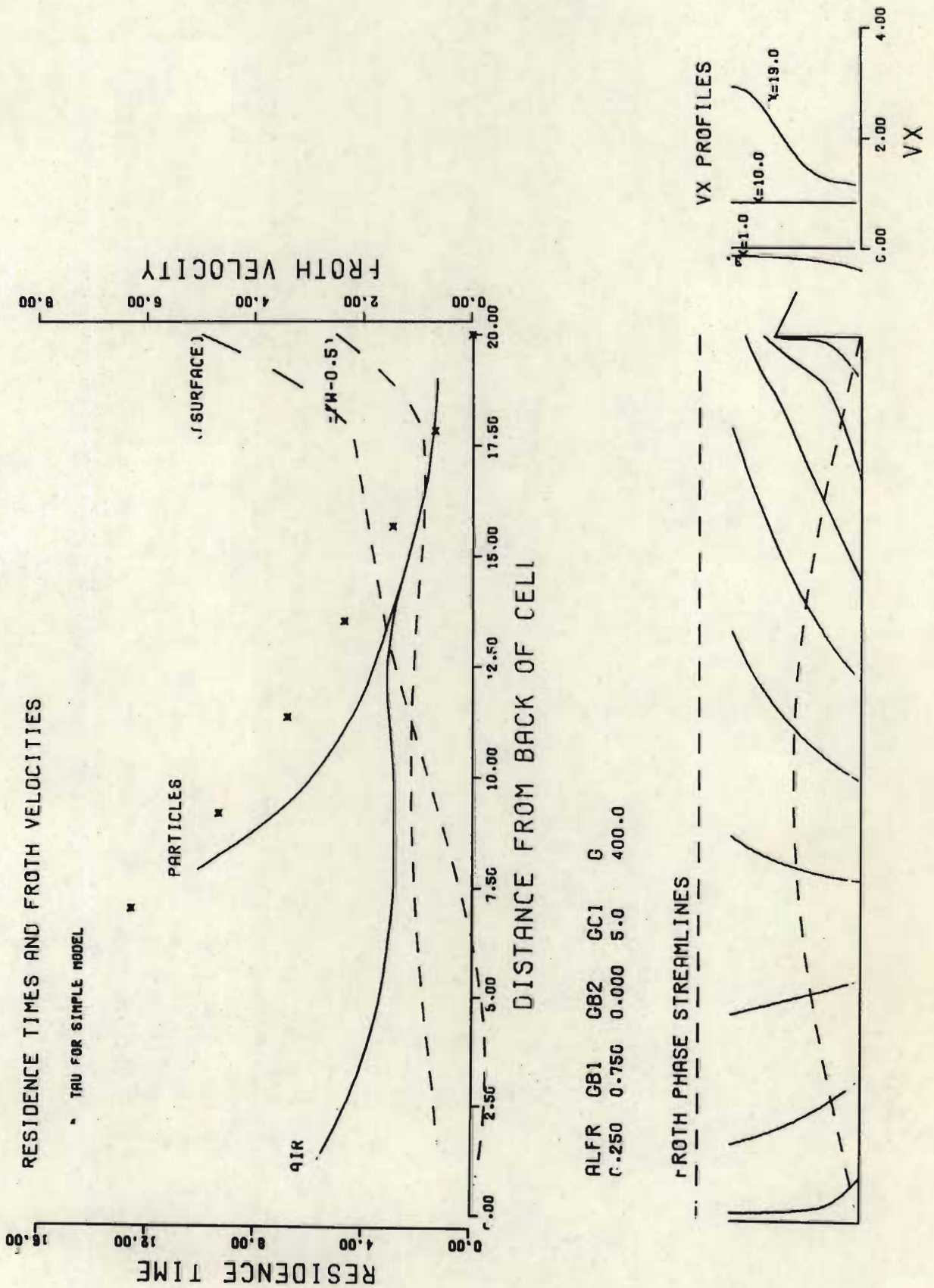


Figure 4.2.14 Simulation of froth behaviour using the solution of the Laplace equation (Refer Table 4.1).

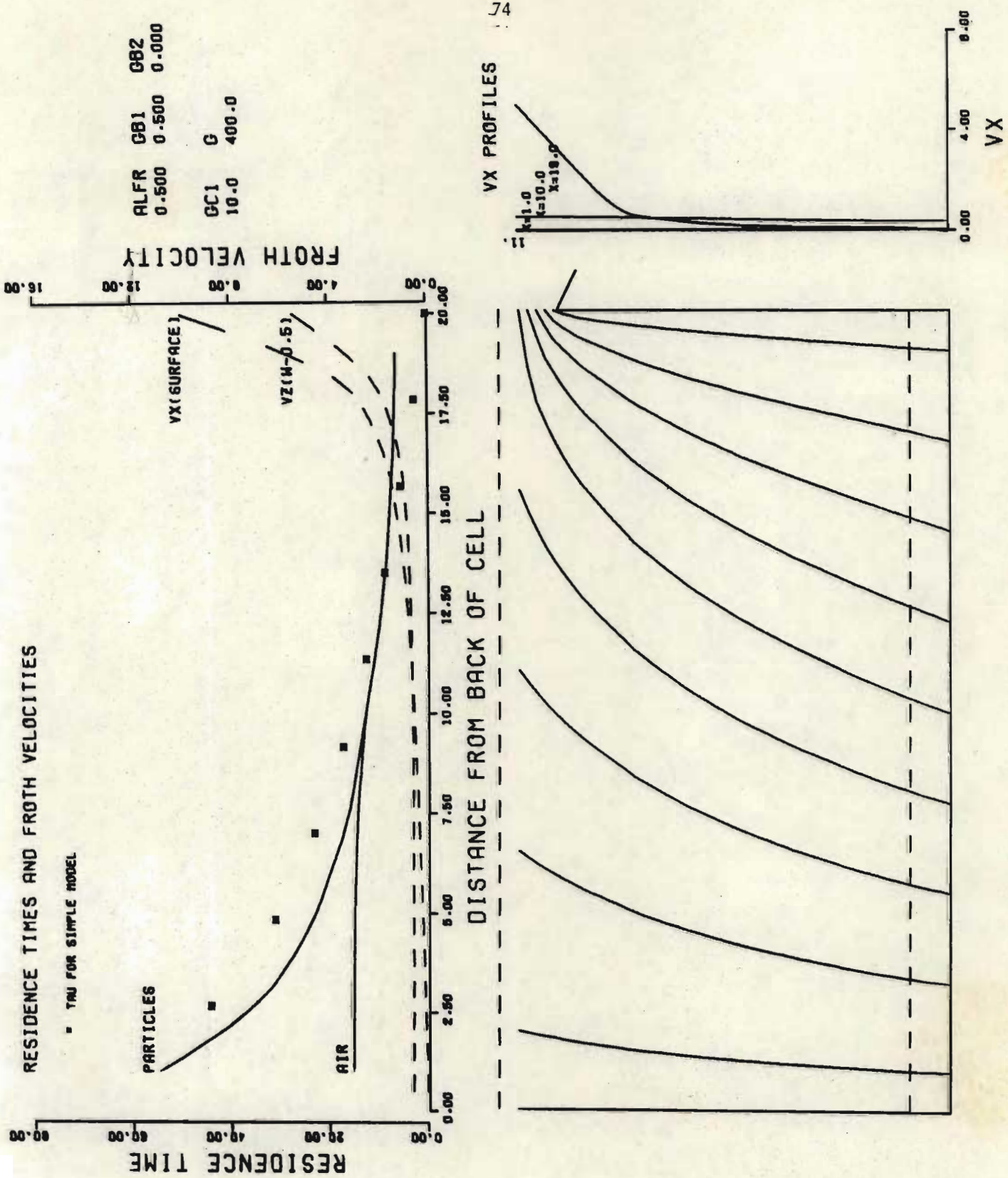


Figure 4.2.15 Simulation of froth behaviour using the solution of the Laplace equation (Refer Table 4.1).

- (iii)  $F(3\tau_{av})$  is the fraction of particles removed after three average residence times.
- (iv)  $F(\infty)$  is the fraction of particles removed at infinite time, assuming that if particles fall back into the pulp, they are not refloated.

The following points are noted on inspection of Table 4.1 and Figures 4.2.1 to 4.2.15.

(1) In general:

both the vertical ("VZ(W-0,5)") and surface ("VX(SURFACE)") velocities have their highest values near the concentrate weir. This implies that the residence time of froth elements that enter the froth near the weir are even smaller than might be expected, and would probably be responsible for most of the entrained gangue and water entering the concentrate stream;

as the froth stability increases, both the maximum and minimum residence times (as taken from the figures) decrease, resulting in increased rate of removal of all components entering the froth phase.

- (2) When a negative slope in the froth breakage function is assumed,  $F(3\tau_{av})$  decreases, implying that a portion of the material entering the froth is subjected to a larger residence time. In some cases (Figures 4.2.2 and 4.2.4) only 78% of this material eventually leaves the froth, because of negative froth velocities near the back of the cell (a phenomenon which has been observed in practice and occurs near regions in the cell where the rate of breakage of froth at a point is very close to or exceeds the rate of entry of froth into the froth phase below that point).

- (3) Negative froth velocities at the back of the cell are also obtained when  $g_f(x)$  is given by equation (4.3) and low froth stabilities or froth heights are used (Figures 4.2.8, 13). This phenomenon decreases the effective volume of the cell and possibly results in oxidation and hence deactivation of floatable particles.
- (4)  $\delta$  increases and  $\tau_{\max}/\tau_{\text{av}}$  decreases as froth height is increased (4.2.12,1,15) resulting in a narrower range of residence times. In the limit as  $h$  tends to very large values the RTD would in the absence of friction tend towards that of a plug flow vessel.
- (5) In Figure 4.3,  $\delta$  is plotted as a function of  $\alpha$  for a range of froth height values, assuming  $g_f(x)$  and  $g_b(x)$  are invariant with  $x$ . (Most of the simulations required to generate this data are not listed in Table 4.1). An empirical function was fitted to this data for use in Section 5.2.2 and has the form

$$\delta(\alpha, h) = 0,55 \exp(-,095\alpha/(h/L)^{1,5}) + 0,45 \exp(-10\alpha) \quad (4.8)$$

If such a relation could be found which fits experimental data, it would reduce by one the number of parameters in the simpler models derived in the next section, and greatly simplify the experimental determination of the remaining parameters.

#### 4.2.2 One-dimensional flow approximation: a tractable model

In the development of this model the following assumptions are made:

- (i) Rate of flux of air bubbles and mineral particles across the froth-slurry interface is invariant with position in that interface.



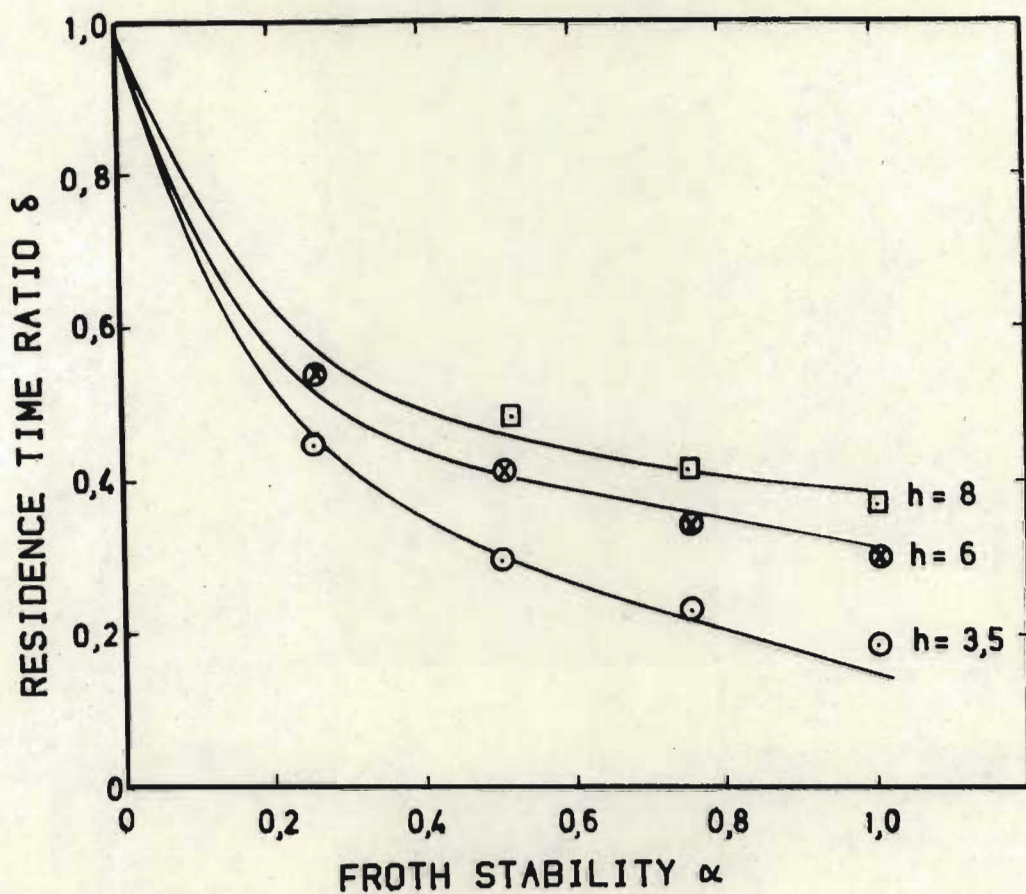


Figure 4.3 Variation of residence time ratio  $\delta$  with froth stability  $\alpha$  (obtained from the solution of the Laplace equation). The lines are obtained from equation (4.8).

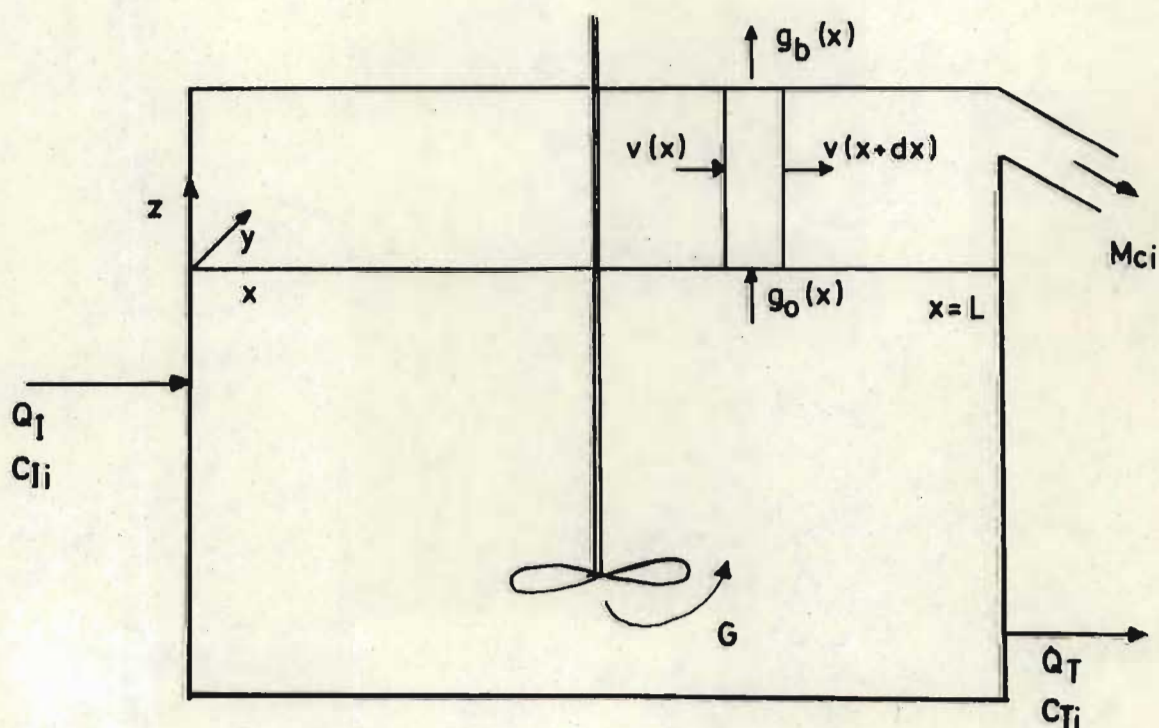


Figure 4.4 Volume balance across a differential element in the froth column.

- (ii) Rate of froth breakage on the surface of the froth phase varies linearly with distance from the back of the cell.
- (iii) Froth moves towards the weir at a velocity  $v(x)$  which does not vary with froth depth.
- (iv) The froth is well-drained, i.e. at any point the volume occupied by liquid and particles is small.

#### 4.2.2.1 Variation of froth velocity with distance from the back of the cell

The streams flowing into and out of a differential element of thickness  $dx$  per unit of froth chamber width are shown in Figure 4.4.

A volume balance gives

$$h \frac{dv(x)}{dx} = g_o - g_b(x)$$

and if

$$g_b(x) = g_{b1} + 2g_{b2}x$$

then

$$v(x) = \frac{x}{h} [(g_o - g_{b1}) - g_{b2}x] \quad (4.9)$$

If  $\alpha$  is the fraction of gas entering the froth phase which leaves in the concentrate, then the amount which leaves due to froth breakage per unit of froth chamber width is

$$(1-\alpha)g_o L = \int_0^L g_b(x) dx$$

Thus

$$(1-\alpha)g_o = g_{b1} + g_{b2}L$$

or  $g_o - g_{b1} = \alpha g_o + g_{b2}L$

Substituting in equation (4.9) gives

$$v(x) = \frac{x}{h} [\alpha g_o + g_{b2}(L-x)] \quad (4.10)$$

#### 4.2.2.2 Froth Residence Time Distribution

The residence time of a froth element entering at point  $x$  is given by

$$\begin{aligned} \tau_1(x) &= \int_x^L \frac{1}{v(x)} dx \\ &= \frac{h}{a} \ln \left[ \frac{L}{x} \frac{(a-g_{b2}x)}{(a-g_{b2}L)} \right] \end{aligned} \quad (4.11)$$

where  $a = \alpha g_o + g_{b2}L$  is introduced to simplify notation.

Note that as  $x \rightarrow L$ ,  $\tau_1(x) \rightarrow 0$  which is not physically realistic since particles entering the froth phase at  $L$  have to rise at least a distance  $\omega$  before entering the concentrate stream, and will hence have a finite residence time,  $\tau_{\min}$ . In terms of the residence time ratio  $\delta$  we have

$$\tau_{\min} = \frac{\delta h}{g_o} \quad (4.12)$$

and write a modified expression for the residence time,

$$\tau_2(x) = \tau_1(x)/\bar{C} + \tau_{\min} \quad (4.13)$$

where  $\bar{C}$  is a normalising constant which ensures that the average residence time is not changed:

$$\tau_{av} = \frac{1}{L} \int_0^L \tau_1(x) dx = \frac{1}{L} \int_0^L \tau_2(x) dx = h/\alpha g_o$$

It can easily be shown that this condition requires that

$$\bar{C} = 1/(1-\alpha\delta) \quad (4.14)$$

The residence time distribution of the froth phase is now easily derived.  $E_c(\tau)$  is the normalised response at the concentrate weir to an impulse of perfectly floatable particles entering at and uniformly distributed across the froth/slurry interface. By definition, the fraction of particles entering between  $x$  and  $x+dx$  will arrive at the concentrate weir at a time between  $\tau+d\tau$  and  $\tau$  later, where  $\tau$  and  $x$  are related by (4.13). Thus

$$E_c(\tau)d\tau = dx/L$$

or

$$\begin{aligned} E_c(\tau) &= \frac{1}{L} \frac{dx}{d\tau} \\ &= \frac{\bar{C}a^2(a-g_{b2}L) \exp\left\{\frac{a\bar{C}}{h}(\tau-\tau_{min})\right\}}{h[g_{b2}L + \alpha g_o \exp\left\{\frac{a\bar{C}}{h}(\tau-\tau_{min})\right\}]^2} \end{aligned} \quad (4.15)$$

for  $\tau \geq \tau_{min}$

The froth phase RTD is related to the concentrate RTD by equation (4.1).

#### 4.2.2.3 Model for Mass Flowrate of Concentrate Components

If the rate of detachment of particles of component  $i$  is such that a fraction

$$r_i(\tau) = \exp(-k_{fi}\tau)$$

remains in the froth after a time  $\tau$ , then the mass flowrate of that component is

$$M_{ci} = \int_{\tau_{\min}}^{\infty} E_f(\tau) e^{-k_{fi}\tau} m_{fio} d\tau$$

where  $m_{fio}$  is the flux of component  $i$  into the froth phase across the froth/slurry interface. Fortunately perhaps, this integral can be solved only for the case where  $g_{b2} = 0$ , in which case

$$M_{ci} = \frac{\epsilon_f \bar{C} \alpha_0 M_{fio} \exp(-k_{fi} \tau_{\min})}{h(k_{fi} + \alpha_0 C/h)} \quad (4.16)$$

$M_{fio}$  is the flowrate of component  $i$  into the froth phase and may be obtained from an appropriate pulp phase model, eg.

$$M_{fio} = k_{pi} A C_{ti}$$

where  $k_{pi}$  is the first-order pulp rate constant,  $A$  is the bubble surface area available for bubble attachment and  $C_{ti}$  is the tailings concentration.

At this point the use of the modified form for  $\tau(x)$  {equation (4.13)} can be justified. If the unmodified form had been used, i.e.  $\delta = 0,0$ ,  $\bar{C} = 1,0$  then

$$M_{ci} = \frac{\epsilon_f \alpha_0 M_{fio}}{h(k_{fi} + \alpha_0/h)} \quad (4.17)$$

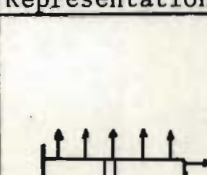
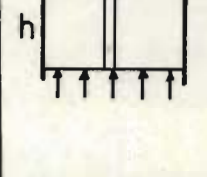
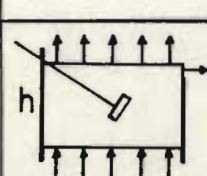
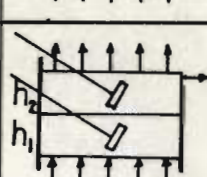
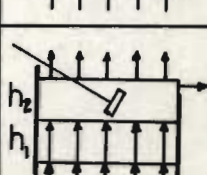
For components which fall out rapidly from the froth, e.g. gangue components, (4.17) predicts much higher concentrate flowrates than (4.16) for given values of the parameters  $k_{fi}$  and  $\alpha$ . Thus if (4.17) is used for estimating parameters from experimental data, inordinately large values of  $k_{fi}$  will be obtained compared with the more realistic values that estimation with (4.16) would yield. The estimation of  $\alpha$  would also be distorted. This being the case, it is unlikely that (4.17) could be used for scale-up purposes, especially for systems where the quantities appearing in the exponent in (4.16) are varied, i.e.  $h$  and  $g_o$  which affect  $\tau_{min}$ .

#### 4.2.2.4 Comparison with other Simple Models of Froth Phase RTD

Several other models may be entertained for describing froth phase behaviour, being based on various combinations of the perfectly mixed and plug flow concepts. These are tabulated in Table 4.2. Models 1 and 2 are for the case where  $g_{b2} = 0$ , to allow comparison with other models. Note that Model 1 has the same form as Model 3, both of them together with Model 4 suffering from the defect that the minimum residence time is zero, which does not accord with experimental reality. Model 2 has the same form as Model 5, and both models have the same number of arbitrary parameters; however, Model 5 is not physically realistic and its second parameter has little physical significance. For these reasons Model 2 is deemed superior to all other models listed.

The equivalence of the RTD expressions for Models 1 and 3 is of more than passing interest. Model 3 is the model of Harris and Rimmer, which is the only froth phase model to have been given serious attention in the literature, and has been used successfully for interpreting experimental data;

Table 4-2 Comparison of Models for Froth Phase RTD

Model No.	Diagrammatical Representation	Description	RTD $E(\tau)$	Cumulative RTD $F(\tau)$	Parameters
1		Plug flow movement of froth towards overflow weir	$E(\tau) = \frac{1}{\bar{\tau}} \exp(-\tau/\bar{\tau})$	$F(\tau) = 1 - \exp(-\tau/\bar{\tau})$	$\alpha$
2			$E(\tau) = \frac{\bar{C}}{\bar{\tau}} \exp\left[-\frac{\bar{C}}{\bar{\tau}}(\tau - \tau_{\min})\right]$ $\tau \geq \tau_{\min}$	$F(\tau) = 1 - \exp\left[-\frac{\bar{C}}{\bar{\tau}}(\tau - \tau_{\min})\right]$ $\tau \geq \tau_{\min}$	$\alpha, \delta$
3		Perfectly mixed froth phase	$E(\tau) = \frac{1}{\bar{\tau}} \exp(-\tau/\bar{\tau})$	$F(\tau) = 1 - \exp(-\tau/\bar{\tau})$	$\alpha$
4		Two perfectly mixed volumes in series	$E(\tau) = \frac{\exp(-\tau/\tau_2) - \exp(-\tau/\tau_1)}{\tau_2 - \tau_1}$	$F(\tau) = 1 - \frac{\tau_2 \exp(-\tau/\tau_2) - \tau_1 \exp(-\tau/\tau_1)}{\tau_2 - \tau_1}$	$\alpha, h_1$ or $h_2$
5		Plug flow volume in series with perfectly stirred volume	$E(\tau) = \frac{1}{\tau_2} \exp\left[-\frac{(\tau - \tau_1)}{\tau_2}\right]$	$F(\tau) = 1 - \exp\left[-\frac{(\tau - \tau_1)}{\tau_2}\right]$	$\alpha, h_1$ or $h_2$

Definition of Terms:  $\bar{\tau} = h/\alpha g_0$ ;  $\tau_1 = h_1/g_0$ ;  $\tau_2 = h_2/\alpha g_0$ ;  $\tau_{\min} = h\delta/g_0$ ;

$$\bar{C} = 1/(1-\alpha\delta)$$

however, as noted in Chapter 1, no claim has been made as to the validity of the model (Harris 1978); in fact, the plug flow concept is generally more conformed to reality. Closer inspection of Model 1 reveals an interesting fact; as shown in Appendix C, the concentration of a component in the froth phase is independent of distance from the back of the cell. Since Model 1 does not allow for vertical variations in the froth phase, this means that Model 1 is in fact identical to Harris and Rimmer's model in terms of the equations that it produces. This may be part of the reason for the usefulness of their model; the equations they derived are in fact applicable to both the perfectly mixed and plug flow concepts.

#### 4.2.2.5 Comparison of Model 2 with the 2-dimensional streamline model

If the streamline model developed in Section 4.2.1 is the best quantitative description of the behaviour of the froth phase available, then it will be instructive to compare Model 2 with it to discover what the relationships between Model 2 parameters and the streamline model parameters are. This was done by computing ten points on the cumulative RTD curve for streamline model simulations for a wide range of conditions, and using the parameter estimation program described in Section 5.2.1.2 to estimate Model 2 parameters by least squares regression for each condition. The results are tabulated in Table 4-3 and illustrated in Figure 4.5. Parameters were estimated for two cases, the first where all the parameters  $\alpha$ ,  $\delta$  and  $g_{b2}$  were assumed variable, and the second where  $g_{b2}$  was held at zero. For all the streamline simulations  $g_{b2}$  was in fact zero. As can be seen from the table, estimating all 3 parameters produced a substantial reduction in the sum of squares, but the parameters differ greatly from those used in the simulation. As is shown in Section 5.2.2, this is due to the high correlation that exists between  $\alpha$  and  $g_{b2}$ . Substantially improved estimates of  $\alpha$  are obtained holding  $g_{b2}$  at zero. In both cases  $\delta$  is substantially underestimated. This is due to the rapid increase in  $F(\tau)$  (for the Laplace simulations) near  $\tau=0$ , which results from the nearly plug flow of froth from the froth-slurry interface near the



Table 4.3 Comparison of Model 2 and Streamline Model

Simulation Specifications			Parameters estimated under these conditions:							$\delta$ estimates from simulation data
No	h	$\alpha$	All 3 parameters free				$\alpha, \delta$ free $g_{b2}=0$			
			$\alpha$	$\delta$	$g_{b2}$	$S^2$	$\alpha$	$\delta$	$S^2$	
1	2,0	,25	,28	,07	-,0021	,00011	,26	,04	,00045	,07
2	2,0	,25	,48	,12	-,036	,004	,38	,016	,016	,22
3	3,0	,25	,51	,19	-,035	,015	,34	,06	,032	,41
4	3,5	,25	,37	,27	-,010	,0021	,28	,12	,008	,34
5	3,5	,50	,64	,12	-,014	,0044	,52	,14	,007	,25
6	3,5	,75	,81	,13	-,009	,0083	,73	,10	,0114	,21
7	3,5	1,00	,95	,09	-,0025	,013	,94	,08	,014	,17
8	8,5	,50	,73	,37	-,013	,013	,62	,33	,021	,47
9	8,5	,75	,87	,30	-,0066	,025	,82	,28	,028	,41
10	8,5	1,00	1,0	,25	0,0	,038	1,0	,25	,038	,36
11	10,0	,25	,58	,52	-,021	,012	,38	,34	,037	,64
12	10,0	,50	,76	,44	-,012	,018	,664	,412	,026	,54

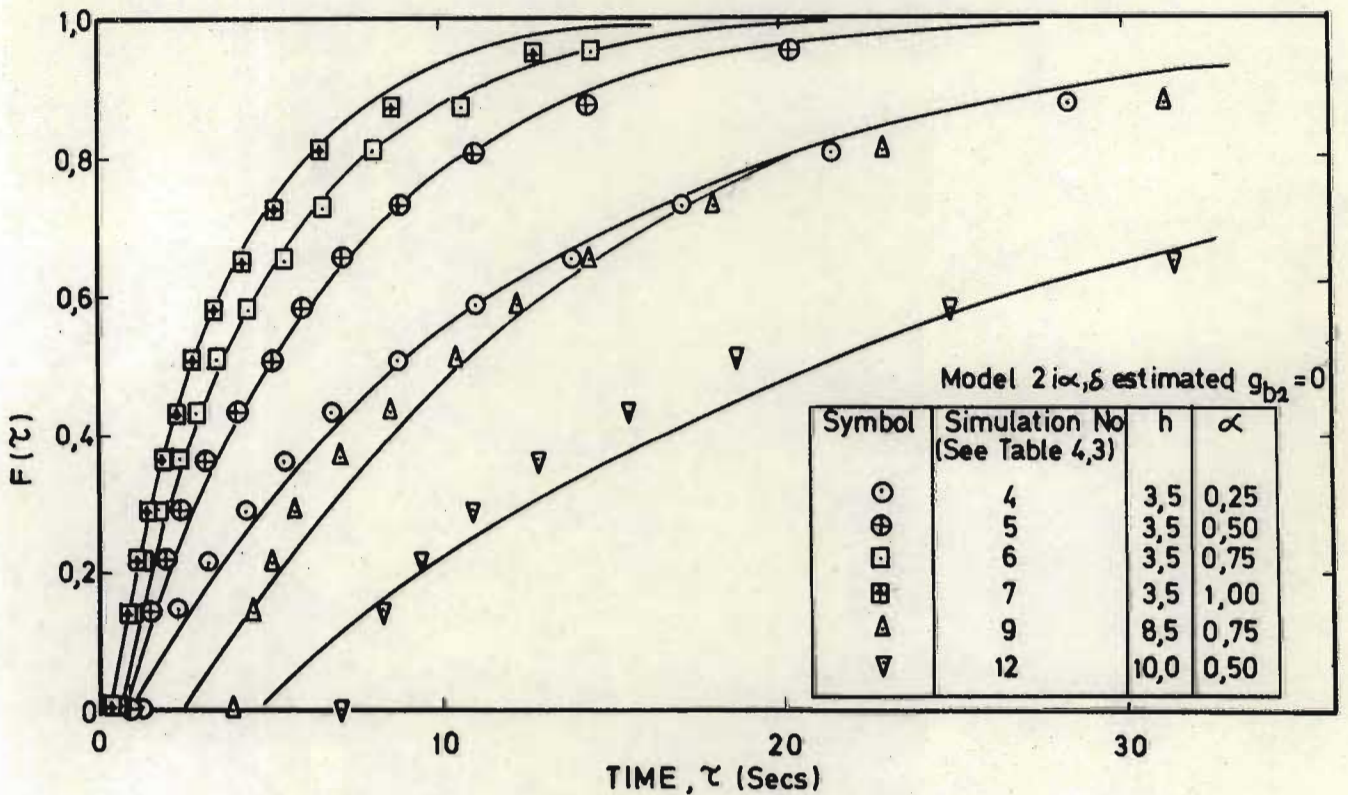


Figure 4.5 Fits of Model 2 to streamline model simulations

concentrate weir. Poor fits are obtained for large froth heights, which is to be expected since in these cases vertical movement of the froth (ignored in the development of Model 2) is substantial.

This analysis indicates that, when using Model 2 for rationalising experimental data, estimating  $g_{b2}$  is unlikely to yield trustworthy insight into the real performance of flotation froths; and that  $\delta$  is likely to be underestimated; and that, if  $g_{b2}$  is given a value of zero, then good estimates of  $\alpha$  will be obtained. The experimental verification of this will now be considered.

## CHAPTER FIVE

### Residence Time Distribution in Flotation Froths : Experimental Determinations

#### 5.1 Development of apparatus and technique

Conventional impulse-response testing was used to obtain RTD data, and these results are supported by an alternative method which is mentioned in section 4.2.2.1 i.e. the measurement of the variation of froth velocity with the distance from the back of the cell. Small polystyrene balls were used as a tracer. Because of their extremely low s.g. of approximately 0,03 (which when compared with the s.g. of water is almost negligible), they are assumed to behave as the bubbles in the froth phase do. In fact they behave as extremely floatable particles would, rising with the bubbles to the top of the froth and then travelling towards the froth lip on the surface of the froth.

The arrangement whereby tracer was introduced into the cell is illustrated in Figure 5.1. A 3 cm. diameter syringe was used to inject a pulse of tracer into the eye of the impeller. The latter distributes the particles throughout the cell volume from where they rise into the base of the froth with a finite distributed residence time  $\tau_p$ . They are then transported to the froth lip by the movement of the froth with residence time  $\tau_f$ . They flow down the projecting concentrate launder with residence time  $\tau_c$ , and are collected in a series of beakers over a number of discrete time intervals. It is evident that  $\tau_p$  and  $\tau_c$  need to be quantified if an estimate of froth residence time  $\tau_f$  is to be obtained. In addition a uniform distribution of particles at the base of the froth phase is essential because of the assumption of constant flux of gas across the froth-slurry interface which was made in the development of the model which is used to interpret the data.

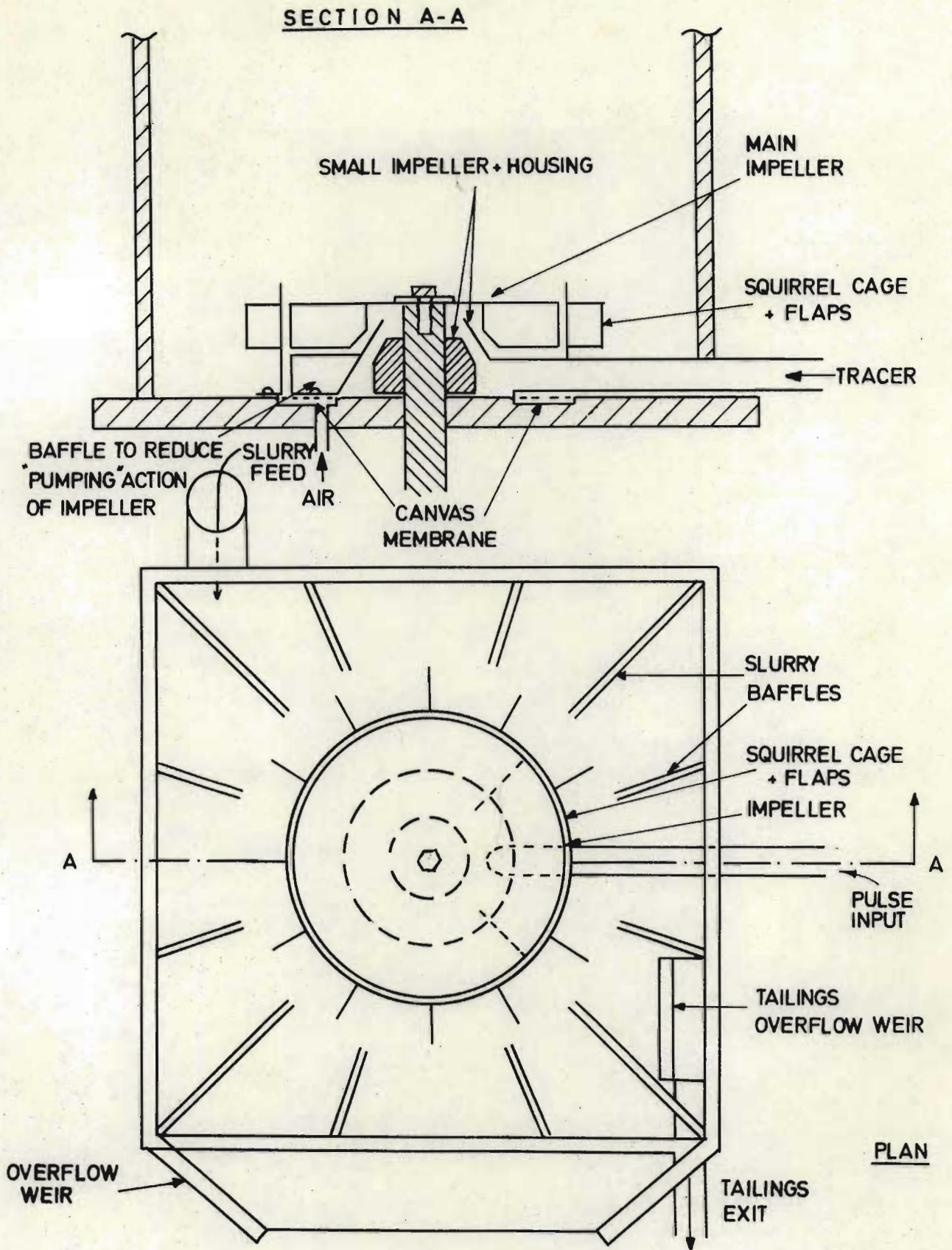


Figure 5.1 Arrangement used for injecting tracer into impeller region, and for achieving a uniform distribution of tracer at the pulp/froth interphase.

### 5.1.1 Production of a uniform tracer distribution at the base of the froth.

Substantial development of equipment was required before a satisfactory distribution of tracer at the base of the froth was obtained. Figure 5.1 illustrates the final arrangement that was used. The following steps were followed in its development, and Table 5.1 shows what improvements were obtained with each step. In each case the distribution was measured by dividing the surface of the liquid into sections with a perspex grid as shown in Figure 5.2. and counting the number of particles that reported in each section. Since the major requirement was that the distribution be uniform with respect to distance from the back of the cell, the total number of particles in sections 1, 2 and 3, 4, 5 and 6 and 7, 8 and 9 are shown. The difference between the largest and smallest of the latter three numbers and the ratio between the standard deviation and the mean for the nine measurements is shown as well, and form measures of the improvement obtained at each step. Initially only the impeller, air induction arrangement and large slurry baffles were present in the cell, as described in section 2.2

- (i) A nylon pipe was inserted through a hole in the side of the cell and directed towards the impeller as shown. Two measurements showed that a large proportion of particles were reporting in partition 5. This was due to the excessive circulation of water above the impeller which caused the low density particles to be attracted to the low-pressure region in the centre of the cell.
- (ii) A "squirrel" cage was constructed which was designed to minimise rotation of the liquid by forcing it to leave the impeller zone in a radial direction, as shown in Figure 5.1. In this case a substantial fraction of the tracer particles reported at the rear of the cell. This was assumed to be due to ineffective mixing of the tracer particles in the impeller zone.
- (iii) A small aluminum cone was used to ensure that particles could only enter the zone beneath the impeller through a

Table 5.1 Attempts to obtain a uniform distribution of tracer particles at the base of the froth.

Modifi- cation No.	Total No. of Particles	% of particles reporting in section no.									Std Dev/ Mean	% of total in sections			Range of last 3 columns
		1	2	3	4	5	6	7	8	9		1+2+3	4+5+6	7+8+9	
(i)	98	6	6	4	19	24	9	12	8	12	.59	16	52	32	36
	99	12	10	4	2	38	17	4	1	12	.97	26	57	17	40
(ii)	122	6	6	5	10	7	14	27	13	12	.61	17	31	52	35
	115	3	5	6	17	8	19	16	10	16	.54	14	44	42	30
	193	11	4	8	12	3	11	19	13	19	.51	23	26	51	28
	197	8	3	4	9	7	10	28	14	17	.69	15	26	59	44
(iii)	188	8	10	13	16	13	6	13	11	10	.27	31	35	34	4
	271	18	6	7	17	7	3	20	11	11	.54	31	27	42	15
	210	17	8	7	15	3	9	19	9	13	.47	32	27	41	14
	366	8	5	10	11	7	14	18	11	16	.38	23	32	45	22
(iv)	256	14	12	5	9	8	21	12	7	12	.42	31	38	31	7
	332	13	15	7	7	9	15	8	8	18	.38	35	31	34	4
	210	9	13	12	13	11	13	10	8	11	.17	34	37	29	8
	506	8	14	9	15	12	10	8	12	12	.23	31	37	32	6

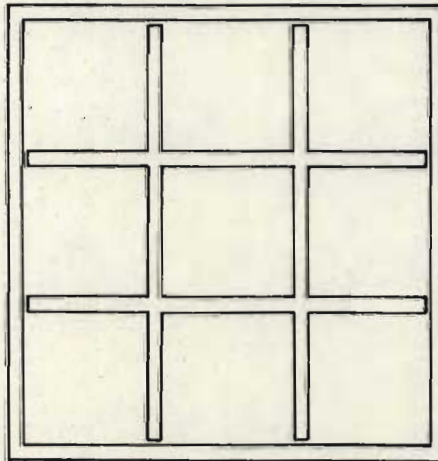


Figure 5.2 Division of pulp surface into 9 segments for measurement of distribution of tracer in the pulp/froth interface

3 mm. annulus around the impeller shaft. A small impeller machined out of an aluminum disc was fastened to the impeller shaft inside the cone to improve mixing of the particles in the cone. Negligible improvement was obtained. Careful examination of the flow patterns in the liquid phase ( as revealed by particles suspended therein) during agitation revealed that the impeller was in fact acting as a pump, sucking water from the front of the cell and pumping it out towards the back; hence the uneven distribution of particles.

- (iv) Three small baffles were inserted below the impeller which effectively eliminated this pumping action of the impeller. After the first two tests shown, certain of the vanes in the squirrel cage were bent to change the distribution of the high-velocity fluid coming from the impeller zone. The improvement obtained was deemed sufficient to allow continuation of the next phase of the program.

#### 5.1.2 Measurement of RTD of tracer particles in the liquid phase.

By removing the particles that had reached the surface of the liquid phase (after a pulse had been injected into the impeller zone) in rapid succession with a series of 6 "scrapers" an estimate of the cell residence time distribution was obtained. The apparatus used is shown in Figure 5.3. The perspex section was fastened to the front of the cell as shown in Figure 5.4 and, before commencement of the experiment the scrapers were clamped in position at the back of the cell. Two pairs of guides, the first just below the surface of the water and the other a fixed distance above them ensured that each scraper moved smoothly across the surface of the cell when the retaining clamp was released. 200 gram weights and rubber bands were used to provide the necessary motive power. The weights were adjusted to give the highest speed of travel which did not result in liquid being thrown from the cell. The elastic band operated only over the first 5 cm of travel, providing a more rapid initial acceleration than could be achieved using gravity alone.

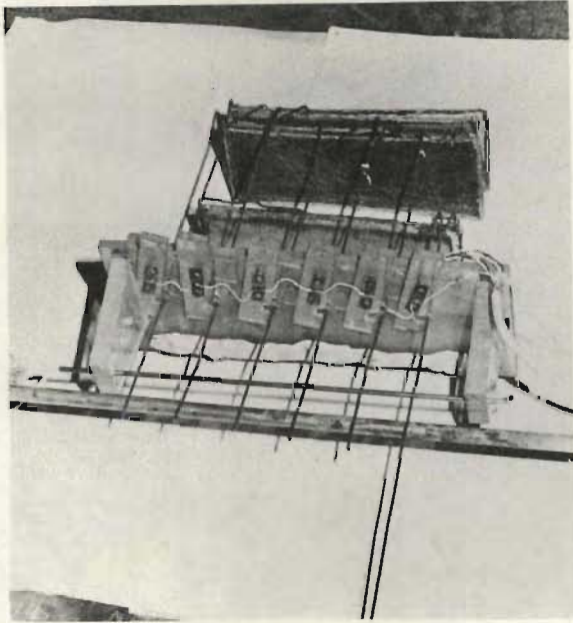


Figure 5.3 Device used for scraping tracer particles from the surface of the cell while measuring the RTD of these particles in the pulp.

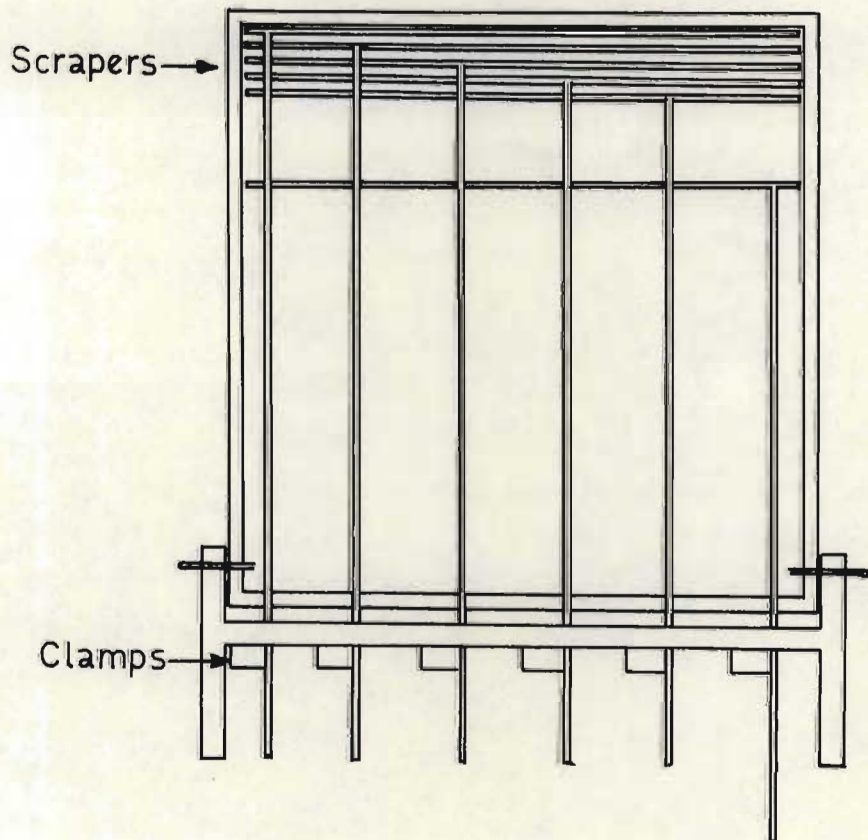


Figure 5.4 Plan View showing how the device illustrated in Figure 5.3 was mounted on the cell.



Timing was done electronically using the circuit shown in Figure 5.5. Initially all the switches were open, and a flat bed recorder (with paper movement set at 500 mm/min) recorded zero volts. Injection of the pulse of tracer particles closed the switch which brought resistor  $R_p$  into the circuit, with a consequent step change in the recorded voltage. The release of each scraper closed the switches which successively brought resistances  $R_1$ - $R_6$  into circuit, resulting each time in a step change in recorded voltage. The resistances were chosen to provide approximately equal steps in voltage, and a recorder output such as that shown in Figure 5.6 was obtained. The first scraper swept most of the particles that had reached the surface of the cell onto a net below the overflow weir. Successive samples were caught between the scrapers and each such sample together with all particles not caught by any of the scrapers were counted. These numbers were normalised to add up to unity and then divided by the relevant time intervals to provide histogram distributions as shown in Figure 5.6.

It was found that the distribution varied with gas rate probably due to the fact that the hydrophobic polystyrene particles were "floated" to the cell surface by attached bubbles. To facilitate interpretation and condensation of the data, the expression

$$E_p(\tau) = \alpha_p^2 \tau e^{-\alpha_p \tau}$$

was used as a model for the distribution.

The cumulative distribution is given by

$$F_p(\tau) = 1 - (1 + \alpha_p \tau) e^{-\alpha_p \tau} \quad (5.1)$$

and  $\alpha_p$  was estimated by least squares regression using Nelder and Mead's (1965) hill-climbing technique. The correspondence between theory and experiment is shown in Figure 5.6 for one of the experiments. Greater precision would obviously be desirable but the large scatter in the data precluded a search for a better model.

The parameter  $\alpha_p$  is plotted as a function of Gas rate in Figure 5.7. A straight line was drawn through the data as shown and its slope and intercept were calculated:

$$\alpha_p = 0,0022 G + 0,833 \quad (5.2)$$

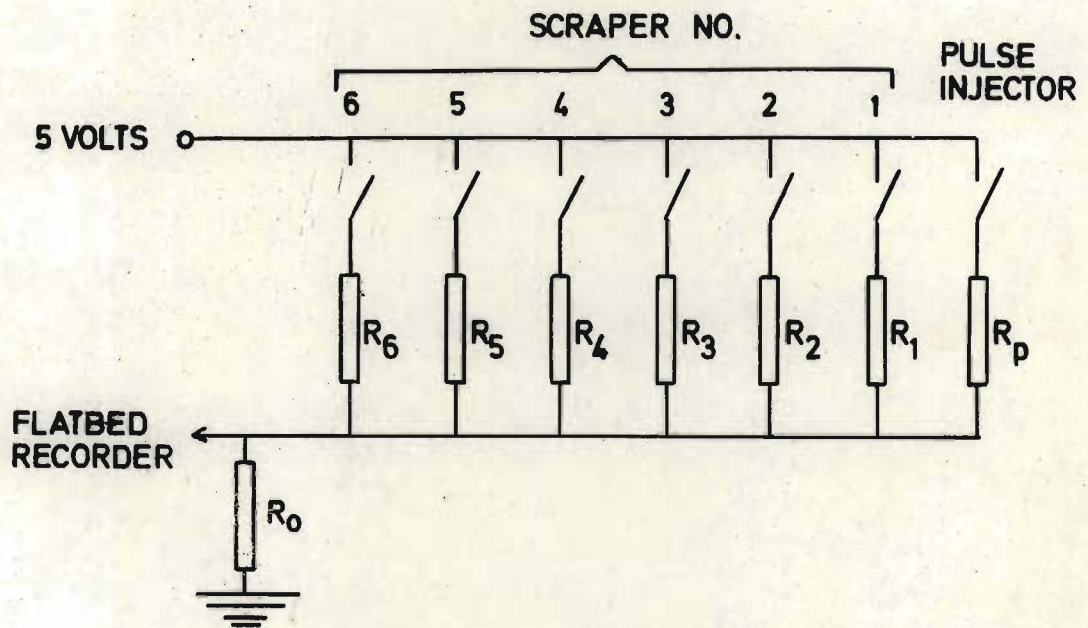


Figure 5.5 Circuit used for timing pulp phase RTD measurements.

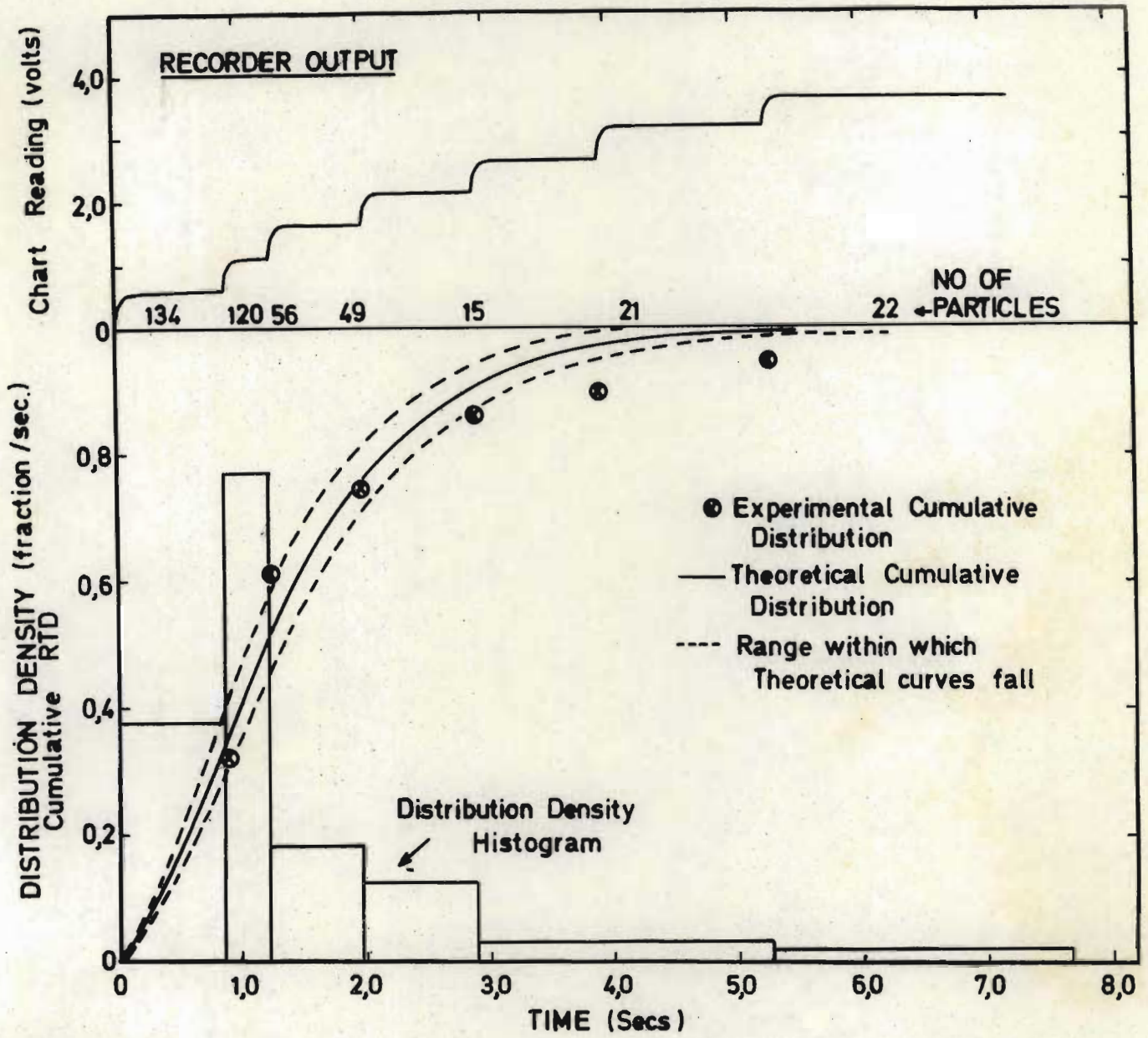


Figure 5.6 Recorder output and data obtained from pulp phase RTD measurements.

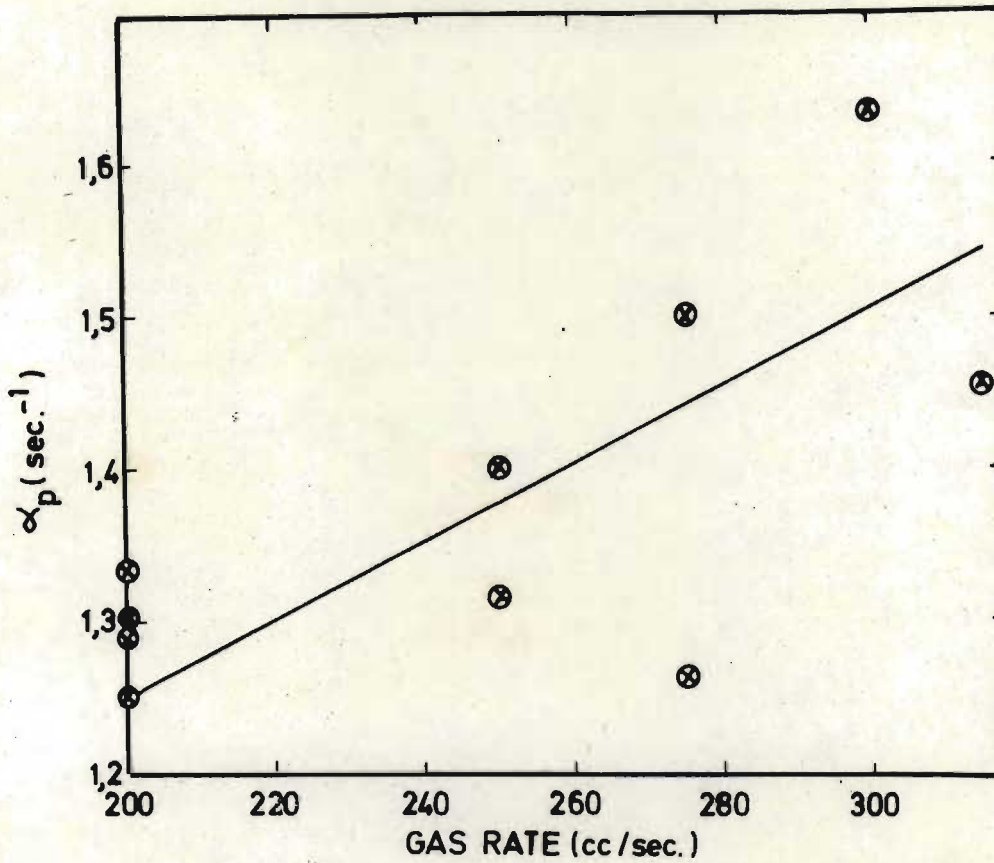


Figure 5.7 Variation of  $\alpha$  with gas rate for pulp phase RTD.

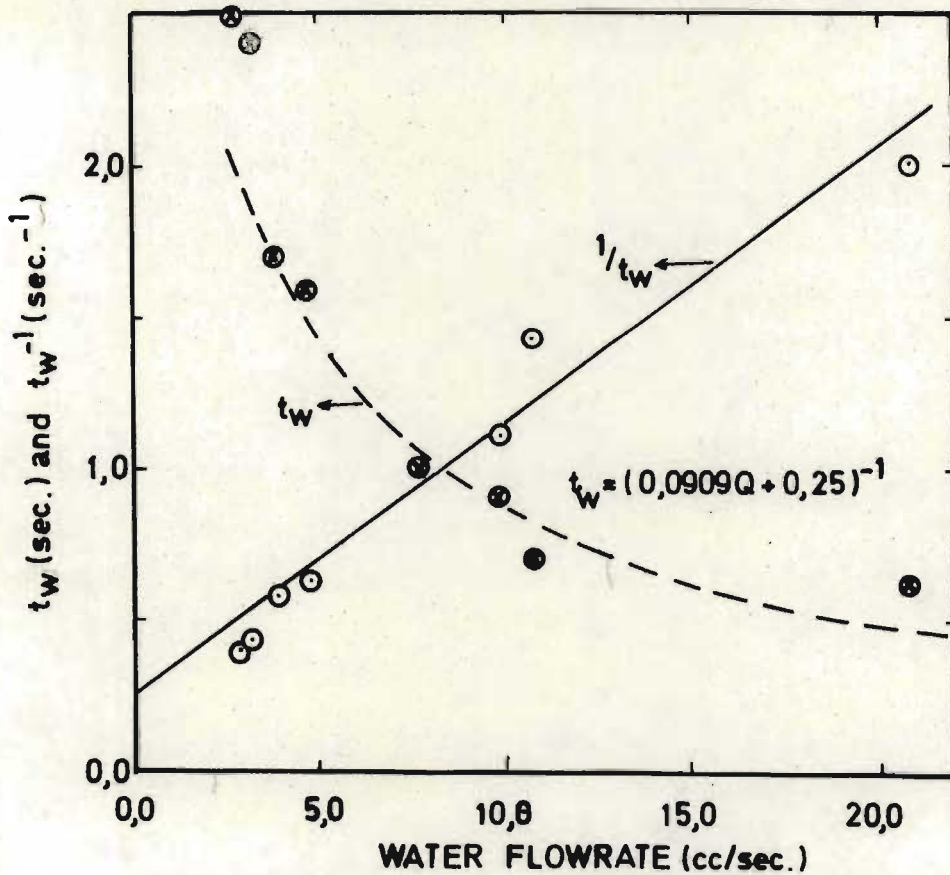


Figure 5.8 Variation of concentrate weir residence time and its inverse with water flowrate.

Besides the fact that an estimate of cell RTD had been obtained, these experiments yielded valuable information in their own right. The average value was larger, and the distribution more scattered than had been expected, and, if bubble behaviour parallels that of polystyrene particles, then this work calls into question the assumption of various authors (e.g. King et al 1970) that bubble residence time in flotation cells can be quantified by using an average value. It also provides a possible method of measuring the RTD of bubbles of any given size if this should be required; again, this depends on the existence of a correlation between the behaviour (probably best quantified in terms of terminal rise velocity) of polystyrene particles and bubbles.

### 5.1.3 Measurement of the Residence Time of Particles on the overflow weir.

An overflow weir of finite length as shown in Figure 5.1 was required to ensure that particles fell into the sampling vessels. The residence time of particles on this weir were measured as a function of gas rate  $G$  and weir height,  $w$  and were found to correlate well with the froth flowrate as shown in Figure 5.8, for various combinations of  $G$  and  $w$  values. The weir residence time could thus be calculated from

$$\tau_c = \frac{1}{.0909Q + .25} \quad (5.3)$$

A maximum error of .4 sec (20%) occurred for very low flow rates.

### 5.1.4 Measurement of the Cell Residence Time Distribution

Timed samples were collected in a train of plastic beakers mounted in a close-fitting channel of galvanised iron. Ten to fifteen concentrate samples allowed sufficient data to be collected to define the cell RTD. Timing was achieved by using an audible signal produced by an electronic metronome at regular preset intervals to regulate the manual insertion of tracer, movement of the sample train, etc. A stop watch was used to obtain the total sampling period.

The following steps were followed for each residence time distribution measurement:

- (i) Load a small volume of tracer particles into the tracer inlet tube and attach syringe to the tube.
- (ii) Set control variables (froth height, gas rate) and allow 5 minutes to attain steady state.
- (iii) Switch on timer to produce audible signals at intervals of  $\Delta t$  (between 2 and 3 secs.).
- (iv) At a chosen signal, insert the first beaker below the concentrate weir, and start the stopwatch. Designate this time  $t = -\Delta t$ .
- (v) At the next signal, ( $t=0$ ) depress the plunger as forcefully as possible to inject the tracer into the impeller zone.
- (vi) For the next few periods, move the beaker train to allow sample collection in successive beakers for one  $\Delta t$  period each. (Beaker no.1 will always contain a sample for two  $\Delta t$  periods).
- (vii) Once most of the tracer (approximately 70%) has been collected, increase the number of periods per sample as seems most appropriate, e.g. if froth is flowing very slowly, use 5 periods per sample, whereas for faster moving froth two periods may be adequate. The requirement that must be met is that all the tracer particles which report in the concentrate must be collected in the sample train.
- (viii) At the end of the last sampling period remove the beaker, stop the stop watch and reduce the gas rate to zero. Record the total time taken and the number of  $\Delta t$  samples

contained by each beaker. The sum of all the individual sample times should add up to this total time.

- (ix) Count the number of particles in each beaker and measure the total volume of water collected during the experiment. This gives a measure of the water flow-rate, which in turn allows one to estimate the residence time of particles on the concentrate weir from the correlation obtained in Section 5.1.3.
- (x) Count the number of particles adhering to each side and the back of the cell.

Analysis of this data is discussed in section 5.2.

#### 5.1.5 Measurement of the Velocity of the Surface of the froth

As shown in section 4.2.2.2, certain assumptions allow the derivation of the following formula for froth velocity as a function of distance from the back of the cell,  $x$ :

$$v(x) = \frac{\bar{C}x}{h} [\alpha g_0 + g_{b2}(L-x)]$$

If the flux of gas across the froth-slurry interface,  $g_0$ , is known, then it should in principle be possible to estimate the froth stability  $\alpha$  and the slope of the froth breakage function,  $g_{b2}$  from experimental data. Alternatively, once  $\alpha$  and  $g_{b2}$  have been estimated from residence time measurements, measurements of froth velocity can be correlated with simulated surface froth velocity profiles obtained from the solution of the Laplace equation described in section 4.2.1. Thus these measurements provide a means of checking parameter values estimated from residence time tests. (see section 5.2.5).

The method used was as follows: a camera was mounted above the cell and focussed on the surface of the flowing froth. A stop watch was clamped in the camera's field of view (see Figure 5.9). The desired operating conditions (frother concentration, froth height and gas rate)



Figure 5.9 Measurement of froth velocity by recording photographically the co-ordinates of blackened polystyrene particles at a sequence of time intervals.



were set and the residence time distribution was measured as described in the previous section. Immediately afterwards a number of blackened polystyrene balls were sprinkled on the surface of the froth, the stop-watch was started and a succession of photographs were taken at intervals of between 2 and 5 seconds duration. Analysis of the photographs thus obtained produced a set of coordinates for selected particles or particle clusters at known times, and thus froth surface velocities could be calculated.

## 5.2. Experimental Design and Analysis of Data

Two sets of experiments were done to obtain RTD measurements as a function of frother concentration, froth height and gas rate. Table 5.2 and Figures 5.10.1 and 5.10.2 indicate the two designs used and Table 5.2 contains the parameters that were estimated from the data. Series A was a fairly comprehensive set of experiments involving measurements at two levels of frother concentration and between one and four levels of the other two variables. Replicate experiments give an indication of the variance that can be expected. Series B were performed once various short-comings in experimental technique had been identified and eliminated. Froth velocities were measured for experiments 41-47.

### 5.2.1 Estimation of parameters in Model 2.

The problem may be broken down into two phases - firstly, the estimation of the froth removal efficiency  $\epsilon_f$  and secondly the estimation of the parameters  $\alpha$ ,  $\delta$  and  $g_{b2}$  in the concentrate residence time distribution function  $E_c(\tau)$

$\epsilon_f$  is the fraction of perfectly floatable particles entering the froth phase which are removed in the concentrate and, for a uniform flux of these particles into the base of the froth, may also be defined as the fraction of the froth/slurry interface involved in producing particles which eventually reach the concentrate weir. Model 2 applies only in cases where the whole interface is thus involved, and so this interfacial area must be calculated before model 2 can be applied to the data (This is not true when the assumption  $g_{b2} = 0$  is made, since in this case



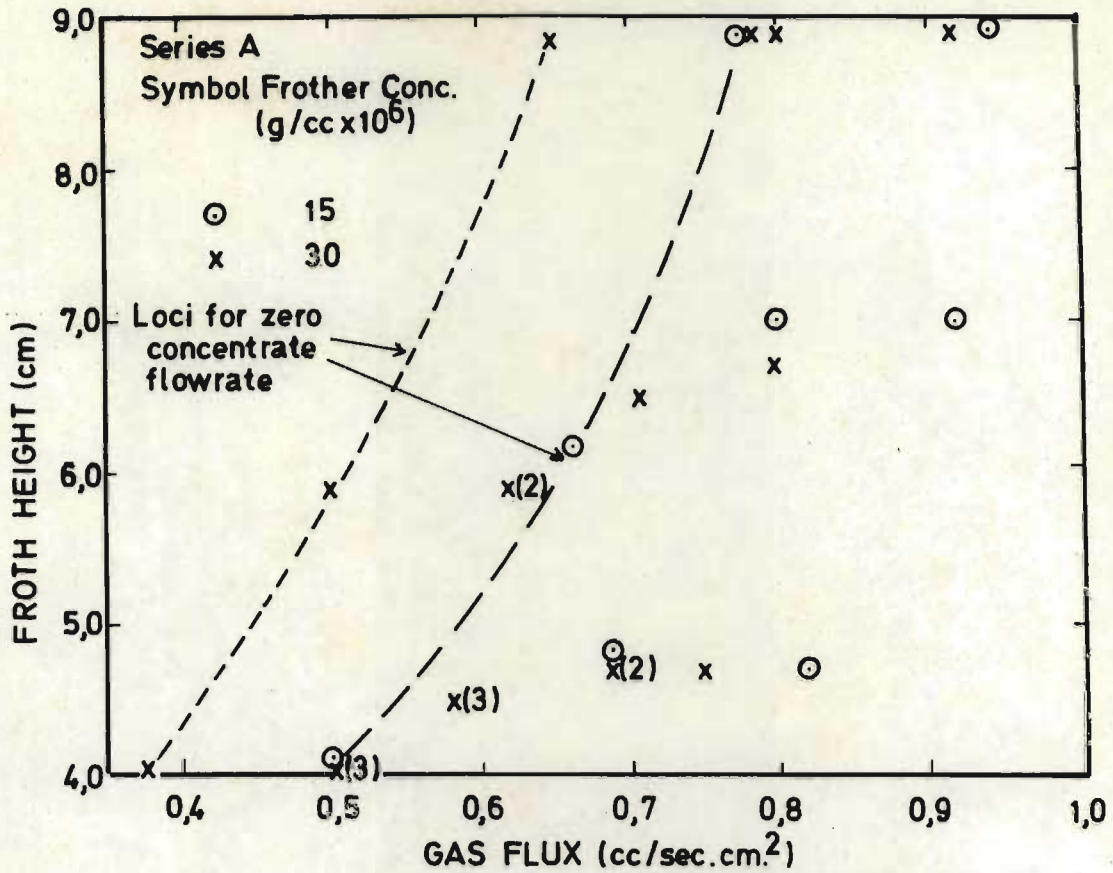


Figure 5.10.1 Points at which froth RTD measurements were performed (Series A, Table 5.2).

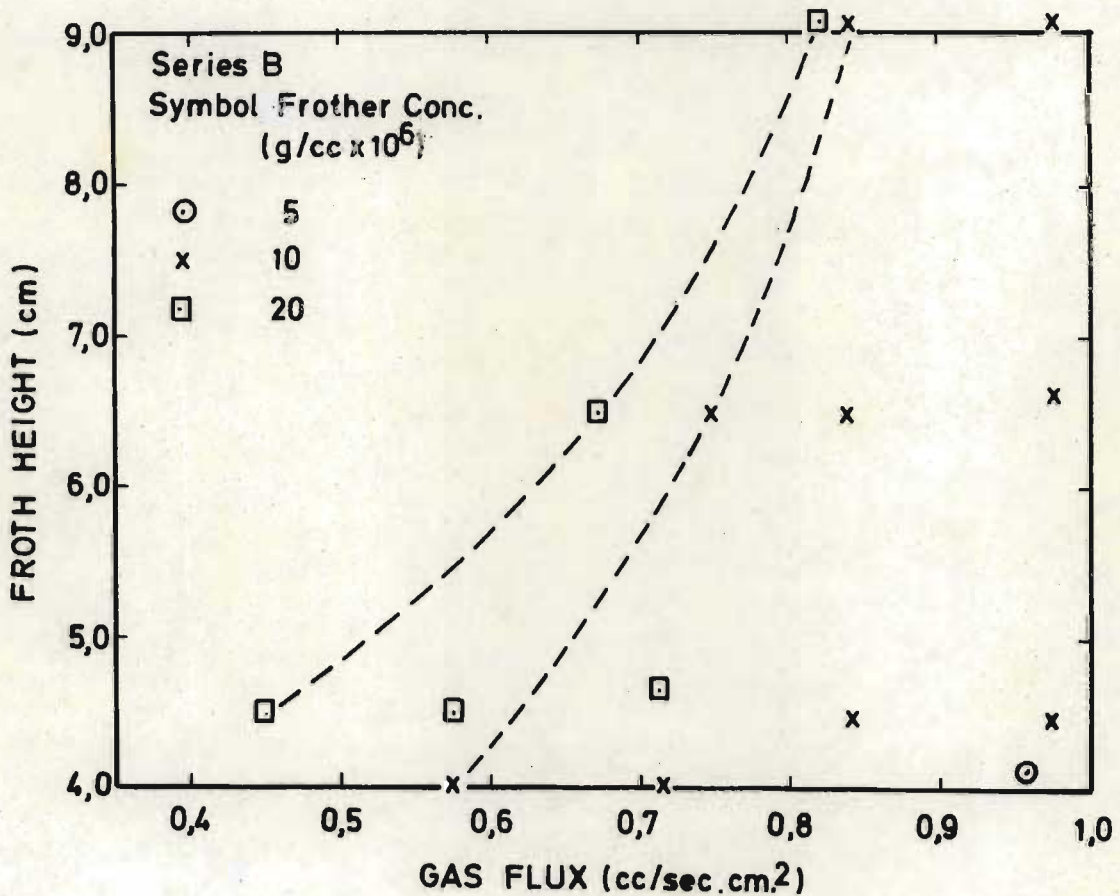


Figure 5.10.2 Points at which froth RTD measurements were performed (Series B, Table 5.2).

$E_c(\tau)$  is independent of the froth chamber length and width). Assuming that the proportion of non-productive surface area near any side of the cell is proportional to the number of particles adhering to that side at the end of a test, we get

$$\epsilon_f = 1 - (r_b + r_s)$$

where  $r_b$  is the fraction of the total number of particles adhering to the back of the cell at the end of the test, and  $r_s$  is the corresponding fraction for the cell sides. The effective length of the cell  $L_e$  is the distance from the point where froth velocity is zero and the froth overflow weir. This is estimated by reducing the two horizontal dimensions (length  $L$  and width  $W$ ) of the cell by amounts proportional to  $r_b$  and  $r_s$ , while ensuring that

$$\frac{L_e W_e}{LW} = \epsilon_f$$

( $W_e$  is the average "effective width" of the area involved in producing froth elements which leave the cell in the concentrate stream).

#### 5.2.1.1 Analysis of $\epsilon_f$ data

As shown in Figure 5.10, the gas flux  $g_o$  must be greater than a certain value  $g_o^0$  to produce a finite concentrate flowrate at a given frother concentration and froth height. When  $g_o = g_o^0$ ,  $\epsilon_f = 0,0$ . Plotting  $\epsilon$  vs  $g_o$  on log-linear paper (see Figure 5.11) we see that froth removal efficiency could be adequately quantified by an expression of the form

$$\epsilon_f = 1 - \exp \{-\beta_e (g_o - g_o^0)\} \quad (5.4)$$

where  $\beta_e$  and  $g_o^0$  are functions of  $h$  and frother concentration, FC. As shown in Section 5.2.4  $g_o^0$  is evaluated with adequate accuracy from

$$g_o^0 = \frac{3 \times 10^{-6}}{FC} + 0,063 h$$

$\beta_e$  (estimated by fitting straight lines through the data by eye and

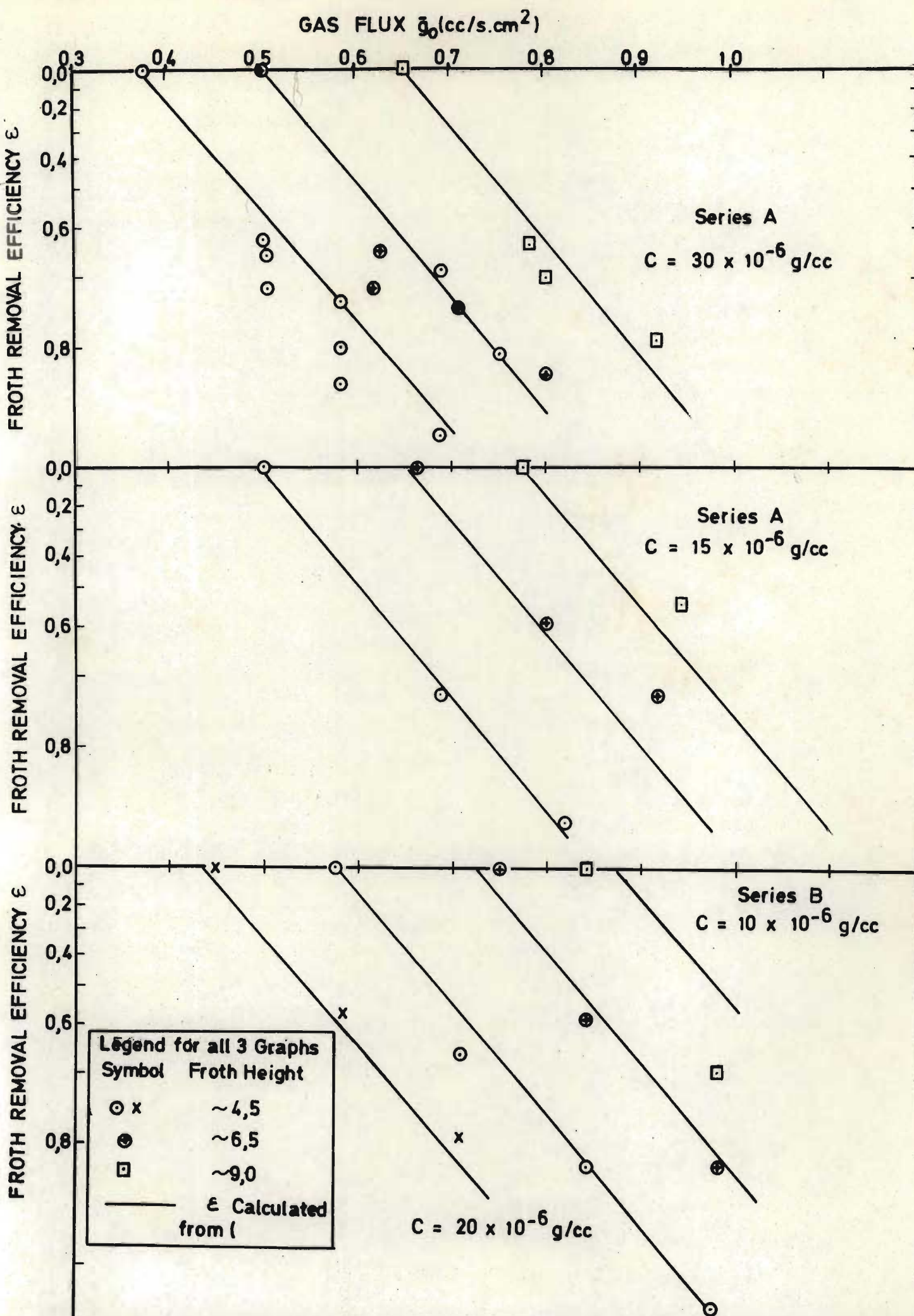


Figure 5.11 Variation of froth removal efficiency  $\epsilon$  with gas flux, froth height and frother concentration

measuring the slope) however, shows no correlation with  $h$  or  $FC$  for this data, and an average value of 6,35 was used to produce the solid lines in Figure 5.11. The correlation with experimental results is surprisingly good.

#### 5.2.1.2 Estimation of parameters for $E_c(\tau)$

The model used for  $E_c(\tau)$  is Model 2 (described in section 5.2.2) involving the parameters  $\alpha$  (froth stability),  $\delta$  (residence time ratio) and  $g_{b2}$  (the slope of the froth breakage function). The regression technique of Nelder and Mead (1965) was used to estimate these parameters by minimising the sum of squares

$$S^2 = \sum_{i=1}^N W_i [F_e(\tau_i) - F_t(\tau_i)]^2$$

where  $W_i$  is a weighting function (default values of 1,0)

$F_e(\tau_i)$  is the experimentally measured cumulative RTD and

$F_t(\tau_i)$  is the corresponding theoretical value, obtained in the following way. As shown in sections 5.3.1 and 5.3.2 the tracer enters the bottom of the froth as an imperfect pulse distributed over a number of seconds characterised by the pulp residence time distribution  $E_p(\tau)$  and takes a finite time  $\tau_c$  to flow down the concentrate weir. Thus the true impulse response is given by the convolution integral

$$E_c^t(t) = \int_0^{\infty} E_p(\tau_p) E_c(t - \tau_p - \tau_c) d\tau_p$$

which is evaluated numerically by assuming that  $E_p(\tau)$  is adequately represented by 5 pulses of fractional content  $f_j$  arriving at times  $\tau_{pj} = 0,2$  0,7 1,3 2,3 and 3,8 seconds. Thus

$$E_c^t(t_i) = \sum_{j=1}^5 f_j E_c(t_i - \tau_{pj} - \tau_c)$$

$E_c^t(t_1)$  is then integrated numerically using Simpson's 3-point formula in each time interval to obtain  $F_t(\tau)$ . Adequate accuracy was obtained since  $F_t(\tau)$  at the largest value of  $\tau$  never exceeded 1,0002 (i.e. maximum error = ,02%)

The following constraints were imposed on the parameters using linear penalty functions which added values to  $S^2$  proportional to the amount by which the constraints were transgressed:

$$0 \leq \alpha \leq 1,0$$

$$0 \leq \delta \leq 1,0$$

$$g_{b2}^2 \leq \{(1-\alpha) g_0/L\}^2$$

The last condition ensures that the breakage rate on the froth surface is never negative.

### 5.2.2 Testing of Hypotheses Concerning the Model

The following hypotheses were entertained concerning the form of the model, and these determined the parameters that had to be estimated (indicated in brackets)

$H_1$ : Model is as formulated in section 4.2.2 ( $\alpha, \delta, g_{b2}$ )

$H_2$ : Froth breakage does not vary with position i.e.  $g_{b2} = 0$   
( $\alpha, \delta$ )

$H_3$ :  $g_{b2} = 0.0$  and  $\delta$  is obtained from equation (4.7) ( $\alpha$ ).

The advantage of the last hypothesis is that it requires the estimation of only one parameter,  $\alpha$ , and this may be easily estimated using froth velocity measurements.

Parameters were estimated for experiments 1-17 in Series A for each of the above hypotheses. The results are summarised in Table 5.3

Table 5.3 Parameters and Sum of Squares for Hypotheses  $H_1$ ,  $H_2$  and  $H_3$   
 (data: Series A, experiments 1-17)

Expt No.	Froth Height cm	Gas Flux $\text{cm}^3/\text{s} \cdot \text{cm}^2$	Parameters estimated for Hypothesis:									
			$H_1$			$H_2$			$H_3$			
			$\alpha$	$\delta$	$g_2$	$S^2$	$\alpha$	$\delta$	$S^2$	$\alpha$	$\delta$	$S^2$
1	4,0	,50	,40	,21	,0053	,0026	,46	,34	,0041	,48	,40	,0077
2	4,0	,50	,58	,12	-,0012	,0026	,55	,13	,0027	,57	,36	,025
3	4,0	,50	,46	,15	-,0055	,0070	,38	,20	,0099	,40	,46	,053
4	4,5	,58	,57	,24	-,0031	,0013	,53	,20	,0015	,54	,41	,016
5	4,5	,58	,73	,29	-,0066	,0012	,63	,24	,0018	,64	,36	,008
6	4,5	,58	,69	,27	-,0060	,0035	,60	,21	,0041	,61	,37	,013
7	4,7	,69	,79	,31	-,0075	,0006	,69	,27	,0011	,70	,34	,0034
8	4,7	,75	,85	,34	-,0060	,0012	,78	,30	,0016	,78	,32	,0018
9	4,7	,69	,83	,21	-,0066	,0015	,75	,17	,0023	,76	,34	,014
11	5,9	,62	,68	,47	-,0107	,0103	,54	,38	,018	,55	,46	,020
12	5,9	,63	,62	,49	-,0093	,0040	,50	,39	,0063	,50	,48	,008
13	6,5	,71	,83	,41	-,0065	,0031	,75	,39	,005	,76	,41	,005
14	6,7	,80	,72	,44	,0118	,0069	,90	,42	,0043	,82	,39	,008
15	8,9	,78	,75	,41	-,0118	,0039	,63	,36	,0064	,66	,51	,022
16	8,9	,80	,89	,42	-,0052	,0016	,84	,40	,0021	,84	,46	,005
17	8,9	,92	,82	,54	,0002	,0001	,83	,53	,0001	,81	,46	,004



and Figures 5.12 and 5.13. The following points are noted:

- (i) Hypothesis  $H_1$  produces the smallest  $S^2$  and hence the best fit of the model to the data. The parameters produced are however suspect, since the  $g_{b2}$  values do not correlate with the operating variables froth height and gas rate. (see Figure 5.12). This is due to the high interaction between  $g_{b2}$  and  $\alpha$  as evidenced in Figure 5.13, where the ratio between  $\alpha(H_1)$  and  $\alpha(H_2)$  is plotted as a function of  $g_{b2}$ . Further doubts are cast on  $H_1$  by the results obtained in Section 4.2.2.4 where it was shown that parameters estimated on the basis of  $H_1$  (using data simulated with the Laplace solution model) bear little relation to the parameters used in the generation of the data. Thus estimation of all 3 parameters gives no reliable extra information concerning the process, and the improved fit is due only to the existence of an extra fitting parameter  $g_{b2}$ .
- (ii)  $H_3$  gives poor fits of the model to the data as evidenced by the large sum of squares that is obtained. This is due to the fact that (4.7) gives values of  $\delta$  that are larger than those obtained by estimation of the basis of  $H_1$  and  $H_2$ . Model 2 cannot reproduce the rapid increase in  $F$  that is obtained with the Laplace solution near  $\tau_{\min}$  and hence is forced to produce an underestimate of  $\tau_{\min}$  (and hence  $\delta$ ) as shown in Figure 4.5. Since a larger value of  $\delta$  is obtained from equation (4.7) a larger value of  $\alpha$  must be estimated to compensate.
- (iii)  $H_2$  thus seems to be preferred, since good fits are obtained and the parameter  $\alpha$  is likely to be close to the true froth stability value as shown in Section 4.2.2.5.  $\delta$ , however, is likely to be underestimated. Various fits of the model to the data on the basis of this hypothesis are shown in Figure 5.14.1 to 5.14.3. The calculation of approximate confidence limits on the parameters allows further conclusions to be drawn from the data.

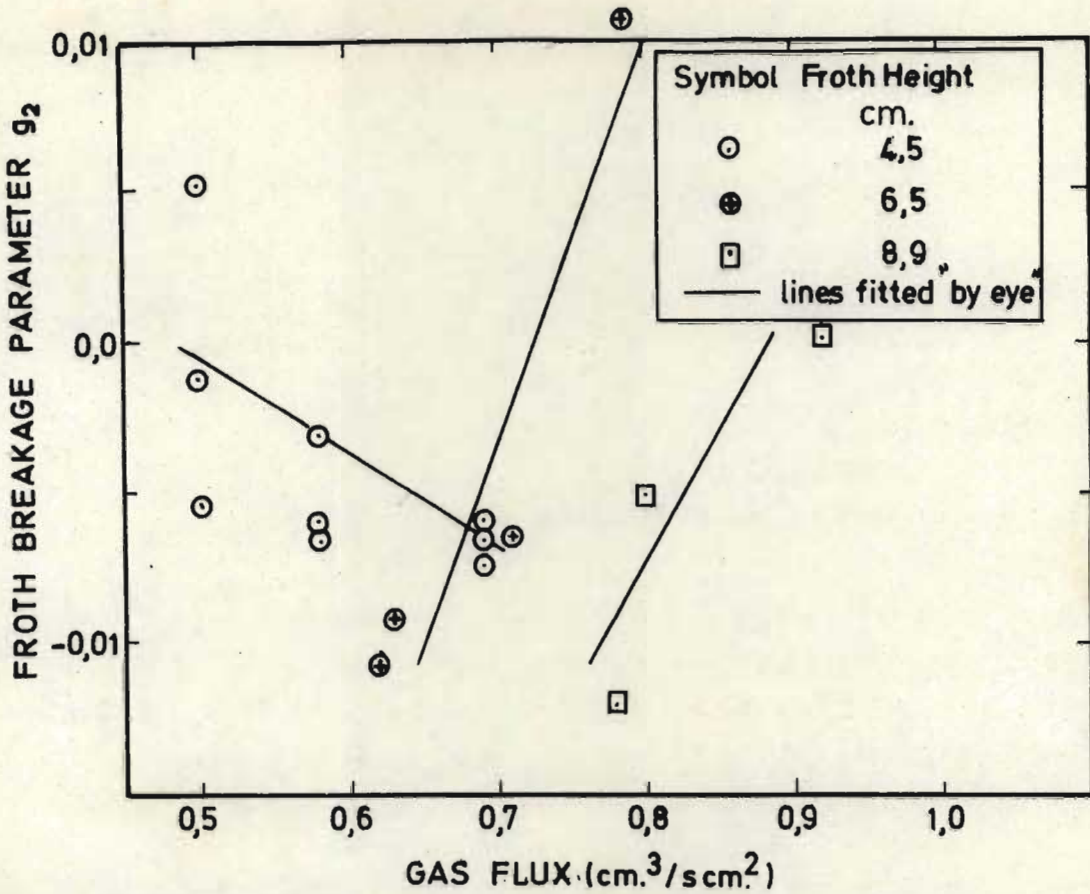


Figure 5.12 Froth breakage parameter  $g_2$  vs gas flux, as a function of froth height. Lack of correlation between  $g_2$ ,  $h$  and  $g$  is evident. (Data: Series A, Experiments 1-17)

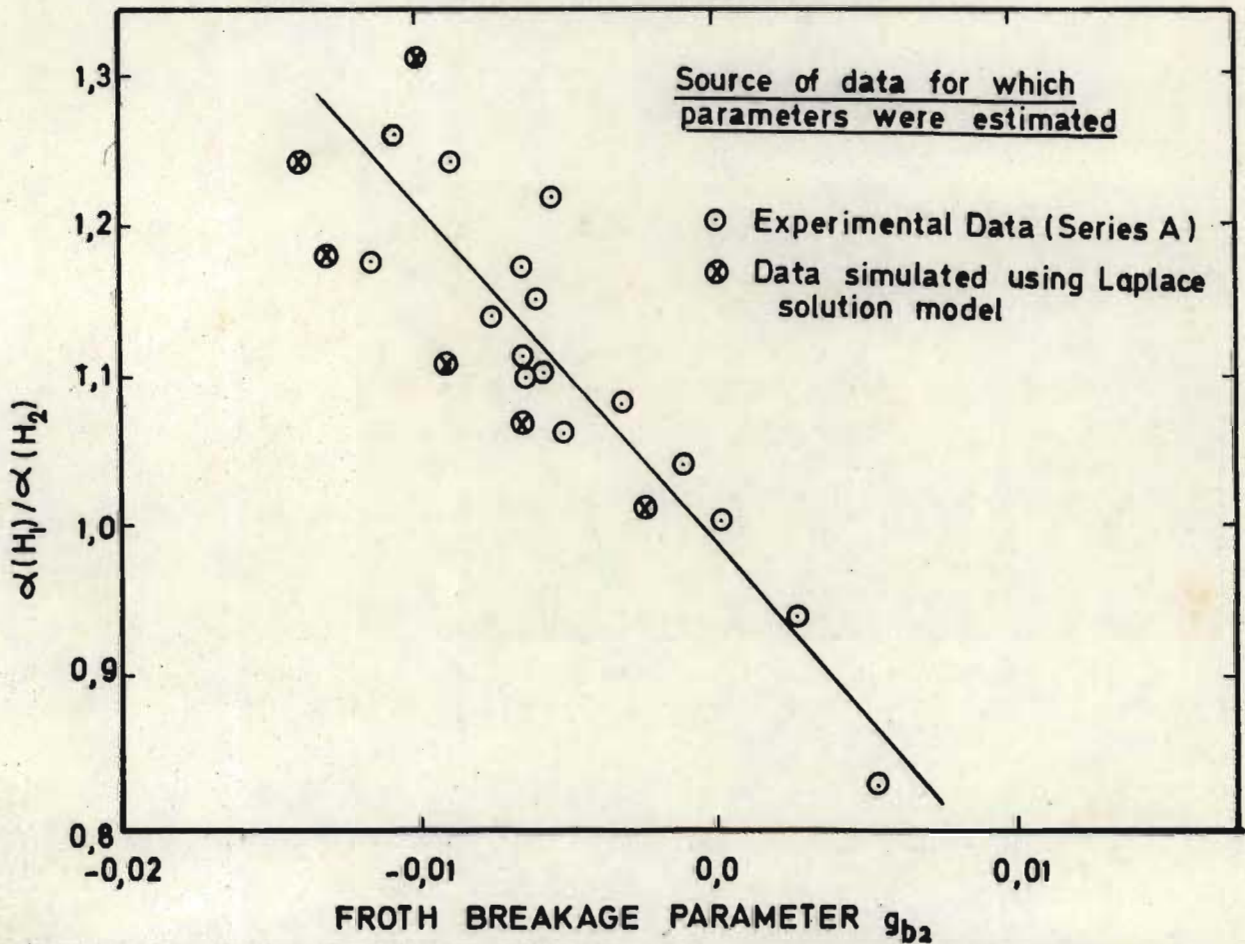
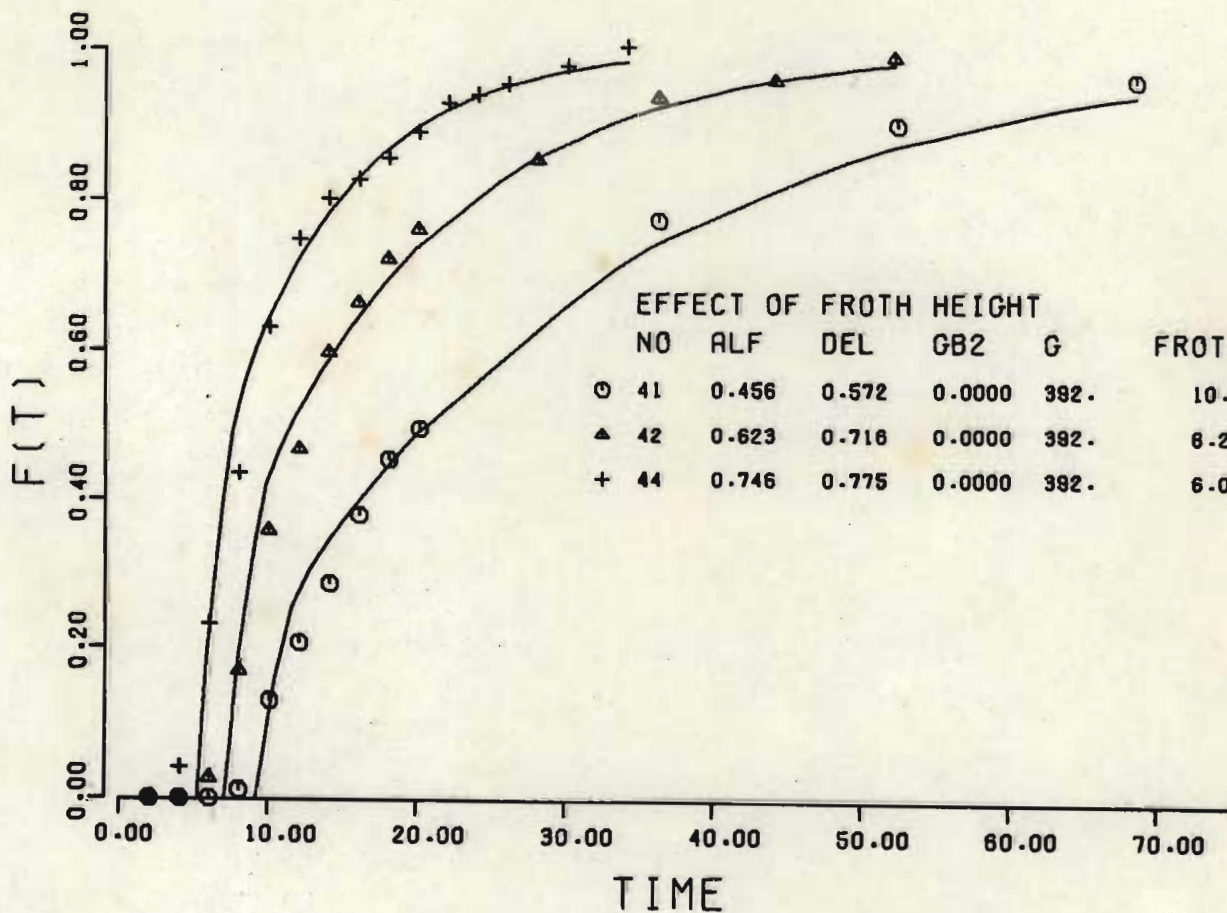
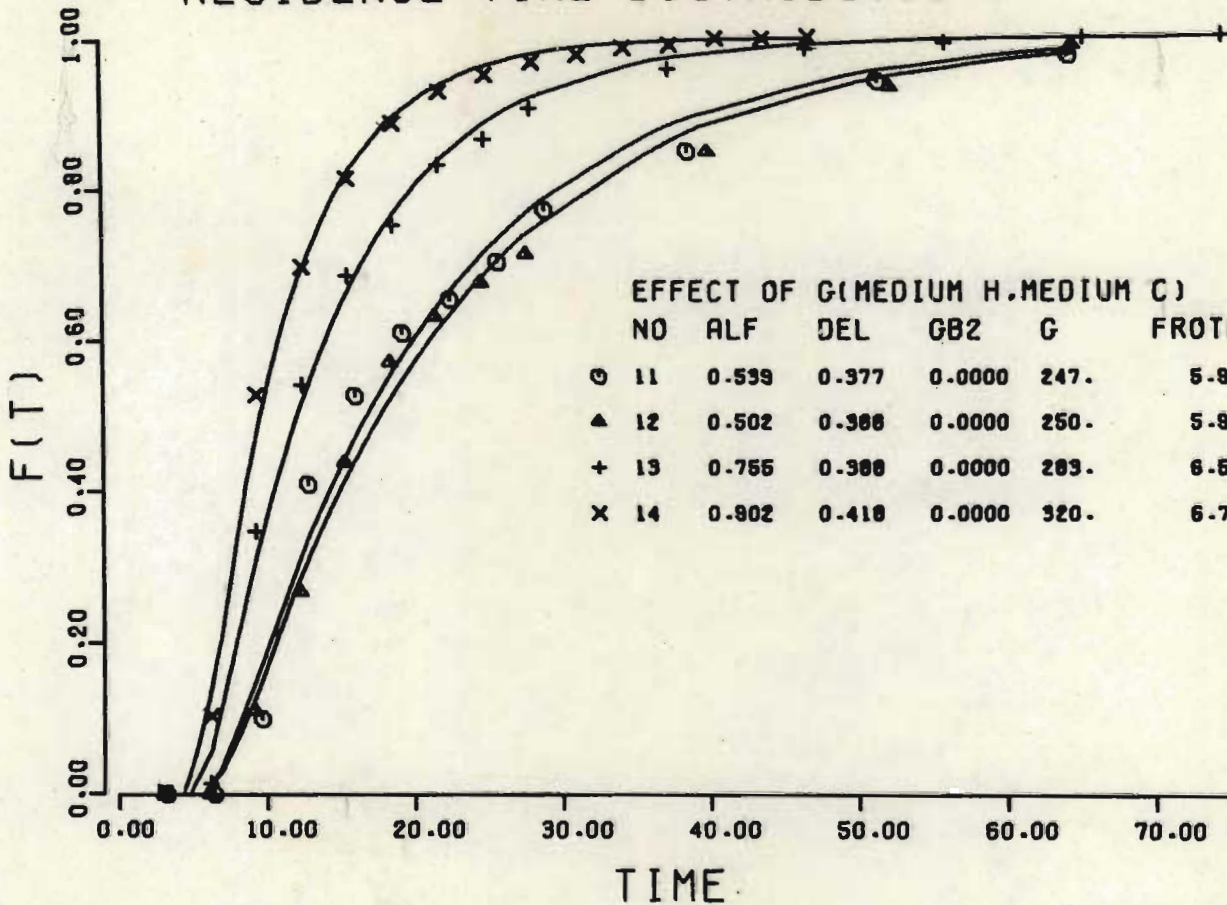


Figure 5.13 Ratio of  $\alpha(H_1)$  to  $\alpha(H_2)$  vs  $g_2$ , demonstrating high correlation between the two estimates of  $\alpha$ .

# RESIDENCE TIME DISTRIBUTIONS



Figures 5.14.1 and 5.14.2 Effect of gas rate and froth height ore concentrate residence time distribution

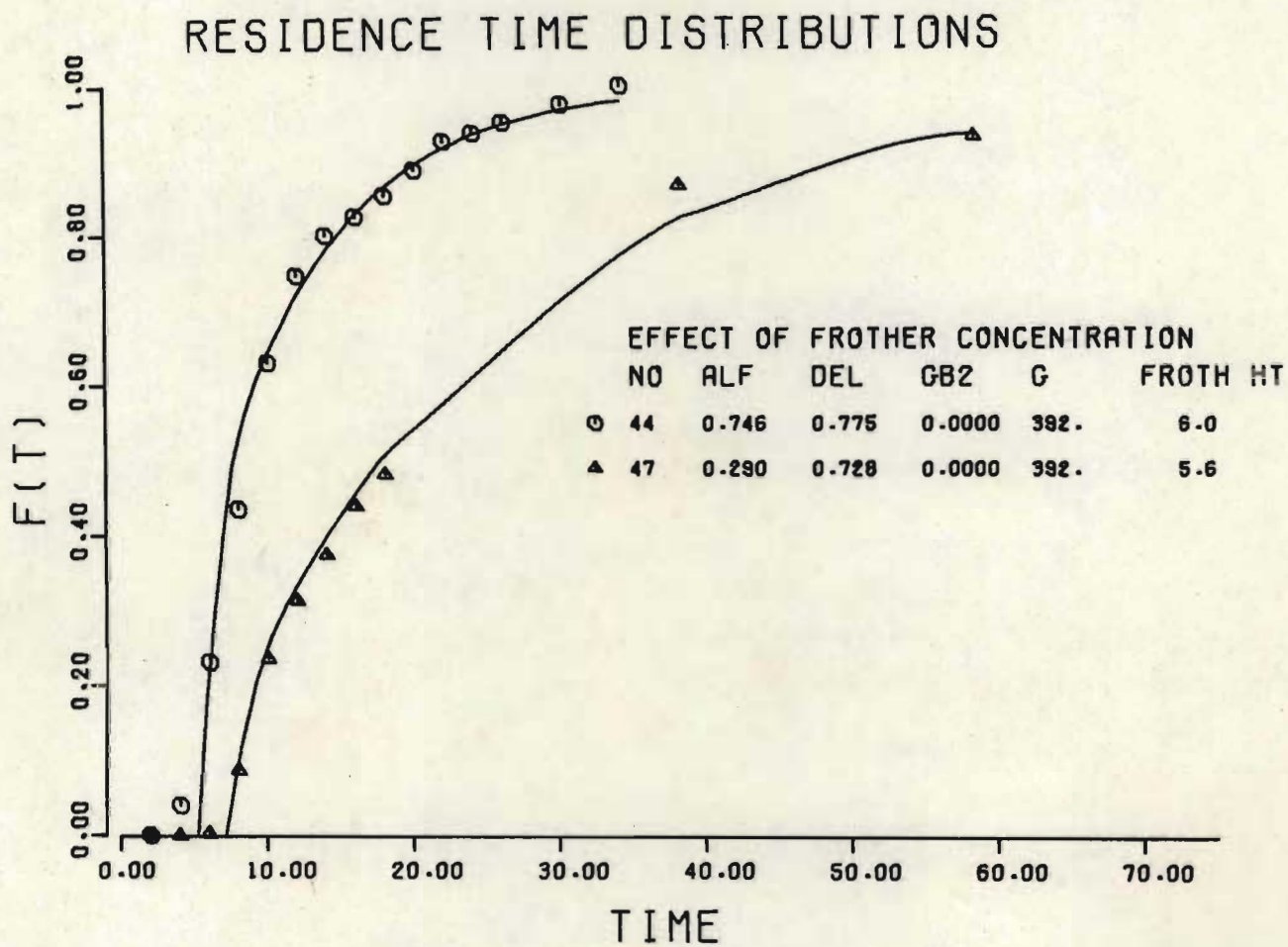


Figure 5.14.3 Effect of frother concentration on concentrate residence time distribution.

### 5.2.3 Confidence Limits on the Parameters

As shown in Appendix D user-defined measures of the 95% confidence limits which can be applied to  $\alpha$  and  $\delta$  are given by

$$\Delta\alpha = \Delta F(\tau_{av}) \alpha e/\bar{C}$$

and

$$\Delta\delta = (\Delta F(\tau_{min}) + \Delta F(\tau_{av}))/\alpha\bar{C}$$

where  $\Delta F(\tau_{av})$  and  $\Delta F(\tau_{min})$  are the 95% confidence variations for the cumulative distribution  $F(\tau)$  at  $\tau_{av}$  and  $\tau_{min}$ . In general  $\Delta F$  is related to the standard deviation  $\sigma_F$  by

$$\Delta F = 1,96\sigma_F$$

An estimate of  $\sigma_F$  at  $\tau_{av}$  and  $\tau_{min}$  is obtained from

- (i) the first 9 experiments of Series A which consist of 3 sets of 3 experiments done at a gas rate of 200, 233 and 275 cc/sec with the exception that experiment 8 is performed at 300 cc/sec; and
- (ii) four pairs of experiments (Nos. 31-38) described in section 6.4.

$\sigma_F$  was calculated for  $\tau$  values near  $\tau_{min}$  and  $\tau_{av}$  respectively for each of the sets of replicates, and the values at the two residence times were obtained by interpolation.  $\sigma_F(\tau_{av})$  correlated well with  $\tau_{av}$  as shown in Figure 5.16 resulting in the expressions given below.  $\sigma_F(\tau_{min})$  did not correlate with any variable and so the maximum values were used. The effect of improvements in experimental technique developed between the two sets of replicates indicated above is evident. The following expressions were used to estimate the variances for the experiments indicated:

$$\sigma_F(\tau_{min}) = 0,5 \quad \sigma_F(\tau_{av}) = 0,003\tau_{av} \quad \text{for Series A experiments}$$

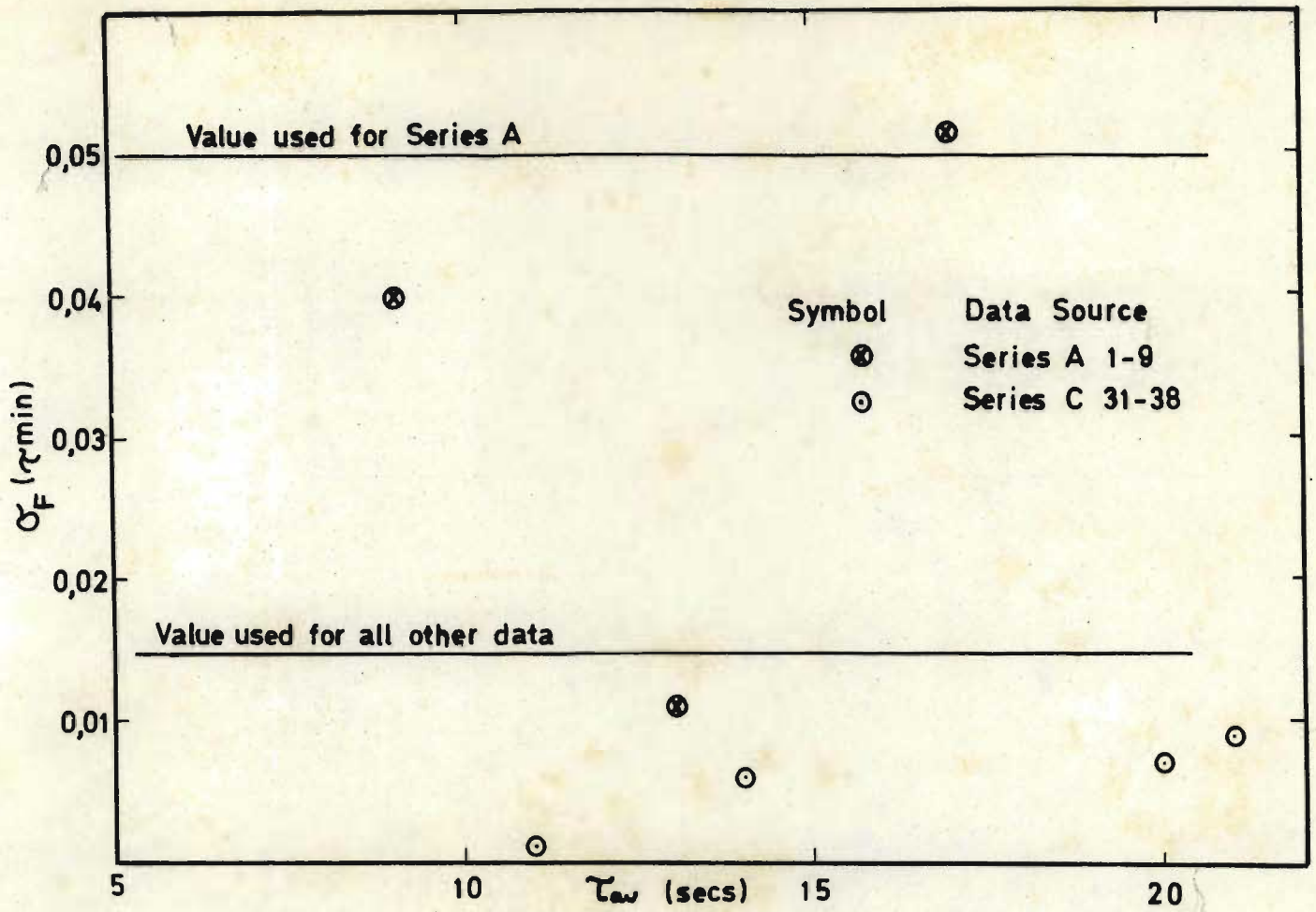


Figure 5.15 Standard Deviation of RTD cumulative distribution at  $\tau_{min} = \delta h / g_0$

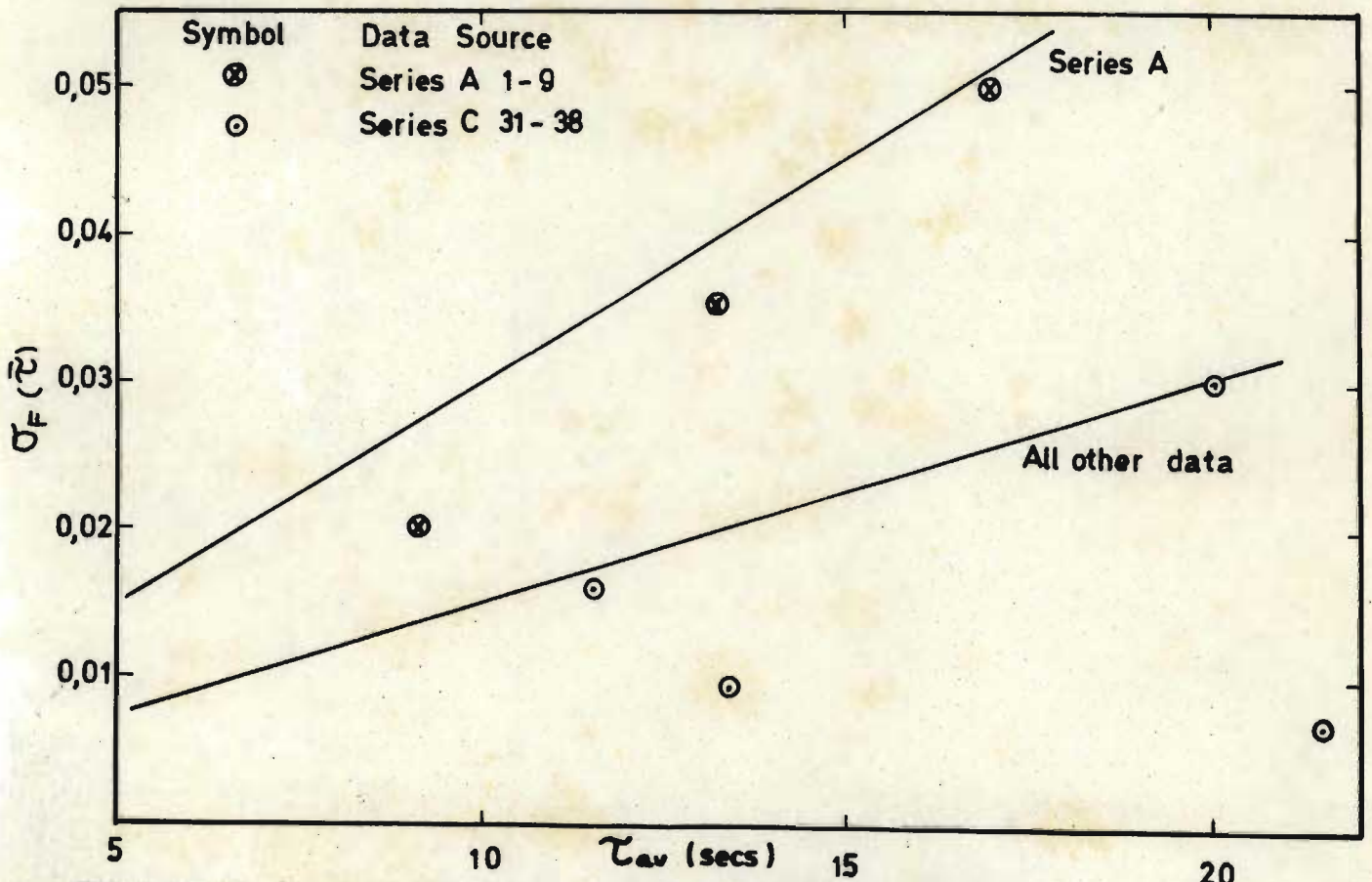


Figure 5.16 Standard Deviation of Cumulative RTD at  $\tau_{av} = h / \alpha g_0$

$$\sigma_F (\tau_{\min}) = ,015 \quad \sigma_F (\tau_{\text{av}}) = 0,0015\tau_{\text{av}} \text{ for all other experiments.}$$

Using the above expressions the confidence variations for  $\alpha$  and  $\delta$  were calculated for all experiments in Series A and B and are given in Table 5.2.

#### 5.2.4 Dependence of RTD Parameters on Control Variables

The variation of  $\alpha$  with gas flux is plotted in Figures 5.20. where the behaviour is similar to that of the froth removal efficiency  $\epsilon_f$  (Figure 5.11) and an expression analogous to (5.4) was used to condense the data:

$$\alpha = 1 - \exp \{-\beta_\alpha (g_o - g_o^0)\} \quad (5.8)$$

Simple graphical techniques reveal that for experiments 1-24

$$\beta_\alpha = (1,27 - m_\beta) h = (1,27 - \frac{8,86 \times 10^{-6}}{FC})h \quad (5.9)$$

and

$$g_o^0 = \hat{g} + 0,063h = \frac{3,0 \times 10^{-6}}{FC} + 0,063 h \quad (5.10)$$

The correlations of  $\hat{g}$  and  $m_\beta$  with  $FC^{-1}$ ,  $\beta_\alpha$  with  $h$  and  $g_o^0$  with  $h$  are shown in Figures 5.17, 18 and 19. The values of  $\alpha$  calculated from this expression appear in Table 5.2 and are plotted together with 95% confidence bands in Figure 5.20.

Good correlations were obtained for experiments 1-24 and also for experiments 41-46. This is probably fortuitous, since poor correlations were obtained for 47-49. Series A and B were performed at different times of the year and because of the notoriously erratic behaviour of froths (eg ambient temperature has a substantial effect on the froth stability) they are not expected to correlate.

It should be noted that all but three of the data points fall within the 95% confidence bands on Figure 5.20, indicating that the expression developed above for  $\Delta\alpha$  provides a reasonable estimate of the confidence we can vest in our estimate of  $\alpha$ .

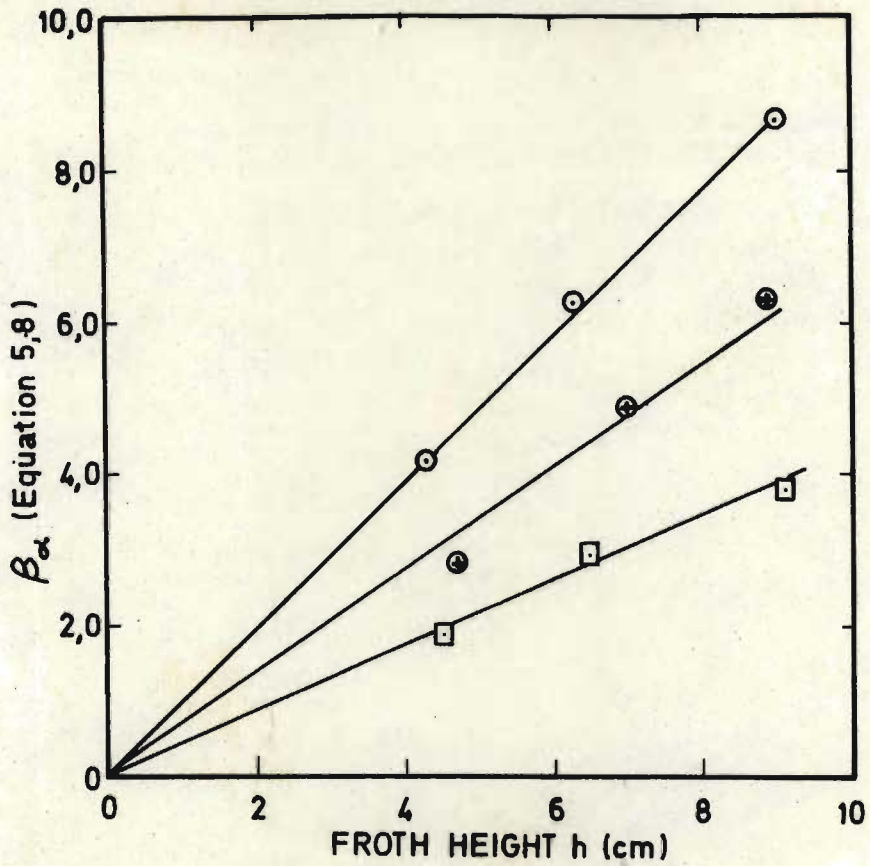


Figure 5.17 Variation of parameter  $\beta_\alpha$  in equation 5.8 with froth height

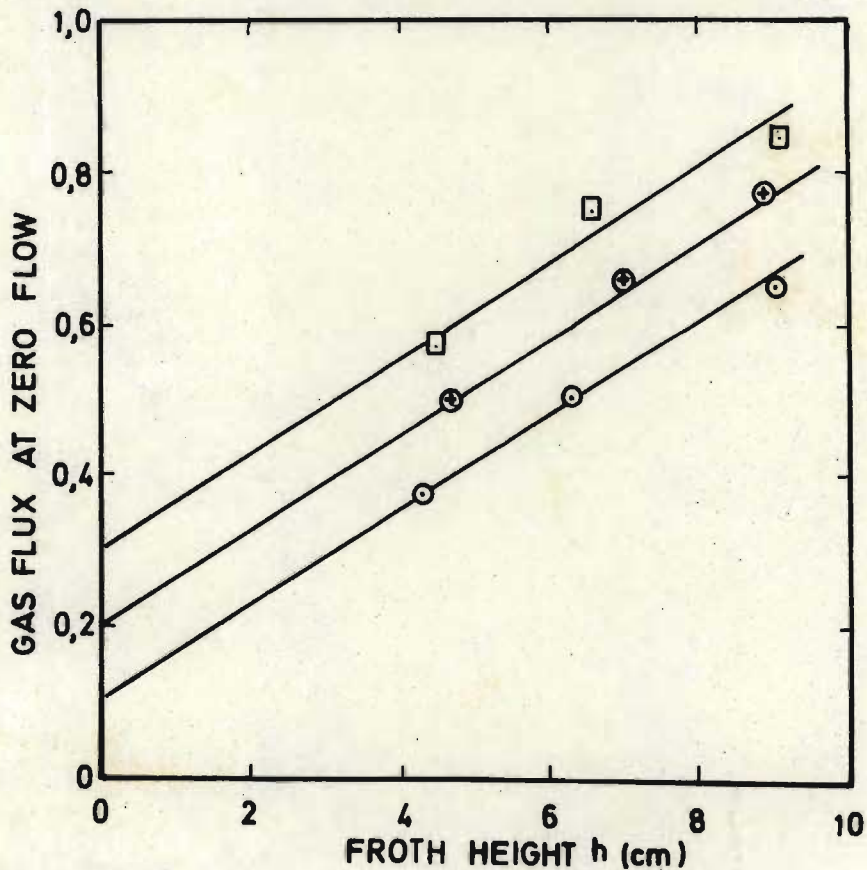


Figure 5.18 Gas flux at zero concentrate flowrate ( $g^0$ ) as a function of froth height



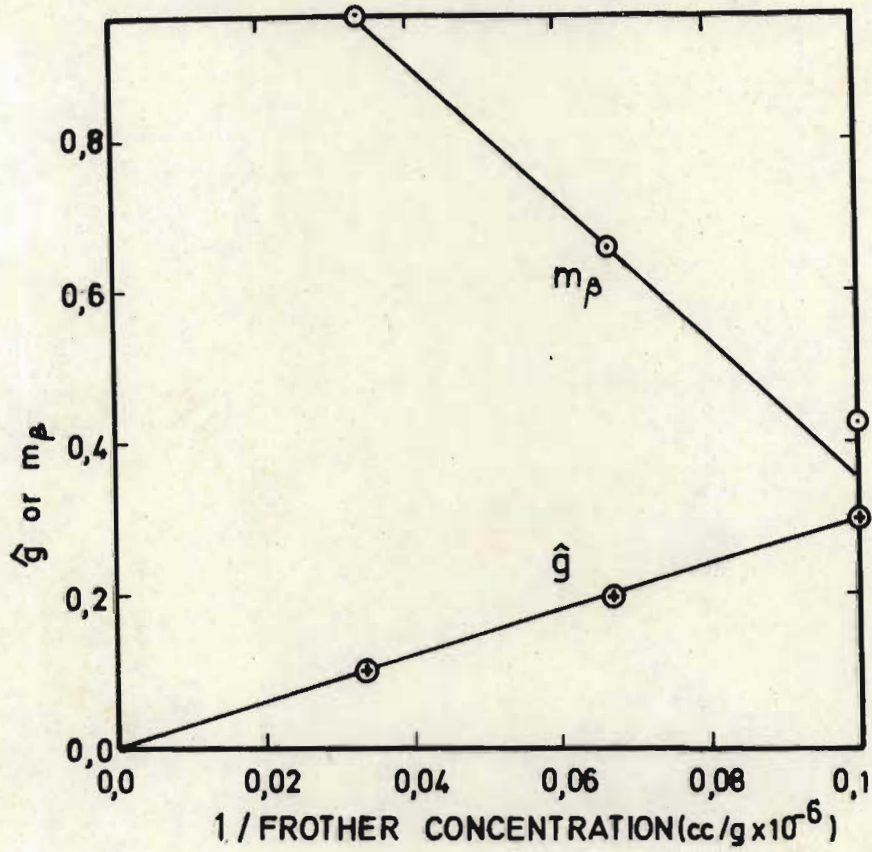


Figure 5.19 Intercept  $\hat{g}$  of gas flux at zero concentrate flowrate and slope of  $\beta_g$  vs  $h$  curves as a function of (frother concentration) $^{-1}$

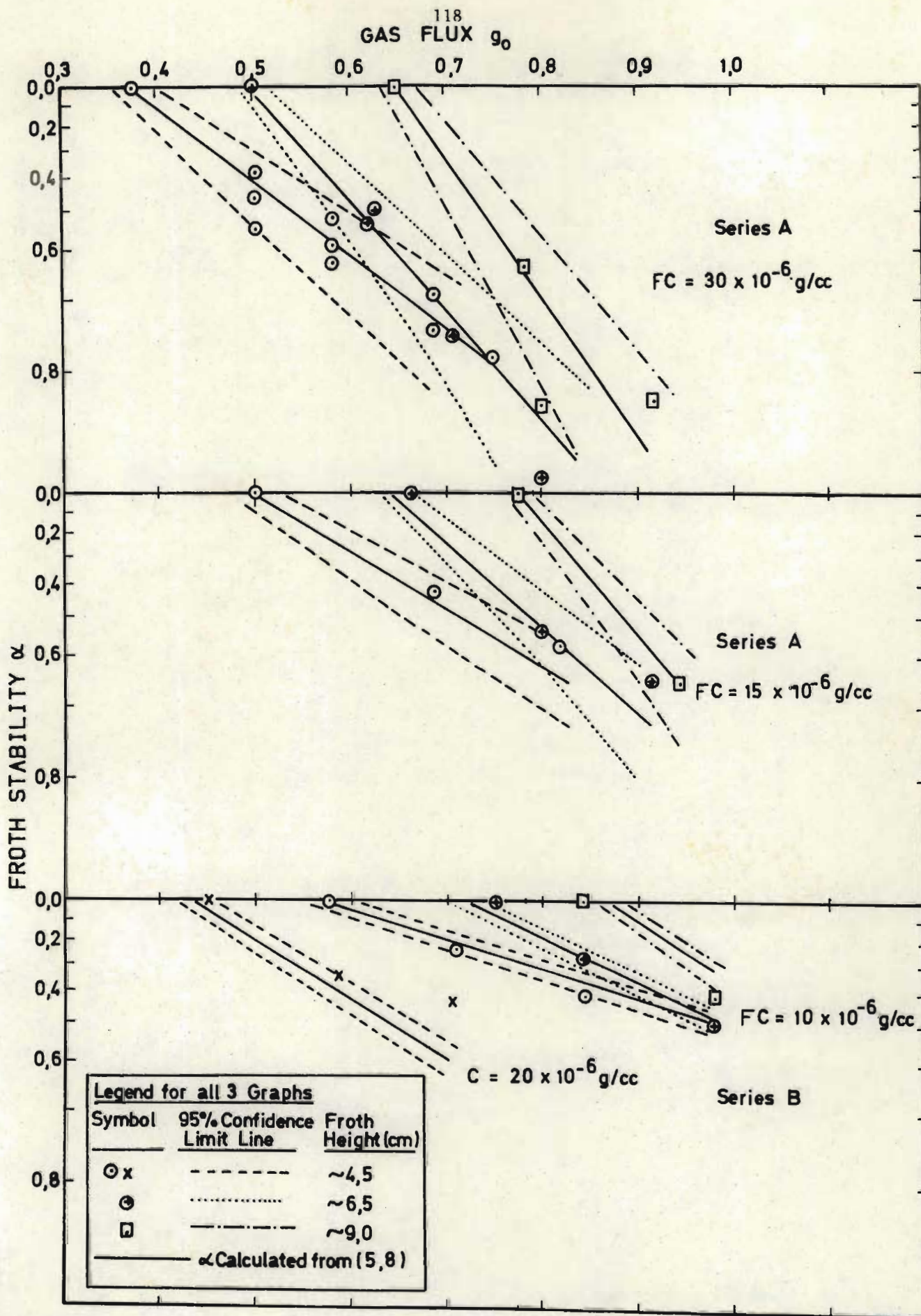


Figure 5.20. Froth stability  $\alpha$  as a function of gas flux, froth height and frother concentration.

The residence time ratio  $\delta$  shows very little correlation with the control variables. This is probably due to a number of factors, among them

- (i) as shown in Section 4.2.2.5,  $\delta$  will generally be underestimated by the regression technique
- (ii)  $\delta$  is determined by the values of  $F(\tau)$  near  $\tau = \tau_{\min}$  and is therefore dependent on the accuracy with which the pulp RTD and concentrate weir residence time were measured. An error of 1 second in these measurements, for example, would produce an error of the order of 30% in the estimates of  $\delta$  at a low froth height; hence the high values obtained for the 95% confidence variations on  $\delta$ .

For these reasons little confidence can be vested in estimates of  $\delta$ , and a value of 0,5 (close to the average -0,48- of  $\delta$  values for the most precisely performed experiments - Series B) will be used where no accurate measurement can be made.

To test this decision,  $\alpha$  was estimated for all the experiments with  $\delta = 0,5$ . Poor fits were obtained near  $\tau_{\min}$ , as expected, but the  $\alpha$  values obtained differed on average from the  $\alpha$  values in Table 5.2 by not more than 1,0%, showing that the assumption of  $\delta = 0,5$  does not minimise the ability of the model to describe the physical process.

It has been shown that the four parameters in equations (5.9) and (5.10) above and a value of 0,5 for  $\delta$  describe the behaviour of the froth for a range of froth heights, frother concentrations and gas rates for the system under consideration. It would obviously be desirable to find a (similar) set of equations to describe the behaviour of 3-phase froths. This is discussed in Chapter 6.

#### 5.2.5 Estimation of Froth Stability from Froth Velocity Measurements

The theoretical froth velocity for Model 2 for  $g_{b2} = 0$  is obtained from Section 4.2.2.2.

$$v_x(x) = \frac{\alpha g_0 (x-x_0)}{h(1-\alpha\delta)} = m_v (x-x_0) \quad (5.11)$$

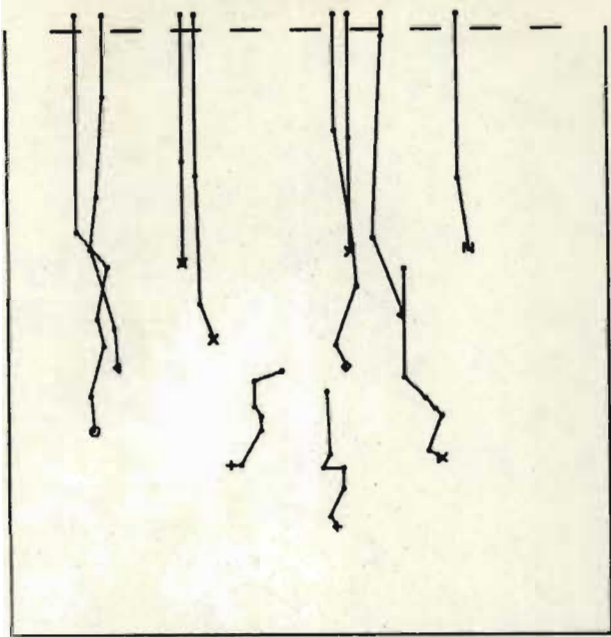
Table 5.4 Comparison of methods for estimating froth RTD parameters

Expt No.	Frother Conc g/ccx10 <sup>6</sup>	Froth Height cm	Gas Flux cm <sup>3</sup> /cm <sup>2</sup> sec	Estimated from RTD data		Estimated from v <sub>f</sub> Measurements	
				α	L <sub>eff</sub>	α	L <sub>eff</sub>
41	10	9,1	,98	,42	17,0	,46	15,0
42	10	6,7	,98	,50	17,8	,50	18,5
43	10	6,5	,84	,28	15,3	,33	15,7
44	10	4,5	,98	,50	19,3	,53	18,0
45	10	4,5	,84	,42	18,4	,49	17,0
46	10	4,0	,71	,23	16,3	,24	17,8
47	5	4,1	,98	,22	17,7	,22	17,4

Figures 5.21.1 to 5.21.7. Trajectories traced by particles on the surface of the froth, and Laplace equation solutions for experiments 41 to 47.

Explanation of Graphs: Most of the features of these graphs are described on the page before Figure 4.2.1. Additional features are as follows

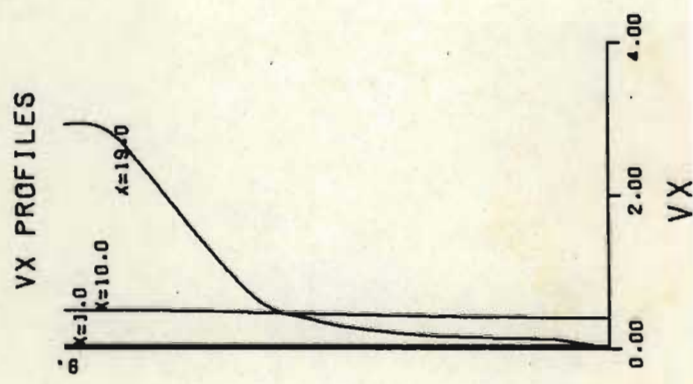
- (i) the trajectories followed by the particles are shown on a plan view of the flotation cell.
- (ii) the velocities calculated from the measured trajectory data are plotted on the "RESIDENCE TIMES AND FROTH VELOCITIES" graph, together with the velocity calculated from equation (5.11).



ALFR 0.420  
 GB1 0.568  
 GB2 0.000  
 GC1 4.1  
 G 392.0

CONCENTRATE LAUNDER

Figure 5.21.1 Froth Velocity data and Laplace Equation solution for Experiment 41; Refer Table 5.4

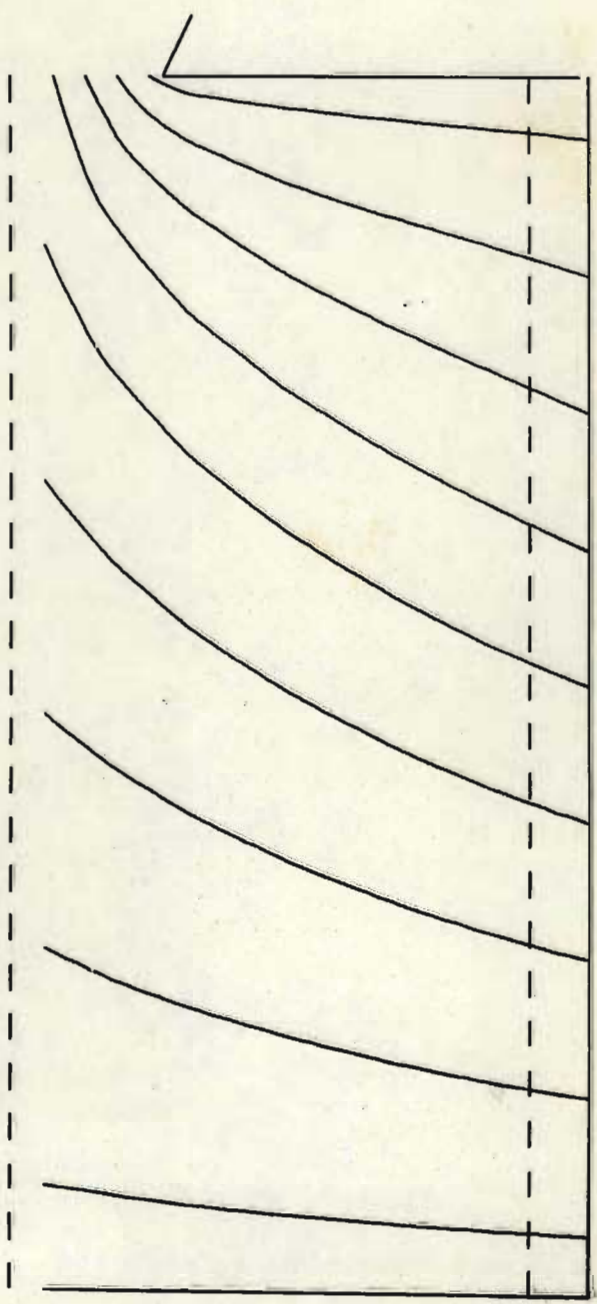


V FOR MODEL NO 2

PARTICLES

DISTANCE FROM BACK OF CELL

FROTH PHASE STREAMLINES



RESIDENCE TIME

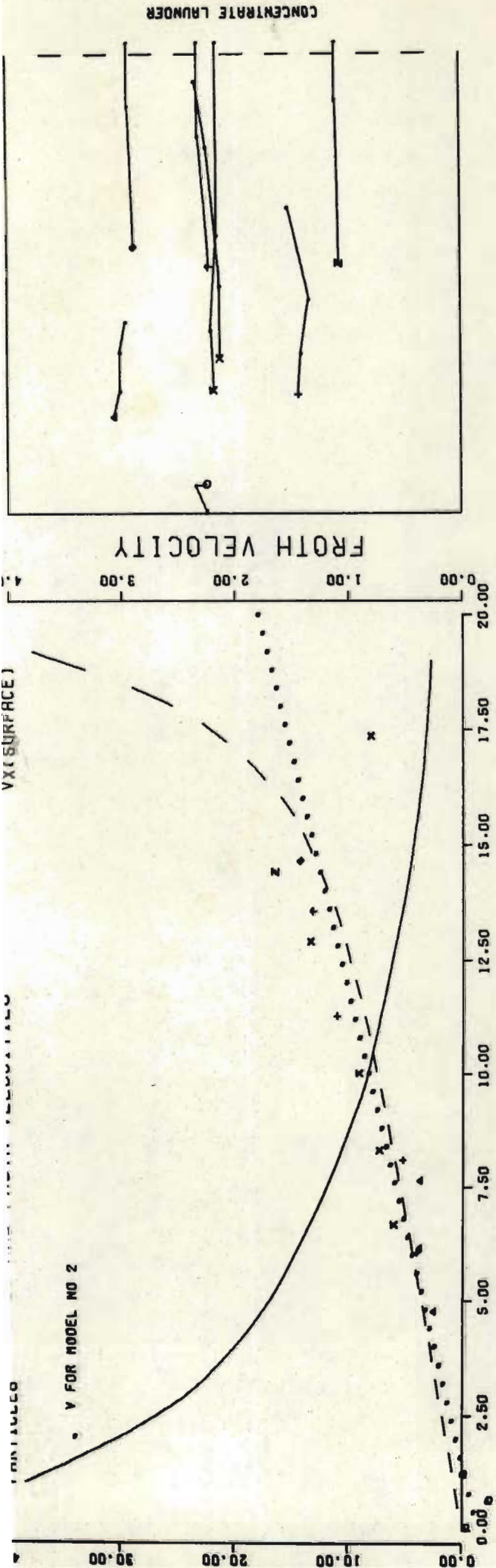
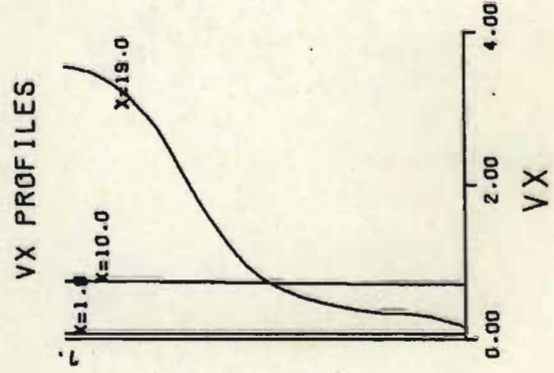
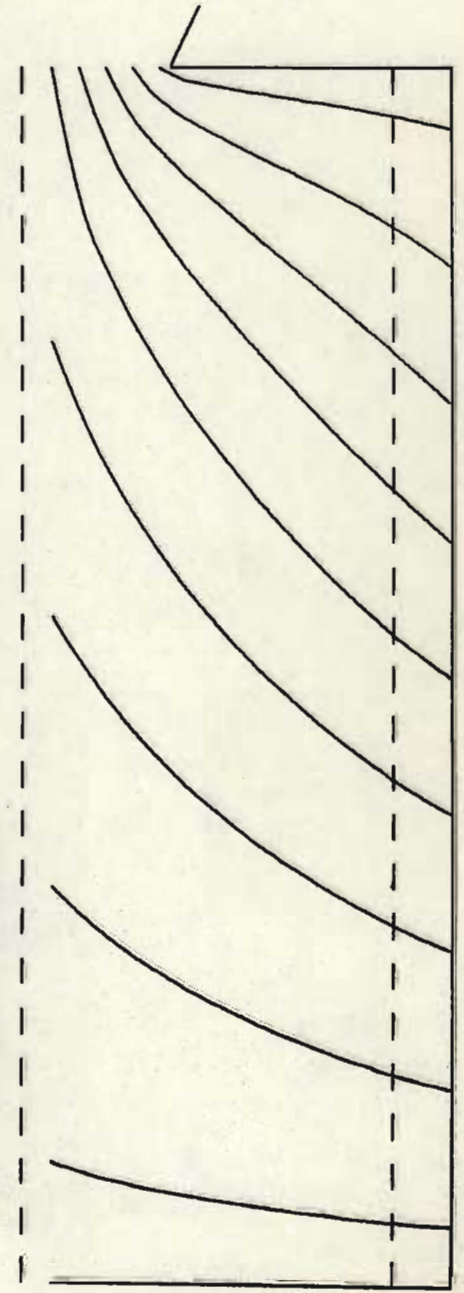


Figure 5.21.2 Froth Velocity data and Laplace Equation solution for Experiment 42; Refer Table 5.4

ALFR	GB1	GB2	GC1	G
0.500	0.490	0.000	4.9	392.0

FROTH PHASE STREAMLINES



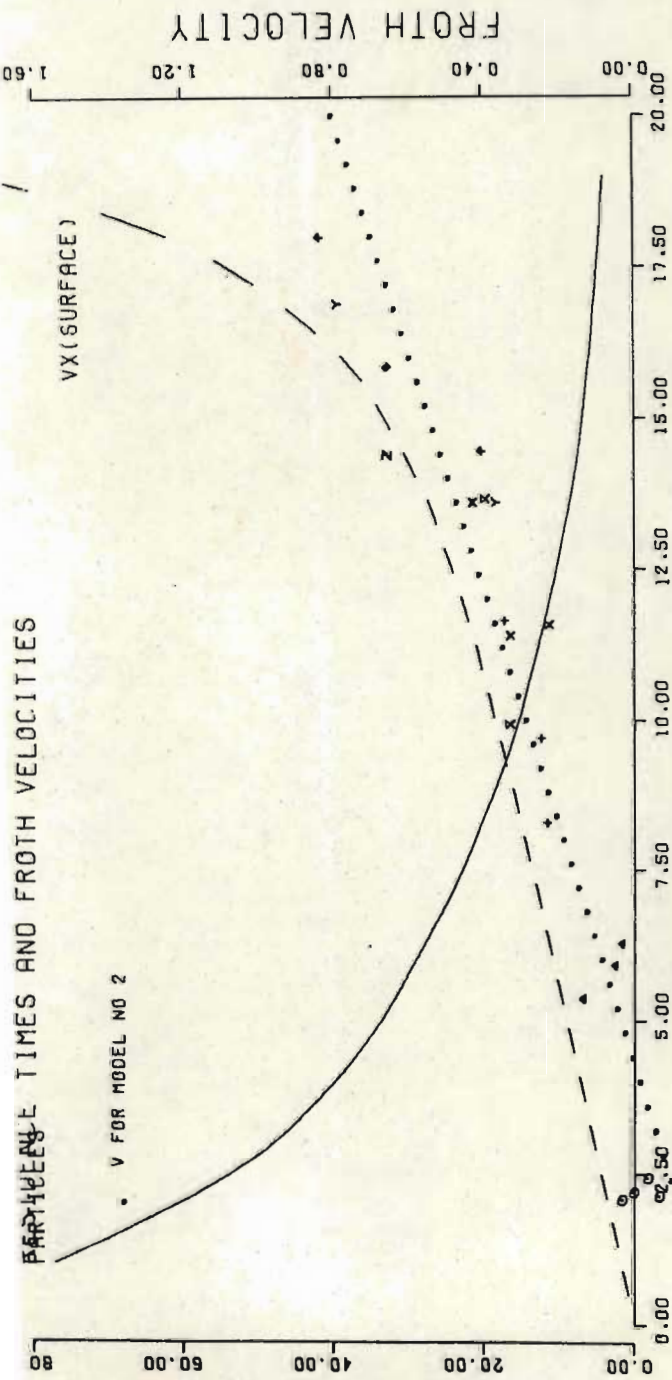
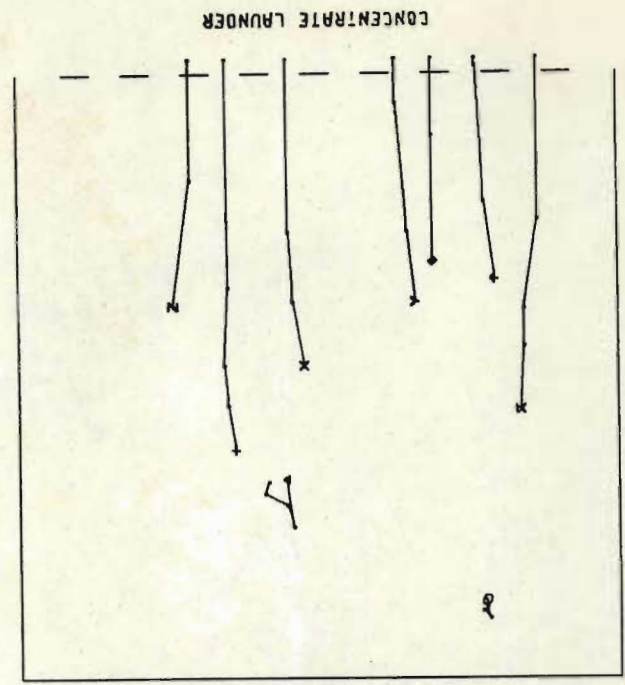
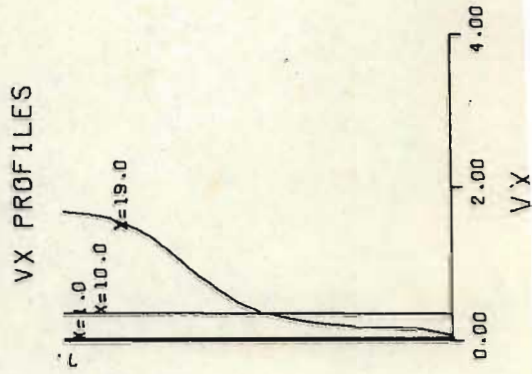
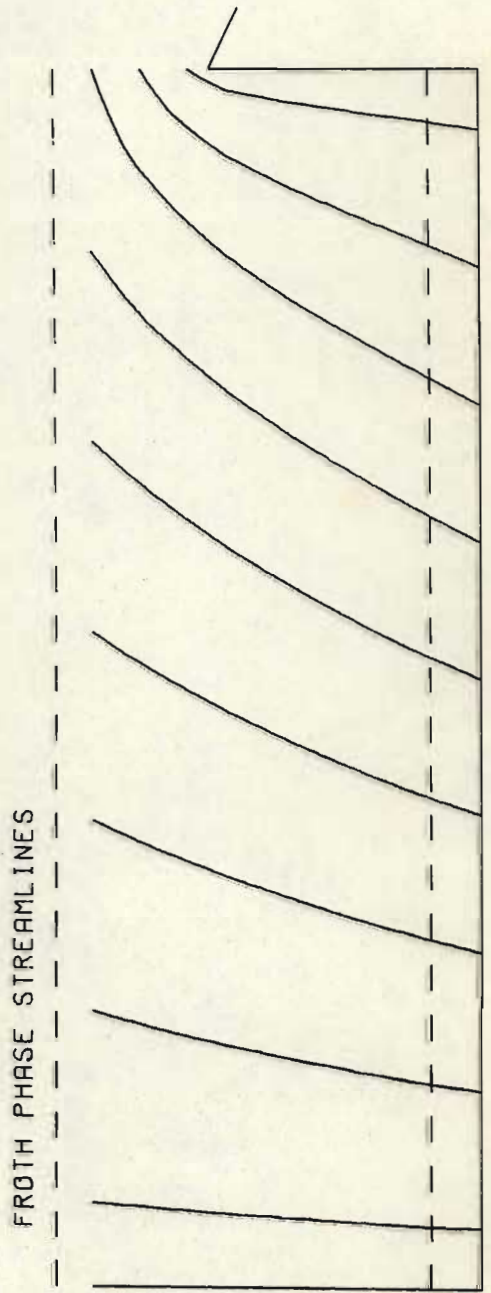


Figure 5.21.3 Froth Velocity data and Laplace Equation solution for Experiment 43; Refer Table 5.4



ALFR	GB1	GB2	GC1	G
0.280	0.606	0.000	2.4	336.7



CONCENTRATE LAUNDER

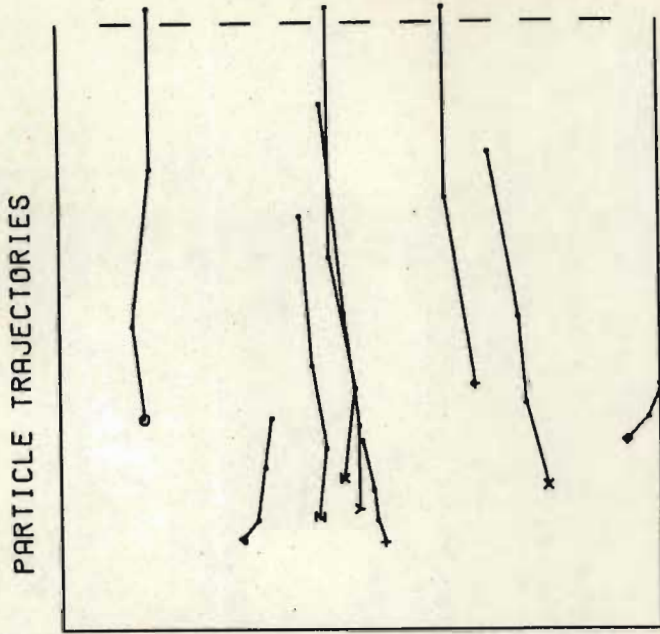
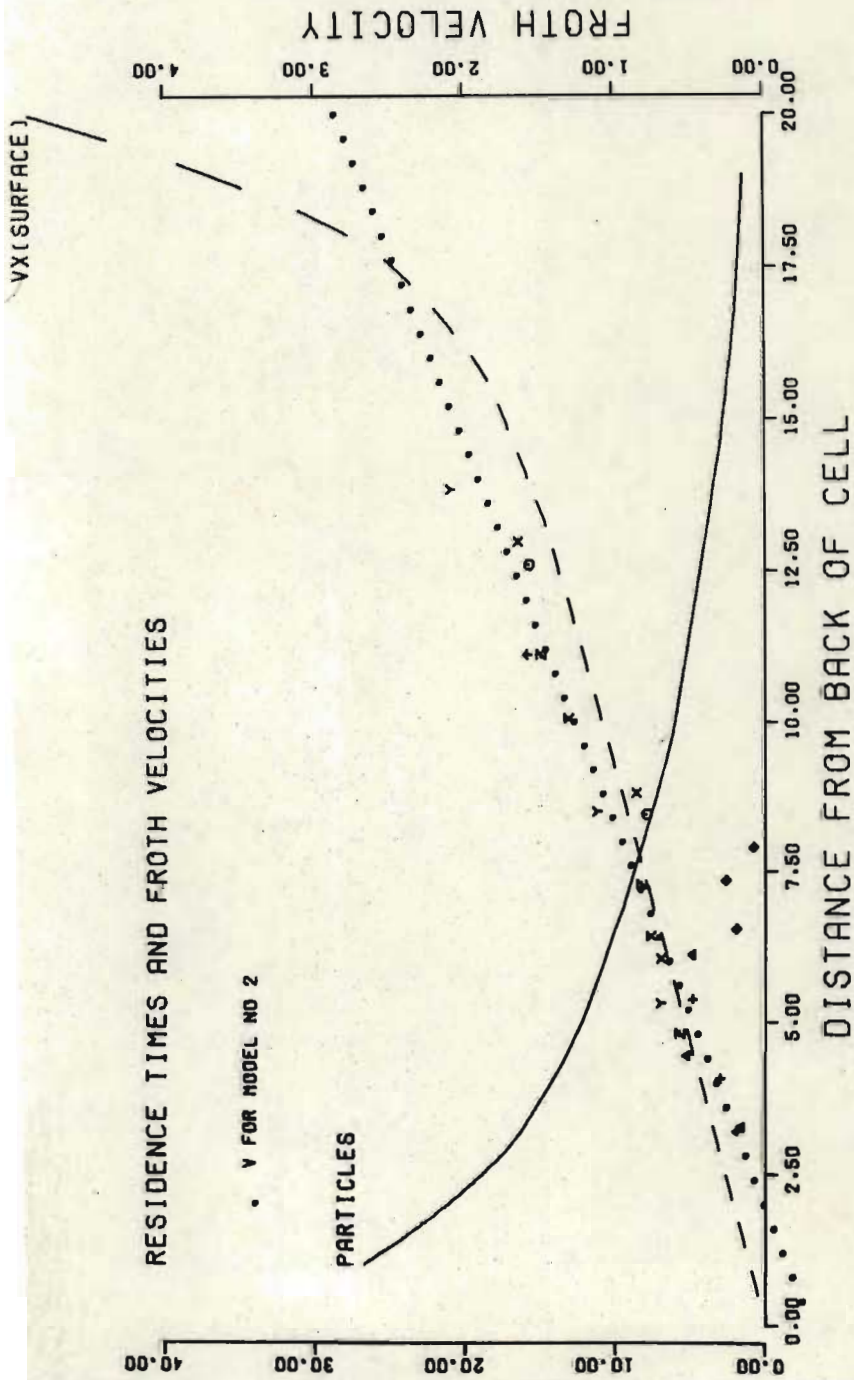
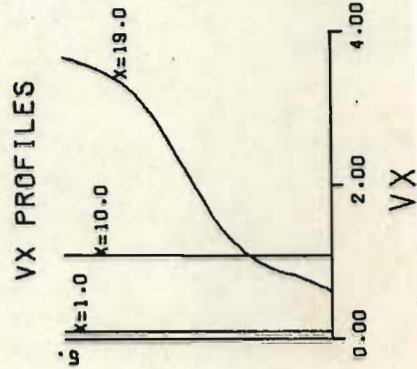
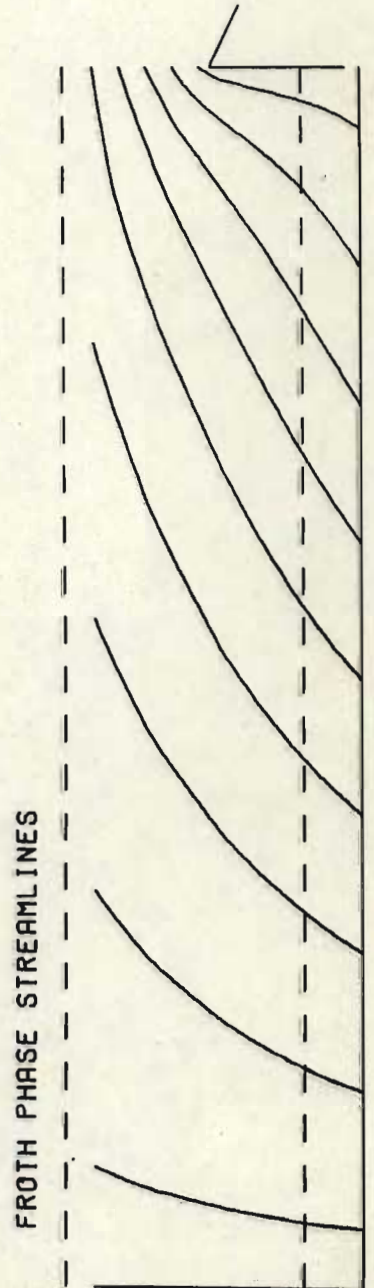


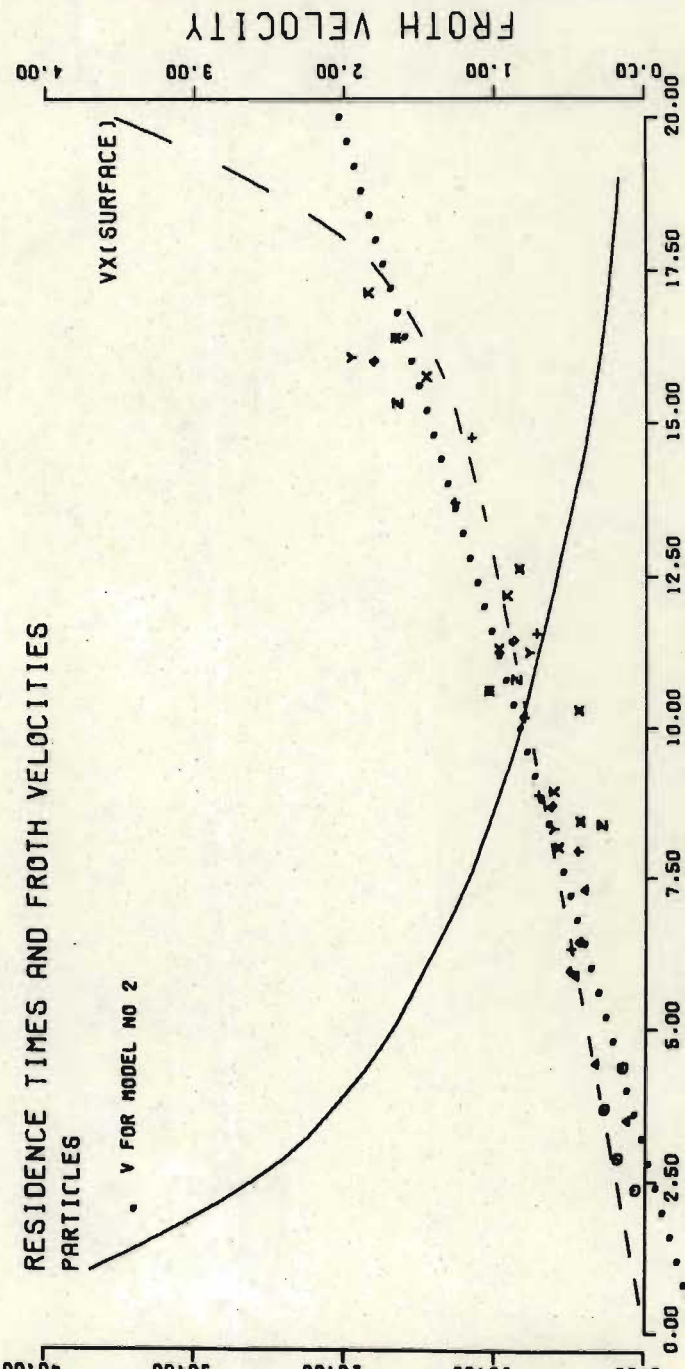
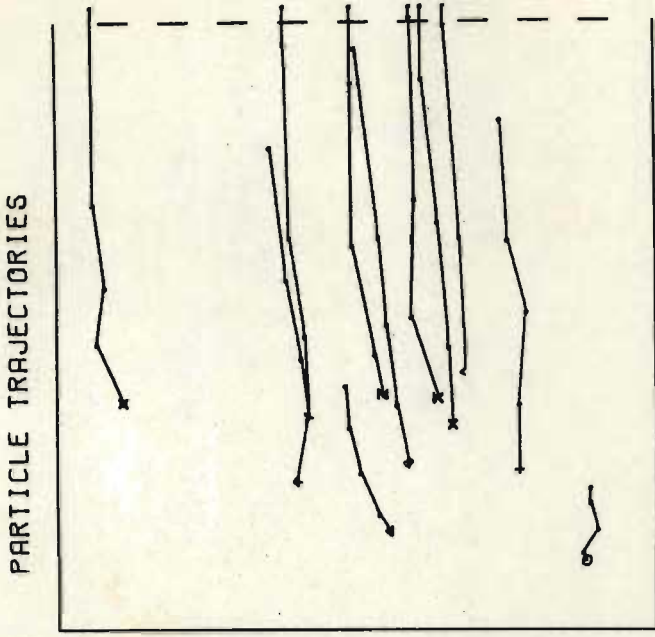
Figure 5.21.4 Froth velocity data and Laplace Equation solution for Experiment 44; Refer Table 5.4



ALFR GB1 GB2 GC1 G  
0.500 0.490 0.000 4.9 392.0







ALFR	GB1	GB2	GC1	G
0.426	0.488	0.000	3.5	336.7

FROTH PHASE STREAMLINES

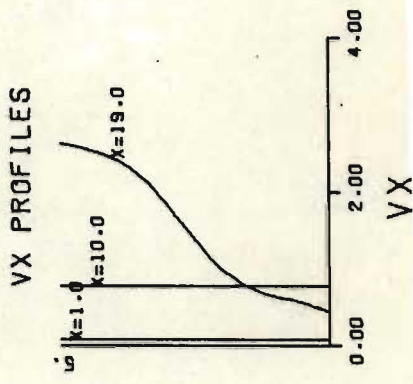
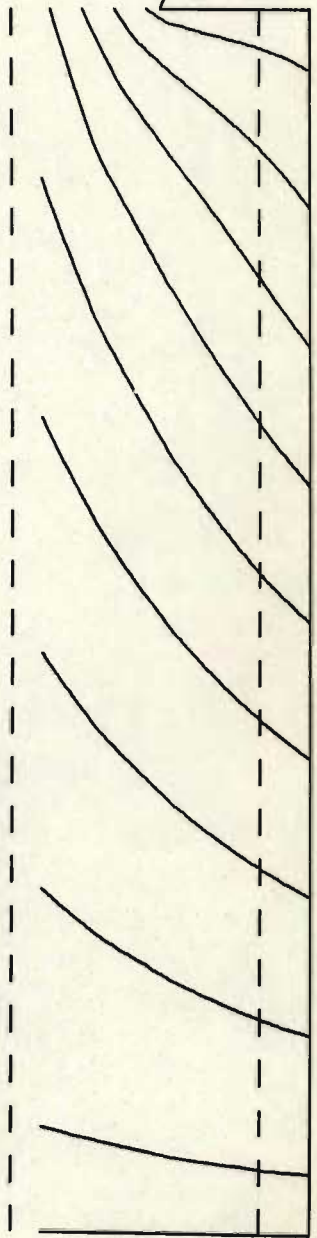


Figure 5.21.5 Froth Velocity data and Laplace Equation solution for Experiment 45; Refer Table 5.4

CONCENTRATE LAUNDER

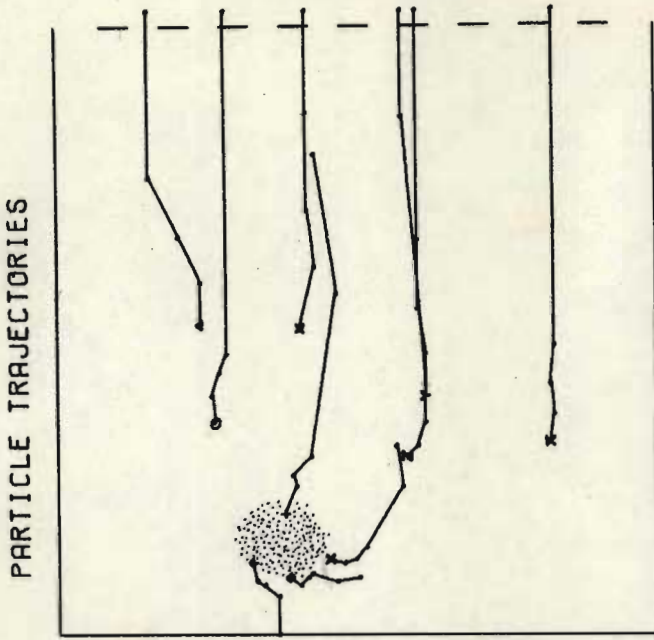
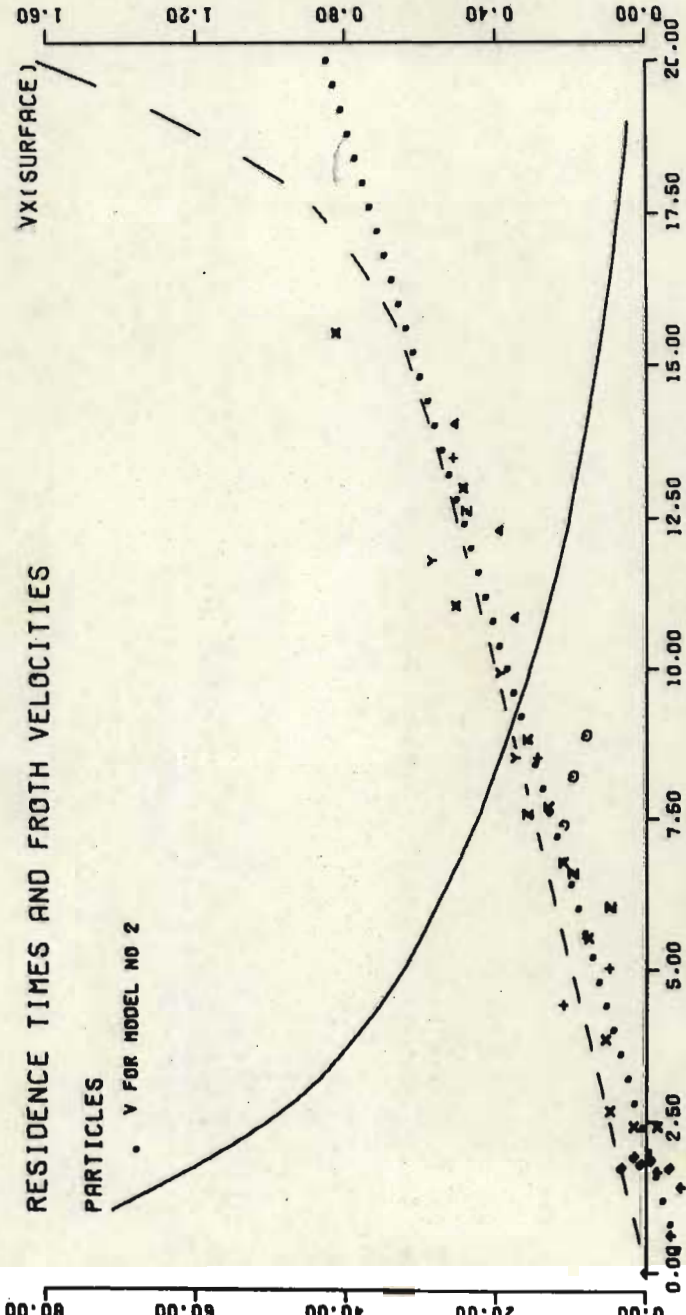


Figure 5.21.6 Froth Velocity data and Laplace Equation solution for Experiment 46; Refer Table 5.4



RESIDENCE TIMES AND FROTH VELOCITIES

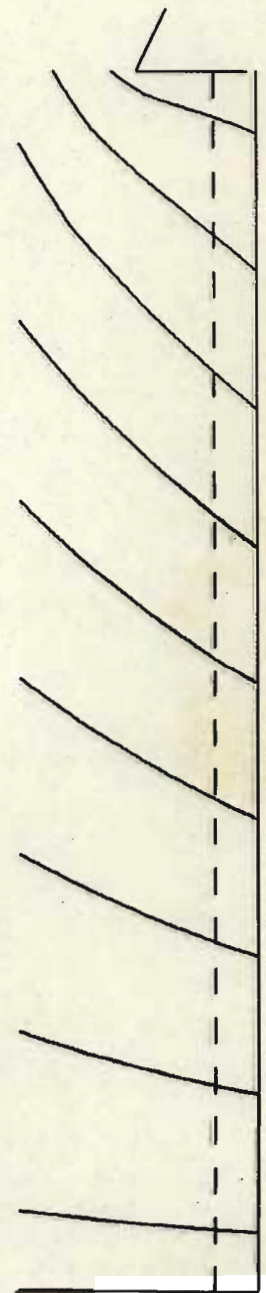
PARTICLES

• V FOR MODEL NO 2

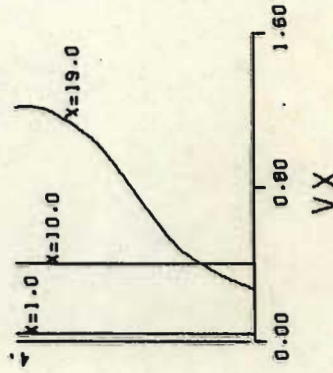
DISTANCE FROM BACK OF CELL

ALFR	GB1	GB2	GCI	G
0.230	0.545	0.000	1.6	283.3

FROTH PHASE STREAMLINES



VX PROFILES



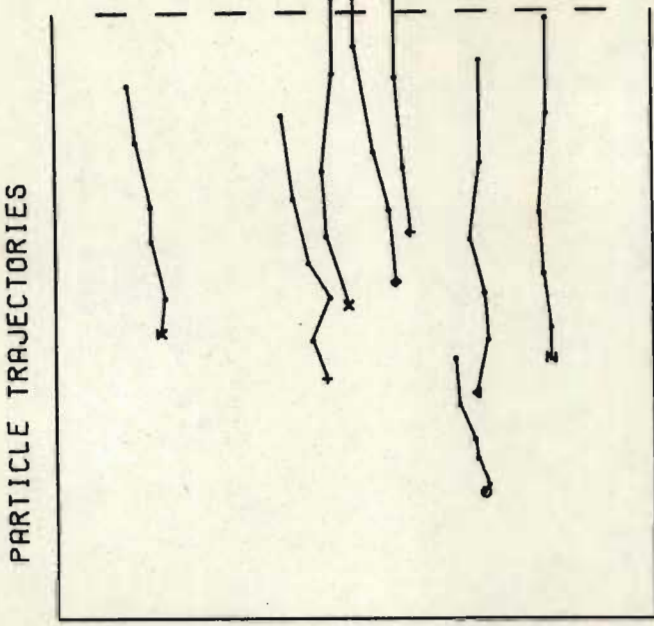
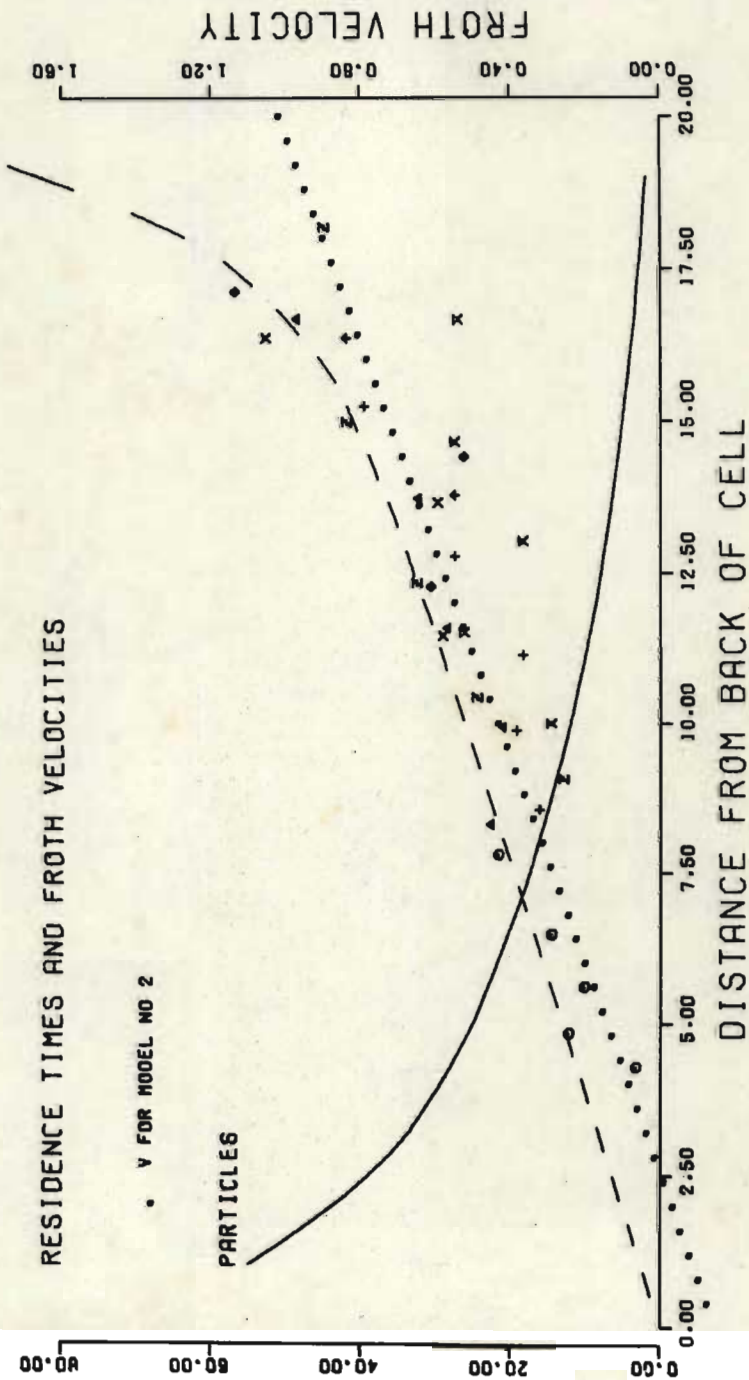
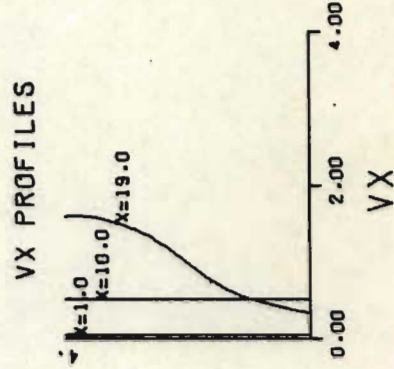
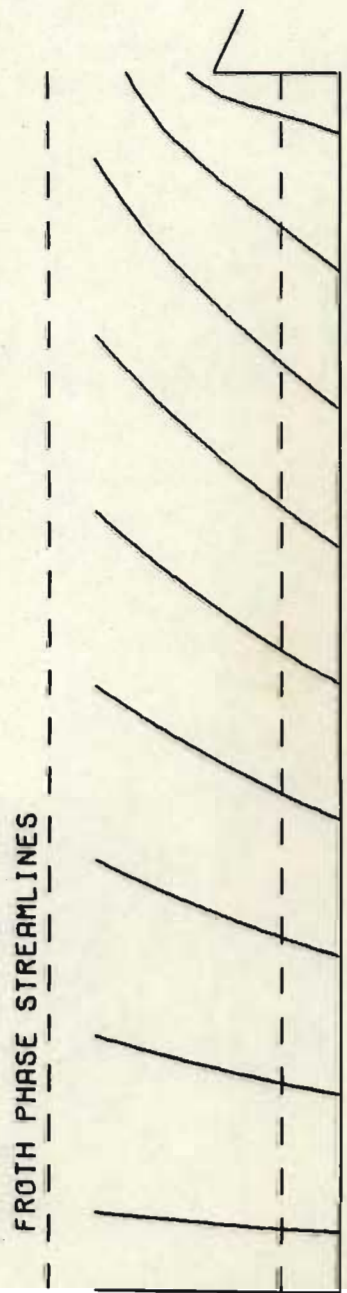


Figure 5.21.7 Froth Velocity data and Laplace Equation solution for Experiment 47; Refer Table 5.4



ALFR	GB1	GB2	GC1	G
0.220	0.764	0.000	2.2	391.7



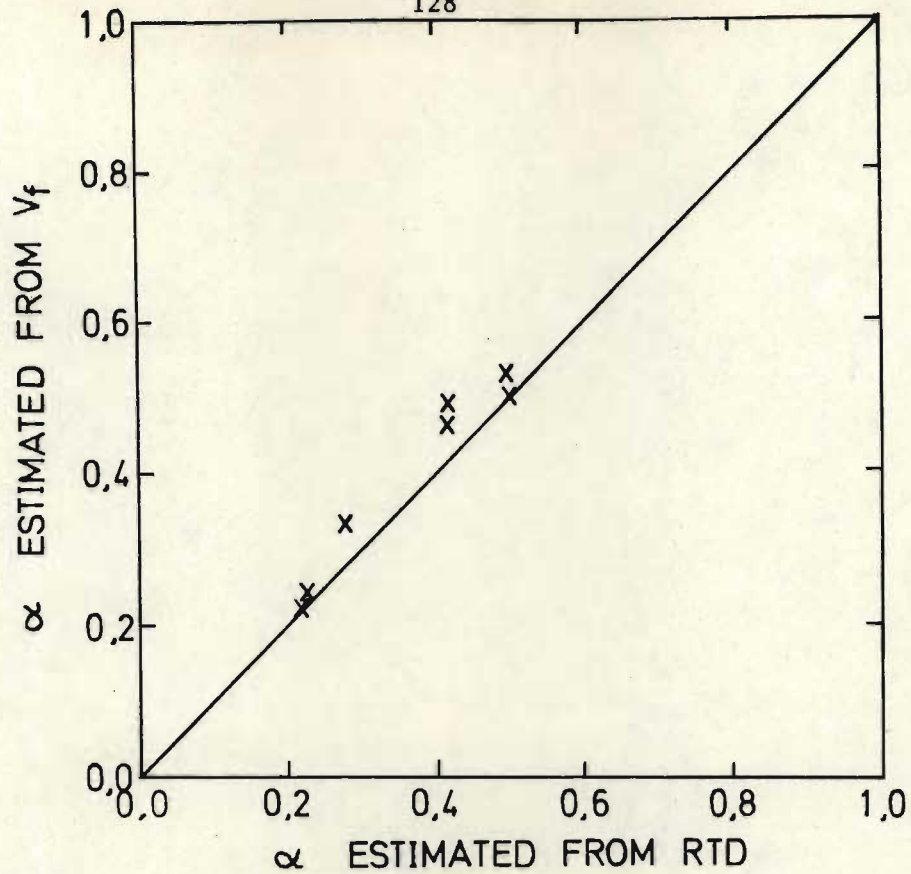


Figure 5.22 Comparison of froth stability values estimated from froth velocity measurements with values estimated from froth RTD measurements.

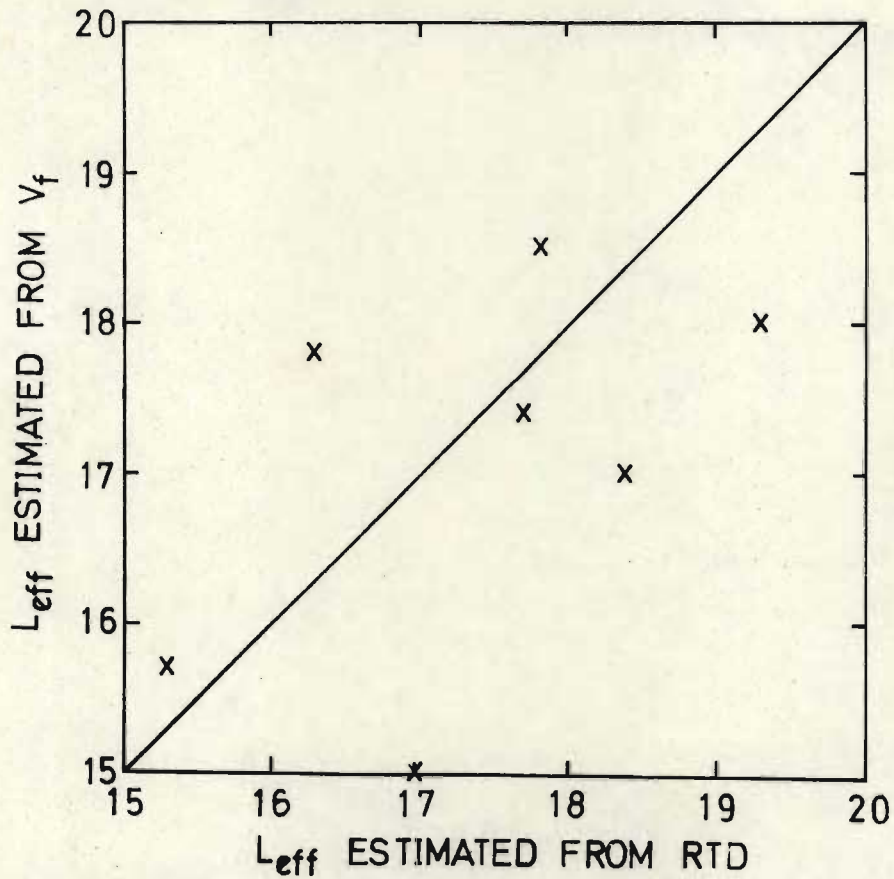


Figure 5.23 Comparison of effective cell length values estimated from froth velocity measurements with values estimated from froth RTD measurements.

where  $m_v$  is the slope of the  $v$  vs  $x$  curve, and  $x_0$  is the point at which  $v(x) = 0$  (not necessarily the back of the cell). If  $v(x)$  can be measured, then estimation of  $m_v$  provides an estimation of  $\alpha$ :

$$\alpha = \frac{m_v h}{g_0 + \delta m_v h}$$

where, as concluded in the previous section,  $\delta$  should be given the value of 0,5 where no measurements are available.

Velocity measurements were performed for experiments 41-47 as described in Section 5.15, and the data is shown in Figures 5.21.1 to 5.21.7. Trajectories of the particles that were traced are shown, and illustrate the various types of behaviour of the surface of the froth. Slow moving froth near the back of the cell results in the erratic behaviour of particles in experiments 41 and 46; for the latter a region of high froth stability (shaded) results in the anomalous behaviour shown. This is evident to a lesser extent for experiment 43. In experiment 44 a particle moves towards the side of the cell and remains there.

Straight lines were fitted by least squares regression through the data in each case, and the slope  $m_v$ , intercept  $x_0$  and hence the froth stability parameter  $\alpha$  were determined. The effective length of froth surface producing froth which reaches the froth lip is

$$L_{\text{eff}} = L - x_0$$

The results of this analysis appear in Table 5.4 and in Figures 5.22 and 5.23 where  $\alpha$  and  $L_{\text{eff}}$  estimated by (i) regression on RTD data (assuming  $g_{b2} = 0$  and  $\delta = 0,5$ ) and (ii) regression on froth velocity data are compared.  $\alpha$  estimated by (ii) is generally larger than that estimated by (i). This is to be expected since Model 2 does not allow for variations of froth velocity at different levels in the froth; thus (5.11) provides a value of the average froth velocity in the  $x$ -direction, and use of the higher surface velocity (measured in these experiments) will produce overestimates of  $\alpha$ . The correlation between the two values of  $L_{\text{eff}}$  is reasonable, considering the indirectness of the methods that are used to estimate them.

The Laplace solution simulator was used to produce predictions of froth surface velocity using the parameters estimated by method (i) and these appear in Figures 5.21.1 to 5.21.7 together with the lines fitted through the velocity data. The apparently wide disparity between the two velocities is due mainly to the fact that the Laplace velocities are constrained to pass through the point  $x=0$ .

#### 5.2.6 Conclusion

It seems fairly well established that, for the two-phase system under consideration

- (i) the cumulative residence time distribution of perfectly floatable particles in the concentrate can be adequately quantified by means of Model 2

$$F_c(\tau) = 1 - \exp \left\{ - \frac{\alpha g_o}{h(1-\alpha\delta)} \left( \tau - \frac{\delta h}{g_o} \right) \right\}$$

- (ii) the residence time ratio  $\delta$  can be assumed to have the value 0,5, unless methods are available for measuring it more accurately
- (iii) the froth stability parameter  $\alpha$  can be obtained by measuring the froth velocity as a function of distance from the back of the cell. Average froth residence time is  $\tau_{av} = h/\alpha g$
- (iv) both  $\alpha$  and the froth removal efficiency  $\epsilon_f$  can be correlated with equations of the form

$$\alpha \text{ or } \epsilon = 1 - \exp (- \beta(g_o - g_o^0))$$

where  $\beta$  and  $g_o^0$  are functions of froth height and frother concentration

- (v) thus the residence time distribution of perfectly floatable particles in the froth phase

$$E_f(\tau) = \epsilon_f E_c(\tau)$$

can be found as a function of frother concentration, froth height and gas rate.

## CHAPTER SIX

### Design of Froth Removal Methods

#### 6.1 Introduction

We now seek to use the tools developed in previous chapters to improve, if possible, the efficiency of the flotation process. This can be done in two ways: we can seek to

- (i) control the properties of the froth (eg stability, viscosity, bubble size, drainage characteristics etc) so that selectivity and recovery are optimised;
- (ii) select the best designs of froth chambers and froth removal methods, or design new ones which will improve the efficiency of the process.

No attempt has been made to control froth properties in this work; however we can make some contribution to objective (i) by recording our observations of the effect of froth properties on flotation performance. Most of the work described in this chapter serves the second objective; a number of modifications to froth chamber geometry and froth removal methods were tested on three different ore types and this allows us to make several recommendations in this area.

The residence time distribution model developed in the previous two chapters has been applied only to the behaviour of two-phase froths; before we can use it for three-phase flotation froths, it must first be shown to be useful for describing them; this is done in the following section. We then use the model to explore the above objectives theoretically, by observing the effect of changing model parameters (eg the froth stability parameter  $\alpha$  which can be controlled with frother addition or the froth removal efficiency  $\epsilon$  which can be independently controlled by modifying chamber design) on grade-recovery curves; we then record results of tests of various design modification suggested by this work on several flotation systems.



## 6.2 Use of the froth RTD model for rationalising real flotation data

Dunne (1975) performed a series of 27 batch tests on a  $3^3$  design to test the effect of air rate, frother concentration and weir height on the flotation characteristics of the Prieska ore. The tests were done in a 1 liter perspex batch cell using 625 g/ton NaCN to depress pyrite, adding lime to bring the pH up to 11,0 and adding 500 g/ton of  $\text{CuSO}_4$  and 75 g/ton of SEX. The levels of the variables were: air rate 3,7 5,6 and 7,5 l#min; frother concentration (FC) 15 30 and 45 g/ton; weir height 2 4 and 6 cm. The time that it took for froth to build up in the cell before coming over the lip was recorded in most cases, and then the flotation response was measured in 4 pans which were changed at intervals over 10 minutes.

Two methods were used for obtaining estimates of froth stability  $\alpha$  from this data:

- (i) The time  $t_0$  that it takes for the froth to build up in the froth chamber to the point where it flows over the froth lip is related to the gas flux  $g_0$ , the weir height  $h$  and the average froth stability parameter  $\bar{\alpha}$  by

$$t_0 = \frac{h}{\bar{\alpha}g_0}$$

Since all parameters except  $\bar{\alpha}$  are known for experiments where  $t_0$  is measured, an estimator for  $\bar{\alpha}$  becomes available, and these estimates are plotted in Figure 6.1 as a function of FC,  $h$  and  $g_0$ . Note that for any particular values of  $g_0$  and FC,  $\bar{\alpha}$  increases with  $h$ , which implies that the instantaneous value of  $\alpha$  increases as the froth builds up, a deduction consonant with what is observed in practice ie that froth breaks very rapidly at the beginning of the build up of froth, and then the breakage rate decreases as the solids that are levitated into the froth produce a stable layer of froth on top of the froth column.

Secondly we note that for a given froth concentration and weir height, the value of  $\bar{\alpha}$  decreases as gas rate increases, an

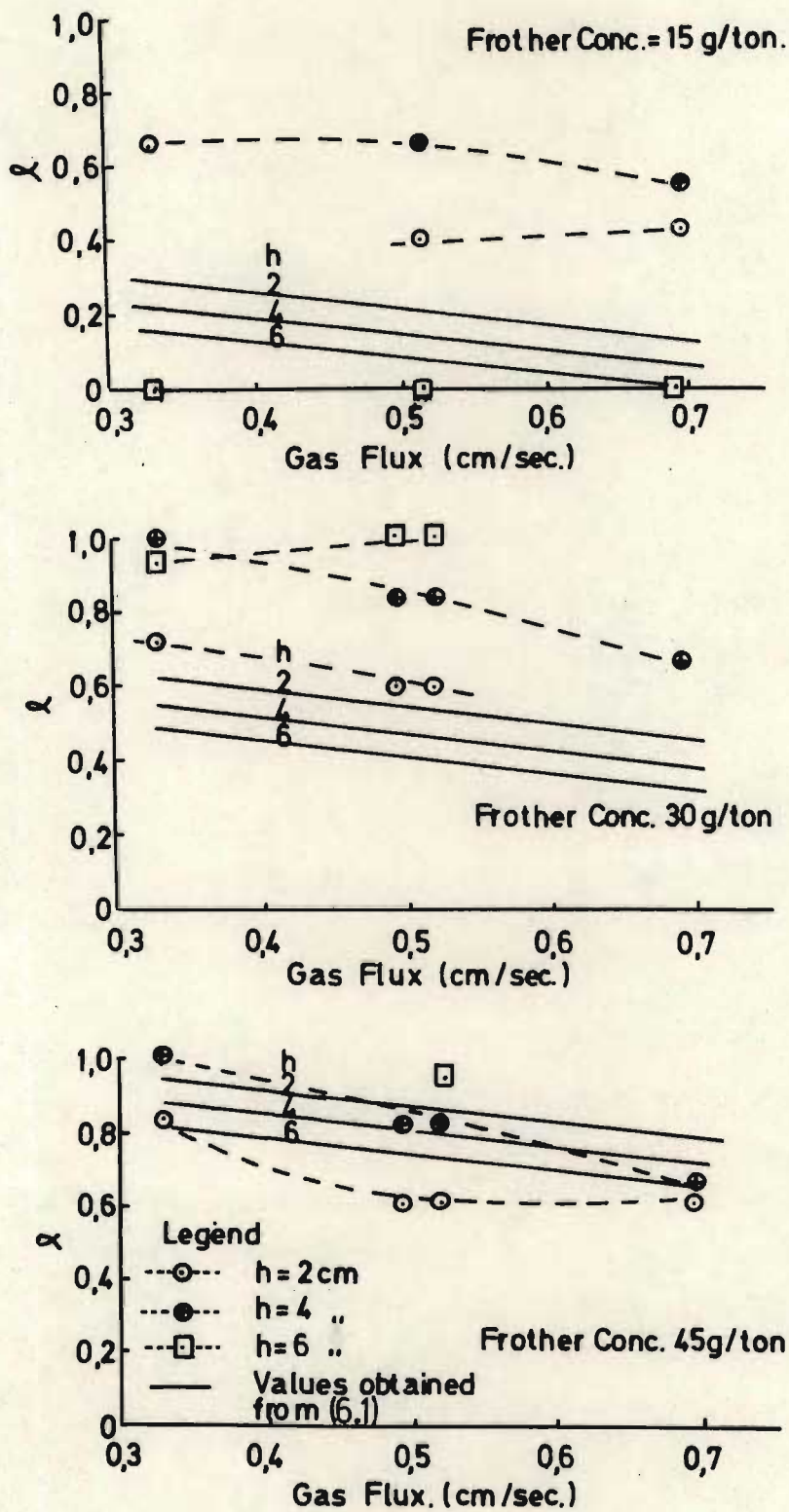


Figure 6.1 Average froth stability calculated from froth rise time measurements, and estimated by regression on froth flow rates.

observation which is contrary to that obtained with 2-phase froths (Section 5.2.4) This is almost certainly due to the fact that froth which is removed at a high rate has a low solids density, resulting in poorly mineralised and hence unstable bubble films.

Thirdly, as expected,  $\bar{\alpha}$  increases as frother concentration increases. This should not be regarded as the norm however, since excess frother is known in many cases to destabilise froth.

- (ii) By regressing on simulated continuous removal rates for each component using the model developed in Section 4.2.2.3,

$$M_{Ci} = \frac{\epsilon_f \alpha g_o \bar{C} M_{fio} e^{-k_{fi} \tau_{min}}}{h(k_{fi} + \alpha g_o \bar{C}/h)}$$

estimates of the parameters in the following expression for  $\alpha$  were obtained:

$$\alpha = a_0 + a_1 FC + a_2 h + a_3 g_o \quad (6.1)$$

The procedure used was as follows:

- a. Obtain simulated continuous flotation removal rates by assuming that these are equal to the average removal rate during the first 30 seconds of the batch test.
- b. Simplify the model by assuming that  $\epsilon_f = 1,0$   $\delta = 0,5$  and that the flowrates of components into the froth phase are given by the expressions given in Table 6.1. Gangue is assumed to be recovered mainly by entrainment in the water flowing into the froth phase.
- c. Obtain first estimates of the parameters  $a_0$  to  $a_3$  using the data shown in Figure 6.1, and regress on the  $k_{fi}$  and the  $k_{pi}$ , assuming that they are unaffected by the experimental variables  $g_o$ ,  $h$  and  $FC$ .

Table 6.1 Results of hypothesis testing of the froth model on Dunne's data.

Hypothesis No.		0	1	2		
Method used for estimating $\alpha$		$\alpha$ calculated from (6.1)	$\alpha$ calculated from $t_o$	$\alpha=1,0$	Method used for calculating $M_{fio}$	
Chalco- pyrite (i=1)	$k_p$	,060	,062	,064	$M_{fio} = k_{pi} A G_{Ti}$	
	$k_f$	,10	,19	,31		
	$S^2$	,22	1,46	2,82		
Sphalerite (i=2)	$k_p$	,061	,060	,06		
	$k_f$	,11	,19	,30		
	$S^2$	,215	1,44	2,77		
Pyrite (i=3)	$k_p$	,66	,57	,65	$M_{f4o} = k_{p4} C_{T4} M_{f5o}$	
	$k_f$	,15	,22	,21		
	$S^2$	,077	,228	,332		
Gangue (i=4)	$k_p$	,37	,41	,40		$M_{f5o} = k_{p5} G$
	$k_f$	,18	,28	,23		
	$S^2$	,016	,069	,106		
Water (i=5)	$k_p$	,0038	,0039	,0017		
	$k_f$	,22	,32	,29		
	$S^2$	,041	,224	,34		

- d. Finally regress on the  $k_{fi}$ ,  $k_{pi}$  and the parameters  $a_0 - a_3$  to obtain the best estimates of all parameters simultaneously.

Results of the above analysis, taken in isolation, would be of minimal significance because of the unproven nature of the model and the gross assumptions made above. For this reason the parameters  $k_{fi}$  and  $k_{pi}$  were also estimated under the following hypotheses

$H_1$ :  $\alpha$  is given by the values calculated from the froth rise times  $t_0$

$H_2$ :  $\alpha=1,0$  ie ignore the effect of froth stability.

(The null hypothesis  $H_0$  is that  $\alpha$  is given by (6.1).) The results of these regressions are compared with results for the null hypothesis in Table 6.1, and the correlation between experimental and predicted recoveries for  $H_0$  is shown graphically in Figure 6.2. The relative values of the sums of squares indicate that assuming  $\alpha=1,0$  produces very poor correlation between experimental and predicted behaviour, and this shows that ignoring froth stability effects can have serious effects on attempts to model flotation behaviour. The use of  $\alpha$ 's calculated from  $t_0$  measurements produce an unsensational improvement in the fit of the model to the data, which is not surprising since these values are calculated from measurements on froths that are not flowing, and hence are unlikely to behave in a similar fashion to those which are. The correlations between experiment and prediction for  $H_0$  as shown in Figure 6.2 are good, considering the wide range of experimental variables tested, and this constitutes an encouraging step towards the verification of the model developed in this work. The values of  $\alpha$  obtained when the final estimates of  $a_0$  to  $a_4$  are substituted in (6.1) are plotted in Figure 6.1. The trends for increasing frother concentration and gas rate are the same as those observed with the  $\alpha$  values calculated from froth rise times. However the regressed  $\alpha$  values decrease as  $h$  increases; this is the effect that is to be expected since froth drainage increases as  $h$  increases, resulting in decreased froth stability for flowing froths.

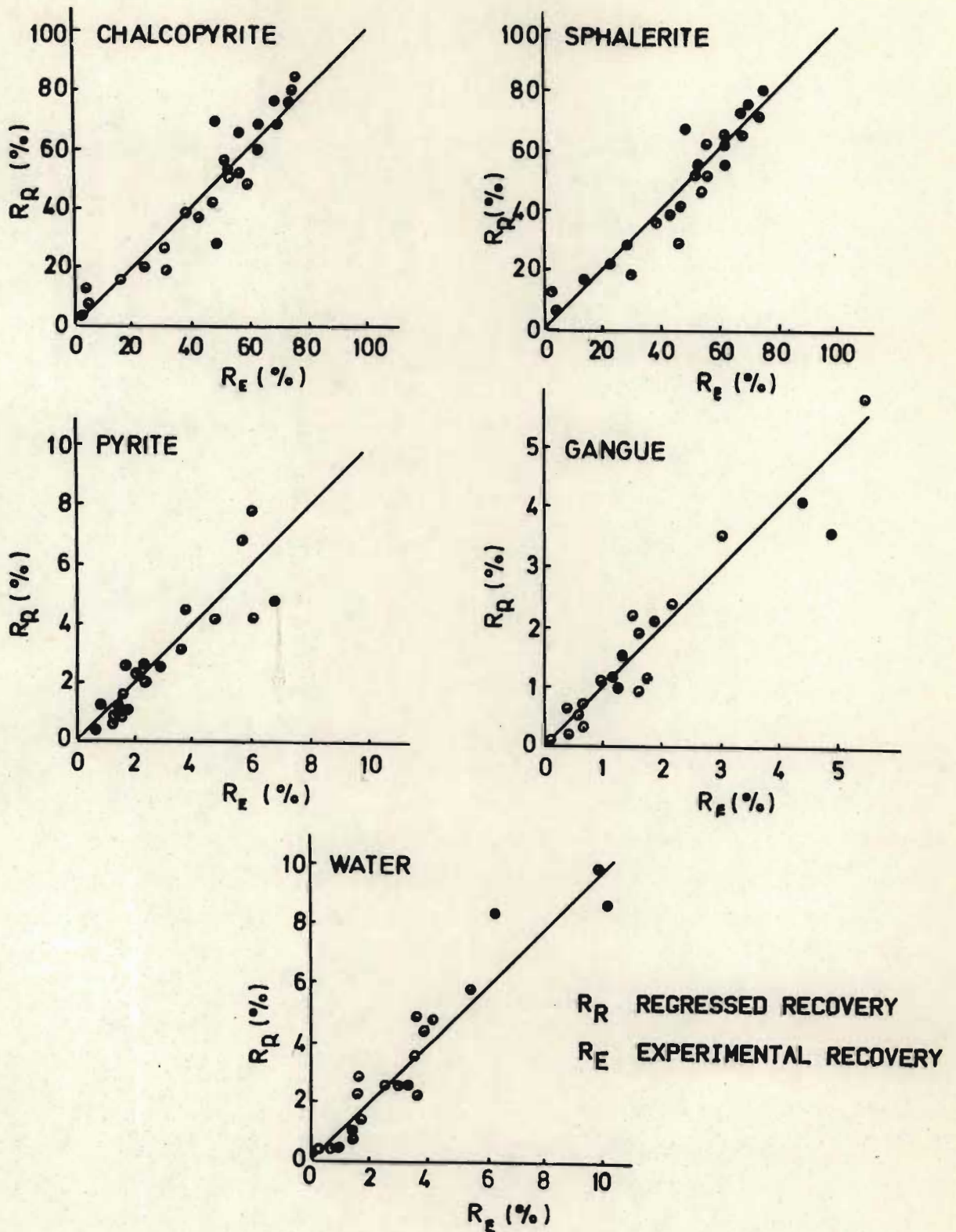


Figure 6.2 Comparison of recoveries produced by the model (using equation (6.1) to evaluate the froth stability) with recoveries obtained experimentally.

### 6.3 Effect of changes in the RTD Model parameters on flotation performance.

We now perform a sensitivity analysis on the RTD Model by observing the effect of changes in the parameters on grade-recovery curves. This gives us an idea of the way in which parameters should be changed to optimise flotation performance, and various design and control actions which may produce such changes are discussed.

#### 6.3.1 Simulation of grade-recovery curves.

To avoid unnecessary complications we simulate the flotation response of a simple 2-component (one mineral, one gangue) system. The rate of transport of mineral, gangue and water into the froth phase are given by the equations for components 1, 4 and 5 respectively in Table 6.1. The head grade of mineral is 10% and the feed enters the cell at 20% solids by weight. Values of the parameters  $k_{fi}$  and  $k_{pi}$  were selected to produce approximately 70% recovery at 70% grade for froth height  $h = 2$ , gas rate = 2,5, froth removal efficiency  $\epsilon = 0,5$  froth stability  $\alpha = 0,5$  (any consistent set of units may be used); their values in vector form are  $k_{fi} = (0,08 \ 0,5 \ 0,6)$  and  $k_{pi} = (700,0 \ 1,0 \ 50,0)$ . Grade-recovery loci were obtained by varying the gas rate between 1,0 and 5,0. The above data were used to generate the "base case" locus in Figure 6.3. Other loci were generated by changing the above parameters one at a time to the values indicated on Figure 6.3. In discussing Figure 6.3 we must bear in mind that in practice all the parameters would change simultaneously with changes in the gas rate, hence these curves cannot simulate what might happen experimentally; this is strictly nothing more than a one by one parameter sensitivity test. The following points are of interest:

- (i) Increasing the froth removal efficiency  $\epsilon$  shifts the grade-recovery curve away from the origin by a substantial amount i.e. flotation efficiency characterised by e.g. recovery at a particular grade is increased over the whole range of gas rates considered. This is because, as  $\epsilon$  increases, the effective surface of the cell area and hence the effective froth volume is increased, resulting in a larger average residence time in the froth phase and greater selectivity.

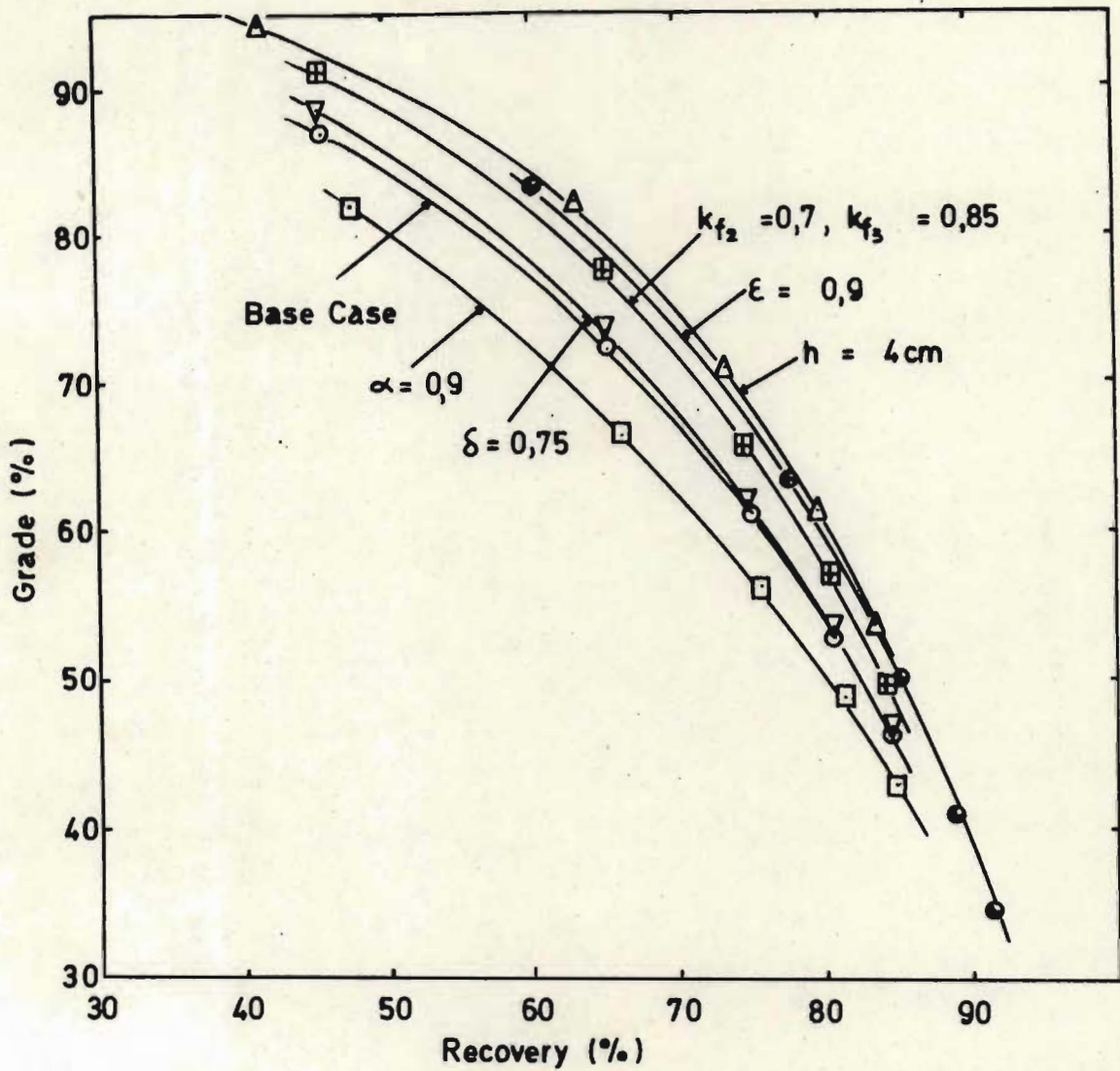


Figure 6.3 Effect of changes in parameters on grade recovery curves  
 (base case parameters are:  $\alpha=0,5$   $\delta=0,5$   $k_{f1}=0,08$   
 $k_{f2}=0,5$   $k_{f3}=0,6$ )



- (ii) Increasing froth stability  $\alpha$  reduces flotation efficiency because both the average and the minimum froth residence times are decreased;  $\tau_{av}$  being inversely proportional to  $\alpha$  for a given froth volume and gas rate, and  $\tau_{min}$  being at least theoretically a strong function of  $\alpha$  (see section 4.2.1).
- (iii) Increasing the residence time ratio  $\delta$  produces a slight improvement in grade at low recoveries, because, as the minimum residence time  $\tau_{min} = \delta h/g_o$  is increased, the amount of entrainment of gangue near the overflow weir is decreased. The amount by which changing  $\delta$  will improve flotation recovery increases as the drainage rate of gangue increases, since gangue recovery is proportional to  $e^{-k_{fi}\tau_{min}}$ .
- (iv) Increasing the froth height increases flotation efficiency by increasing froth volume and hence froth residence time.
- (v) Increasing the drainage rate constants for gangue and water has the obvious effect.

As indicated above, for any real flotation system  $\alpha$  and  $\epsilon$  (and probably the  $k_{fi}$  and  $\delta$ ) will be strong functions of control variables such as gas rate  $g_o$ , frother concentration FC and froth height  $h$ , and the design of the frother chamber and froth removal method. Two further sets of simulations (shown in Figures 6.4 and 6.5) were performed assuming that  $\alpha$  and  $\epsilon$  were given by

- (a) equations (5.8) and (5.4) respectively which were determined for two-phase froths in chapter 5; and
- (b) equation (6.1) and  $\epsilon=1$  i.e. the values obtained/used in analysing Dunne's data (section 6.2).

Case (a) is also unrealistic because the equations were derived from 2-phase froth data; however a few interesting points are illustrated:

- (i) Increasing the frother concentration from  $10$  to  $20 \times 10^{-6}$  g/cc produces a substantial decrease in flotation efficiency; a further increase to  $30 \times 10^{-6}$  g/cc produces little change. Similar behaviour is obtained in case (b) where FC is changed over the range 15-45 g/ton.
- (ii) Increasing  $h$  produces an improvement in both cases, this being most marked in case (b)

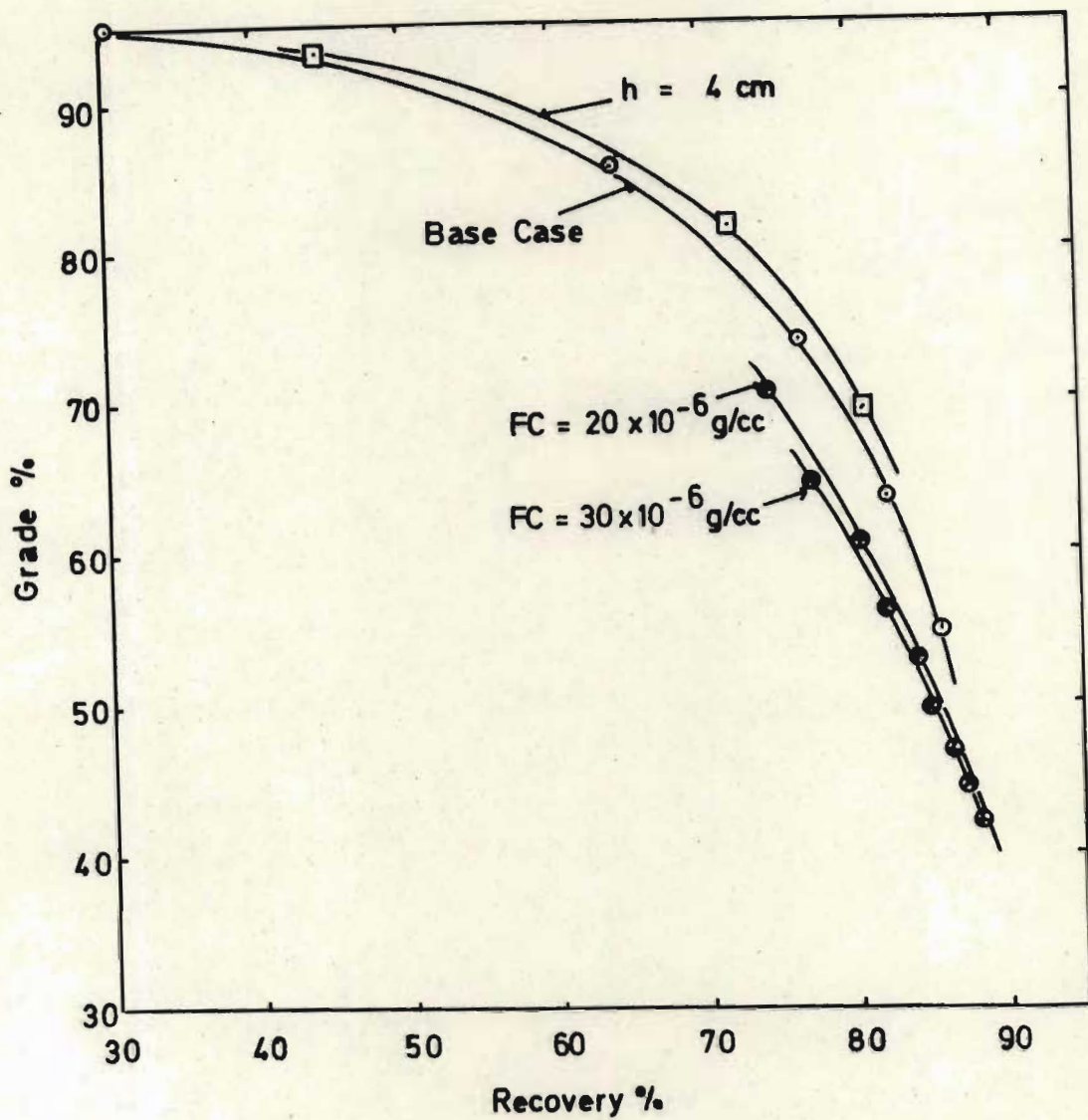


Figure 6.4 Grade-recovery curves using expressions for  $\alpha$  and  $\epsilon$  determined in Chapter 5: effect of variations in froth height  $h$  and frother concentration  $FC$  (base case:  $h=2$  cm and  $FC=10 \times 10^{-6}$  g/cc)

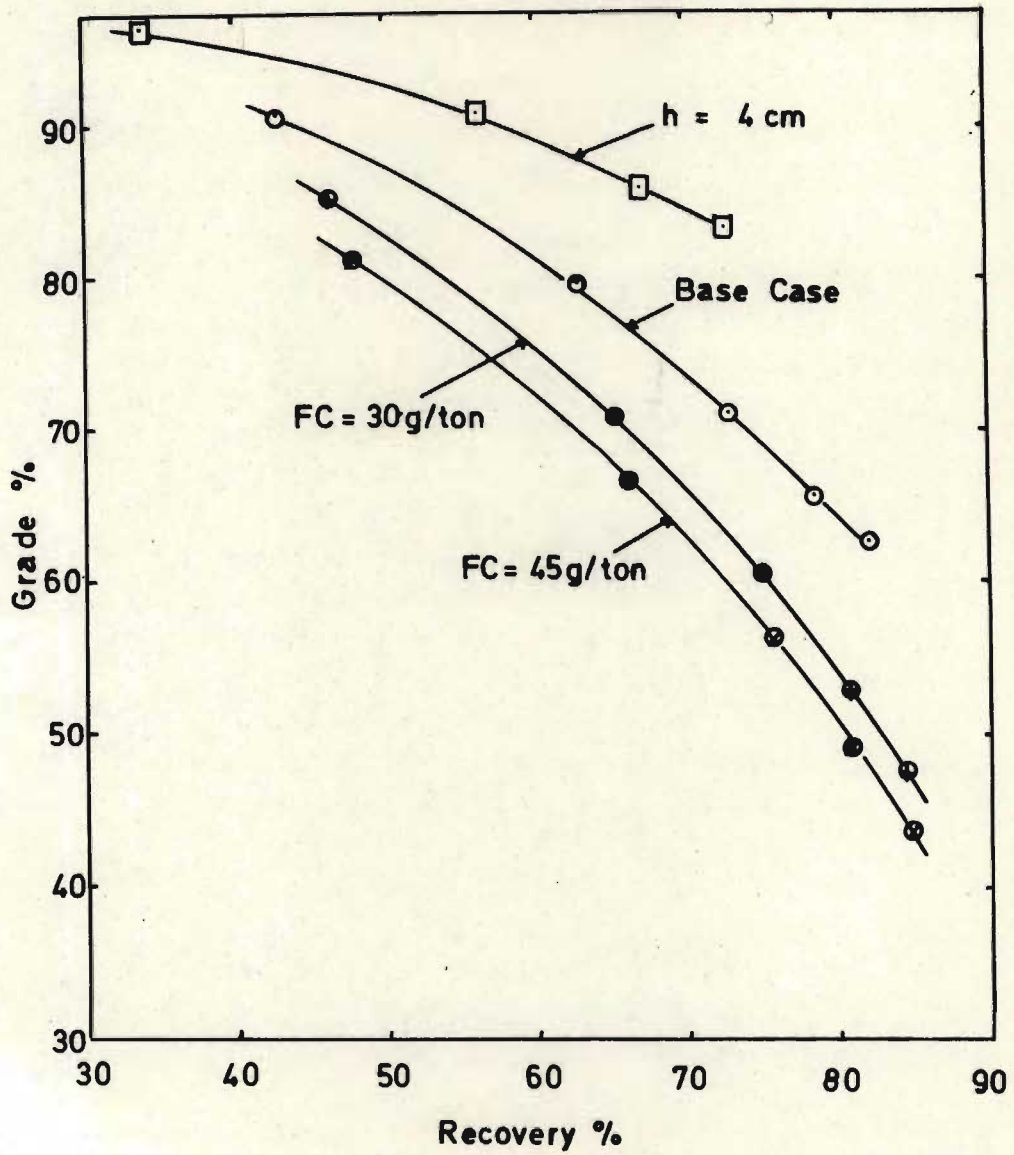


Figure 6.5 Grade-recovery curves using expressions for  $\alpha$  and  $\epsilon$  determined in Section 6.2 (Dunne's data): effect of variations in froth height  $h$  and frother concentration  $FC$ . (base case:  $h=2$  cm,  $FC=15$ g/ton)

(iii) In case (b) the shape of the curves is very different from that shown in the previous two figures, the slopes of the loci changing more slowly over the range of recoveries considered. This is because  $\alpha$  decreases as  $g_0$  increases resulting in a slower decrease in selectivity at high recoveries.

All of these simulations illustrate the complex dependence of flotation efficiency on froth parameters, and also provide some indicators as to how this efficiency may be improved as discussed in the next section.

### 6.3.2 Implications for design and control.

Certain desirable objectives can be formulated for each of the above parameters, and the latter can be manipulated in the following ways to achieve these objectives:

- (i) froth removal efficiency  $\epsilon$  should be maximised ie no dead areas should exist in the froth phase. This results in efficient use of the available volume of the froth chamber, resulting in maximum drainage of the froth at a given froth removal rate.  $\epsilon$  is maximised by
- a. having concentrate launders on both sides of the cell, so that dead froth volumes do not build up at the back of the cell;
  - b. better still, having removal of froth on all sides of the cell and even within the froth phase using launders mounted in the froth as is the case with Maxwell cells. In the latter no dead froth volumes exist, the length of overflow lip per unit surface area of froth is large, and no element has to travel a great distance before entering the concentrate launder. This allows the use of a lower gas rate per unit of pulp volume, with resulting improved agitation of the pulp at lower impeller speeds and lower power requirements.
  - c. a crowder can be mounted at the back of a conventional cell to force froth towards the froth lip; this suffers from the disadvantage of reducing froth volume.

- d. an innovation not conceived of before would be to have paddles at the back of the cell which continually move froth away from that area.
- e. better still, a baffle could be mounted in the cell as shown in Figure 6.6 which forces all bubbles to rise near the back of the cell. The froth thus formed would then flow across the cell towards the froth lip as shown; all froth elements would be subject to the same residence time and would thus be well drained; gangue and water draining from the froth would be recycled to the pulp phase through the slit shown in Figure 6.6. This could be applied to cells with froth discharge on both sides of the cell and even to Maxwell cells in an obvious way. One disadvantage of this would be that the baffle would encourage the coalescence of bubbles while they coursed up towards its edge; this together with the distance to be travelled by the froth before it reaches the concentrate launder seems to dictate that this method would work best for systems with very stable bubbles and froths.
- (ii) Froth stability  $\alpha$  will have an optimum value for any particular system. If  $\alpha$  is too low, high gas rates will be required to produce an appreciable flow of concentrate; these high gas rates may produce undesirable effects in the pulp phase eg poor agitation, oversize bubbles etc. High values of  $\alpha$  imply very stable froths (producing dead volumes in the froth phase, particularly at the back of the cell), low rates of drainage (hence low froth enrichment), low froth residence times and other problems associated with stable froths (eg flooding of launders, poor pumping characteristics for concentrates etc). Besides these macroscopic effects we should also consider the microscopic aspects of bubble breakage on the surface of the froth. What happens to the water and load of particles associated with a bubble when it bursts? Some high-speed photographic work not reported in this volume revealed that single phase bubble films break into tiny droplets which are scattered over neighbouring bubbles. Photographs of

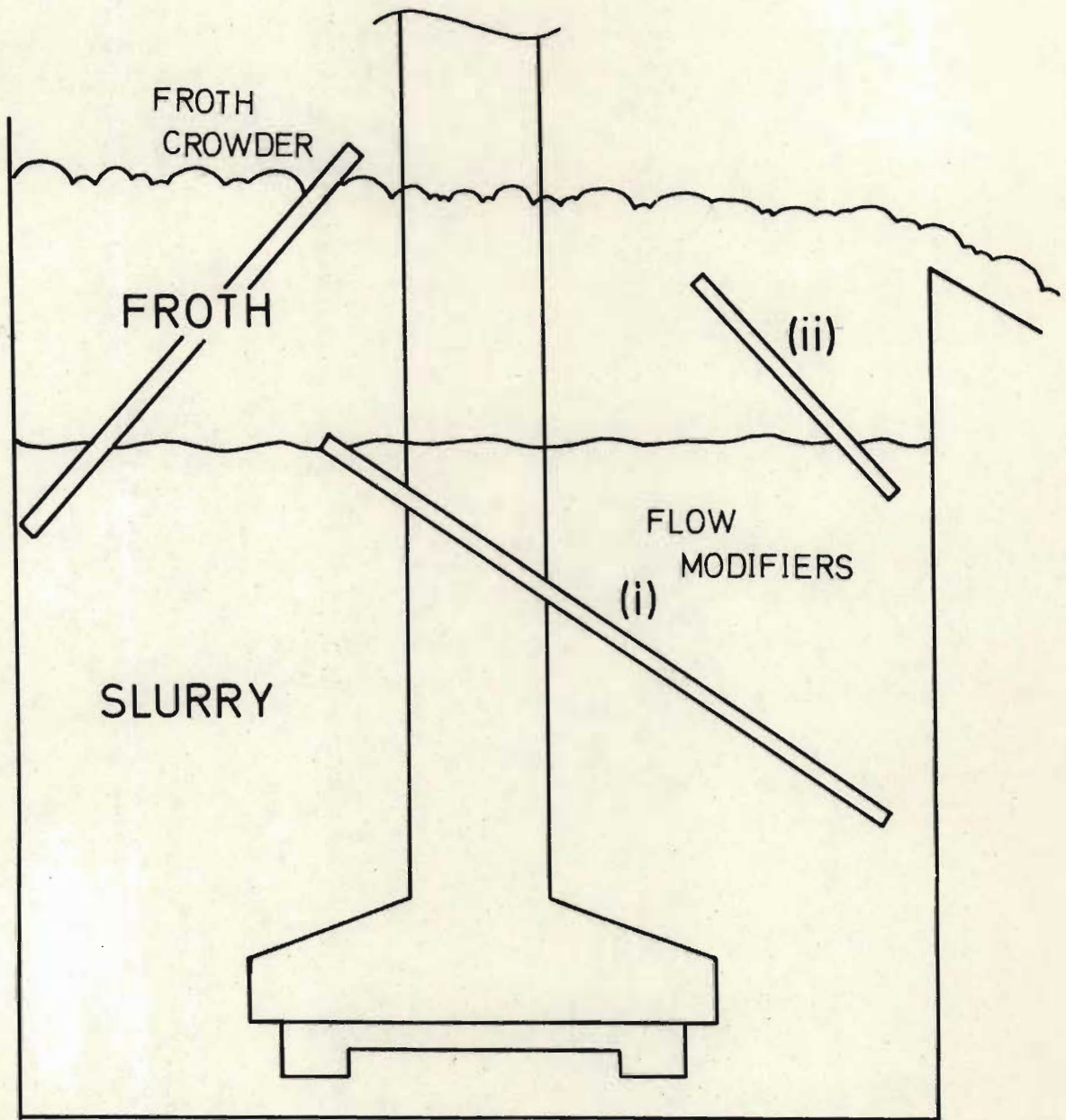


Figure 6.6 - The froth crowder and two versions of flow modifier discussed in (i) section 6.3.2 and (ii) section 6.4

three-phase froths were inconclusive; it was not possible to establish whether the same mechanism operated, or whether the film elements were pulled down to the base of the bubble by the receding edge of the hole in the film. The first mechanism would maximise the chances of hydrophobic particles sticking to films upon which they fall. This mechanism is supported by what is observed at the end of a batch float in a glass flotation cell; the otherwise clean froth contains a thin layer of the last remaining hydrophobic particles on the top of the froth. The second mechanism would maximise the chances of the constituents of the broken film entering Plateau borders and draining back to the base of the froth; hydrophobic particles (especially small ones) would have a reduced chance of being reattached to a bubble film, while the drainage of gangue particles would certainly be increased. In either event, to a greater or lesser extent, a certain amount of bubble breakage should result in improving the grade of the concentrate.

$\alpha$  can be changed by

- a. adding flotation reagents which modify the properties of the froth. Guest (1979) added Cresylic acid (known as a "froth stiffener") which changed a "wet, slimy" froth to a "crisp" one, and increased recovery of  $\text{CaF}_2$  at grade from 49 to 80%. Another attempt with power paraffin, however, produced a stable froth with the appearance of "whipped cream" and was accompanied by a loss in recovery.
- b. Controlling the froth depth which produces better drainage of the froth and hence increased bubble breakage in some cases.
- c. Spraying or dousing of the froth which replaces water lost in the upper regions of the froth, and hence increases  $\alpha$ . If spraying is too vigorous, or if water has an inherent destabilising effect (eg due to removal of frother molecules) then  $\alpha$  will be decreased.

- d. changing the distance travelled by the froth before it enters the concentrate launder. Thus the Maxwell cell would be suitable for systems with very unstable froths, while modification (i) e above would decrease  $\alpha$  for very stable froths.
- e. other methods e.g. the novel approach of Guest (op. cit.) who changed the quality of a fluorspar froth by adding a certain low-grade ore to the ore he was floating. This transformed a wet, slimy, stable froth to a so-called "brittle" froth which carried less water and broke very easily. Improvements in recovery at a grade of 95.5%  $\text{CaF}_2$  ranged between 2 and 20% for cases where the froth quality was changed in this manner. When no change in froth quality was evident no improvement in recovery was obtained.
- (iii) The drainage rate coefficients  $k_{fi}$  for gangue materials should be as high as possible, while those for valuable minerals should be minimised. Since the  $k_{fi}$  will be directly related to the pulp rate constants  $k_{pi}$ , the flotation chemist who develops the flotation reagent recipe makes a large contribution in this area. The  $k_{pi}$  can however be modified in the froth phase by
- decreasing the amount of bubble surface area in the froth phase by encouraging coalescence to the point where competition between particles for attachment sites begins, resulting in rejection of weakly attached material (see Section 3.5).
  - dousing or spraying the froth so that weakly attached and entrained particles are washed back into the pulp phase. This however may increase  $\alpha$  and produce little or no overall improvement.
- (iv) The residence time ratio  $\delta$  is proportional to  $\tau_{\min} (= \delta h / g_0)$  and should thus be maximised. According to the model this is particularly important if the  $k_{fi}$  for floatable and unfloatable components differ widely, because of the exponential dependence of concentrate flowrate  $M_{ci}$  on  $\tau_{\min}$ .  $\delta$  can be increased by



- a. increasing froth height  $h$  as shown theoretically in Section 4.2.1.4. This should apply in practice, but the accuracy of experimental data was not sufficient to prove it. (In any case  $\tau_{\min}$  is increased by increasing  $h$  irrespective of whether  $\delta$  is changed. Decreasing  $g_o$  will also increase  $\tau_{\min}$  and may also increase  $\delta$  by producing a decrease in  $\alpha$  - see Section 4.2.1.4).
- b. inserting a flow modifier such as that described in (i)e above which increases the distance travelled by the froth before entering the concentrate launder.

#### 6.4 Effect of changes in froth removal method on concentrate RTD

The effect of changes in standard control variables such as froth height, gas rate and frother concentration on concentrate RTD's is illustrated in Figures 5.14.1 to 5.14.3. The effect of two of the design modifications recommended above, viz.

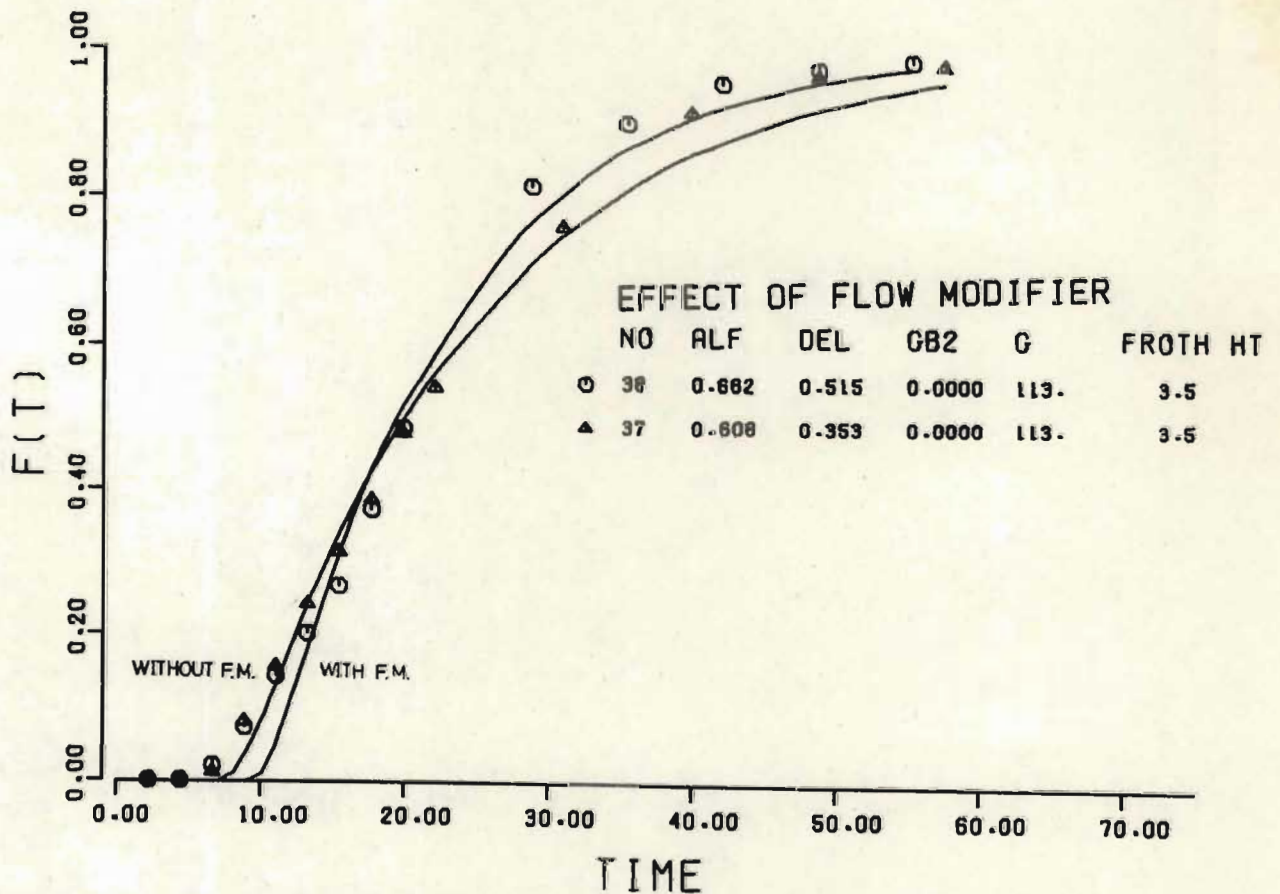
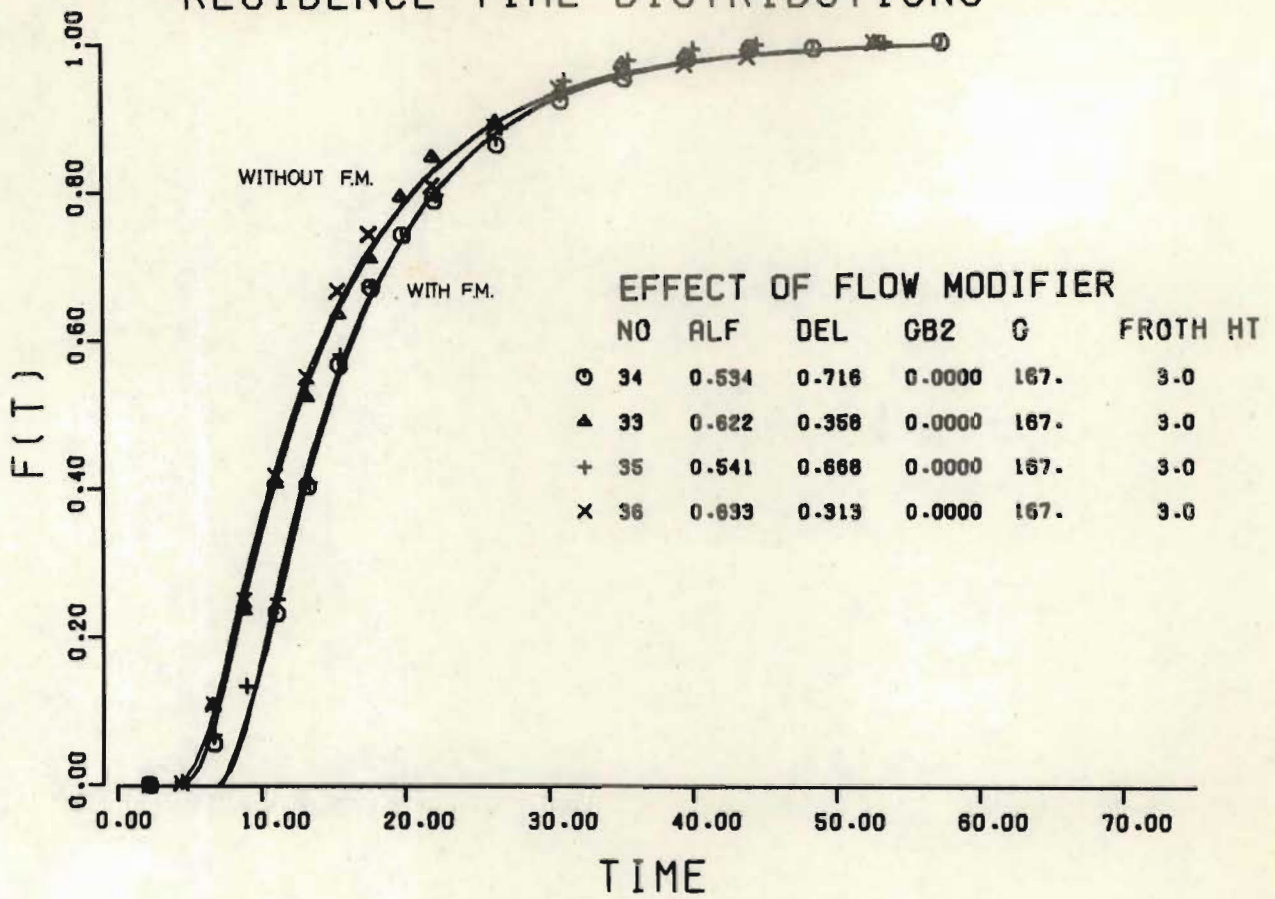
- (i) a flow modifier similar to that discussed in 6.3.2 (i)e and
- (ii) the crowder discussed in 6.3.2 (i)c

is now considered. Perspex baffles were fabricated to achieve these two modifications as shown in Figure 6.6. The flow modifier was smaller than that discussed in (i)e and was almost entirely situated in the froth phase as shown. Eight tests were done consisting of replicates at two gas rates (113 and 167 cc/sec) with and without the flow modifier.

The RTD's are shown in Figures 6.7.1, 6.7.2 and 6.7.3 and the data is summarised in Table 6.1. The results at the high gas rate (Figure 6.7.1) showed excellent reproducibility while the others showed a variability characteristic of the performance obtained in general at low gas rates. In spite of this all the data showed that the introduction of the flow modifier resulted in a consistent increase in the parameter  $\delta$  and a decrease in the parameter  $\alpha$  at both gas rates producing increases in both  $\tau_{\min}$  and  $\tau_{AV}$  as shown in Table 6.1. No significant effect on  $\epsilon$  was observed.

The effect of the sloping rear crowder on the RTD is shown in Figure 6.8. Three experiments were performed at approximately constant gas rates

# RESIDENCE TIME DISTRIBUTIONS



Figures 6.7.1 (top) and 6.7.2 (bottom) Effect of flow modifier on froth phase residence time distribution.

# RESIDENCE TIME DISTRIBUTIONS

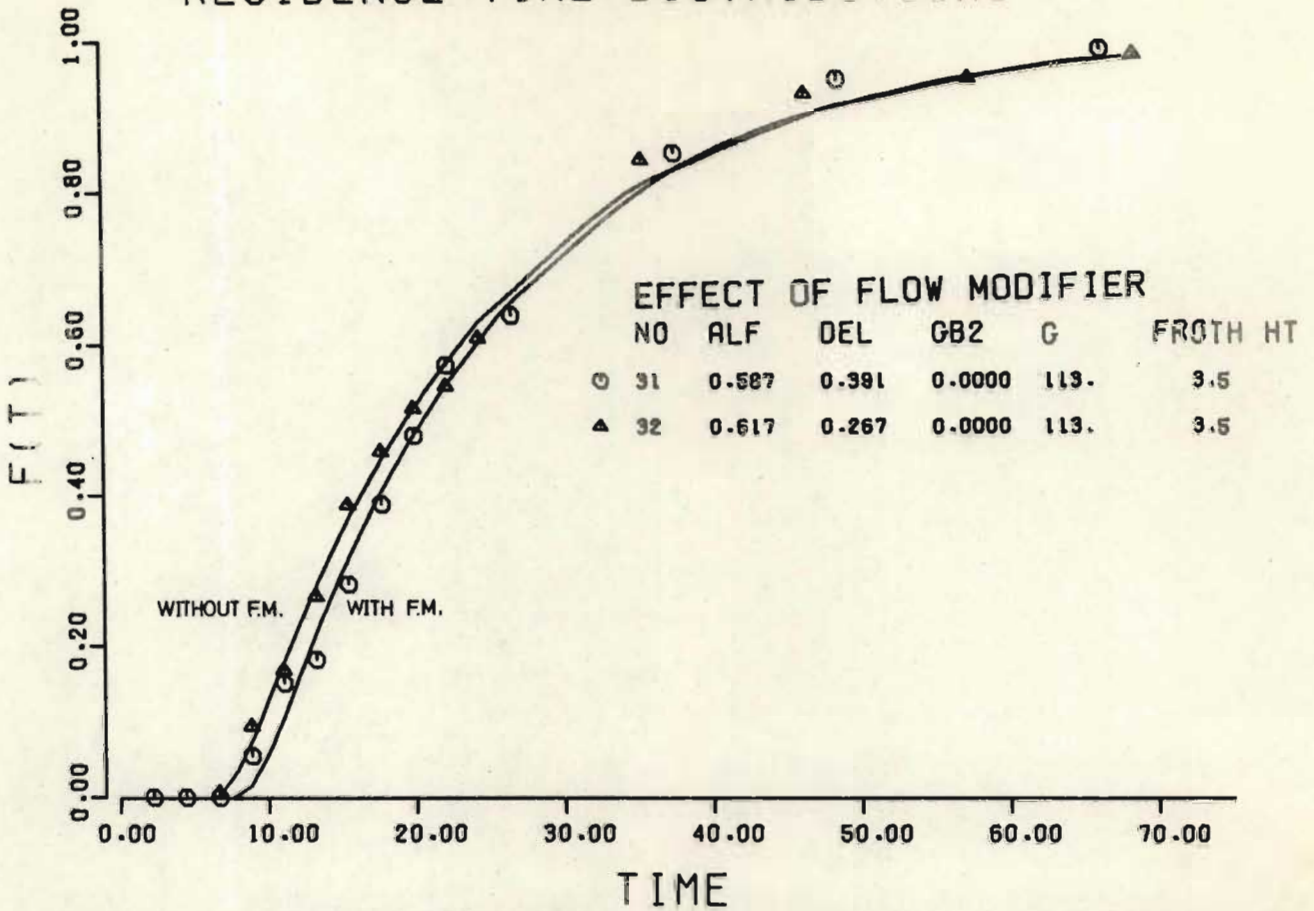


Figure 6.7.3 Effect of flow modifier on froth phase residence time distribution

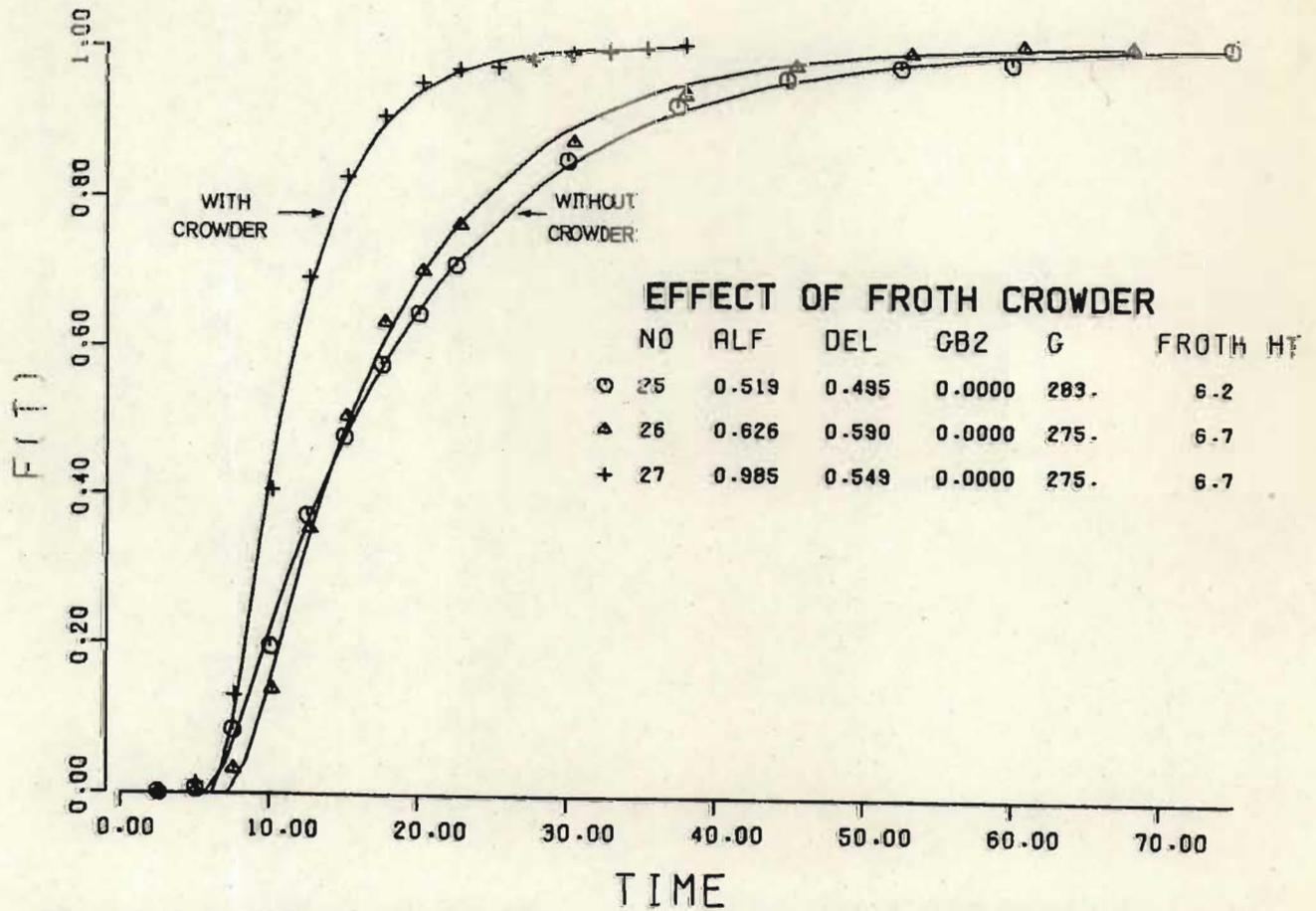


Figure 6.8 Effect of froth crowder on froth phase residence time distribution

Table 6.2 Residence Time Distribution parameters as affected by presence or absence of flow modifier.

Expt No.	Gas Flux cc/s.cm <sup>2</sup>	Flow Modifier Present?	Froth Height (cm)	Froth Removal Efficiency $\epsilon$	Froth Stability $\alpha$	Residence Time Ratio $\delta$	95% Confidence Variations for		Minimum Residence Time $\tau_{min}$	Average Residence Time $\tau_{av}$
							$\alpha$	$\delta$		
31	,28	yes	3,5	,86	,59	,39	,08	,12	4,9	21,2
38	,28	yes	3,5	,99	,52	,49	,08	,14	6,1	24,0
32	,28	no	3,5	,90	,62	,27	,09	,12	3,4	20,2
37	,28	no	3,5	,93	,61	,35	,08	,12	4,4	20,5
34	,42	yes	3,0	,95	,53	,72	,04	,08	5,1	13,5
35	,42	yes	3,0	,95	,54	,67	,04	,08	4,8	13,2
33	,42	no	3,0	,96	,62	,36	,05	,08	2,6	11,5
36	,42	no	3,0	,94	,63	,31	,05	,08	2,2	11,3

(the gas rate for experiment 25 is 3% higher than that for the other two experiments). Experiment 27 was performed with the crowder inserted and  $\alpha$  was thereby increased by approximately 40% to 0,985.  $\epsilon$  was also increased from 0,85 to 0,95.

## 6.5 Experimental tests of various froth removal methods

A number of froth removal methods were tested\* with the flotation systems described below. Each froth removal method consisted of various combinations of the following "design elements"

- (i) the conventional froth removal paddle;
- (ii) the flow modifier } discussed in Section 6.4;
- (iii) the froth crowder }
- (iv) a "froth douser" which allowed one to add water gently and evenly to the top of the froth;
- (v) the option of scraping the froth manually from the back of the cell towards the overflow weir.

### 6.5.1 Tests on Prieska Ore (performed at University of Natal).

As shown in Section 6.4, insertion of a flow modifier (as shown in Figure 6.6) into the froth phase changes the residence time of particles passing through the froth phase. What effect does this have on actual flotation performance? To answer this question tests were performed on a slurry conditioned for bulk sulphide flotation (see Section 2.3.4) in the cell described in Section 2.2. Feed solids concentration was 30% solids by weight and the feedrate was 3,0 l/min. Experiments were performed at three gas rates (10,7 13,9 and 17,0 l/min). Concentrate and tailings samples were taken with and without the flow modifier inserted in the froth phase. The results of these experiments are shown graphically in Figure 6.9 where grade-recovery curves for chalcopyrite, sphalerite, pyrite and gangue are presented. The effect of the presence of the flow modifier on the chalcopyrite and sphalerite curves is quite marked; a substantial shift away from the origin is obtained. The effect on the pyrite curve is

\* Some of the experiments were done at the University; the rest were done subsequently at the author's present place of employment, the National Institute for Metallurgy, Randburg, Transvaal.

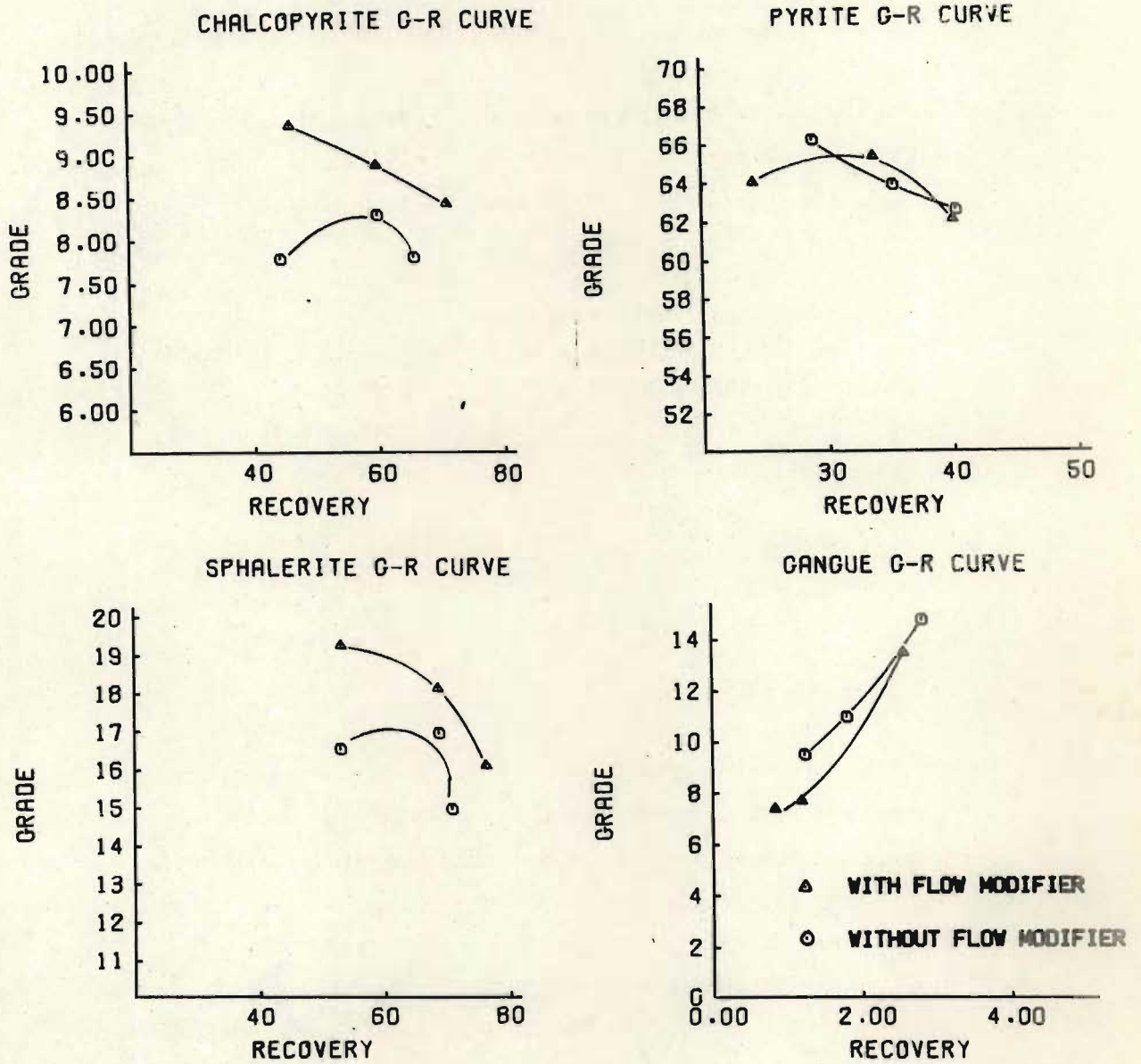


Figure 6.9 Effect of flow modifier on grade-recovery curves for components of the Prieska ore.

ambiguous, the points at intermediate gas rate contradicting our expectations. Note, however, the expanded scale; these two points differ in grade by only 1 in 65 percent which is not very significant. The gangue grade-recovery curve confirms our expectations; the presence of the flow modifier shifts the curve towards the origin.

Particle size effects are shown in Figures 6.10.1 and 6.10.2 where grade is shown as a function of particle size for each component (each graph shows the effect of the froth crowder at a given gas rate). At low gas rates the flow modifier produces an improvement in grade for small particles, while the grade for larger particles is hardly affected. This supports the hypothesis that the presence of the flow modifier encourages drainage of the froth, reducing entrainment of fine gangue particles and hence producing an improvement in grade of the floatable particles in these size ranges. At high gas rates the effect is less marked - a trend not followed in the tests described in the next section.

#### 6.5.2 Tests on Gasifier Cinder from African Explosives and Chemical Industries' Ammonia Plant

These tests were performed at the National Institute for Metallurgy. The gasifier cinder required no grinding since it was already very fine (73,5% - 75  $\mu$ ). A 30% solids by weight slurry was made up in a 1,5 m<sup>3</sup> stirred cell. This was pumped to a 60 litre conditioner at a steady rate of 4,5 l/min with a monopump and diluted to about 17% solids, providing a flowrate of 8,0 l/min to the test cell. Kerosene (25 kg/ton) was used as conditioner; no frother was required.

The test cell was a 25 l Denver-type cell with a Denver "Sub-A" No 7 impeller. Seven froth removal methods were tested which involved all the "design elements" listed in Section 6.5 except the froth crowder (the froth crowder was not used since the froth produced in this system is extremely stable and a large bank of it always builds up near the back of the cell, providing a natural froth crowder. Unless this is continuously removed by scraping (froth removal method (7) below) it ensures that only about 50% of the available froth phase volume is in use). The froth

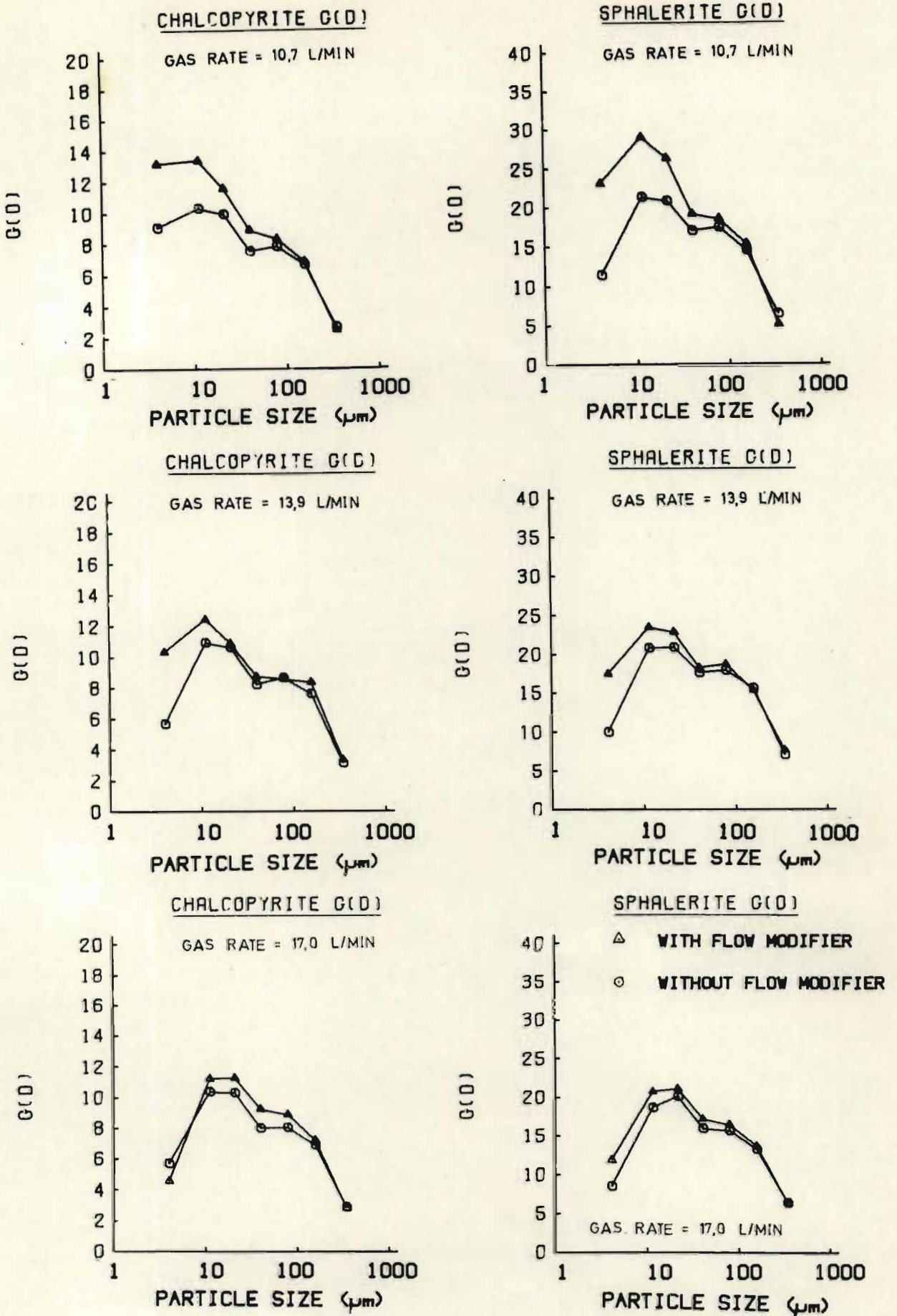


Figure 6.10.1 Effect of flow modifier on grades within particle size classes for chalcopyrite and sphalerite (Prieska ore)



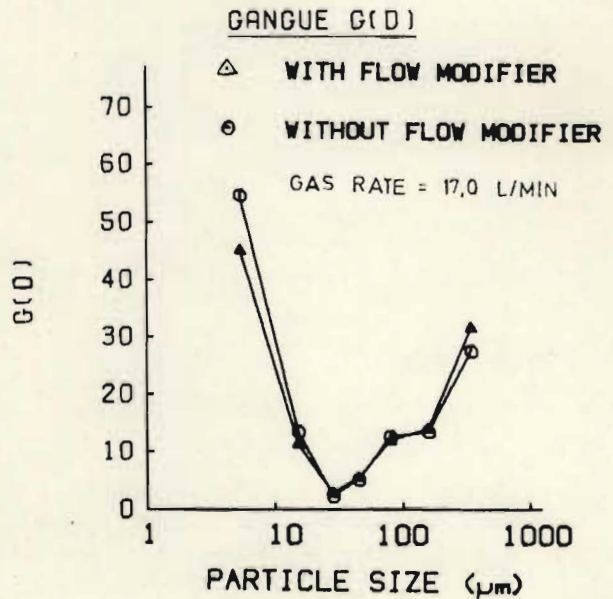
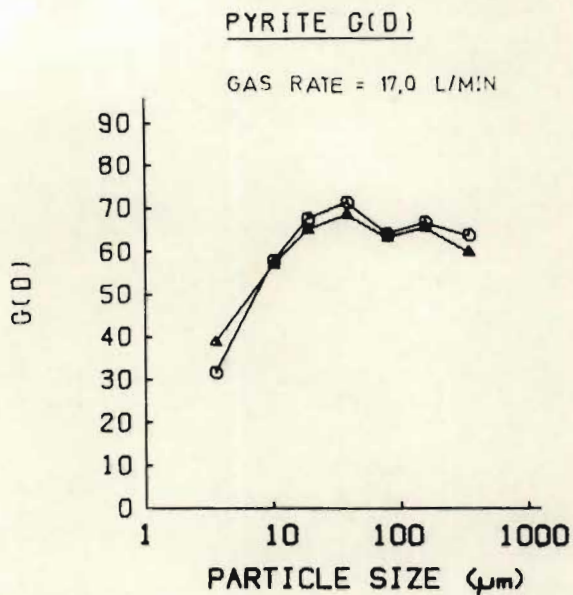
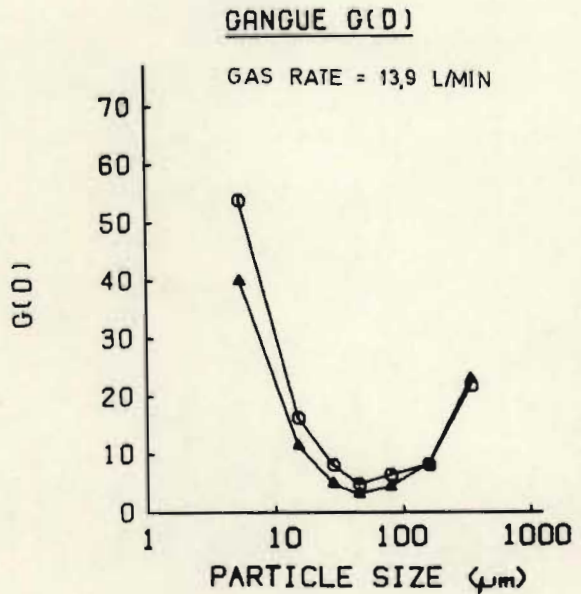
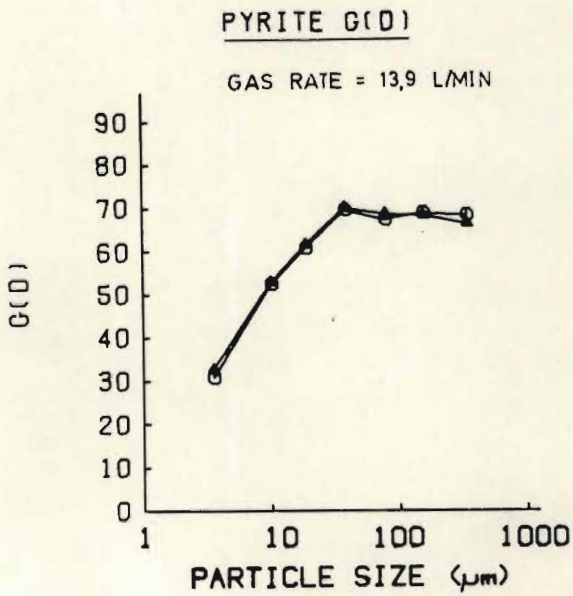
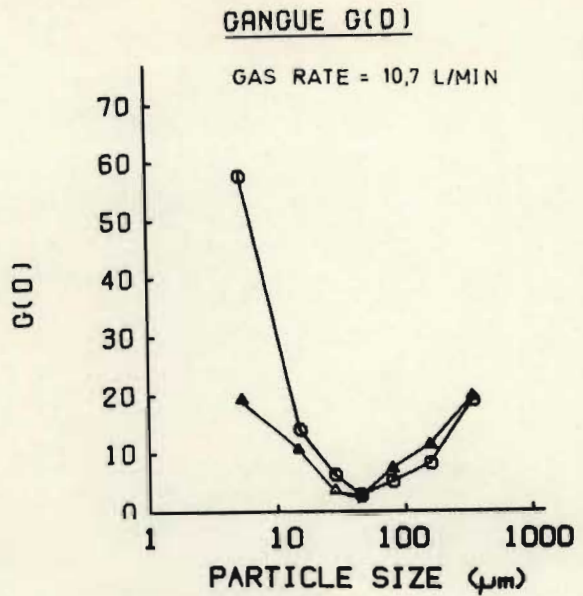
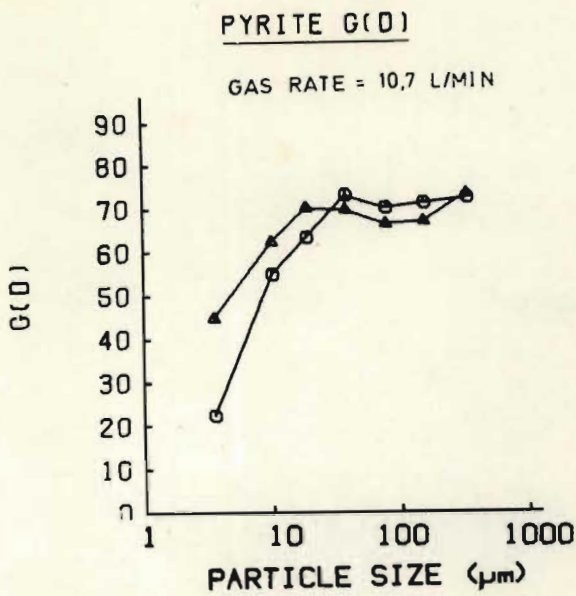


Figure 6.10.2 Effect of flow modifier on grades within particle size classes for pyrite and gangue. (Prieska ore)

removal methods were:

- (1) No extra design element (gas rate only)
- (2) Froth removal paddle only
- (3) Flow modifier only
- (4) Dousing only
- (5) Flow modifier plus paddle
- (6) Flow modifier plus dousing
- (7) Flow modifier plus continuous scraping of froth from the back of the cell. This was done with a flat perspex paddle by inserting it alternatively on the left and right side of the cell behind the froth at the back of the cell and moving it forwards to a line through the impeller shaft parallel with the back of the cell.

The dousing water was distributed over most of the froth surface by forcing it through a canvas membrane stretched over a piece of PVC plate cut in the shape of the froth chamber. The impeller shaft had to be accommodated by a broad slot in the distributor, with the result that the froth immediately behind the shaft received no dousing water.

Measurements of both concentrate and tailings flowrate were obtained for between two and four gas rates for each froth removal method. Dousing rates were either 0,5 or 1,0 l/min. Standard tests were done using froth removal method (1) at a gas rate of 30 l/min near the beginning, middle and end (tests 3, 9 and 19) of the test series. These provided an indication of any systematic change in the characteristics of the feed with time. No systematic change was observed ie the recovery values were respectively 36,5 32 and 37 percent with one percent variation in grade.

The samples from three tests were screened to obtain particle size data. All analyses for percent carbon were performed by ashing the samples at 820°C.

The grade-recovery curves obtained for each froth removal method are shown in Figure 6.11. Note that the maximum variation in grade at any particular recovery is only 4%. The experimental error being of the order of 1%, we can only make statements with confidence about grade-recovery lines which are separated by a variation in grade larger than 1%. Thus from these tests we may conclude that

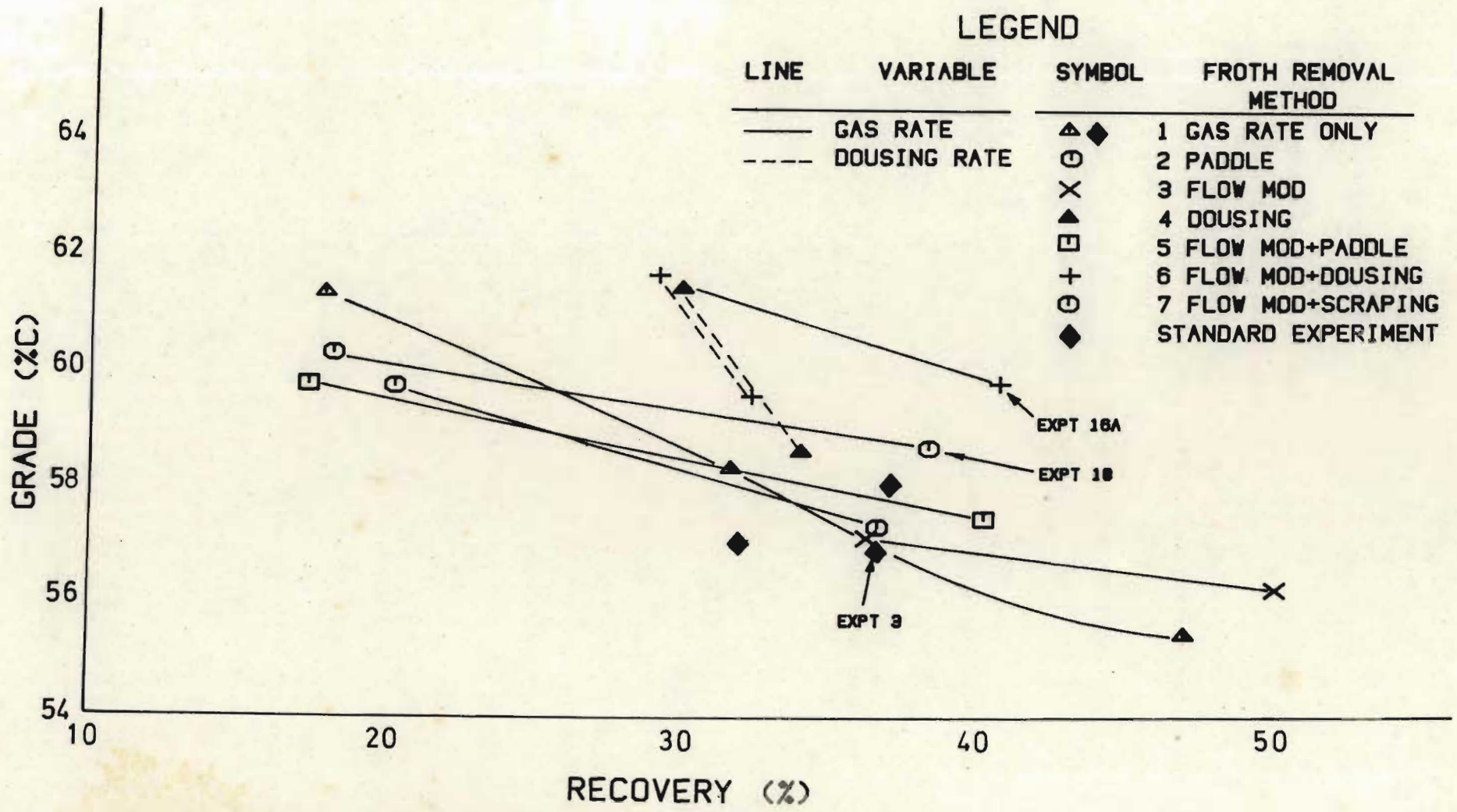


Figure 6.11 Grade-recovery curves for flotation of gasifier cinder

- (a) dousing the froth {methods (4) and (6)} produces a significant improvement in grade (between two and four percent, depending on the rate of dousing). The presence or absence of the flow modifier makes little difference.
- (b) The use of flow modifier plus froth scraping {method (7)} produces an increase in grade at high froth removal rates. This is presumably due to the fact that the growth of a bank of stable froth near the back of the cell is prevented, resulting in a more efficient use of the available volume of the froth phase and hence more efficient drainage of entrained materials.
- (c) In general, use of the flow modifier reduces the slope of the grade-recovery curve, producing a decrease in grade at low recoveries and an increase in grade at high recoveries.

Particle size effects are illustrated in Figure 6.12 for experiments 3, 16A and 18 which are indicated in Figure 6.11. These were chosen because they cover a relatively wide range of grade values at a recovery of  $38,3 \pm 2\%$  and will allow comparisons to be made of the effect of flow modifier (experiments 16A, 18) and dousing (experiment 16A) with the situation in which no attempt was made to assist froth to flow (experiment 3). The particle size distribution and distribution of carbon in the feed and the recovery of carbon and ash are shown as a function of average size within each class (the average size of the  $-38\mu$  class is taken as  $20\mu$ ). Most (54%) of the total solid and 40% of the carbon in the feed to the cell occurs in the  $-38\mu$  fraction, and it is this fraction which is most strongly affected by the control actions. The use of the flow modifier plus scraping produces a 3,7% increase in recovery of carbon in this fraction, while the use of the flow modifier plus dousing produces an 11,7% improvement. Little change in the recovery of ash is observed, which is surprising and indicates that ash is not recovered mainly by entrainment as was at first supposed. This was borne out by photomicrographical investigations performed by Loo (1979) which showed that some of the ash and the carbon are finely intergrown even in the  $-38\mu$  fraction. The recovery of ash is slightly increased in the larger size fractions for experiment 3. This is due either to the fact that the flow modifier was absent in this experiment or to a possible drift in the floatability of the ash in the long time interval (3,5 hours) that elapsed between this experiment and experiments 16A and 18.

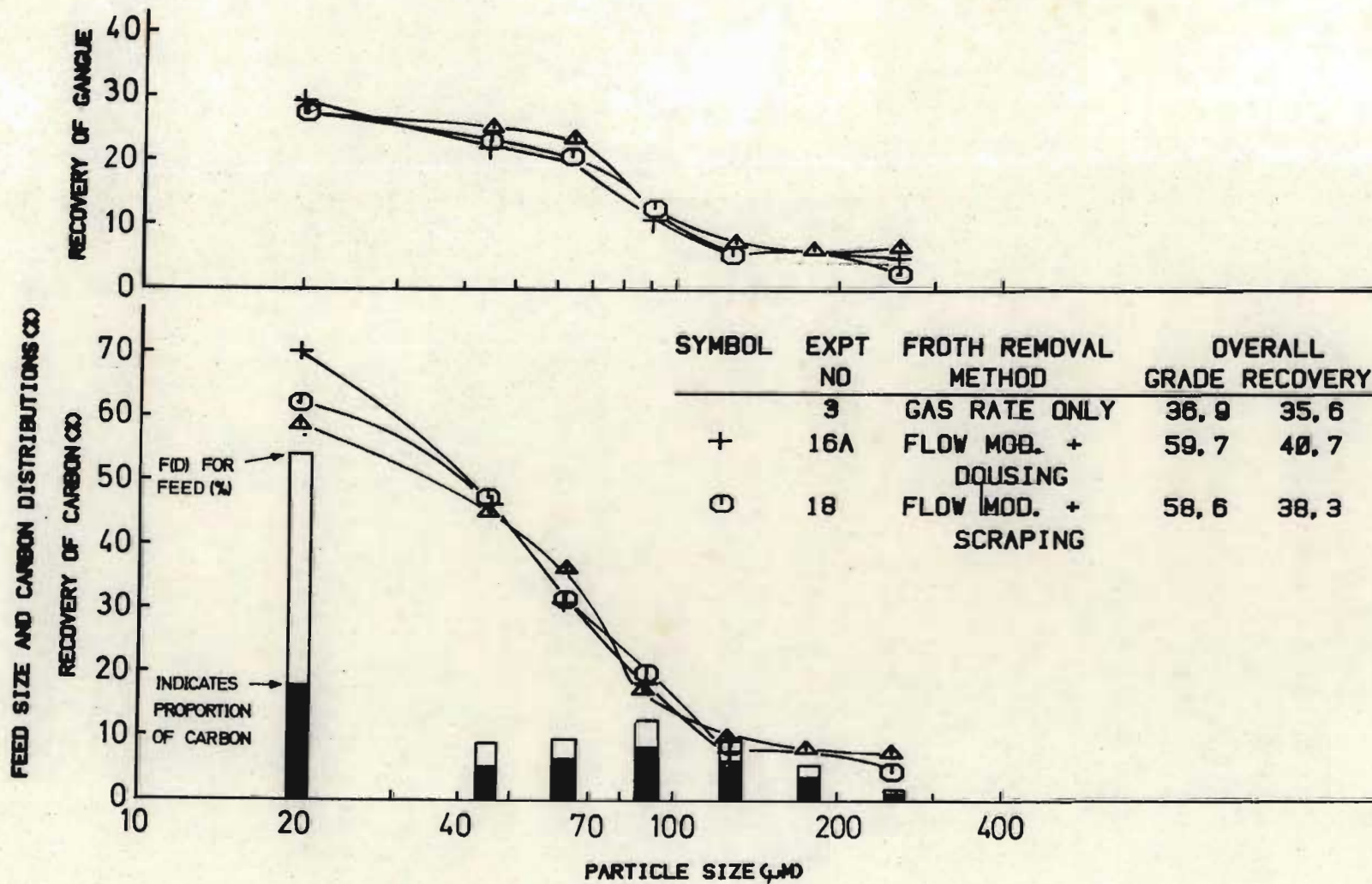


Figure 6.12 Variation of various experimental parameters with particle size for experiments 3,16A and 18 (experiments with gasifier cinder).

## CHAPTER SEVEN

### CONCLUSIONS

In response to the need for greater understanding of the processes occurring in the froth phase expressed by various researchers as recorded in the first chapter, some progress has been made. On the mathematical modelling front, Mika and Fuerstanau's ideal of "a detailed representation of the froth subprocesses" is still shrouded in the mists of obscurity, and will probably remain so; it is questionable whether such a representation can be formulated or is worth the attempt given the complexity of the problem and the large amount of experimentation that would be required to estimate the parameters that would be involved. In any case, no two froths are identical, even on the same ore under similar conditions. However, in pursuit of more reasonable goals three advances have been made:

(i) a model has been formulated which describes various processes occurring when froth is removed vertically in plug flow fashion from a cell. This work builds on the foundations laid by Watson and Grainger-Allen, confirming their observations relating to the behaviour of a steady-state froth column, and contributing additional observations concerning the effect of froth removal on concentration gradients in the froth. The effect of competition for attachment sites in the froth caused by coalescence of bubbles and resulting in inflections in the concentration gradient of the less hydrophobic mineral has also not been reported before. This work also illustrated how two mechanisms occurring in the froth conflict and must be traded off against each other to obtain the best performance i.e. the mechanism of drainage, which increases the grade of the froth but decreases its mobility and stability; and the mechanism of froth removal which requires (at least for conventional froth removal methods) a high degree of mobility if it is to be removed before it collapses. The model is rather complex however and involves a lot of parameters which limits its potential for practical purposes; its main value is its contribution to our understanding of selected subprocesses occurring in the froth.

(ii) a second model has been obtained by solving the two-dimensional Laplace equation to obtain a description of the frictionless flow of a well-drained froth in a conventional flotation cell. This model was used to explore the effect of the profiles of gas flux crossing the various boundaries of the froth volume (ie flux entering the base of the froth from the pulp, flux across the surface of the froth due to bubble breakage and flux of gas leaving the cell in the concentrate stream.) Various phenomena observed in practice were simulated eg stagnant areas at the back of the froth or in areas of low froth stability, and the rapid rate of rise of froth from the froth-slurry interface into the concentrate stream near the froth overflow lip. Residence time distributions were calculated for various froth heights and froth stabilities; this illustrated the effect of these variables on the minimum residence time of froth in the cell and highlighted a weakness in conventional cell design, which ensures that the lowest grade of froth occurs near the point of removal. This also brought into question the use of paddles for froth removal which ensure mixing of froth near the froth lip and removal of poorly drained froth, producing low froth grades.

Again, this model is limited to academic purposes because of the complex numerical methods required to solve the Laplace equation.

(iii) A third model was developed which was essentially a one-dimensional simplification of the second model. This model takes into account the fact that all froth spends a time longer than a certain value  $\tau_{\min}$  in the froth, and describes the behaviour of froths of varying stability. Residence time distribution measurements on two-phase froths (air + water) established the ability of this model to describe the behaviour of real systems and that the froth stability estimated from RTD data was a good estimate of the true froth stability. The latter was established by comparing this model with the Laplace model, and by comparing froth stability estimates obtained by two different experimental methods. Froth stability  $\alpha$  and froth removal efficiency  $\epsilon$  were found to be simple functions of froth depth, frother concentration and gas rate.

The application of the last model to practical industrial problems was then considered. The model is extremely tractable and can be combined with models of pulp phase processes to produce a comprehensive model of cell behaviour. It takes into account cell geometry and operating variables such as gas rate, froth depth and froth concentration and hence should be of use in the scale-up and control of flotation processes. Relatively simple methods exist for estimation of the important parameters: the parameter  $\delta$  defining  $\tau_{\min}$  can be fixed at a value of 0,5, the froth stability  $\alpha$  can be estimated by measuring the velocity of the froth moving towards the froth lip using the method described in Sections 5.1.5 and 5.2.5. and the froth removal efficiency can be obtained by estimating the fraction of the cell surface cross-sectional area which is producing froth which eventually reaches the froth overflow weir.

The model was shown to be capable of describing the behaviour of a 4-component complex sulphide float; it was demonstrated that ignoring the effect of froth stability made it impossible to do so.

By simulating grade-recovery curves for various systems the following points were made which are relevant when designing froth removal methods:

- (i) The froth removal efficiency should be maximised: an absence of stagnant froth zones ensures that froth volume is efficiently utilised, and that a minimum of floatable particles are returned to the pulp phase.
- (ii) The froth stability should be optimised: too stable a froth generally means a low froth residence time and hence a low-grade froth and problems in handling the froth once it has been removed (a certain amount of bubble coalescence will in general result in an additional increase in froth grade because of competition for attachment sites and increased drainage of unwanted particles) while if the froth is too unstable high gas rates are required to obtain recovery, which reduces the efficiency of pulp phase processes, produces increased mixing in the froth phase and increased power requirements.



(iii) The minimum froth residence time should be maximised so that entrainment is reduced.

Most of these conditions are admirably met by the Maxwell cell which has a large froth removal lip length per cell cross-sectional area, ensuring maximum froth removal efficiency, the ability to cope with low stability froths and hence low power and reagent costs. (Low froth stability also ensures a high minimum froth residence time as shown in Section 4.2.1).

Insight obtained from this work led to

- (i) the design of one novel froth removal method ie scraping the froth towards the front of the cell in a region near the back of the cell rather than using a paddle to remove froth from the front of the cell; and
- (ii) the selection of or modification of a number of other methods eg. froth dousing or the insertion of a flow modifier (see section 6.5.1) which seemed to serve the above objectives. Testing of these methods in two pilot plant applications confirmed their power to increase the efficiency of the froth removal process. These methods will be tested further and hopefully applied in industrial situations.

o o o o o o o

One last comment must be added. The flotation field is littered with many a deflated ambition to obtain generalised understandings. If the author has learnt one thing in his work, it is this : no two floats are the same; each is a Cinderella, with its unique glass slipper to be found only by diligent searching.

REFERENCES

- Arbiter, N. and Harris, C.C., 1962. Flotation kinetics. In: D.W. Fuerstenau (Editor), Froth Flotation. AIME, 50th Anniversary Volume, pp. 215-246.
- Ball, B., and Fuerstenau, D.W., 1970. A two-phase distributed-parameter model of the flotation process. Proc. IX Int. Miner. Proc. Congr., Prague.
- Ball, B. and Fuerstenau, D.W., 1974. On the determination of rate constants from semi-batch flotation tests. Quarterly of the Colo. Sch. Mines, 1974 69: 27-40.
- Ball, B., Kapur, P.C. and Fuerstenau, D.W., 1970. Prediction of grade recovery curves from a flotation kinetic model. Trans. Soc. Min. Eng. AIME, 247:263-269.
- Bishop, J.P. and White, M.E., 1974. Prediction of gangue recovery in flotation concentrates. Tech. Report Julius Kruttschnitt Mineral Research Centre, Univ. of Queensland, pp. 47-58.
- Boutin, P. and Wheeler, D., 1967. Column Flotation. World Mining, March, 1967. pp. 47-50.
- Bushell, C.H.G., 1962. Kinetics of flotation. Trans. Am. Inst. Min. Eng., AIME 223: 266-273.
- Casson, G., 1973. Mathematical Models of Flotation Processes. Thesis, Univ. of Leeds.
- Carlsan, H.S. and Jaeger, J.C., 1959. Conduction of Heat in Solids; 2nd ed., Oxford, Clarendon Press.
- Cooper, H.r., 1966. Feedback process model of mineral flotation. Part 1. Development of a Model for Froth Flotation. Trans. Soc. Min. Eng. AIME, 235: 439-446.
- Cutting, G.W. and Devenish, M., 1975. A steady state model of flotation froth structures. Soc. Min. Eng. AIME, Preprint 75-B-56 at AIME Annu. Meet., Feb. 1975.
- Dawson, 1976. Private communication.
- De Kok, S.K., 1972. Differential flotation of copper-zinc at Prieska Copper Mines (Pty) Limited: a preliminary report. J. S.A. Inst. Min. Metall. Vol 72, July 1972. pp. 305-321.
- Dunne, R. and Dawson, M.F., 1975. Private communication.
- Dunne, R., 1975. Private communication.
- Dunne, R.C., Moys, M.H., Harris, P.J., Forbes, A.W. and Hulse, N.D., 1976. The measurement of bubble size distributions in flotation pulps. Tech. Mem., S.Afr. Natl. Inst. Metall.
- Finlayson, R., 1976. Private communication.

- Flint, L.R., 1973. Factors Influencing the Design of Flotation Equipment. Miner. Sci. Engng 5: 232-241.
- Flint, L.R., 1974. A mechanistic approach to flotation kinetics. Trans. Inst. Min. Metall., 83:C90-95.
- Gaudin, A.M., 1932. Flotation. McGraw-Hill Book Co., New York.
- Guest, R.N., 1979. Confidential Report No. 2004. National Institute for Metallurgy, 1979.
- Harris, C.C., 1976. A recycle flow flotation machine model: response of model to parameter changes. Int. J. Min. Process., 3: 9-25.
- Harris, C.C. and Chakravarti, A., 1970. Semi-batch froth flotation kinetics: species distribution analysis. Trans. Am. Inst. Min. Eng., 247: 162-172.
- Harris, C.C., Chakravarti, A. and Degaleesan, S.N., 1975. A recycle flow flotation machine model. Int. J. Miner. Process., 2: 39-58.
- Harris, C.C., Jowett, A. and Ghosh, S.K., 1963. Analysis of data from continuous flotation testing. Trans. Am. Inst. Min. Eng., 226: 444-447.
- Harris, C.C. and Rimmer, H.W., 1966. Study of a two-phase model of the flotation process. Trans. Inst. Min. Metall., Sect. C, 75: C153-C162.
- Hulbert, D.G., 1977. Multivariable Control of a Grinding circuit. PhD. Thesis, Univ. of Natal.
- Johnson, N.W., McKee, D.J. and Lynch, A.J., 1972. Flotation Rates of Non-Sulphide Materials in Chalcopyrite Flotation Processes. Trans. Soc. Min. Eng., AIME 256: 204-209.
- Jowett, A., 1966. Gangue Mineral contamination of froth. Brit. Ch. Eng., ii (5): 330-333.
- King, R.P., Te Riele, W.A.M. and Buchalter, E., 1970. An improved distributed parameter model for the kinetics of mineral flotation. S. Afr. Nat. Inst. Metall., Rep. 996.
- Klassen, V.I., 1941. Flotation of Andalusite. Non Ferr. Metals, Moscow, No. 22-23 (1941) as quoted in Mokrousov (1958).
- Klassen, V.I. and Mokrousov, V.A., 1959. An introduction to the Theory of Flotation. Butterworth, London (translated from the Russian by J. Leja and G.W. Poling, 1963).
- Klassen, V.I., Pikkat Ordynsky, G.A. and Gurevich, R.I., 1956. Increasing the effectiveness of flotation by spraying the froth. Non-ferr. metals, Moscow, No. 5 (1956).
- Livshits, A.L. and Dudenkov, S.V., 1960. The influence of the solid phase on froth stability. Tsvetnye Metally. 33(11): 23.
- Loo, J., 1979. Private Communication.

- Livshits, A.K. and Dudenkov, S.V., 1964. Some factors in flotation froth stability. 7th Int. Min. Proc. Congr. 367-371.
- Lukina, K.I. and Bogatikov, A.S., 1971. Mechanical flotation machines with adhesion drums. Sov. J. of Non-Ferr. Met. 12(6): 77-79.
- Lynch, A.J., Johnson, N.W., McKee, D.J. and Thorne, G.C., 1974. The behaviour of minerals in sulphide flotation processes, with reference to simulation and control. J. South African Inst. Mining and Met. 1974, pp. 349-361.
- Maksimov, I.I. and Khainman, V.Ya. Effect of processes, occurring in the froth layer, on the rate and selectivity of flotation. (Vses. Nauch. - Issled. Proekt. Inst. Mekh. Obrab. Polez. Iskop.), 38(5) 1965 (Pub 1967), 1, 442-59 (Russ).
- Malinovski, V.A., 1970. Froth separation. Sov. J. of Non-Fer. Metals. II (8) 1970.
- Malinovskii, V.A. and Lukina, K.I., 1968. Tsvetinye Metally, 1968 (1)
- Mathieu, G.I., 1972. Comparison of flotation column with conventional flotation for concentration of a molybdenum ore. Can. Min. and Metall. Bull. 65(721): 41-45.
- Meshcheryakov, N.F., Ryabov, Yu. V., Khan, A.A., Khomkov, V.N. and Podvigin, M.A., 1975. Comparative tests on fluidized-bed flotation machines and froth separation machines. Sov. J. of Non-Fer. Met., 16(8): 87-89.
- Millar, F.G., 1969. The effect of froth sprinkling on coal flotation efficiency. Trans. Soc. Min. Engrs., AIME 244:158-167.
- Mika, T., 1967. Discussion of paper by H.R. Cooper. Trans. Soc. Min. Eng. AIME, 238: 479-483.
- Mika, T. and Fuerstenau, D.W., 1969. The microscopic model of the flotation process. Proc. 7th Int. Miner. Process. Conf., Leningrad, pp. 246-269.
- Moys, M.H., 1978. A study of a plug-flow model for flotation froth behaviour. Int. J. Miner. Process., 5: 21-38.
- Nelder, J.A. and Mead, R., 1965.
- Sadler, L.Y., 1973. Dynamic response of the continuous mechanical froth flotation cell. Trans. Soc. Min. Eng. AIME, 254: 336-342.
- Waksmundzki, A., Neczaj-Hruziwicz, J. and Planik, M., 1972. Mechanism of carry-over of gangue shales during flotation of sulphur ore. 81(793): C249-C251. Trans. Inst. Min. Metall.
- Watson, D. and Grainger-Allen, T.J.N., 1974. Study of froth flotation using a steady state technique. Trans. Soc. Min. Eng. AIME, 256: 242-247.
- Woodburn, E.T., 1976. Flotation kinetics. Prepared for Handbook of Min. Proc.
- Woodburn, E.T., Kropholler, H.W., Greene, J.C.A. and Cramer, L.A., 1976. The utility and limitations of mathematical modelling in the prediction of the properties of flotation networks. In: M.C. Fuerstenau (Editor), Flotation. A.M. Gaudin Memorial Volume, 2. American Institute of Mining, Metallurgical, and Petroleum Engineers, New York, N.Y., pp. 638-674.

Zakhvatkin, V.K., 1970. Efficiency of pneumomechanical flotation machines.  
Sov. J. of Non-Ferr. Met. 11 (2): 69-77.

APPENDIX ADISCUSSION OF PAPER BY GREAVES AND ALLAN  
ON TRANSIENT RESPONSE OF CONCENTRATE FLOWRATE  
TO CHANGES IN SLURRY FEED RATE

Greaves and Allan (1974) have compared the predictions of the unsteady-state continuous version of Harris and Arbiter's 2-phase model with data obtained from the measurement of startup and step change responses of a continuous flotation cell. The model is only marginally successful in the transient zone. Arbitrary adjustment of the estimated air-free volume of froth produced substantially improved correlations between theory and practice. The authors do not attempt to interpret this observation and thereby miss an opportunity to improve their model for air-free froth volume,  $V_f$ . (Another reason why they obtained poor correlations for the startup experiments is that they neglected to take into account the time required for the froth to rise in the froth chamber before it could flow over the concentrate weir.

To estimate  $V_f$  they assume that the residence times  $\tau_a$  and  $\tau_f$  of the air and air-free fractions passing through the froth chamber are identical. Thus

$$\tau_f = \frac{V_f}{Q_c} = \frac{V_a}{G} = \tau_a$$

where  $G$  is the air rate,  $Q_c$  is the volumetric flow rate of air-free concentrate and  $V_a$  is the volume of air in the froth phase. Now the measured total froth volume is 0,75 litre:

$$V_f + V_a = 0,75$$

$V_a$  is eliminated to give

$$V_f = \frac{0,75}{1 + G/Q_c} \quad (\text{A.1})$$

However  $\tau_a$  and  $\tau_f$  are identical only under two conditions, i.e.

- (i) No drainage of water and particles occurs
- (ii) No gas escapes through the surface of the froth due to bubble breakage, i.e. froth stability parameter  $\alpha = 1,0$ .

In general drainage does occur and  $\alpha < 1,0$ . If we neglect drainage in the absence of means to measure or estimate it, or assume that the froth is "well drained" as it enters the froth phase, then we get

$$\tau_f = V_a / \alpha G = \tau_a / \alpha$$

Hence a more realistic expression for  $V_f$  is

$$V_f = \frac{0,75}{1 + \alpha G / Q_c} \quad (\text{A.2})$$

Relevant data obtained from the paper are shown in Table A.1. The final concentrate rate and the gas rate were obtained from graphs and hence are approximate. The "Froth volume for best correlation" was obtained as follows. Greaves and Allan obtained predictions of the transient response of the cell under startup conditions (i.e. feed rate changing from zero to the indicated amount) for theoretical froth volumes ranging from  $0,1 V_f$  to  $8 V_f$  ( $V_f$  calculated from (A.1)). At each of the values for  $V_f$  the time-average error (defined as the area between the theoretical and experimental curves divided by the total measured response time) is quoted. Using difference analysis it was possible to estimate the multiple of  $V_f$  at which

the minimum error occurred. This is shown in Table A.1. Note that this value decreases steadily as the concentrate flowrate increases, until for experiment 9G a value of 1,1 is obtained, i.e.  $V_f$  calculated by equation (A.1) is close to the best value. This implies that  $\alpha \approx 1$  in equation A.2. The data in Greaves and Allan's paper allows one to calculate a value of  $\alpha$  for each experiment (see Table A.1);  $\alpha = 0,88$  for run 9G, and decreases rapidly as the rate of solid removal decreases. This corroborates what is found in practice, i.e. that  $\alpha$  increases as the amount of solid in the froth increases, since the solids stabilise the bubbles.

Thus introduction of the effect of froth stability into Greaves and Allan's model produces a marked improvement in its ability to describe experimental reality, and provides information about the variation of froth stability with various parameters such as feed density and concentrate removal rate.



Case No.	Final Feed Rate		Step Change 1 / min.	Final conc. Rate kg KCl / min.	Froth volume for best correlation	Approximate Gas Rate l / min.	$\alpha$
	l / min.	kg KCl / min.					
9A	2,65	,74	2,65	,68	5,5 $V_f$	4 <sup>+</sup> 1	,05
9B	3,79	1,02	3,79	,85	3,6 $V_f$	"	,12
9C	4,73	,80	4,73	,68	4,0 $V_f$	7 <sup>+</sup> ,3	,134
9D	6,06	,91	6,06	,73	4,7 $V_f$	"	,101
9E	7,19	1,27	7,19	1,08	2,3 $V_f$	"	,293
9F	7,57	1,31	7,57	1,02	2,0 $V_f$	"	,387
9G	11,92	2,0	11,92	1,4	1,1 $V_f$	"	,88

$V_f$  determined from equation A1.

Table A.1 Analysis of data from Greaves and Allan's paper

APPENDIX BUSE OF THE MODEL OF HARRIS AND RIMMER  
FOR ESTIMATING FROTH VOLUME

If we assume that the Harris and Rimmer model can be used to describe the behaviour of water as well as solid particles, then we can use the model for predicting the air-free volume of the froth. Equation (1.1) gives the mass of component  $i$  in the froth phase, and froth volume is then

$$V_f = \sum M_i / \rho_i$$

where  $\rho_i$  is the density of component  $i$ .

The performance of a single cell floating a mineral consisting of two components {one mineral ( $i = 1$ ), one gangue ( $i = 2$ ); water has index  $i = 3$ } was simulated and  $V_f$  was obtained as a function of feed rate, feed density and froth pulling rate. Table B.1 gives the values of the various parameters that were used, and the variation of froth volume with the abovementioned parameters is shown in Figure B.1. The grade recovery curve is shown in Figure B.1 as well.

The following points may be noted:

- (i)  $V_f$  is a strong function of  $Q_F$ ,  $Q_I$  and  $C_I$ , especially at low values of  $Q_F$ .  $V_f$  decreases as  $Q_F$  increases and increases as  $Q_I$  and  $C_I$  increase, i.e. as the amount of solids available for flotation increases.

- (ii) All points fall on the same grade-recovery curve, i.e. the model does not allow for improvements in flotation efficiency by adjustment of  $Q_F$ ,  $Q_I$  or  $C_I$  which can be obtained in practice. The only way of moving onto a different grade recovery curve is to change either the pulp or the froth phase rate constants.

Component	Mineral	Gangue	Water
$i =$	1	2	3
$k_{pi}$	830	83	16,7
$k_{fi}$	,33	,5	,83
for $Q_I = 16,7$ and $33,3$ and $66,7$ cc/sec. } $C_i$ at 33% solids	,05	,4	,90
Extra values of $C_i$ { 19% Solids	,025	,2	,95
at $Q_I = 16,7$ cc/sec. { 44% Solids	,075	,6	,85
Density (g/cc)	4,5	4,5	1,0

(Note : The apparently strange values for rate constants and flow rates given above are due to the fact that minutes were originally taken as the time unit in this analysis, not seconds; thus  $Q_I$  values were 1000 2000 and 4000 cc/min. etc.)

Table B.1 Values of parameters and control variables used in simulations

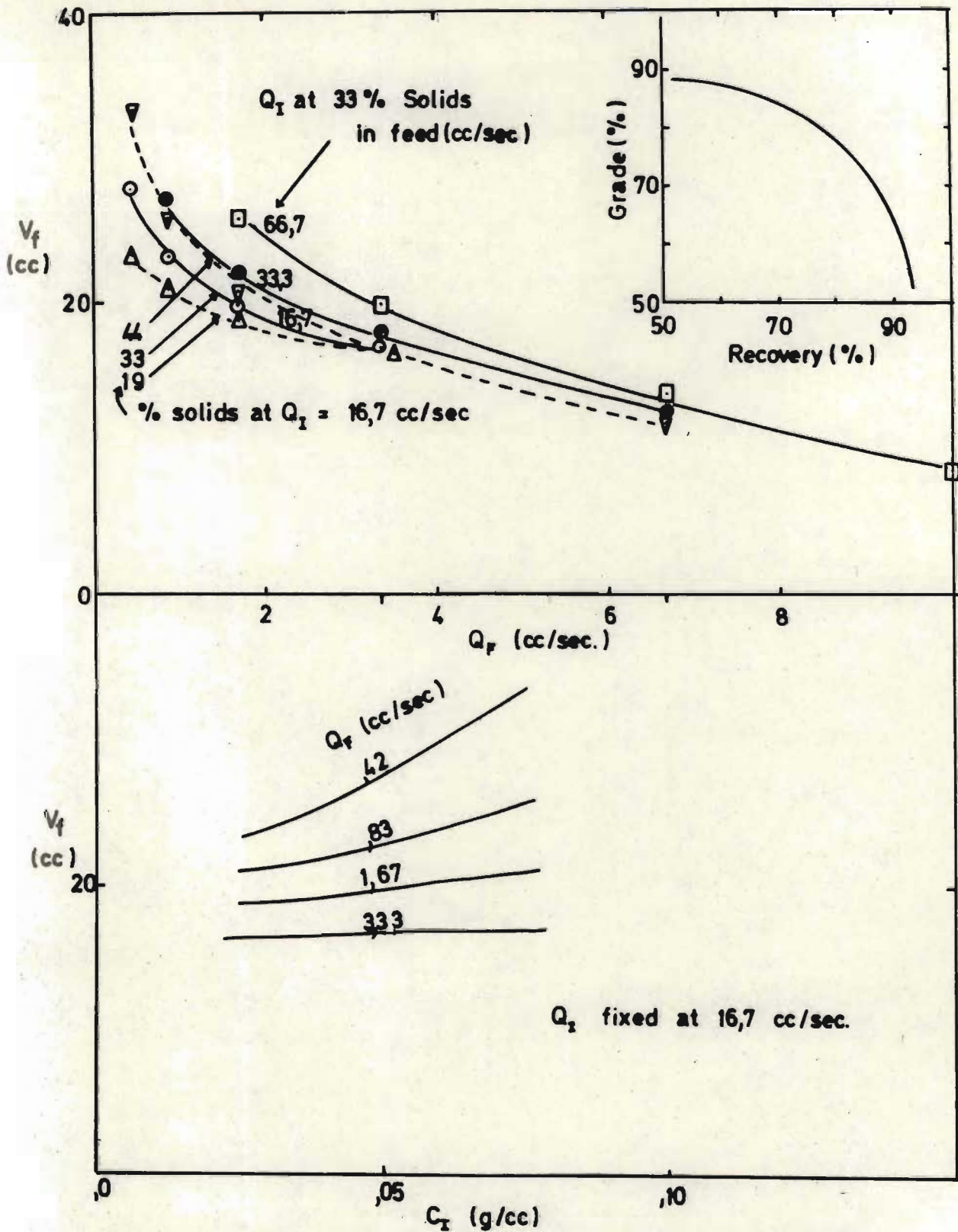


Figure B-1. Variation of air-free froth volume  $V_f$  with operating parameters feed rate, feed concentration and froth removal rate.

APPENDIX C

## CONCENTRATION OF COMPONENTS IN THE FROTH PHASE: PLUG FLOW MODEL

Refer to Figure 4.4. We assume that  $g_b(x)$ ,  $g_f(x)$  and  $m_{f0}$ , the flux of any component into the froth phase, are uniform, i.e. independent of  $x$ .

We define a unit froth element for any component as the mass of that component which enters the base of the differential slice in a time  $d\tau$ . Assuming that drainage of this component results in an exponential rate of decrease of the mass of the element, we find that the mass of the element is given by

$$dm(\tau) = M_{f0} dx d\tau e^{-k_f \tau}$$

Consider the flux of froth through a plane of height  $h$  and unit width at point  $x$ . The number of froth elements flowing through this plane is equal to the number entering the froth phase between the back of the cell and position  $x$ :

$$N(x) = x/dxdt$$

Using the method used in section 4.2.2.2 we can show that the residence time distribution of elements crossing a plane at  $x$  is given by

$$E(\tau/x) = \frac{e^{-\tau/\bar{\tau}}}{\bar{\tau}}$$

Thus the mass flowrate of a component through the plane is

$$\begin{aligned}
 \dot{M}(x) &= \int_0^{\infty} dm(\tau) E(\tau/x) N(x) d\tau \\
 &= \frac{M_{fo} x}{\bar{\tau} (k_f + 1/\bar{\tau})}
 \end{aligned}$$

and the concentration of particles at position  $x$  is given by

$$\begin{aligned}
 C(x) &= \dot{M}(x) / hv(x) \\
 &= \frac{M_{fo}}{h(k_f + 1/\bar{\tau})}
 \end{aligned}$$

i.e. it is independent of  $x$ .

APPENDIX D: Confidence Limits for the parameters  $\alpha$  and  $\delta$  in the froth residence time distribution

The froth residence time  $F(\tau)$  is given by

$$F(\tau) = 1 - \exp \left\{ \frac{-\alpha g_o C}{h} (\tau - \tau_{\min}) \right\} = 1 - \bar{F}$$

where

$$\tau_{\min} = \delta h / g_o \text{ and } C = 1 / (1 - \alpha \delta)$$

and  $\bar{F}$  is introduced to simplify notation

We wish to estimate variations in  $\alpha$  and  $\delta$ , denoted by  $\Delta\alpha$  and  $\Delta\delta$  which are measures of the confidence we have in these parameters, given that the data used in the estimation of the parameters {ie  $F(\tau)$ } has been determined with experimental errors denoted by  $\Delta F(\tau)$ .

For small variations,

$$\Delta F(\tau) = \frac{\partial F(\tau)}{\partial \alpha} \Delta\alpha + \frac{\partial F(\tau)}{\partial \delta} \Delta\delta \quad (D-1)$$

and we can show that

$$\frac{\partial F(\tau)}{\partial \alpha} = \frac{g_o C^2}{h} (\tau - \tau_{\min}) \bar{F}$$

which has a value of zero at  $\tau = \tau_{\min}$  and a maximum value at  $\tau = \tau_{av} = h / \alpha g_o$ ; and

$$\frac{\partial F(\tau)}{\partial \delta} = \alpha C \bar{F} \left\{ \frac{\alpha g_o C}{h} (\tau - \tau_{\min}) - 1 \right\}$$

which has a maximum (numerical) value at  $\tau = \tau_{\min}$  and has a value of zero at  $\tau = \tau_{av}$ .

Typical variations with  $\tau$  of  $F$  and the above derivatives are shown in Figure D-1 for the case where  $g_o = 0,5$   $h = 5\text{cm}$   $\delta = 0,5$  and  $\alpha = 0,5$ . Bearing (D-1) in mind, we observe that near  $\tau = \tau_{av}$ ,  $\Delta F(\tau)$  is a strong function of  $\Delta\alpha$  (at  $\tau = \tau_{av}$ ,  $\Delta F(\tau)$  is unaffected by  $\Delta\delta$ ).

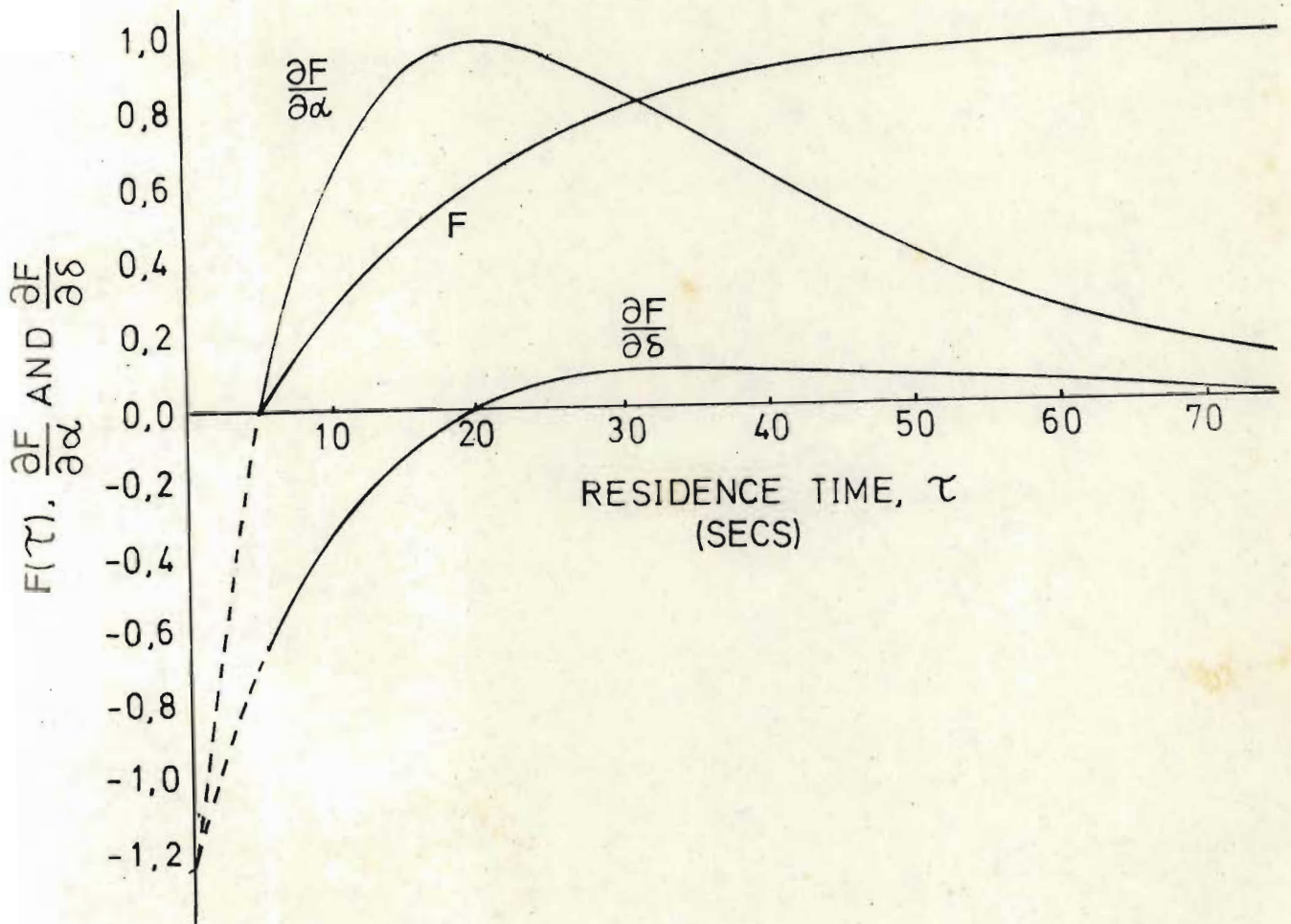


Figure D-1. Variation of residence time distribution  $F(\tau)$  and its derivatives with  $\tau$  for  $g_0 = 0,5$   $h = 5$  cm  $\delta = 0,5$  and  $\alpha = 0,5$



$\Delta F(\tau)$  near  $\tau = \tau_{\min}$  is most strongly affected by  $\Delta\delta$ ; however as  $\tau$  increases in value,  $\Delta\alpha$  increases its effect on  $\Delta F$ , so that, in the example portrayed in Figure D-1, at  $\tau = 8$  seconds,  $\Delta\alpha$  and  $\Delta\delta$  have equal effects on  $\Delta F$  (ie  $\frac{\partial F}{\partial \alpha} = \frac{\partial F}{\partial \delta}$  at  $\tau = 8$  seconds). Thus an error in  $\alpha$  will introduce errors in our estimation of  $\delta$ ; on the other hand, errors in  $\delta$  have little effect on our estimation of  $\alpha$  as was shown in section 5.2.4, where fixing the value of  $\delta$  at 0,5 (rather than estimating a value for it) did not change estimates of  $\alpha$  by more than 1,0%. Thus we can be justified in using (D-1) to obtain a measure of the error in our estimate of  $\alpha$  by evaluating (D-1) at  $\tau = \tau_{av}$  and solving for  $\Delta\alpha$

$$\Delta\alpha = \pm \Delta F(\tau_{av}) \alpha e / C$$

However to estimate errors in  $\delta$  we must take into account errors in  $\alpha$ . Solving (D-1) for  $\Delta\delta$  at  $\tau = \tau_{\min}$ , but using  $\frac{\partial F}{\partial \alpha}(\tau_{av})$  instead of its zero value at  $\tau_{\min}$ , we get

$$\Delta\delta = \pm (\Delta F(\tau_{\min}) \pm \Delta F(\tau_{av})) / \alpha C$$

If the  $\Delta F$ 's are given positive values for the purposes of calculation, then the + option of the  $\pm$  sign in the brackets must be used to obtain the maximum effect of the interaction between  $\alpha$  and  $\delta$ .

Obviously these estimates for  $\Delta\alpha$  and  $\Delta\delta$  are not measures of error with any specified degree of confidence in the rigorous statistical sense. They do however give us a "feel" for the accuracy with which  $\alpha$  and  $\delta$  are estimated, and since they are obtained from regions in the  $\tau$  domain where  $F(\tau)$  is most strongly affected by these parameters, they are at least as stringent as the 95% confidence values defined in the accepted statistical sense.

NOMENCLATURE

Note: Some symbols that appear in this thesis are not listed below, because they are defined and used only in very limited contexts eg. only in a single paragraph.

Roman Symbols

A	Total bubble surface area in the pulp phase.
$A_c$	Cross-sectional area of flotation cell in the froth phase.
$C_{fi}$ $C_{Ii}$ $C_{Ti}$	Concentration of ith component in the froth, feed and tailings streams respectively.
$\bar{C}$	Normalising constant in the froth residence time equation, defined in section 4.2.2.2
$E_c(\tau)$ , $E_f(\tau)$ , $E_p(\tau)$	Residence time distribution density functions for particles in the concentrate stream, the froth phase and the pulp phase respectively.
$F(\tau)$	Cumulative residence time distribution function; with subscripts e or t, it denotes experimental or theoretical values respectively.
FC	Frother concentration
G	Gas rate to impeller region of the flotation cell.
$G(D)$	Mineral grade as a function of diameter.
$g_b(x)$ ; $g_{b1}$ , $g_{b2}$	Functional form for the gas flux through the froth surface due to bubble breakage, and the two parameters that appear in its algebraic form.
$g_c(z)$ ; $g_{c1}$	Functional form for the gas flux in the concentrate stream across the concentrate weir and the constant value that is assigned to it.
$g_f(x)$ ; $g_o$	Functional form for the gas flux across the froth-slurry interface and the constant value that is assigned to it.
$g_o^o$	Gas flux across the froth-slurry interface below which no concentrate is produced.

$h$	Height of the surface of the froth above the froth-slurry interface.
$k_{ei}$	Rate constant governing the rate at which particles of component $i$ move from the upward-flowing stream of slurry to the downward-flowing stream of slurry in the froth phase.
$k_{fi}$	Rate constant governing the rate at which particles of component $i$ move from the froth phase to the pulp phase.
$k_{pi}$	Rate constant governing the rate at which particles are attached to bubbles in the pulp phase and removed into the froth phase.
$k_q$	Rate constant governing the rate at which water in the upward-flowing stream diffuses into the downward-flowing stream in the froth phase.
$L$	Distance between the back of the cell and the concentrate weir.
$L_{eff}$	Distance between the point at which froth begins to move forwards and the concentrate weir.
$M_{ci}, m_{ci}$	Mass flowrate of component $i$ in the concentrate stream.
$M_{ei}(z)$	Upward mass flowrate of particles of component $i$ attached to bubble films at level $z$ in the froth phase.
$M_{ri}(z)$	Downward mass flowrate of particles of component $i$ at level $z$ in the froth phase.
$m_{\beta}$	Slope of the parameter $\beta_{\alpha}$ with respect to froth height $h$ .
$Q_f, Q_I, Q_T$	Volumetric flowrate of concentrate, feed and tailings streams, respectively.
$q_1(z), q_2(z)$	Upward and downward volumetric flowrates of slurry at level $z$ in the froth phase.
$R_E, R_R$	Experimental and regressed recovery of a component.
$u(z)$	Downward velocity of slurry returning to the pulp phase, at level $z$ in the froth phase.

$V_f$	Volume of the froth phase.
$V_p$	Volume of the pulp phase.
$v(z)$	Upward velocity of bubbles and associated particles and slurry at level $z$ in the froth phase.
$v_x$	Velocity of a froth element towards the concentrate weir in the froth phase (derived from the stream function).
$v_z$	Vertical velocity of a froth element in the froth phase (derived from the stream function).
$w$	Height of concentrate weir above froth-slurry interface.
$x$	Distance from the back of the cell.
$z$	Height above the froth-slurry interface.
$z_{di}$	Height above the froth-slurry interface at which detachment of weakly attached particles commences.

#### Greek Symbols

$\alpha$	Froth stability, defined in section 4.2.1
$\beta_\alpha \beta_\epsilon$	Parameters in the relationships which express $\alpha$ and $\epsilon$ respectively as functions of $g_0$ .
$\Delta F \Delta \alpha \Delta \delta$	95% confidence limits on $F$ , $\alpha$ and $\delta$ as defined in Appendix D.
$\epsilon$	Froth removal efficiency defined in section 4.1
$\sigma_F$	Standard deviation of measured values of $F(\tau)$
$\tau, \tau_c$	Residence time of a froth element in the froth phase and on the concentrate weir, respectively.
$\tau_p$	Residence time of a tracer particle in the pulp phase.
$\tau_{min} \tau_{av} \tau_{max}$	Minimum, average and maximum residence time of froth elements in the froth phase.
$\phi(x, z), \phi$	Functional form and value respectively of the stream function which defines the streamlines followed by froth elements in the froth phase.